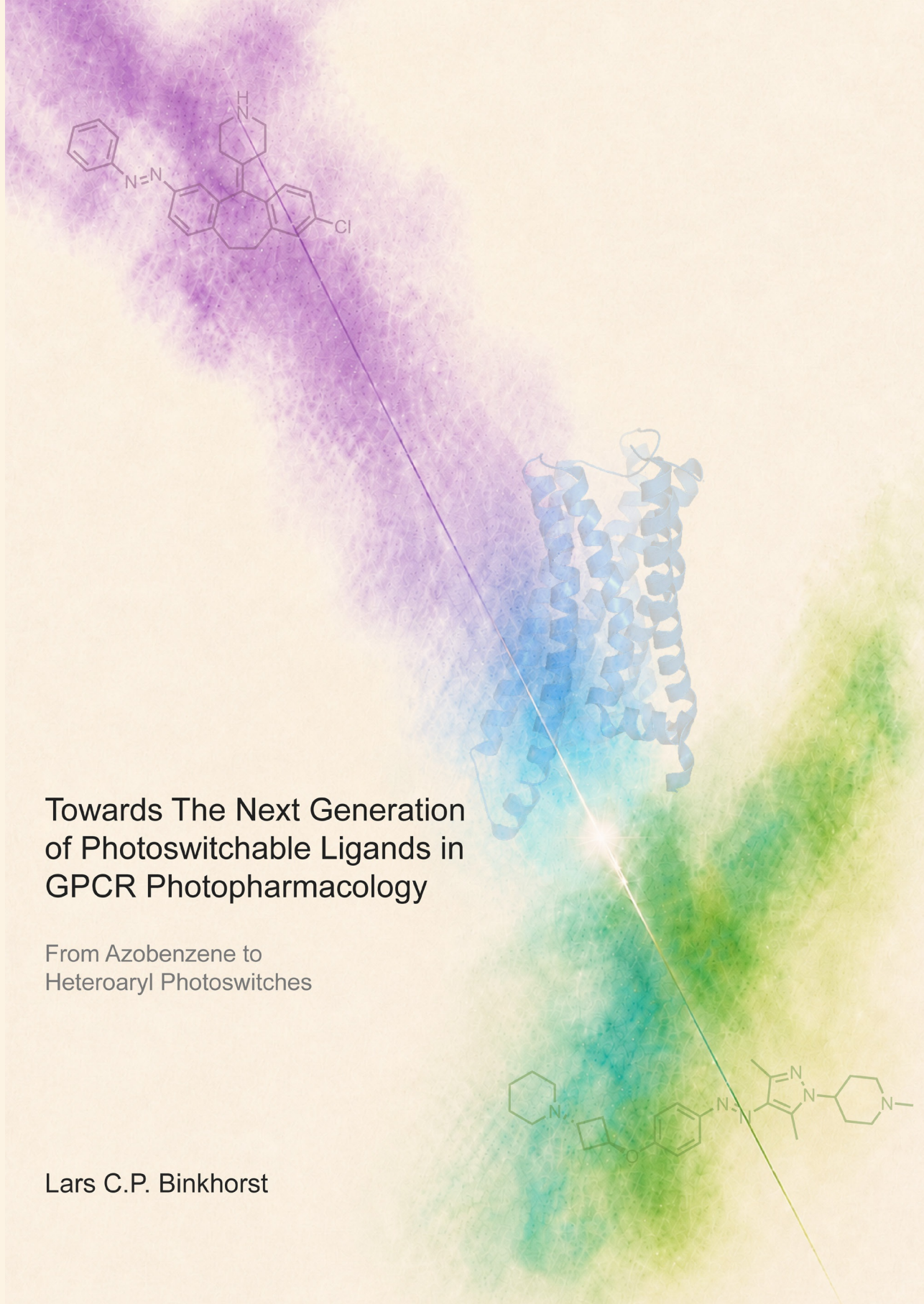

Towards The Next Generation of Photoswitchable Ligands in GPCR Photopharmacology

From Azobenzene to Heteroaryl Photoswitches

Lars C.P. Binkhorst

Towards the Next Generation of Photoswitchable Ligands in GPCR Photopharmacology

From Azobenzenes to Heteroaryl Photoswitches

Lars C.P. Binkhorst

The work in this thesis was performed at the Amsterdam Insitute of Molecular and Life Sciences (AIMMS), Division of Medicinal Chemsitry, Faculty of Science, Vrije Universiteit Amsterdam, De Boelelaan 1108, 1081 HZ, Amsterdam, The Netherlands.

Towards the Next Generation of Photoswitchable Ligands in GPCR Photopharmacology
From Azobenzenes to Heteroaryl Photoswitches

Printed by: ProefschriftMaken // www.proefschriftmaken.nl

©Copyright Lars Binkhorst, 2026

DOI: 10.5463/thesis.1683

This work in this thesis was supported by The Dutch Research Council (NWO, OCENW.KLEIN.532, “Towards the next frontiers in GPCR photopharmacology”).

VRIJE UNIVERSITEIT

Towards the Next Generation of Photoswitchable Ligands in GPCR Photopharmacology

From Azobenzenes to Heteroaryl Photoswitches

ACADEMISCH PROEFSCHRIFT

ter verkrijging van de graad Doctor aan
de Vrije Universiteit Amsterdam,
op gezag van de rector magnificus
prof.dr. J.J.G. Geurts,
volgens besluit van de decaan
van de Faculteit der Bètawetenschappen
in het openbaar te verdedigen
op woensdag 30 september 2026 om 13.45 uur
in de universiteit

door

Lars Cornelis Pieter Binkhorst

geboren te Haarlem

promotor:	prof.dr. R. Leurs
copromotor:	dr. M. Wijtmans
promotiecommissie:	dr. S.A.K. Jongkees prof.dr. D.J. Vugts prof.dr. W.C. Szymanski dr. X. Gomez-Santacana dr. N.J. Hauwert

Table of contents

Chapter 1	Introduction and aim	7
Chapter 2	A radiolabeled photoswitchable G proteincoupled receptor antagonist enlightens ligand binding kinetics associated with photoswitching	43
Chapter 3	'Photoswitch hopping' in Photopharmacology: A Comparative Study on Photochemical and Pharmacological Properties	91
Chapter 4	Design and synthesis of photoswitchable desloratadine ligands for histamine H_1 receptor photopharmacology	155
Chapter 5	Investigating the effect of positional arylazopyrazole isomers of a photoswitchable H_3R agonist	211
Chapter 6	Discussion and future perspectives	231
Appendix	English Summary	257
	Acknowledgements	263

Chapter 1

Introduction and aim

Light-based approaches to modulate biological processes

The use of light as an external stimulus to control biological processes has gained significant interest over the past decades. Light-based approaches offer precise spatial and temporal regulation, enabling the targeting of specific cells or tissues. Conversely, standard pharmacotherapy often lacks this specificity, leading to the potential for off-target effects.[1,2] Light-based approaches can overcome these limitations by reducing off-target effects through dynamic control over biological processes. Moreover, the use of light, specifically photons, is minimally invasive. Generally, light-based approaches can be divided into the areas of photodynamic therapy, optogenetics, and photopharmacology.

Photodynamic therapy

A well-established approach is photodynamic therapy (Figure 1A), which combines the use of light with a photosensitizer.[3,4] Upon absorption of light, the photosensitizer is activated at a specific location, and an electron is excited to a higher-energy orbital.[3] This system can undergo intersystem crossing to produce a triplet state. In this excited state, it can react with cellular substrates or molecular oxygen to generate reactive oxygen species, such as short-lived singlet oxygen ($^1O_2$).[4] These reactive species can react with a wide range of biological molecules and eventually lead to cell death. This approach is mainly used in oncology, where cell death is desired, as it is less invasive and more selective compared to standard therapies.[3]

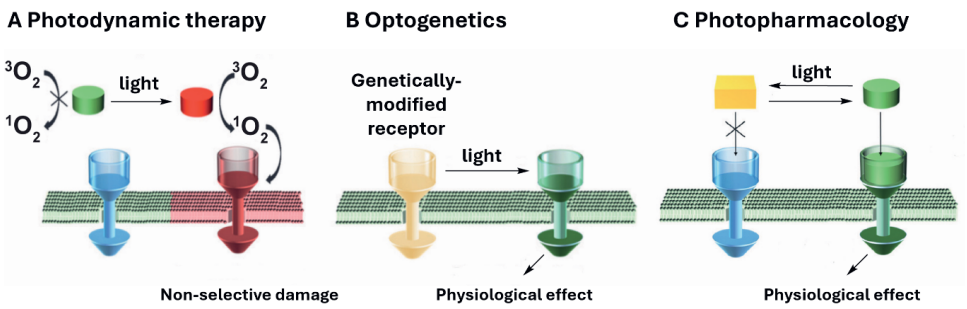

Figure 1. Overview of the different light-based approaches to control biological processes. (A) Photodynamic therapy, (B) Optogenetics, and (C) Photopharmacology. Figure adapted from Lerch *et al*.[5]

Optogenetics

Another light-based approach, used primarily in neuroscience, is optogenetics (Figure 1B). This method combines optical methods and genetic modification. Specific cell types are genetically modified to express light-responsive proteins, such as GPCRs, ion channels (e.g.,

channelrhodopsins, halorhodopsins), and enzymes (e.g., photoactivated adenylyl cyclases).[6,7] Illumination then allows precise control over their activity. Examples of optogenetics involve activating or inactivating neurons.[8] Channelrhodopsin, which is activated by blue light, functions as a cation channel that opens upon illumination. It allows influx of cations into the cell, leading to depolarization and neuronal activation.[6] In contrast, halorhodopsin, which is activated by yellow light, is a chloride pump that transports chloride ions into the cell. This results in hyperpolarization and inhibition of neuronal signaling.[9] This method is mainly used for studying brain function, as it enables precise activation or inhibition of specific cell types, with optogenetics providing a powerful tool for exploring neuronal circuits with high spatial and temporal resolution. [8]

Photopharmacology

Although both photodynamic therapy and optogenetics demonstrate the potential of light to modulate biological processes, they also pose challenges. Photodynamic therapy induces irreversible cell death, while optogenetics requires genetic modification. A third, complementary approach to photodynamic therapy and optogenetics is photopharmacology (Figure 1C). This approach uses light-responsive ligands to modulate biological processes without the need for genetic modification. By incorporating photoresponsive moieties into biological ligands, precise control over protein targets can be achieved. [2,5]

Photopharmacology

Photopharmacology represents a field in which light-responsive moieties are incorporated into bioactive ligands to achieve control over biological signaling. The field of photopharmacology can be subdivided into two main subfields: photocaging[10] and photoswitchable ligands. [2,11,12] In this thesis, the primary focus will be on the latter.

Photocaging

In photocaging, a biological ligand is made inactive by incorporation of a photocleavable protecting group. Upon illumination with light, the photocaged ligand is deprotected ('uncaged'), releasing both the active ligand and the byproduct of the photocleavable group (Figure 2). Although this approach provides spatial and temporal control, its main limitation is that uncaging is irreversible. As a result, the active ligand can only be released once. Additionally, the byproduct of the cleaved photoprotecting group (i.e., a nitrosobenzaldehyde in Figure 2) may also absorb light, exhibit reactivity, and potentially induce toxicity.[13] For example, o-Nitrobenzyl, coumarin and BODIPY are well-known caging groups, but some of their derivatives are used as photosensitizers in PDT.[10,14]

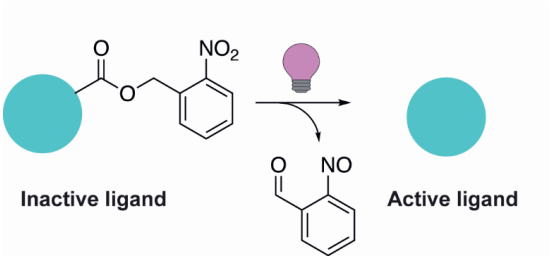

Figure 2. Schematic representation of photocaging where the ligand (cyan) is caged with a photocleavable group. Upon illumination with light, the active ligand is released.

Photoswitchable ligands

Also in the field of photoswitchable ligands, photoresponsive moieties are incorporated into a bioactive ligand. [2,11,12] Upon illumination, an isomerization takes place (often a *trans-cis* isomerization). As a result, these ligands change shape and chemical properties (such as dipole moment), with the potential to give distinct biological properties. An advantage of this approach is that photoswitching from the thermodynamically stable *trans* isomer to the metastable *cis* isomer is reversible.[15] Thus, it allows precise and dynamic control over a protein target without generating additional byproducts. Among the various photoswitch scaffolds, azobenzenes have emerged as a prototypical photoswitch due to their extensively investigated isomerization, robust photoswitching properties, and well-established synthesis. Azobenzenes are also widely employed in other fields such as metal catalysis, materials science, imaging, and supramolecular chemistry.[16–19] Photoswitching from the *trans* isomer to the *cis* isomer (Figure 3) requires illumination with a specific wavelength, often ultraviolet (UV) light. This process is reversible, either by illumination with a different wavelength, often blue light in the 400-450 nm region, or by thermal relaxation in the dark.

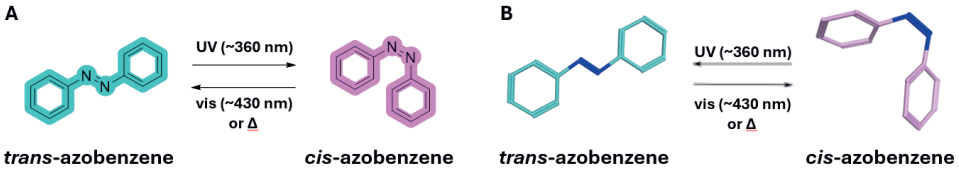

Figure 3. Isomerization of an azobenzene. (A) 2D representation and (B) 3D crystal structures of *trans* and *cis* azobenzene (deposition numbers 1104320 and 1104150), showing the change in shape accompanying the isomerisation.[20,21] UV light is used to switch from the thermodynamically stable *trans* isomer (cyan) to the metastable *cis* isomer (pink). Upon illumination with a different wavelength, the *cis* isomer is reverted to the *trans* isomer or by thermal relaxation.

Properties, design, and synthesis of photoswitchable ligands

Photochemical parameters

Several photochemical properties define the performance of photoswitches. The first property is the quantum yield (ϕ), i.e., the ratio of the number of molecules undergoing a photochemical event (e.g., isomerization) to the number of photons absorbed.[22] Photoswitches absorb light at various wavelengths (λ) and usually exhibit distinct absorption spectra for the *trans and cis* isomers, typically displaying two characteristic absorption bands (Figure 4A). The first absorption band of the azobenzene corresponds to the π-π* transition, which has a maximum absorption (λ_{max}) around 320 nm. The second absorption band is the n-π* transition, which is above 400 nm for azobenzenes with the λ_{max} value around 450 nm.[23,24]

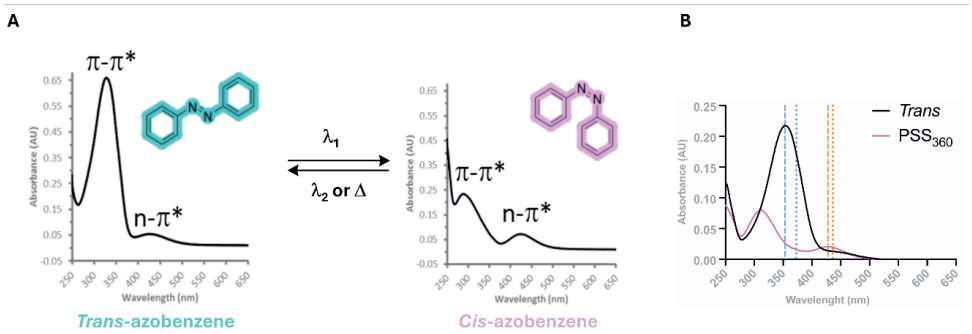

Figure 4. (A) Representative UV-Vis absorption spectra of the parent *trans*-azobenzene and *cis*-azobenzene. (B) Example of a UV-Vis absorption spectrum showing the λ_{max} (striped) and optimal wavelengths for irradiation (dotted). The photostationary state at 360 nm (PSS_{360}) is a mixture of isomers enriched in the *cis* isomer. Figures adapted from Wijtmans *et al.*[25]

Efficient switching can be achieved by selecting wavelengths where the absorption difference between the two isomers is the highest. The wavelength (λ_1) used for *trans* to *cis* isomerization of azobenzenes is often located in the π-π* absorption band, typically requiring a wavelength of around 360-370 nm (Figure 4B). Another wavelength (λ_2) is chosen to illuminate the *cis* isomer and revert it to the *trans* isomer. In this case, a wavelength is selected where the *cis* isomer absorbs more strongly than the *trans* isomer. This wavelength is often near the n-π* absorption band of azobenzenes (Figure 4B).

After illumination with a specific wavelength for either isomerisation, a photochemical equilibrium is reached. This photochemical equilibrium is called the photostationary state (PSS) and gives a ratio in which both isomers are present. For *trans* to *cis* isomerization, PSS_{cis} is achieved, i.e., the amount of *cis* isomer present at photochemical equilibrium.[25] When photoswitching from the *cis* isomer to the *trans* isomer, the PSS_{trans} is reached, i.e., the amount of *trans* isomer present at photochemical equilibrium. Additionally, the metastable

cis isomer can revert to the *trans* isomer by thermal relaxation in the dark, with the rate defined by its half-life ($t_{½}$).[23]

Types of photoswitches

Although the focus in photopharmacology is often on linear azobenzenes, a broad range of photoswitches can be selected, including diarylethenes,[26] Stenhouse switches,[27] spiropyrans,[28] acylhydrazone switches,[29] BF_2-coordinated azo compounds,[30] stilbenes,[31] hemithioindigos,[32] and diazocines (Figure 5).[33]

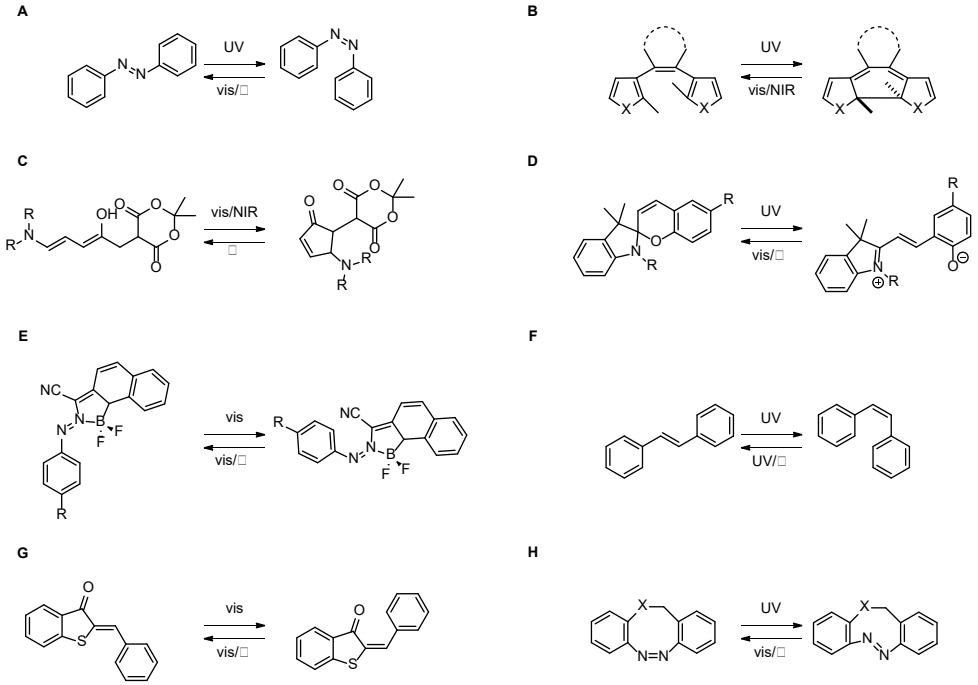

Figure 5. Examples of different types of photoswitches. (A) azobenzene, (B) diarylethene, (C) Stenhouse switch, (D) spiropyran, (E) BF_2-coordinated azoswitch, (F) stilbene, (G) hemithioindigo, (H) diazocine. UV = UV light, vis = visible light, Δ = thermal relaxation.

Although many of these classes exhibit interesting and diverse photochemical properties, such as switching with visible light, most of these switches have not yet been widely applied in the field of photopharmacology. Instead, the most extensively used photoswitch in photopharmacology remains the azobenzene due to its well-established switching properties and ease of synthesis.[13,25,34] However, incorporating the azobenzene also has a key limitation. For the switching from the *trans* to the *cis* isomer, UV light is often used. This may lead to toxicity in biological settings.[2] Additionally, the penetration depth of light with shorter wavelengths is limited through the skin (Figure 6).[2,35] Therefore, the use of UV and blue light is limited to superficial tissues. In contrast, longer wavelengths such as red and near-infrared light penetrate much deeper, making them more suitable for applications in biological

systems.[36] In recent years, efforts have therefore focused on 'red-shifting' photoswitch units, i.e., photoswitches that use wavelengths in the visible light spectrum for switching in both directions.[37–39] For biological applications, an ideal photoswitch can operate at wavelengths near the near-infrared (NIR) region, which offer deep tissue penetration without the toxicity associated with higher-energy wavelengths.[37]

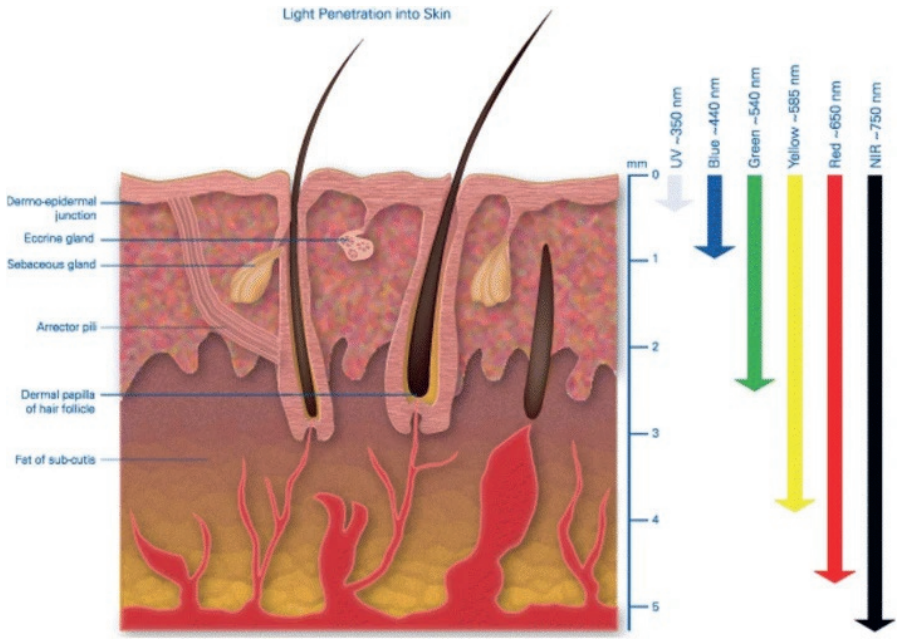

Figure 6. Penetration depth of different wavelengths through the skin, adapted from Clement *et al*.[35]

Tetra-ortho-substituted azobenzenes

One strategy to achieve red-shifting is to introduce substituents at the *ortho* position of azobenzenes. Although there are a variety of combinations with *ortho* substituents, to date, only the tetra-*ortho*-fluoro azobenzenes and tetra-*ortho*-chloro azobenzenes (Figure 7A) have made their way into photoswitchable ligands used in photopharmacology.[38] These *ortho* substituents affect the electronic properties and geometry of these molecules. As a result, the n-π* bands of the tetra-*ortho*-substituted azobenzenes show significant separation, which allows the use of visible light for *trans* to *cis* isomerization instead of UV light. Additionally, other properties, such as the PSS and thermal stability/dark stability, are significantly influenced by these substituents.[38]

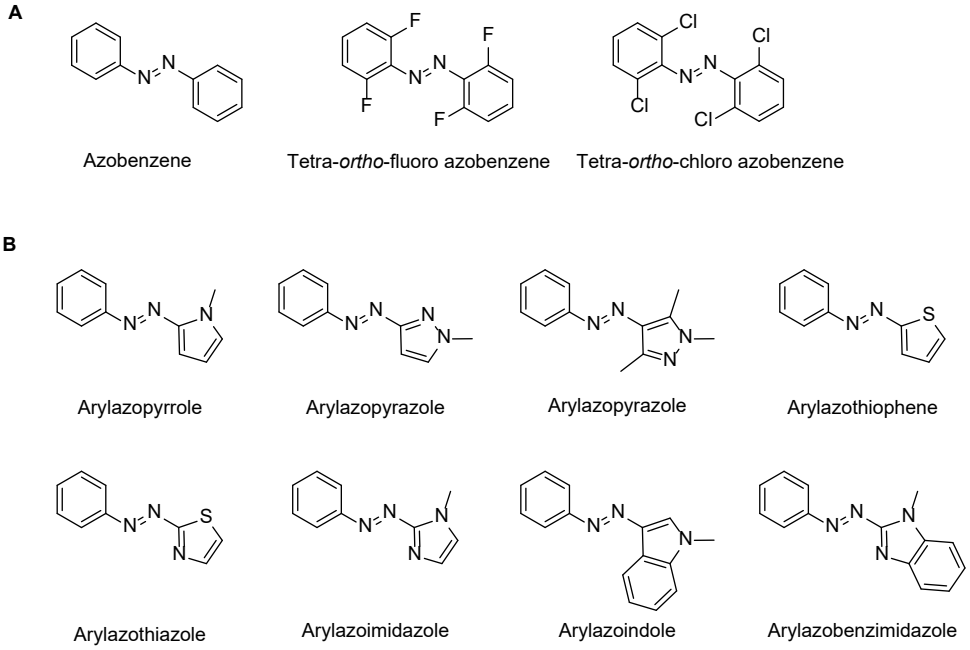

Figure 7. A selection of available photoswitches. (A) Azobenzene and tetra-*ortho*-substituted azobenzenes. (B) Examples of five-membered or fused heteroaromatic photoswitches, including pyrrole, pyrazole,[40] thiophene,[41] thiazole,[42] imidazole,[43] indole,[44,45] and benzimidazole.[45]

Tetra-*ortho*-fluoro azobenzenes retain a nearly planar geometry comparable to that of unsubstituted azobenzenes, since fluorine atoms are similar in size to hydrogen. The absorption maxima are located around 305 nm for the π-π* band and 456 nm for the n-π* band. The inductive effects of the fluorine atoms lead to a 43 nm separation for the n-π* bands of *trans* and *cis* isomers.[38] As a consequence, visible light can be used for photoswitching, i.e., wavelengths of >500 nm, can be used for *trans* to *cis* isomerization. Wavelengths around 410 nm can be used to switch the *cis* isomer back to the *trans* isomer. Additionally, these compounds display remarkably high thermal stability, i.e., half-lives up to years at 25 ºC in DMSO.[46]

In contrast to the tetra-*ortho*-fluoro azobenzenes, the tetra-*ortho*-chloro azobenzenes adopt a twisted conformation in the *trans* configuration due to the steric effects of the larger chlorine atoms relative to the smaller hydrogen and fluorine atoms. The absorption maxima of the parent tetrachloro-azobenzene are located around ~280 nm for the π-π* transition and at 457 nm for the n-π* absorption band.[47] Due to the band separation in the n-π* absorption band, higher wavelengths, i.e., red light, can be used to reach PSS_{cis}. Moreover, blue light can be used to efficiently switch to the *trans* isomer, with PSS trans values of 82-90% for the unsubstituted tetra-*ortho*-chloro azobenzenes.[47] However, substituents can significantly impact these properties.[47]

Heteroaryl photoswitches

In addition to *ortho*-substituted azobenzenes, heteroaryl photoswitches have recently gained attention in various fields where photoswitches are utilized, including photopharmacology.[39,48] For heteroaryl photoswitches, one phenyl ring of the azobenzene is substituted by a heteroaromatic ring. These photoswitches exhibit broad structural diversity, as the heterocyclic rings can be extensively tuned. Some heteroaryl switches exhibit attractive properties, including high PSS_{trans} values, high thermal stability of the *cis* isomer, and shifting of the wavelength used for *trans* to *cis* isomerization from the UV to blue light (~400 nm).[39] These heteroarylazo switches primarily contain five-membered or fused heterocycles, including pyrrole, pyrazole,[40] thiophene,[41] thiazole,[42] imidazole,[43] indole, [44,45] and benzimidazole[45] switches (Figure 7B).

One of the heteroaryl switches that is becoming more popular in photopharmacology is the arylazopyrazole (Figure 7B).[49–57] Specifically, arylazopyrazoles with two methyl substituents in the *ortho* positions of the pyrazole ring exhibit interesting properties, including near-quantitative switching both ways. Interestingly, these five-membered heteroaryl photoswitches can adopt conformations of the *cis* isomer that are not standard for an azobenzene. Without both methyl substituents, it can adopt a T-shape conformation as a result of a H-π interaction, while with a substituent present on the *ortho* position, it will adopt a twisted conformation because of steric constraints disabling the H-π interaction (Figure 8).[58]

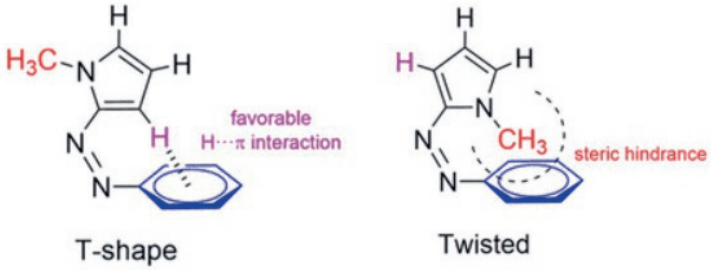

Figure 8. The T-shape and twisted conformation of *cis* isomers of five-membered heteroarylazo photoswitches, as exemplified for a pyrrole with one methyl substituent at the *ortho* position. Figure adapted from Calbo *et al*.[58]

Significant separation of the π-π* absorption bands of the *trans* and *cis* isomers leads to high PSS_{cis} values, although still requiring UV light. Secondly, because of the twisted conformation adopted in the *cis* configuration, the n-π* band of the *trans* isomer is lower compared to the n-π* band of the *cis* isomer. As a result, green light (~500 nm) can be used to irradiate in the tail of the n-π* band to afford high PSS_{trans} values. Without the two methyl substituents, the intensity of the n-π* absorption band for the *trans* and *cis isomers* is comparable, resulting in a lower PSS_{trans} value.[40]

Synthesis of azo compounds

The key synthetic step in the synthesis of photoswitchable ligands is the formation of the azo bond (-N=N-). Incorporation of this moiety requires careful synthetic planning, as it can significantly influence reactivity, can be unstable under reductive conditions and is sensitive to light. The two most common methods for the formation of azo bonds are the diazonium coupling or the Mills reaction (Scheme 1).[59]

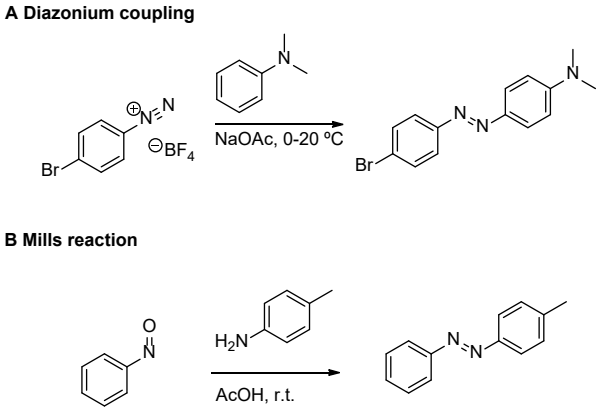

Scheme 1. Examples of a diazonium coupling[60] and a Mills reaction.[61]

In the diazonium coupling, a diazonium salt, which can be prepared by diazotization of an aniline, is reacted with an electron-rich arene nucleophile. This nucleophile often contains an electron-donating group (e.g., an amine or hydroxyl group), and reaction occurs at the *para* position or at the *ortho* position if the *para* position is occupied.[59] The stability of the diazonium salt strongly depends on the counterion. While chloride diazonium salts can be unstable, diazonium salts with counterions like tetrafluoroborate, disulfonimide, hexafluorophosphate, and zinc chloride can be isolated and stored.[59]

The Mills reaction provides an alternative approach, in which a nitroso derivative is reacted with an aniline in acetic acid. A range of oxidation agents can be used to prepare these nitroso compounds, but the most common approach to obtain the nitroso derivatives is by oxidation of an aniline with Oxone. However, these methods all require excess amounts of oxidant, the reaction can be slow, and overoxidation to the nitrobenzene can occur.[59]

In addition to these well-established methods, several other methods have been reported. However, these are less widely adopted. The development of red-shifted photoswitches (e.g., the tetra-*ortho*-substituted azobenzenes and heteroarylazo benzenes) requires new synthetic strategies to address challenges, such as steric effects, reactivity or instability. For the synthesis of tetra-substituted azobenzenes, Hansen *et al*. reported a method, which relies on the *ortho* lithiation of 1,3-disubstituted aromatic compounds containing fluoro, chloro, or methoxy substituents. These lithiated species can react as nucleophiles with diazonium salts.[62] Earlier studies already demonstrated that diazonium salts can be reacted with organometallics such as Grignard, cadmium, lithium, zinc, and mercury reagents to form azo

bonds.[63–65] More recently, a method using a trimethylsilyl derivative of a thiazole has been *used to react with diazonium salts to form the azo bond.*[66]

Design of photoswitchable ligands

For the design of photoswitchable ligands, two approaches can be chosen. The first method is azologization (Figure 9A), in which an azobenzene isoster (Figure 9B, also referred to as azostere) is substituted for a photoswitchable moiety in the core of a bioactive template ligand.[11,67] Recent applications of the azologization strategy include the design of a ligand for the gamma aminobutyric acid type A receptor ($GABA_AR$). Specifically, substitution of the benzylether group in the positive allosteric modulator abecarnil with an azo bond yields the photoswitchable ligand azocarnil.[68] Similarly, an amide group in VU0415374, a positive allosteric modulator of metabotropic glutamate 4 receptor (mGlu4), was replaced by an azo bond to give photoswitchable ligand optogluram.[69] Another example of azologization involved the replacement of an amide group in an the atypical chemokine receptor 3 (ACKR3) ligand with an azo bond, resulting in the first small-molecule photoswitchable agonist targeting ACKR3.[70]

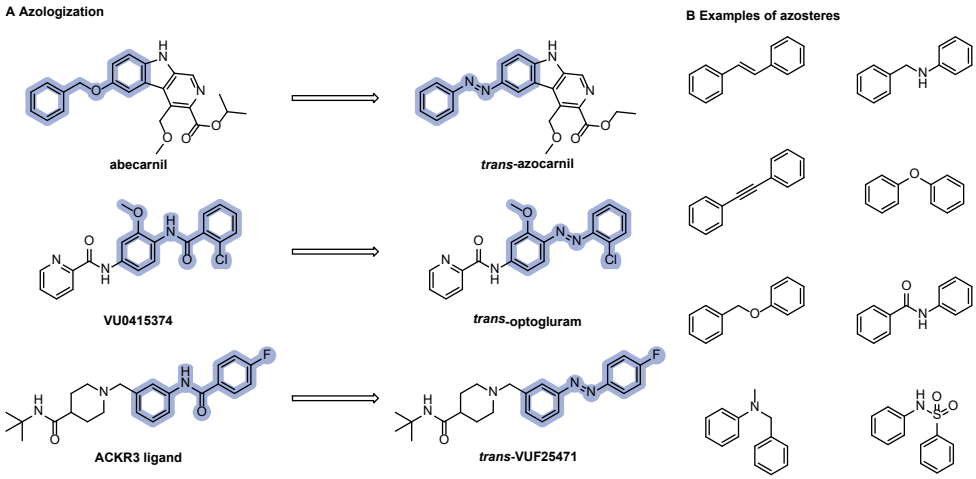

Figure 9. (A) Representative examples of photoswitchable ligands designed by using an azologization strategy.[68–70] (B) Examples of azosteres.

The second approach is azoextension (Figure 10), in which the template ligand is extended with a photoswitch unit. An example is the design of a photoswitchable casein kinase Iα (CKIα) inhibitor, in which azoextension of the parent compound longdaysin affords a light-responsive analog.[51] Another example is a photoswitchable analog of a transient receptor potential vanilloid 6 (TRPV6) inhibitor, obtained by extending the parent ligand with an azobenzene unit.[71] Besides these experimental examples, also computational methods are applying these strategies. For example the PSW-designer platform reported by Simon *et al.* enables the design and virtual screening of new photoswitchable ligands by applying these azologization and azoextension strategies on known ligands for biological targets.[72]

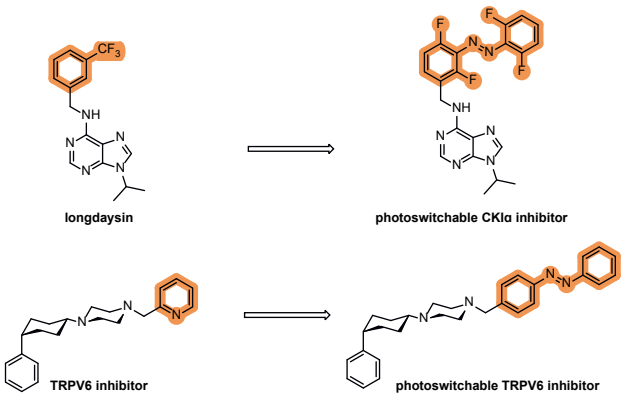

Figure 10. Representative examples of photoswitchable ligands designed by using an azoextension strategy.[51,71]

An example that shows that ligands designed based on azobenzene isomerization can ultimately be advanced to the clinic is KIO-301 (Figure 11), a photoswitchable ligand that is currently in phase II clinical trials for patients with retinitis pigmentosa.[73] Retinitis pigmentosa is a degenerative disease where the loss of rod and cone photoreceptor cells leads to loss of vision.[74] This ligand can potentially treat visually impaired patients. This photoswitch can be used to modulate light-dependent ion channels reversibly. The *trans* isomer of KIO-301 is inactive, whereas the *cis* isomer can block ion channels upon illumination.[75–77] As a result, signaling to the brain is restored, improving vision. In the dark, the *cis* isomer rapidly relaxes back to the *trans* isomer. Studies suggest that KIO-301 can partially restore visual function in patients with blindness, emphasizing the potential of photoswitchable ligands and photopharmacology.

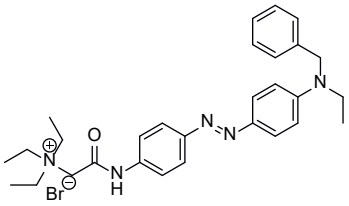

Figure 11. Structure of clinical candidate KIO-301 by Kiora Pharmaceuticals.

Notwithstanding the clinical promise outlined here, the design and properties of photoswitchable ligands require careful balancing.

G-Protein Coupled Receptors

Photoswitchable ligands can, in principle, be applied to any protein target. Over the past few decades, significant progress has been made in the development of photoswitchable ligands, including those targeting enzymes, ion channels, and GPCRs.[13,67] In this thesis, the focus is on

histamine receptors, which belong to the G-protein coupled receptors (GPCRs). GPCRs are one of the largest families of membrane proteins, comprising approximately 800 proteins.[78,79] These proteins share a common motif consisting of seven transmembrane helices connected by intracellular and extracellular loops.[78] GPCRs can be divided into different subfamilies based on their sequence and structural features: rhodopsin-like (class A), secretin and adhesion (class B), glutamate (class C), frizzled (class F), and taste2 (class T). [78,80,81] GPCRs are a highly relevant protein family for drug discovery. This family is targeted by 516 approved drugs, which is approximately 36% of all approved drugs.[79] These approved drugs target 131 different GPCRs with the most drugged targets being aminergic receptors, i.e., class A GPCRs that bind biogenic amines such as endogenous ligands, including dopamine, muscarinic, serotonin, adrenergic, and histamine receptors.[79]

Over the past two decades, the number of structures available for GPCRs in their active and inactive states has increased significantly, contributing to a better understanding of the structural and functional aspects of these receptors.[82,83] Challenges, including low membrane expression and conformational flexibility, initially hindered this progress. A breakthrough was achieved in 2000 with the publication of the first GPCR crystal structure, rhodopsin, followed by the β_2-adrenergic receptor in 2007.[79] Since then, advances in crystallography and the introduction of cryo-electron microscopy (cryo-EM) have led to a rapid increase in the number of resolved GPCR structures in recent years.[81]

GPCRs can be activated extracellularly by a variety of ligands, leading to signaling events through various pathways, the most well-known ones are through heterotrimeric G proteins, consisting of α-, β-, and γ-subunits, or β-arrestins (Figure 12).[79,81] The G proteins consist of four different families, i.e., $G\alpha_s$, $G\alpha_i$, $G\alpha_q$, and $G\alpha_{12}$.[84] The heterotrimer remains inactive when bound to GDP. Upon binding of an agonist to the receptor, the GPCR adopts an active conformation, enabling G protein recruitment and activation, thus leading to downstream signaling events (Figure 12). Guanosine diphosphate (GDP) bound to the Gα subunit is replaced with guanosine triphosphate (GTP). Consequently, the Gα subunit dissociates from the Gβɣ-subunit. In addition to signaling via G proteins, GPCRs can also signal via β-arrestins pathways (Figure 12). Agonists can, in principle, selectively activate one signaling pathway over another. A preference for one signaling pathway over another is referred to as biased signaling.[85,86] This phenomenon, also known as biased agonism, enables the selective modulation of cellular responses initiated by the same receptor.[87] While activation of one pathway may have beneficial outcomes, the other could be unfavorable and result in side effects. Exogenous GPCR ligands are diverse, and they can stimulate or inhibit receptor activation by its natural ligand through multiple mechanisms. That is, ligands can bind the orthosteric site, i.e., the site where the endogenous ligands bind, but also allosterically, i.e., an alternative binding site.[88] Also, exogenous ligands, including antagonists and inverse agonists, have the potential to modulate signaling pathways selectively.

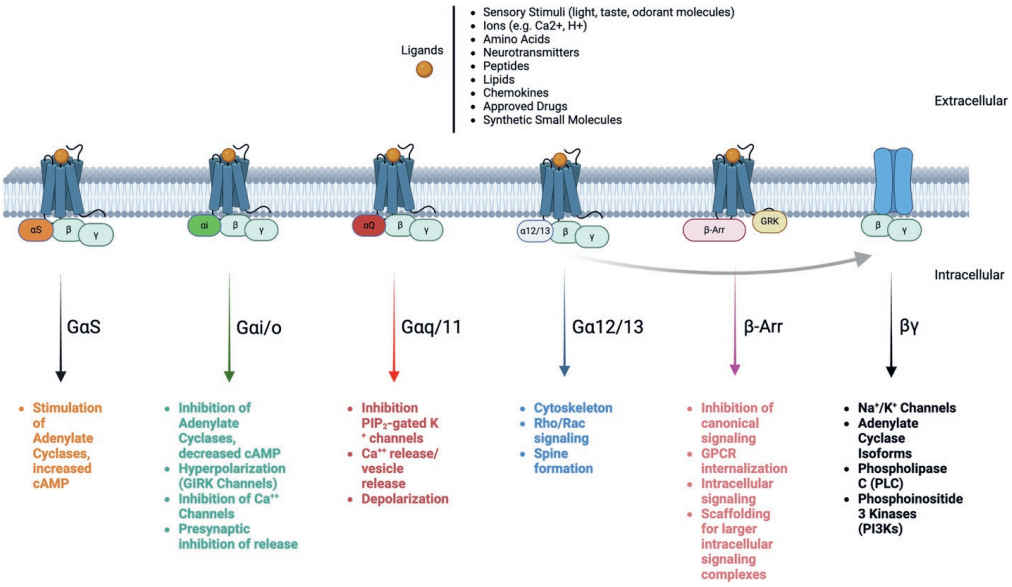

Figure 12. Overview of common GPCR signaling pathways upon stimulation with various ligands. Figure adapted from Krumm *et al*.[89]

Histamine Receptors

Among the aminergic GPCR subfamilies, the histamine receptors are a significant group with diverse physiological and pharmacological implications. These receptors are activated by the endogenous amine histamine, which is found in high concentrations in the skin, lungs, and gastrointestinal tract.[90] Histamine is produced from histidine via the enzyme histidine decarboxylase and stored in basophils and mast cells.[90–92] In the nervous system, histamine acts as a neurotransmitter, whereas in the gut, skin, and immune system, it functions as a local mediator.[90] The histamine receptor family has low sequence identity (16-35%), but all bind histamine as their endogenous ligand and signal mostly through G proteins.[93] Four different receptor subtypes exist: H_1R, H_2R, H_3R, and H_4R. The histamine H_1 and H_2 receptors have relatively low affinity for histamine (pK_i hH_1R = 4.6 and pK_i hH_2R = 5.1)[90] compared to the H_3 and H_4 receptors (pK_i hH_3R = 8.2 and pK_i hH_4R = 8.1).[90] Additionally, they signal through different G proteins, resulting in distinct intracellular signaling effects (Figure 13).[94]

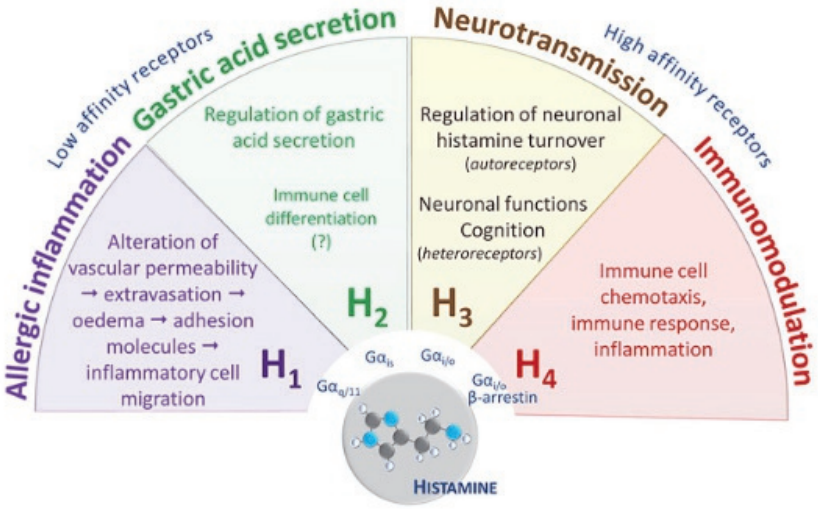

Figure 13. The functions and signaling proteins of the histamine H_1-H_4 receptors. Adapted from Tiligada *et al*.[91]

Histamine H_1 receptor

The histamine H_1 receptor (H_1R) is the second most targeted GPCR by marketed drugs, with 59 drugs targeting this receptor.[79] This receptor is expressed widely throughout the body in e.g. epithelial, smooth muscle, neuronal, glial, and immune cells.[90,95] Upon activation, the receptor couples to $G\alpha_q$, leading to the activation of phospholipase C (PLC). As a result, calcium ions are released into the cell, leading to depolarization and contraction of smooth muscle cells.[90] H_1R is targeted primarily to treat allergic diseases, like urticaria, allergic rhinitis, and allergic conjunctivitis.[93] To treat allergic diseases, H_1-antihistamines are used. These drugs act as inverse agonists, thereby stabilizing the receptor in its inactive state.[96] First-generation antihistamines, like diphenhydramine and chlorpheniramine (Figure 14A), are known to have poor selectivity and to penetrate the blood-brain barrier, causing sedation.[97] The structure of first-generation antihistamines consists of two aromatic rings combined by a linker to a tertiary aliphatic amine. Second-generation antihistamines, such as desloratadine and cetirizine (Figure 14B), have lower BBB penetration, higher H_1R selectivity, and bind preferentially to peripheral H_1R.[96] Their structures often retain the core pharmacophore but have additional polar substituents, e.g., carboxyl or hydroxyl groups.

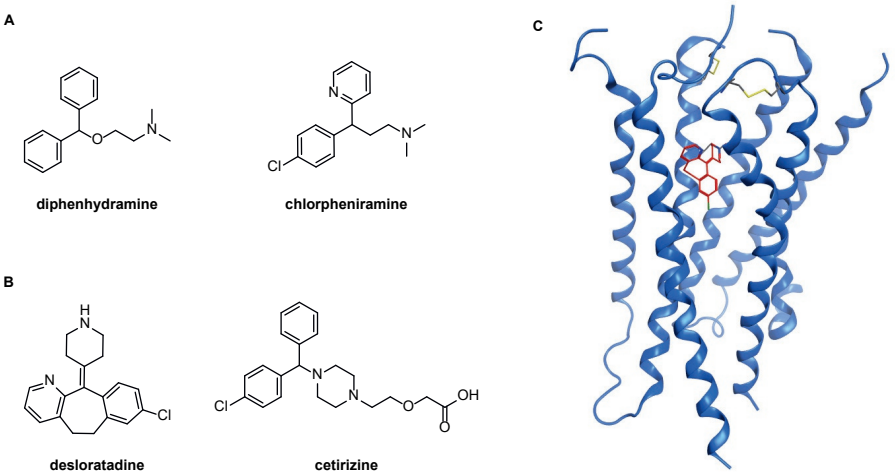

Figure 14. Structures of (A) first-generation inverse agonists, (B) second-generation inverse agonists, (C) cryo-EM structure of H_1R in complex with desloratadine (red), derived from PDB 8X64 as deposited by Wang *et al*.[98]

In 2011, the first X-ray crystal structure of H_1R in complex with the first-generation ligand doxepin was released.[99] This revealed that doxepin was buried deep in the ligand-binding pocket and showed an important hydrophobic interaction with $W428^{6.48}$ and an ionic interaction with $D107^{3.32}$. $W428^{6.48}$ is a highly conserved residue in GPCRs and is involved in switching the receptor from its inactive state to its active state.[100,101] In the past five years, more structures of H_1R have appeared. In addition to the inactive structure, an active H_1R structure in complex with the $G\alpha_q$ protein was published.[100] Additionally, H_1R cryo-EM structures were released with three second-generation antihistamines, mepyramine, astemizole, and desloratadine (Figure 14C), which confirmed the role of $W428^{6.48}$ as an important switch for H_1R activity.[98]

Histamine H_2 receptor

The histamine H_2 receptor (H_2R) was the second histamine receptor identified. It is primarily found in the gastrointestinal tract, where it regulates the secretion of gastric acid.[102] These receptors are also found in nerve cells, airway and vascular smooth muscles, as well as other immune cells, contributing to a variety of physiological responses.[95] Upon activation, H_2R couples mainly to the $G\alpha_s$ protein, leading to stimulation of adenylyl cyclase and subsequent increases in intracellular cAMP levels.[90] Eventually, this leads to acid secretion. H_2R is a well-established target in the treatment of gastroesophageal reflux diseases, dyspepsia, and gastric ulcers.[90,91] Inverse agonists targeting H_2R, such as cimetidine, nizatidine, ranitidine, and famotidine (Figure 15A), reduce gastric acid secretion.[90,103]

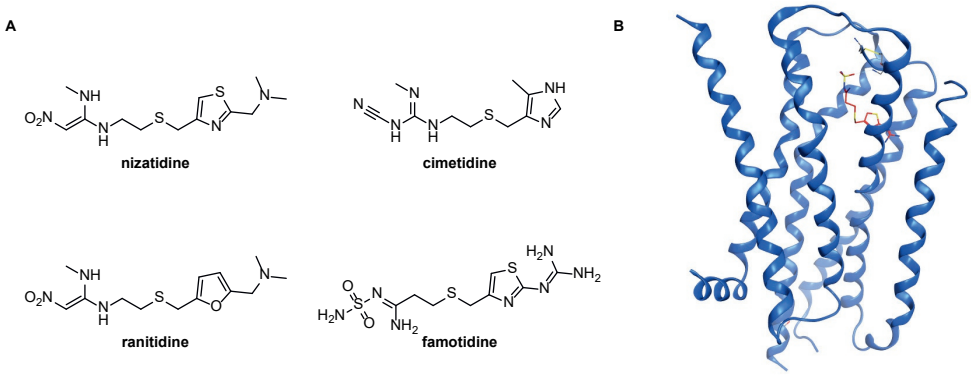

Figure 15. (A) Structures of H_2R inverse agonists nizatidine, cimetidine, ranitidine, and famotidine. (B) cryo-EM structure of H_2R in complex with famotidine (red), derived from PDB 7UL3 as deposited by Robertson *et al*.[104]

The first cryo-EM structure of H_2R was reported in 2022,[104] with the receptor bound to the inverse agonist famotidine (Figure 15B). This structure revealed some interesting differences compared to H_1R. In H_2R, the hydrophobic pocket that accommodates the diphenyl moiety in H_1R is significantly altered. Specifically, the substitution of aromatic amino acids, as well as hydrophobic and π-π stacking interactions, are present in H_1R. In addition, an inward movement of TM6 partially closes the binding site.[104] These structural rearrangements explain how H_2R accommodates different ligands, such as famotidine, compared to the pharmacophore for H_1R inverse agonists. In addition to the inactive structure, active structures of H_2R coupled to $G\alpha_s$ were recently published.[105,106]

Histamine H_3 receptor

The histamine H_3 receptor (H_3R) is mainly expressed in the central nervous system.[107] This receptor functions as an auto-receptor and thus modulates the release of histamine. Additionally, it can also function as a hetero-receptor, regulating the release of other neurotransmitters, including dopamine, acetylcholine, noradrenaline, and serotonin.[108] Upon activation, H_3R couples primarily to $G\alpha_{i/o}$ proteins. As a result, adenylyl cyclase is inhibited and cAMP production is decreased.[90,109] H_3R has been associated with a wide range of neurological and psychiatric disorders, including schizophrenia, Alzheimer's disease, Tourette's syndrome, Parkinson's, and sleep disorders such as narcolepsy.[90,110,111] Pitolisant (Figure 16A) is currently the only approved drug for this target. It is used as a treatment for patients with narcolepsy (Wakix®) and for the treatment of adults with obstructive sleep apnea (Ozawade®).[112,113]

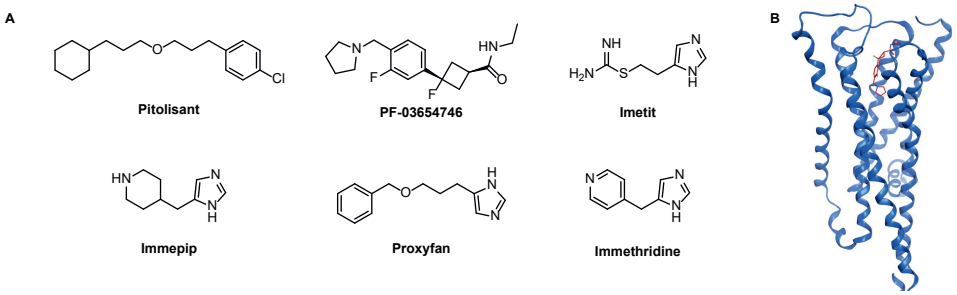

Figure 16. (A) Structures of H_3R inverse agonist pitolisant, antagonist PF-03654746, and agonists imetit, immepip, proxyfan, and immethridine. (B) crystal structure of H_3R in complex with PF-03654746 (red), derived from PDB 7F61 as deposited by Peng *et al*.[114]

Currently, the crystal structure of H_3R with antagonist PF-03654746[114] (Figure 16B) and cryo-EM structures with agonists proxyfan, immethridine, imetit, and immepip (Figure 16A) and histamine have been published.[105,106]

Histamine H_4 receptor

The histamine H_4 receptor (H_4R) represents the most recently discovered member of the histamine receptor family.[90,115–117] It is primarily expressed in bone marrow and hematopoietic cells, like mast cells, basophils, dendritic cells, and T cells.[93,116] H_4R couples mainly to $G\alpha_{i/o}$, leading to inhibition of adenylyl cyclase and reduced cAMP production.[117] This signaling stimulates chemotaxis as well as cytokine release, implicating that H_4R is involved in inflammatory responses.[90] H_4R is considered a target for several immune and inflammatory diseases, such as asthma, atopic dermatitis, pruritus, rheumatoid arthritis, and allergies.[118]

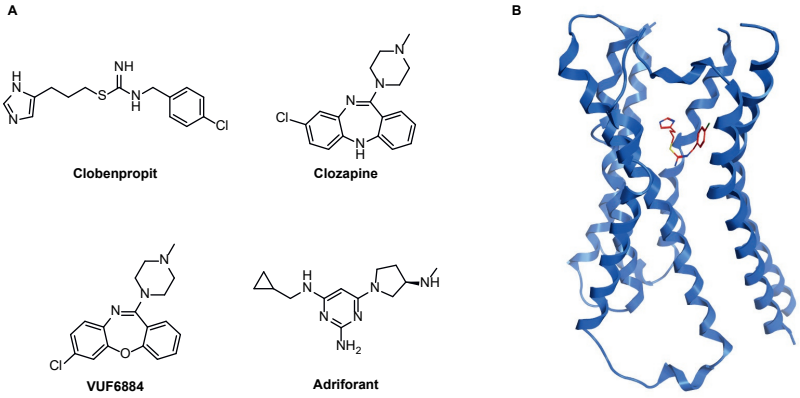

Figure 17. Structures of H_4R agonists clobenpropit, clozapine, and VUF6884 and antagonist adriforant. (B) cryo-EM structure of H_4R in complex with clobenpropit (red), derived from PDB 8JXX as deposited by Xia *et al*. [119]

Previously, only active structures of H_4R coupled to G_q were resolved with agonists histamine or imetit[120] bound, as well as H_4R coupled to G_i with agonists clobenpropit, clozapine, and VUF6884 (Figure 17) bound.[119] Recently, the inactive structure of H_4R bound to antagonist adriforant has been disclosed.[121]

GPCR Photopharmacology

For GPCRs, a significant number of photoswitchable ligands have been disclosed.[122–125] The first example of a photoswitchable ligand targeting a GPCR was Bis-Q (Figure 18A), which targets the muscarinic receptor and was disclosed in the 1980s. Upon illumination of the *trans* isomer to the *cis* isomer, a threefold decrease in affinity was observed. [126]

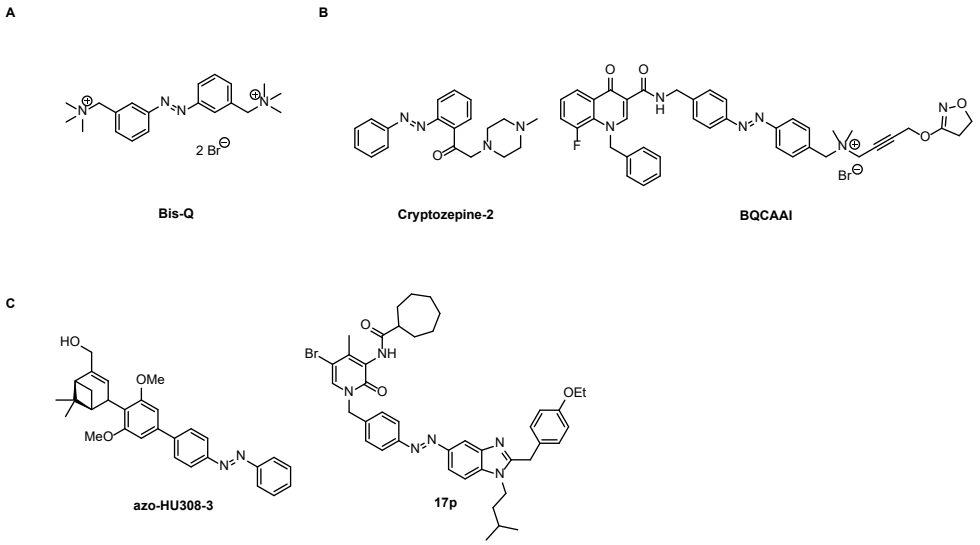

Figure 18. Structures of selected photoswitchable GPCR ligands. (A) Bis-Q, (B) examples of photoswitchable M_1R ligands,[127,128] (C) examples of photoswitchable CB_2 ligands.[129,130]

For more than 30 years, no new photoswitchable ligands for class A GPCRs were published until 2014 (opioid receptor).[125] In the past decade, an increase in GPCRs being targeted has been evident, and a detailed analysis has revealed that the muscarinic and cannabinoid receptors (M_1 and CB_2, Figure 18B,C and Figure 19A) have been studied most.[125]

Resarchers in the field use roughly similar strategies towards finding new photoswitchable ligands for GPCR photopharmacology, although details can vary. Our in-house approach is displayed in Figure 19B. First, a GPCR target is selected, after which known structure-activity relationships (SAR) and/or structure-activity functional relationships (SFR) are studied, sometimes in combination with molecular modeling. This is followed by deciding whether to use an azologization approach or an azoextension approach. In the former case, the identification of possible azosteres is required. Subsequently, a concise library is synthesized,

where photochemical properties, such as the PSS and half-life, are established. Often, pharmacological experiments are monitored in parallel. A key compound is selected based on its photochemical and pharmacological properties. For this key compound, in-depth photochemical characterization and advanced pharmacological assays are performed.

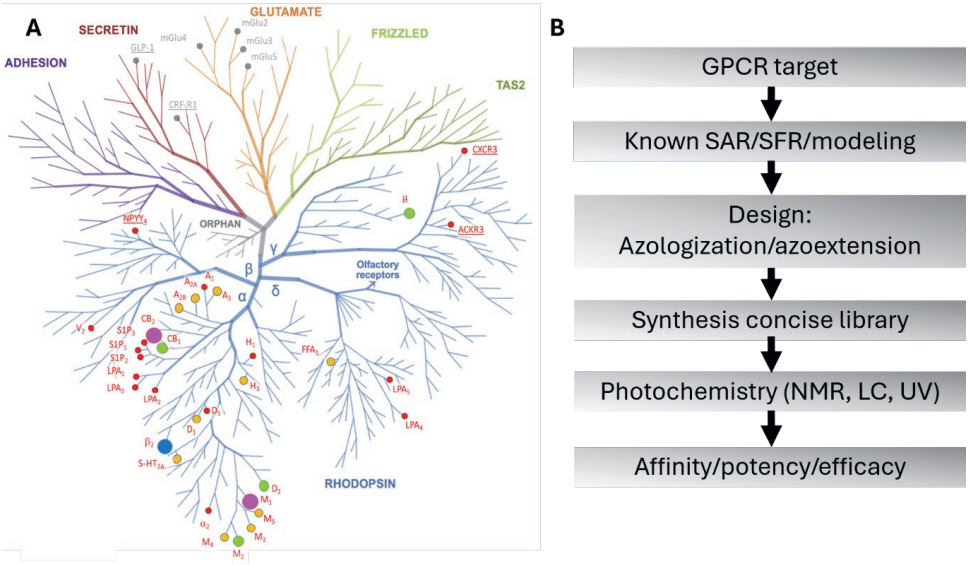

Figure 19. (A) Phylogenetic tree illustrating which GPCRs have been targeted with photoswitchable ligands. The size and color of the circles stand for the number of publications (red = 1, orange = 2, green = 3, blue = 4, magenta = 6). Adapted and updated from Wijtmans *et al*.[125] (B) A workflow for designing new photoswitchable GPCR ligands.

Photoswitchable ligands targeting GPCRs can be broadly classified into different generations. First-generation series typically consist of photoswitchable antagonists or agonists, in which light exposure modulates the affinity and potency of the ligand. Representative examples include photoswitchable H_3R antagonists VUF14862 and VUF14738, and agonist VUF15000 (Figure 20).[131] Antagonist VUF14862 exhibits high affinity in the *trans* state (pK_i *trans* = 8.7). Upon illumination with UV light, an 11-fold decrease in H_3R affinity was observed (pK_i PSS_{cis} = 7.7), and this ligand displayed a long half-life of 29 days. In contrast, antagonist VUF14738 displayed low affinity in the *trans* state (pK_i *trans* = 6.2) and exhibited a 13-fold increase in H_3R affinity upon illumination with UV light (pK_i PSS_{cis} = 7.3). This ligand also showed a long thermal half-life of 122 days. On the other hand, agonist VUF15000 showed high affinity in the *trans* state (pK_i *trans* = 8.4) and an 8.5-fold decrease in affinity upon illumination with UV light (pK_i PSS_{cis} = 7.5). Additionally, a 20-fold decrease in potency (pEC_{50} *trans* = 7.6 & pEC_{50} PSS_{cis} = 6.3) was observed upon illumination.

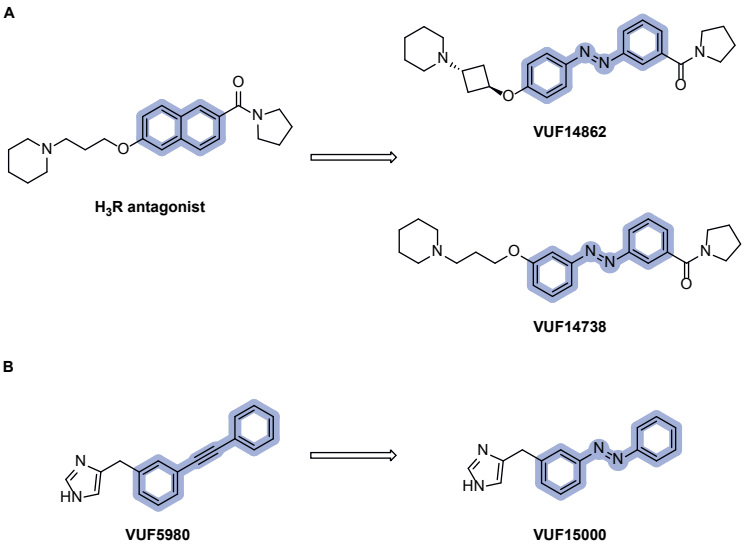

Figure 20. Photoswitchable ligands targeting H_3R and their parent molecules. (A) Parent ligand by Roche[132] and photoswitchable antagonists VUF14862 and VUF14738. (B) Parent ligand VUF5890 and agonist VUF15000.[131,133]

In recent years, the field has moved toward expanding and refining the GPCR photopharmacology toolbox. Second-generation series can enable a change in ligand efficacy upon illumination, thus establishing a photoswitch from, e.g., antagonism to agonism (Figure 21A).[134] Research on next-generation photoswitchable ligands has also addressed allosteric ligands. The ligands have the potential to optically control the activity of endogenous ligands (Figure 21B).[135]

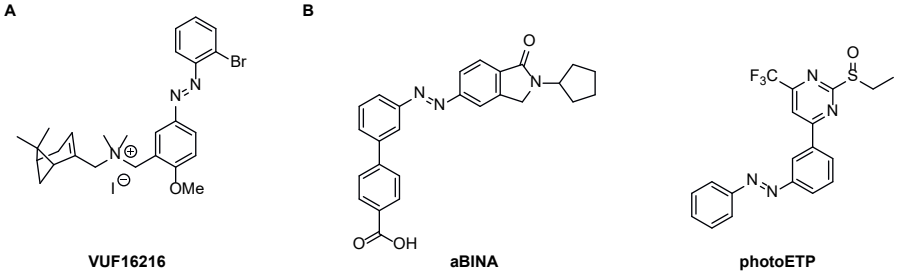

Figure 21. Structure of photoswitchable ligands. (A) Efficacy photoswitch VUF16216. (B) Allosteric photoswitchable ligands aBINA[136] and photoETP.[137]

Future generations of GPCR photoswitchable ligands await several challenges. One challenge is the design of photoswitchable ligands that can induce GPCR signaling bias. GPCRs are known to signal through both G proteins and/or β-arrestins, and ligands that preferentially

modulate one signaling pathway over the other can produce profoundly different physiological outcomes.[138] The integration with photopharmacology offers unique opportunities to investigate GPCR signalling. To date, four biased, photoswitchable GPCR ligands have been reported (Figure 22).[139–142] While these biased photoswitchable ligands can preferentially modulate either G-protein or β-arrestin pathways, ligands capable of reversibly switching between these two signaling pathways have not yet been achieved.

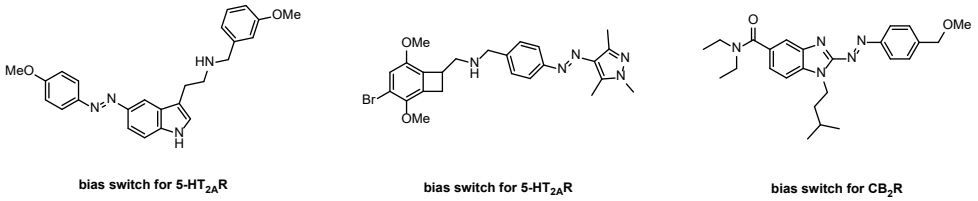

Figure 22. Examples of small molecule biased photoswitchable ligands.

Other challenges the (GPCR) photopharmacology field currently faces include drawbacks associated with azobenzenes. In 2021, over 80% of the reported photoswitchable ligands in class A GPCR photopharmacology contained an azobenzene moiety.[125] However, incorporating azobenzenes in bioactive ligands poses several limitations. Their hydrophobic character often leads to poor aqueous solubility.[12,143] Additionally, the use of UV light is required to switch the thermodynamically stable *trans* isomer to the metastable *cis* isomer. The use of UV light can cause problems in biological settings due to its low tissue penetration. Isomerization of the *cis* isomer to the *trans* isomer involves illumination with blue light (400-450 nm). However, the n-π* bands of the two isomers overlap in this range, which limits the photostationary state (PSS) values.[34] To overcome these issues, recent efforts have focused on enabling bidirectional switching with visible light.[37,38] As described (paragraph *types of switches*), tetra-*ortho*-substituted azobenzenes are known for their ability to switch using visible light.[38] However, bulky *ortho* substituents (e.g., chlorine) may cause problems with protein binding compared to unsubstituted analogues due to sterics. Recently, an increase in the use of heteroarylazo switches has been evident, given their excellent switching properties.[12,39,40,58,144] However, systematic comparisons of their properties are lacking, making the design more challenging. Further studies on other heteroaromatics are needed to refine the photoswitch toolbox.

The rational design of (GPCR) photoswitchable ligands remains particularly challenging. Although computational modeling is being increasingly used, it is often used retrospectively to explain observed differences, with relatively few cases using prospective prediction. As a result, the design process is still often driven by trial-and-error. This challenge is likely to become more significant in the future with the development of diverse new photoswitch classes, including various red-shifted photoswitches. An increase in the choice of potential photoswitches and associated substitution patterns will present substantial design challenges.

Lastly, most ligand development has focused on optimizing photoswitching efficiency (e.g., PSS) and affinity. However, the photoswitching behavior of photoswitchable ligands within a protein binding pocket is poorly understood, i.e., whether the isomerization event occurs before and/or after binding. How the protein environment influences this process can have a profound impact on the binding kinetics and functional selectivity of the *trans* and *cis* isomers. A deeper understanding of these processes will be essential for refining the rational design of photoswitchable ligands.

Aim and outline

The aim of this PhD thesis is to address current challenges in the field of GPCR photopharmacology by exploring emerging photoswitch moieties and concepts. Primarily, the histamine H_3 receptor was used as a prototypical class A GPCR to probe the various concepts. Instead of using the typical workflow to find new photoswitchable ligands for GPCRs (Figure 19B), previously reported photoswitchable H_3R antagonists[133] and agonists[131] were used as a basis for the development of new-generation photoswitchable ligands that served to explore emerging moieties, concepts and questions in the field. Additionally, efforts were made to develop a photoswitchable ligand for the human H_1R, as such ligands have remained elusive.

In **Chapter 2**, the azobenzene photoswitch of a known H_3R photoswitchable antagonist was replaced with an arylazopyrazole moiety to improve its physicochemical, photochemical, and pharmacological properties. Incorporation of a tritium radiolabel in the key compound allowed investigation of light-dependent ligand-protein binding kinetics in real time, which provides evidence that the compound is switching in the protein binding pocket.

In **Chapter 3**, a 'photoswitch hop' was performed by installing known and less known heteroarylazo switches. The physicochemical, photochemical, and pharmacological properties of 12 heteroarylazo photoswitchable ligands were systematically compared to their azobenzene counterpart. These results can help in providing design blueprints for the field.

In **Chapter 4**, the design of photoswitchable ligands for the human H_1R is described. An 'azoscan' on the antihistamine desloratadine was performed. Functionalization of the aromatic positions of the desloratadine scaffold and installation of azobenzenes on the piperidine ring gave a total of 9 photoswitchable ligands.

In **Chapter 5**, positional arylazopyrazole isomers as photoswitchable H_3R agonists were explored. Building on azobenzene-based agonists, analogues containing arylazopyrazoles at peripheral, but also central positions were designed and synthesized with the aim to investigate the influence of photoswitch placement, while simultaneously improving the photochemical and pharmacological properties.

In **Chapter 6**, a summary and discussion of the data reported in this thesis will be given, as well as future perspectives.

References

(1) Hashim, P. K.; Shaji, A. T.; Amrutha, A. S.; Ahmad, S. Conceptual Expansion of Photomedicine for Spatiotemporal Treatment Methods. *RSC Med Chem* **2025**, *16* (6), 2360–2372. https://doi.org/10.1039/d4md01005a.

(2) Velema, W. A.; Szymanski, W.; Feringa, B. L. Photopharmacology: Beyond Proof of Principle. *J Am Chem Soc* **2014**, *136* (6), 2178–2191. https://doi.org/10.1021/ja413063e.

(3) Correia, J. H.; Rodrigues, J. A.; Pimenta, S.; Dong, T.; Yang, Z. Photodynamic Therapy Review: Principles, Photosensitizers, Applications, and Future Directions. *Pharmaceutics 2021, Vol. 13, Page 1332* **2021**, *13* (9), 1332. https://doi.org/10.3390/pharmaceutics13091332.

(4) Chilakamarthi, U.; Giribabu, L. Photodynamic Therapy: Past, Present and Future. *Chemical Record* **2017**, *17* (8), 775–802. https://doi.org/10.1002/tcr.201600121.

(5) Lerch, M. M.; Hansen, M. J.; van Dam, G. M.; Szymanski, W.; Feringa, B. L. Emerging Targets in Photopharmacology. *Angew Chem Int Ed Engl* **2016**, *55* (37), 10978–10999. https://doi.org/10.1002/anie.201601931.

(6) Deisseroth, K. Optogenetics. *Nat Methods* **2011**, *8* (1), 26–29. https://doi.org/10.1038/nmeth.f.324.

(7) Emiliani, V.; Entcheva, E.; Hedrich, R.; Hegemann, P.; Konrad, K. R.; Lüscher, C.; Mahn, M.; Pan, Z. H.; Sims, R. R.; Vierock, J.; Yizhar, O. Optogenetics for Light Control of Biological Systems. *Nature reviews. Methods primers* **2022**, *2* (1), 55. https://doi.org/10.1038/S43586-022-00136-4.

(8) Williams, S. C. P.; Deisseroth, K. Optogenetics. *Proc Natl Acad Sci U S A* **2013**, *110* (41), 16287. https://doi.org/10.1073/pnas.1317033110.

(9) Kandori, H. Biophysics of Rhodopsins and Optogenetics. *Biophys Rev* **2020**, *12* (2), 355–361. https://doi.org/10.1007/s12551-020-00645-0.

(10) Josa-Culleré, L.; Llebaria, A. In the Search for Photocages Cleavable with Visible Light: An Overview of Recent Advances and Chemical Strategies. *ChemPhotoChem* **2021**, *5* (4), 298–316. https://doi.org/10.1002/cptc.202000253.

(11) Broichhagen, J.; Frank, J. A.; Trauner, D. A Roadmap to Success in Photopharmacology. *Acc Chem Res* **2015**, *48* (7), 1947–1960. https://doi.org/10.1021/acs.accounts.5b00129.

(12) Fuchter, M. J. On the Promise of Photopharmacology Using Photoswitches: A Medicinal Chemist's Perspective. *J Med Chem* **2020**, *63* (20), 11436–11447. https://doi.org/10.1021/acs.jmedchem.0c00629.

(13) Hüll, K.; Morstein, J.; Trauner, D. In Vivo Photopharmacology. *Chem Rev* **2018**, *118* (21), 10710–10747. https://doi.org/10.1021/acs.chemrev.8b00037.

(14) Klán, P.; Šolomek, T.; Bochet, C. G.; Blanc, A.; Givens, R.; Rubina, M.; Popik, V.; Kostikov, A.; Wirz, J. Photoremovable Protecting Groups in Chemistry and Biology: Reaction Mechanisms and Efficacy. *Chem Rev* **2013**, *113* (1), 119–191. https://doi.org/10.1021/cr300177k.

(15) Hoorens, M. W. H.; Szymanski, W. Reversible, Spatial and Temporal Control over Protein Activity Using Light. *Trends Biochem Sci* **2018**, *43* (8), 567–575. https://doi.org/10.1016/j.tibs.2018.05.004.

(16) Mukherjee, A.; Seyfried, M. D.; Ravoo, B. J. Azoheteroarene and Diazocine Molecular Photoswitches: Self-Assembly, Responsive Materials and Photopharmacology. *Angew. Chem. Int. Ed.* **2023**, *62* (42), e202304437. https://doi.org/10.1002/anie.202304437.
(17) Olesińska-Mönch, M.; Deo, C. Small-Molecule Photoswitches for Fluorescence Bioimaging: Engineering and Applications. *Chemical Communications* **2023**, *59* (6), 660–669. https://doi.org/10.1039/d2cc05870g.
(18) Jerca, F. A.; Jerca, V. V.; Hoogenboom, R. Advances and Opportunities in the Exciting World of Azobenzenes. *Nature Reviews Chemistry 2021 6:1* **2021**, *6* (1), 51–69. https://doi.org/10.1038/s41570-021-00334-w.
(19) Thaggard, G. C.; Haimerl, J.; Park, K. C.; Lim, J.; Fischer, R. A.; Maldeni Kankanamalage, B. K. P.; Yarbrough, B. J.; Wilson, G. R.; Shustova, N. B. Metal-Photoswitch Friendship: From Photochromic Complexes to Functional Materials. *J Am Chem Soc* **2022**, *144* (51), 23249–23263. https://doi.org/10.1021/jacs.2C09879.
(20) Brown, C. J. A Refinement of the Crystal Structure of Azobenzene. *urn:issn:0365-110X* **1966**, *21* (1), 146–152. https://doi.org/10.1107/s0365110x66002445.
(21) Mostad, A.; Rømming, Chr.; Rømming, Chr.; Hammarström, S.; Lousberg, R. J. J. C.; Weiss, U. A Refinement of the Crystal Structure of Cis-Azobenzene. *Acta Chem Scand* **1971**, *25*, 3561–3568. https://doi.org/10.3891/acta.chem.scand.25-3561.
(22) Braslavsky, S. E. Glossary of Terms Used in Photochemistry 3rd Edition: (IUPAC Recommendations 2006). *Pure and Applied Chemistry* **2007**, *79* (3), 293–465. https://doi.org/10.1351/pac200779030293.
(23) Bandara, H. M. D.; Burdette, S. C. Photoisomerization in Different Classes of Azobenzene. *Chem Soc Rev* **2012**, *41* (5), 1809–1825. https://doi.org/10.1039/c1cs15179g.
(24) Forber, C. L.; Kelusky, E. C.; Bunce, N. J.; Zerner, M. C. Electronic Spectra of Cis-and Trans-Azobenzenes: Consequences of Ortho Substitution. *J Am Chem Soc* **1985**, *107* (21), 5884–5890. https://doi.org/10.1021/ja00307a009.
(25) Wijtmans, M.; Josimovic, I.; Vischer, H. F.; Leurs, R. Optical Control of Class A G Protein-Coupled Receptors with Photoswitchable Ligands. *Curr Opin Pharmacol* **2022**, *63*, 102192. https://doi.org/10.1016/j.coph.2022.102192.
(26) Irie, M.; Fukaminato, T.; Matsuda, K.; Kobatake, S. Photochromism of Diarylethene Molecules and Crystals: Memories, Switches, and Actuators. *Chem Rev* **2014**, *114* (24), 12174–12277. https://doi.org/10.1021/cr500249p.
(27) Lerch, M. M.; Szymański, W.; Feringa, B. L. The (Photo)Chemistry of Stenhouse Photoswitches: Guiding Principles and System Design. *Chem Soc Rev* **2018**, *47* (6), 1910–1937. https://doi.org/10.1039/c7cs00772h.
(28) Kortekaas, L.; Browne, W. R. The Evolution of Spiropyran: Fundamentals and Progress of an Extraordinarily Versatile Photochrome. *Chem Soc Rev* **2019**, *48* (12), 3406–3424. https://doi.org/10.1039/c9cs00203k.
(29) Van Dijken, D. J.; Kovaříček, P.; Ihrig, S. P.; Hecht, S. Acylhydrazones as Widely Tunable Photoswitches. *J Am Chem Soc* **2015**, *137* (47), 14982–14991. https://doi.org/10.1021/jacs.5b09519.
(30) Yang, Y.; Hughes, R. P.; Aprahamian, I. Visible Light Switching of a BF 2-Coordinated Azo Compound. *J Am Chem Soc* **2012**, *134* (37), 15221–15224. https://doi.org/10.1021/ja306030d.
(31) Waldeck, D. H. Photoisomerization Dynamics of Stilbenes. *Chem Rev* **1991**, *91* (3), 415–436. https://doi.org/10.1021/cr00003a007.

(32) Wiedbrauk, S.; Dube, H. Hemithioindigo—an Emerging Photoswitch. *Tetrahedron Lett* **2015**, *56* (29), 4266–4274. https://doi.org/10.1016/j.tetlet.2015.05.022.
(33) Lentes, P.; Stadler, E.; Röhricht, F.; Brahms, A.; Gröbner, J.; Sönnichsen, F. D.; Gescheidt, G.; Herges, R. Nitrogen Bridged Diazocines: Photochromes Switching within the Near-Infrared Region with High Quantum Yields in Organic Solvents and in Water. *J Am Chem Soc* **2019**, *141* (34), 13592–13600. https://doi.org/10.1021/jacs.9b06104.
(34) Tavassoli, A.; Hamilton, A. D.; Spring, D. R.; Beharry, A. A.; Woolley, G. A. Azobenzene Photoswitches for Biomolecules. *Chem Soc Rev* **2011**, *40* (8), 4422–4437. https://doi.org/10.1039/c1cs15023e.
(35) Clement, M.; Daniel, G.; Trelles, M. Optimising the Design of a Broad-Band Light Source for the Treatment of Skin. *Journal of Cosmetic and Laser Therapy* **2005**, *7* (3–4), 177–189. https://doi.org/10.1080/14764170500344575.
(36) Weissleder, R. A Clearer Vision for in Vivo Imaging. *Nature Biotechnology 2001 19:4* **2001**, *19* (4), 316–317. https://doi.org/10.1038/86684.
(37) Dong, M.; Babalhavaeji, A.; Samanta, S.; Beharry, A. A.; Woolley, G. A. Red-Shifting Azobenzene Photoswitches for in Vivo Use. *Acc Chem Res* **2015**, *48* (10), 2662–2670. https://doi.org/10.1021/acs.accounts.5b00270.
(38) Cardano, F.; Márquez García, R.; Szymanski, W. Manipulation of Chemistry and Biology with Visible Light Using Tetra-ortho-Substituted Azobenzenes and Azonium Ions. *Angewandte Chemie International Edition* **2025**. https://doi.org/10.1002/anie.202423506.
(39) Dang, T.; Zhang, Z. Y.; Li, T. Visible-Light-Activated Heteroaryl Azoswitches: Toward a More Colorful Future. *J Am Chem Soc* **2024**, *146* (29), 19609–19620. https://doi.org/10.1021/jacs.4c03135.
(40) Weston, C. E.; Richardson, R. D.; Haycock, P. R.; White, A. J. P.; Fuchter, M. J. Arylazopyrazoles: Azoheteroarene Photoswitches Offering Quantitative Isomerization and Long Thermal Half-Lives. *J Am Chem Soc* **2014**, *136* (34), 11878–11881. https://doi.org/10.1021/ja505444d.
(41) Heindl, A. H.; Wegner, H. A. Rational Design of Azothiophenes—Substitution Effects on the Switching Properties. *Chemistry – A European Journal* **2020**, *26* (60), 13730–13737. https://doi.org/10.1002/chem.202001148.
(42) Lin, R.; Hashim, P. K.; Sahu, S.; Amrutha, A. S.; Cheruthu, N. M.; Thazhathethil, S.; Takahashi, K.; Nakamura, T.; Kikukawa, T.; Tamaoki, N. Phenylazothiazoles as Visible-Light Photoswitches. *J Am Chem Soc* **2023**, *145* (16), 9072–9080. https://doi.org/10.1021/jacs.3c00609.
(43) Dolai, A.; Box, S. M.; Bhunia, S.; Bera, S.; Das, A.; Samanta, S. Photoisomerization of 2-Arylazoimidazoles under Visible Light: Identifying a Predictive Tool to Anticipate and Tune Likely Photoswitching Performance and Cis Half-Life. *J Org Chem* **2023**. https://doi.org/10.1021/acs.joc.3c00211.
(44) Simeth, N. A.; Crespi, S.; Fagnoni, M.; König, B. Tuning the Thermal Isomerization of Phenylazoindole Photoswitches from Days to Nanoseconds. *J Am Chem Soc* **2018**, *140* (8), 2940–2946. https://doi.org/10.1021/jacs.7b12871.
(45) Steinmüller, S. A. M.; Odaybat, M.; Galli, G.; Prischich, D.; Fuchter, M. J.; Decker, M. Arylazobenzimidazoles: Versatile Visible-Light Photoswitches with Tuneable Z-Isomer Stability. *Chem Sci* **2024**, *15* (14), 5360–5367. https://doi.org/10.1039/d3sc05246j.

(46) Bléger, D.; Schwarz, J.; Brouwer, A. M.; Hecht, S. O -Fluoroazobenzenes as Readily Synthesized Photoswitches Offering Nearly Quantitative Two-Way Isomerization with Visible Light. *J Am Chem Soc* **2012**, *134* (51), 20597–20600. https://doi.org/10.1021/ja310323y.

(47) Lameijer, L. N.; Budzak, S.; Simeth, N. A.; Hansen, M. J.; Feringa, B. L.; Jacquemin, D.; Szymanski, W. General Principles for the Design of Visible-Light-Responsive Photoswitches: Tetra-Ortho-Chloro-Azobenzenes. *Angewandte Chemie - International Edition* **2020**, *59* (48), 21663–21670. https://doi.org/10.1002/anie.202008700.

(48) Crespi, S.; Simeth, N. A.; König, B. Heteroaryl Azo Dyes as Molecular Photoswitches. *Nature Reviews Chemistry*. Nature Publishing Group March 1, 2019, pp 133–146. https://doi.org/10.1038/s41570-019-0074-6.

(49) Matsuo, K.; Ogawa, H.; Yamaoka, S.; Waku, T.; Kobori, A. A Chemical Platform for the Efficient Screening of Arylazopyrazole-Based Photoswitchable CENP-E Inhibitors Using Mild Cyclization Reactions. *Bioorg Med Chem Lett* **2024**, *111*, 129892. https://doi.org/10.1016/j.mbcl.2024.129892.

(50) Wirth, U.; Raabe, K.; Kalaba, P.; Keimpema, E.; Muttenthaler, M.; König, B. Photoswitchable Probes of Oxytocin and Vasopressin. *J Med Chem* **2023**, *66* (21), 14853–14865. https://doi.org/10.1021/acs.jmedchem.3c01415.

(51) Kolarski, D.; Miró-Vinyals, C.; Sugiyama, A.; Srivastava, A.; Ono, D.; Nagai, Y.; Iida, M.; Itami, K.; Tama, F.; Szymanski, W.; Hirota, T.; Feringa, B. L. Reversible Modulation of Circadian Time with Chronophotopharmacology. *Nature Communications 2021 12:1* **2021**, *12* (1), 1–12. https://doi.org/10.1038/s41467-021-23301-x.

(52) Sink, A.; Gerwe, H.; Hübner, H.; Boivin-Jahns, V.; Fender, J.; Lorenz, K.; Gmeiner, P.; Decker, M. "Photo-Adrenalines": Photoswitchable B2-Adrenergic Receptor Agonists as Molecular Probes for the Study of Spatiotemporal Adrenergic Signaling. *Chemistry – A European Journal* **2024**, *30* (11), e202303506. https://doi.org/10.1002/chem.202303506.

(53) Wirth, U.; Erl, J.; Azzam, S.; Höring, C.; Skiba, M.; Singh, R.; Hochmuth, K.; Keller, M.; Wegener, J.; König, B. Monitoring the Reversibility of GPCR Signaling by Combining Photochromic Ligands with Label-Free Impedance Analysis. *Angewandte Chemie* **2023**, *135* (21), e202215547. https://doi.org/10.1002/ange.202215547.

(54) Aguirre, T.; Teichmann, E.; Römpp, F. Q.; Vivier, R.; Bryant, C.; Hulverson, M. A.; Van Voorhis, W. C.; Ojo, K. K.; Doggett, J. S.; Fiedler, D.; Hecht, S. Photoswitchable Inhibitors to Optically Control Specific Kinase Activity. *ACS Chem Biol* **2023**, *18* (6), 1378–1387. https://doi.org/10.1021/acschembio.3c00119.

(55) Sarkar, H. S.; Mashita, T.; Kowada, T.; Hamaguchi, S.; Sato, T.; Kasahara, K.; Matubayasi, N.; Matsui, T.; Mizukami, S. Arylazopyrazole-Based Photoswitchable Inhibitors Selective for Escherichia Coli Dihydrofolate Reductase. *ACS Chem Biol* **2023**, *18* (2), 340–346. https://doi.org/10.1021/acschembio.2c00749.

(56) Schulte, A. M.; Kolarski, D.; Sundaram, V.; Srivastava, A.; Tama, F.; Feringa, B. L.; Szymanski, W. Light-Control over Casein Kinase 1δ Activity with Photopharmacology: A Clear Case for Arylazopyrazole-Based Inhibitors. *Int J Mol Sci* **2022**, *23* (10), 5326. https://doi.org/10.3390/ijms23105326.

(57) Lahmy, R.; Hübner, H.; Lachmann, D.; Gmeiner, P.; König, B. Development of Photoswitchable Tethered Ligands That Target the μ-Opioid Receptor. *ChemMedChem* **2023**, *18* (23), e202300228. https://doi.org/10.1002/cmdc.202300228.

(58) Calbo, J.; Weston, C. E.; White, A. J. P.; Rzepa, H. S.; Contreras-García, J.; Fuchter, M. J. Tuning Azoheteroarene Photoswitch Performance through Heteroaryl Design. *J Am Chem Soc* **2017**, *139* (3), 1261–1274. https://doi.org/10.1021/jacs.6b11626.
(59) Merino, E. Synthesis of Azobenzenes : The Coloured Pieces of Molecular Materials. *Chem Soc Rev* **2011**, *40* (7), 3835–3853. https://doi.org/10.1039/c0cs00183j.
(60) Gutsmiedl, K.; Wirges, C. T.; Ehmke, V.; Carell, T. Copper-Free "click" Modification of Dna via Nitrile Oxide-Norbornene 1,3-Dipolar Cycloaddition. *Org Lett* **2009**, *11* (11), 2405–2408. https://doi.org/10.1021/ol9005322.
(61) Scheiner, M.; Sink, A.; Hoffmann, M.; Vrigneau, C.; Endres, E.; Carles, A.; Sotriffer, C.; Maurice, T.; Decker, M. Photoswitchable Pseudoirreversible Butyrylcholinesterase Inhibitors Allow Optical Control of Inhibition in Vitro and Enable Restoration of Cognition in an Alzheimer's Disease Mouse Model upon Irradiation. *J Am Chem Soc* **2022**, *144* (7), 3279–3284. https://doi.org/10.1021/jacs.1c13492.
(62) Hansen, M. J.; Lerch, M. M.; Szymanski, W.; Feringa, B. L.; Hansen,] M J; Lerch, M. M.; Szymanski, W.; Eringa, B. L. F. Direct and Versatile Synthesis of Red-Shifted Azobenzenes. *Angewandte Chemie International Edition* **2016**, *55* (43), 13514–13518. https://doi.org/10.1002/anie.201607529.
(63) Barbero, M.; Degani, I.; Dughera, S.; Fochi, R.; Perracino, P. Preparation of Diazenes by Electrophilic C-Coupling Reactions of Dry Arenediazonium o-Benzenedisulfonimides with Grignard Reagents. *Synthesis (Stuttg)* **1998**, *1998* (09), 1235–1237. https://doi.org/10.1055/s-1998-6102.
(64) Curtin, D. Y.; Tveten, J. L. Reaction of Diarylzinc Reagents with Aryldiazonium Salts. Direct Formation of Cis-Azo Compounds. *Journal of Organic Chemistry* **1961**, *26* (6), 1764–1768. https://doi.org/10.1021/JO01065A017/ASSET/JO01065A017.FP.PNG_V03.
(65) Curtin, D. Y.; Arnheim Ursprung, J. Reaction of Organometallic Compounds with Diazonium Salts. Synthesis of Arylazoalkanes. *Journal of Organic Chemistry* **1956**, *21* (11), 1221–1225. https://doi.org/10.1021/jo01117a005.
(66) Sahu, S.; Tamaoki, N. A Versatile One-Pot Strategy for Thiazolylazo Extensions: Visible Light-Driven Photoswitches. *J Am Chem Soc* **2025**. https://doi.org/10.1021/jacs.5c08259.
(67) Kobauri, P.; Dekker, F. J.; Szymanski, W.; Feringa, B. L. Rational Design in Photopharmacology with Molecular Photoswitches. *Angew. Chem. Int. Ed.* **2023**, *62* (30), e202300681. https://doi.org/10.1002/anie.202300681.
(68) Maleeva, G.; Nin-Hill, A.; Wirth, U.; Rustler, K.; Ranucci, M.; Opar, E.; Rovira, C.; Bregestovski, P.; Zeilhofer, H. U.; König, B.; Alfonso-Prieto, M.; Gorostiza, P. Light-Activated Agonist-Potentiator of GABAA Receptors for Reversible Neuroinhibition in Wildtype Mice. *J Am Chem Soc* **2024**, *146* (42), 28822–28831. https://doi.org/10.1021/jacs.4c08446.
(69) Panarello, S.; González-Díez, A.; Berizzi, A. E.; Malhaire, F.; Borràs-Tudurí, R.; Rovira, X.; Serra, C.; Prézeau, L.; Pin, J. P.; Goudet, C.; Llebaria, A.; Gómez-Santacana, X. Photoswitchable Positive Allosteric Modulators of Metabotropic Glutamate Receptor 4 to Improve Selectivity. *iScience* **2024**, *27* (6), 110123. https://doi.org/10.1016/j.isci.2024.110123.
(70) Bérenger, S.; Adamska, J. M.; Deflorian, F.; de Graaf, C.; Palmer, C. B.; Szpakowska, M.; Chevigné, A.; de Esch, I. J. P.; Zarzycka, B.; Vischer, H. F.; Wijtmans, M.; Leurs, R. Design, Synthesis and Pharmacological Characterization of the First Photoswitchable

Small-Molecule Agonist for the Atypical Chemokine Receptor 3. *ACS Omega* **2025**, *10* (8), 8675–8686. https://doi.org/10.1021/acsomega.4c11583.

(71) Cunha, M. R.; Bhardwaj, R.; Lindinger, S.; Butorac, C.; Romanin, C.; Hediger, M. A.; Reymond, J. L. Photoswitchable Inhibitor of the Calcium Channel TRPV6. *ACS Med Chem Lett* **2019**, *10* (9), 1341–1345. https://doi.org/10.1021/acsmedchemlett.9b00298.

(72) Simon, I. A.; Homan, E. J.; Wijtmans, M.; Sundström, M.; Leurs, R.; De Esch, I. J. P.; Zarzycka, B. A. PSW-Designer: An Open-Source Computational Platform for the Design and Virtual Screening of Photopharmacological Ligands. *J Chem Inf Model* **2023**, *63* (21), 6696–6705. https://doi.org/10.1021/acs.jcim.3c01050.

(73) *Study Details | NCT06628947 | A Phase II Study of Intravitreal KIO-301 in Patients With Late-stage Retinitis Pigmentosa | ClinicalTrials.gov*. https://clinicaltrials.gov/study/NCT06628947?spons=Kiora%20Pharmaceuticals,%20Inc.&rank=1 (accessed 2025-09-02).

(74) Hartong, D. T.; Berson, E. L.; Dryja, T. P. Retinitis Pigmentosa. *Lancet* **2006**, *368* (9549), 1795–1809. https://doi.org/10.1016/s0140-6736(06)69740-7.

(75) Tochitsky, I.; Trautman, J.; Gallerani, N.; Malis, J. G.; Kramer, R. H. Restoring Visual Function to the Blind Retina with a Potent, Safe and Long-Lasting Photoswitch. *Scientific Reports 2017 7:1* **2017**, *7* (1), 1–8. https://doi.org/10.1038/srep45487.

(76) Tochitsky, I.; Polosukhina, A.; Degtyar, V. E.; Gallerani, N.; Smith, C. M.; Friedman, A.; Van Gelder, R. N.; Trauner, D.; Kaufer, D.; Kramer, R. H. Restoring Visual Function to Blind Mice with a Photoswitch That Exploits Electrophysiological Remodeling of Retinal Ganglion Cells. *Neuron* **2014**, *81* (4), 800–813. https://doi.org/10.1016/j.neuron.2014.01.003.

(77) *KIO-301 | Inherited Retinal Disease - Kiora Pharmaceuticals*. https://kiorapharma.com/pipeline-science/kio-301/ (accessed 2025-09-02).

(78) Rosenbaum, D. M.; Rasmussen, S. G. F.; Kobilka, B. K. The Structure and Function of G-Protein-Coupled Receptors. *Nature* **2009**, *459* (7245), 356–363. https://doi.org/10.1038/nature08144.

(79) Lorente, J. S.; Sokolov, A. V; Ferguson, G.; Schiöth, H. B.; Hauser, A. S.; Gloriam, D. E. GPCR Drug Discovery: New Agents, Targets and Indications. *Nat Rev Drug Discov* **2025**, ASAP. https://doi.org/10.1038/s41573-025-01139-y.

(80) Fredriksson, R.; Lagerström, M. C.; Lundin, L. G.; Schiöth, H. B. The G-Protein-Coupled Receptors in the Human Genome Form Five Main Families. Phylogenetic Analysis, Paralogon Groups, and Fingerprints. *Mol Pharmacol* **2003**, *63* (6), 1256–1272. https://doi.org/10.1124/mol.63.6.1256.

(81) Zhang, M.; Chen, T.; Lu, X.; Lan, X.; Chen, Z.; Lu, S. G Protein-Coupled Receptors (GPCRs): Advances in Structures, Mechanisms and Drug Discovery. *Signal Transduction and Targeted Therapy 2024 9:1* **2024**, *9* (1), 1–43. https://doi.org/10.1038/s41392-024-01803-6.

(82) Congreve, M.; de Graaf, C.; Swain, N. A.; Tate, C. G. Impact of GPCR Structures on Drug Discovery. *Cell* **2020**, *181* (1), 81–91. https://doi.org/10.1016/j.cell.2020.03.003.

(83) Yang, D.; Zhou, Q.; Labroska, V.; Qin, S.; Darbalaei, S.; Wu, Y.; Yuliantie, E.; Xie, L.; Tao, H.; Cheng, J.; Liu, Q.; Zhao, S.; Shui, W.; Jiang, Y.; Wang, M. W. G Protein-Coupled Receptors: Structure- and Function-Based Drug Discovery. *Signal Transduction and Targeted Therapy 2020 6:1* **2021**, *6* (1), 1–27. https://doi.org/10.1038/s41392-020-00435-w.

(84) Syrovatkina, V.; Alegre, K. O.; Dey, R.; Huang, X. Y. Regulation, Signaling, and Physiological Functions of G-Proteins. *J Mol Biol* **2016**, *428* (19), 3850–3868. https://doi.org/10.1016/j.jmb.2016.08.002.
(85) Smith, J. S.; Lefkowitz, R. J.; Rajagopal, S. Biased Signalling: From Simple Switches to Allosteric Microprocessors. *Nat Rev Drug Discov* **2018**, *17* (4), 243–260. https://doi.org/10.1038/nrd.2017.229.
(86) Wootten, D.; Christopoulos, A.; Marti-Solano, M.; Babu, M. M.; Sexton, P. M. Mechanisms of Signalling and Biased Agonism in G Protein-Coupled Receptors. *Nat Rev Mol Cell Biol* **2018**, *19* (10), 638–653. https://doi.org/10.1038/s41580-018-0049-3.
(87) Michel, M. C.; Charlton, S. J. Biased Agonism in Drug Discovery—Is It Too Soon to Choose a Path? *Mol Pharmacol* **2018**, *93* (4), 259–265. https://doi.org/10.1124/mol.117.110890.
(88) Jeffrey Conn, P.; Christopoulos, A.; Lindsley, C. W. Allosteric Modulators of GPCRs: A Novel Approach for the Treatment of CNS Disorders. *Nat Rev Drug Discov* **2009**, *8* (1), 41–54. https://doi.org/10.1038/nrd2760.
(89) Krumm, B. E.; Roth, B. L. Intracellular GPCR Modulators Enable Precision Pharmacology. *npj Drug Discovery 2025 2:1* **2025**, *2* (1), 1–9. https://doi.org/10.1038/s44386-025-00011-8.
(90) Panula, P.; Chazot, P. L.; Cowart, M.; Gutzmer, R.; Leurs, R.; Liu, W. L. S.; Stark, H.; Thurmond, R. L.; Haas, H. L. International Union of Basic and Clinical Pharmacology. XCVIII. Histamine Receptors. *Pharmacol Rev* **2015**, *67* (3), 601–655. https://doi.org/10.1124/pr.114.010249.
(91) Tiligada, E.; Ennis, M. Histamine Pharmacology: From Sir Henry Dale to the 21st Century. *Br J Pharmacol* **2020**, *177* (3), 469–489. https://doi.org/10.1111/bph.14524.
(92) Parsons, M. E.; Ganellin, C. R. Histamine and Its Receptors. *Br J Pharmacol* **2006**, *147*. https://doi.org/10.1038/sj.bjp.0706440.
(93) Thurmond, R. L.; Gelfand, E. W.; Dunford, P. J. The Role of Histamine H1 and H4 Receptors in Allergic Inflammation: The Search for New Antihistamines. *Nat Rev Drug Discov* **2008**, *7* (1), 41–53. https://doi.org/https://doi.org/10.1038/nrd2465.
(94) Ravhe, I. S.; Krishnan, A.; Manoj, N. Evolutionary History of Histamine Receptors: Early Vertebrate Origin and Expansion of the H3-H4 Subtypes. *Mol Phylogenet Evol* **2021**, *154*, 106989. https://doi.org/10.1016/j.ympev.2020.106989.
(95) Jutel, M.; Akdis, M.; Akdis, C. A. Histamine, Histamine Receptors and Their Role in Immune Pathology. *Clinical & Experimental Allergy* **2009**, *39* (12), 1786–1800. https://doi.org/10.1111/J.1365-2222.2009.03374.X.
(96) Simons, F. E. R.; Simons, K. J. Histamine and H1-Antihistamines: Celebrating a Century of Progress. *Journal of Allergy and Clinical Immunology* **2011**, *128* (6), 1139-1150.e4. https://doi.org/10.1016/j.jaci.2011.09.005.
(97) Kay, G. G. The Effects of Antihistamines on Cognition and Performance. *Journal of Allergy and Clinical Immunology* **2000**, *105* (6), S622–S627. https://doi.org/10.1067/mai.2000.106153.
(98) Wang, D.; Guo, Q.; Wu, Z.; Li, M.; He, B.; Du, Y.; Zhang, K.; Tao, Y. Molecular Mechanism of Antihistamines Recognition and Regulation of the Histamine H1 Receptor. *Nature Communications 2024 15:1* **2024**, *15* (1), 1–10. https://doi.org/10.1038/s41467-023-44477-4.

(99) Shimamura, T.; Shiroishi, M.; Weyand, S.; Tsujimoto, H.; Winter, G.; Katritch, V.; Abagyan, R.; Cherezov, V.; Liu, W.; Han, G. W.; Kobayashi, T.; Stevens, R. C.; Iwata, S. Structure of the Human Histamine H 1 Receptor Complex with Doxepin. *Nature* **2011**, *475* (7354), 65–72. https://doi.org/10.1038/nature10236.

(100) Xia, R.; Wang, N.; Xu, Z.; Lu, Y.; Song, J.; Zhang, A.; Guo, C.; He, Y. Cryo-EM Structure of the Human Histamine H1 Receptor/Gq Complex. *Nature Communications 2021 12:1* **2021**, *12* (1), 1–9. https://doi.org/10.1038/s41467-021-22427-2.

(101) Olivella, M.; Caltabiano, G.; Cordomí, A. The Role of Cysteine 6.47 in Class A GPCRs. *BMC Structural Biology 2013 13:1* **2013**, *13* (1), 1–11. https://doi.org/10.1186/1472-6807-13-3.

(102) Del Valle, J. D.; Gantz, I. Novel Insights into Histamine H2 Receptor Biology. *Am J Physiol Gastrointest Liver Physiol* **1997**, *273* (5 36-5). https://doi.org/10.1152/ajpgi.1997.273.5.g987.

(103) Hu, W.; Chen, Z. The Roles of Histamine and Its Receptor Ligands in Central Nervous System Disorders: An Update. *Pharmacol Ther* **2017**, *175*, 116–132. https://doi.org/10.1016/j.pharmthera.2017.02.039.

(104) Robertson, M. J.; Papasergi-Scott, M. M.; He, F.; Seven, A. B.; Meyerowitz, J. G.; Panova, O.; Peroto, M. C.; Che, T.; Skiniotis, G. Structure Determination of Inactive-State GPCRs with a Universal Nanobody. *Nature Structural & Molecular Biology 2022 29:12* **2022**, *29* (12), 1188–1195. https://doi.org/10.1038/s41594-022-00859-8.

(105) Zhang, X.; Liu, G.; Zhong, Y.-N.; Zhang, R.; Yang, C.-C.; Niu, C.; Pu, X.; Sun, J.; Zhang, T.; Yang, L.; Zhang, C.; Li, X.; Shen, X.; Xiao, P.; Sun, J.-P.; Gong, W. Structural Basis of Ligand Recognition and Activation of the Histamine Receptor Family. *Nat Commun* **2024**, *15* (1), 1–16. https://doi.org/10.1038/s41467-024-52585-y.

(106) Shen, Q.; Tang, X.; Wen, X.; Cheng, S.; Xiao, P.; Zang, S. K.; Shen, D. D.; Jiang, L.; Zheng, Y.; Zhang, H.; Xu, H.; Mao, C.; Zhang, M.; Hu, W.; Sun, J. P.; Zhang, Y.; Chen, Z. Molecular Determinant Underlying Selective Coupling of Primary G-Protein by Class A GPCRs. *Advanced Science* **2024**, *11* (23). https://doi.org/10.1002/advs.202310120.

(107) Leurs, R.; Bakker, R. A.; Timmerman, H.; de Esch, I. J. P. The Histamine H3 Receptor: From Gene Cloning to H3 Receptor Drugs. *Nat Rev Drug Discov* **2005**, *4* (2), 107–120. https://doi.org/10.1038/nrd1631.

(108) Leurs, R.; Hoffmann, M.; Wieland, K.; Timmerman, H. H3 Receptor Gene Is Cloned at Last. *Trends Pharmacol Sci* **2000**, *21* (1), 11–12. https://doi.org/10.1016/S0165-6147(99)01411-X.

(109) Schlicker, E.; Kathmann, M. Role of the Histamine H3 Receptor in the Central Nervous System. In *Handbook of Experimental Pharmacology*; Springer New York LLC, 2017; Vol. 241, pp 277–299. https://doi.org/10.1007/164_2016_12.

(110) Cheng, L.; Liu, J.; Chen, Z. The Histaminergic System in Neuropsychiatric Disorders. *Biomolecules* **2021**, *11* (9), 1345. https://doi.org/10.3390/biom11091345.

(111) Harwell, V.; Fasinu, P. S. Pitolisant and Other Histamine-3 Receptor Antagonists—An Update on Therapeutic Potentials and Clinical Prospects. *Medicines* **2020**, *7* (9), 55. https://doi.org/10.3390/medicines7090055.

(112) Sarfraz, N.; Okuampa, D.; Hansen, H.; Alvarez, M.; Cornett, E. M.; Kakazu, J.; Kaye, A. M.; Kaye, A. D. Pitolisant, a Novel Histamine-3 Receptor Competitive Antagonist, and Inverse Agonist, in the Treatment of Excessive Daytime Sleepiness in Adult Patients with Narcolepsy. *Health Psychol Res* **2022**, *10* (2), 34222. https://doi.org/10.52965/001c.34222.

(113) Meskill, G. J.; Davis, C. W.; Zarycranski, D.; Doliba, M.; Schwartz, J. C.; Dayno, J. M. Clinical Impact of Pitolisant on Excessive Daytime Sleepiness and Cataplexy in Adults With Narcolepsy: An Analysis of Randomized Placebo-Controlled Trials. *CNS Drugs* **2022**, *36* (1), 61–69. https://doi.org/10.1007/s40263-021-00886-x.
(114) Peng, X.; Yang, L.; Liu, Z.; Lou, S.; Mei, S.; Li, M.; Chen, Z.; Zhang, H. Structural Basis for Recognition of Antihistamine Drug by Human Histamine Receptor. *Nat Commun* **2022**, *13* (1), 1–9. https://doi.org/10.1038/s41467-022-33880-y.
(115) Zampeli, E.; Tiligada, E. The Role of Histamine H4 Receptor in Immune and Inflammatory Disorders. *Br J Pharmacol* **2009**, *157* (1), 24–33. https://doi.org/10.1111/j.1476-5381.2009.00151.x.
(116) Thurmond, R. L. The Histamine H4 Receptor: From Orphan to the Clinic. *Front Pharmacol* **2015**, *6* (MAR), 134341. https://doi.org/10.3389/fphar.2015.00065.
(117) De Esch, I. J. P.; Thurmond, R. L.; Jongejan, A.; Leurs, R. The Histamine H4 Receptor as a New Therapeutic Target for Inflammation. *Trends Pharmacol Sci* **2005**, *26* (9), 462–469. https://doi.org/10.1016/j.tips.2005.07.002.
(118) Marson, C. M. Targeting the Histamine H4 Receptor. *Chem Rev* **2011**, *111* (11), 7121–7156. https://doi.org/10.1021/cr900166w.
(119) Xia, R.; Shi, S.; Xu, Z.; Vischer, H. F.; Windhorst, A. D.; Qian, Y.; Duan, Y.; Liang, J.; Chen, K.; Zhang, A.; Guo, C.; Leurs, R.; He, Y. Structural Basis of Ligand Recognition and Design of Antihistamines Targeting Histamine H4 Receptor. *Nature Communications 2024 15:1* **2024**, *15* (1), 1–13. https://doi.org/10.1038/s41467-024-46840-5.
(120) Im, D.; Kishikawa, J. ichi; Shiimura, Y.; Hisano, H.; Ito, A.; Fujita-Fujiharu, Y.; Sugita, Y.; Noda, T.; Kato, T.; Asada, H.; Iwata, S. Structural Insights into the Agonists Binding and Receptor Selectivity of Human Histamine H4 Receptor. *Nature Communications 2023 14:1* **2023**, *14* (1), 1–11. https://doi.org/10.1038/s41467-023-42260-z.
(121) Jin, S.; Zhang, H.; Yan, J.; Wu, C.; Cai, X.; Wu, K.; Wang, M.-W.; Xu, H. E.; Yang, D.; Jiang, Y. Decoding Ligand Recognition and Constitutive Activation of Histamine H3 and H4 Receptors. *Acta Pharmacologica Sinica 2025* **2025**, 1–11. https://doi.org/10.1038/s41401-025-01633-4.
(122) Panarello, S.; Rovira, X.; Llebaria, A.; Gómez-Santacana, X. Photopharmacology of G - Protein-Coupled Receptors. In *Molecular Photoswitches*; John Wiley & Sons, Ltd, 2022; Vol. 2–2, pp 921–944. https://doi.org/10.1002/9783527827626.ch37.
(123) Ricart-Ortega, M.; Font, J.; Llebaria, A. GPCR Photopharmacology. *Mol Cell Endocrinol* **2019**, *488*, 36–51. https://doi.org/10.1016/j.mce.2019.03.003.
(124) Berizzi, A. E.; Goudet, C. Strategies and Considerations of G-Protein-Coupled Receptor Photopharmacology. *Adv Pharmacol* **2020**, *88*, 143–172. https://doi.org/10.1016/bs.apha.2019.12.001.
(125) Wijtmans, M.; Josimovic, I.; Vischer, H. F.; Leurs, R. Optical Control of Class A G Protein-Coupled Receptors with Photoswitchable Ligands. *Current Opinion in Pharmacology*. Elsevier Ltd April 1, 2022. https://doi.org/10.1016/j.coph.2022.102192.
(126) Nargeot, J.; Lester, H. A.; Birdsall, N. J. M.; Stockton, J.; Wassermann, N. H.; Erlanger, B. F. A Photoisomerizable Muscarinic Antagonist. Studies of Binding and of Conductance Relaxations in Frog Heart. *Journal of General Physiology* **1982**, *79* (4), 657–678. https://doi.org/10.1085/jgp.79.4.657.
(127) Agnetta, L.; Kauk, M.; Canizal, M. C. A.; Messerer, R.; Holzgrabe, U.; Hoffmann, C.; Decker, M. A Photoswitchable Dualsteric Ligand Controlling Receptor Efficacy.

Angewandte Chemie International Edition **2017**, *56* (25), 7282–7287. https://doi.org/10.1002/anie.201701524.

(128) Riefolo, F.; Sortino, R.; Matera, C.; Claro, E.; Preda, B.; Vitiello, S.; Traserra, S.; Jiménez, M.; Gorostiza, P. Rational Design of Photochromic Analogues of Tricyclic Drugs. *J Med Chem* **2021**, *64* (13), 9259–9270. https://doi.org/10.1021/acs.jmedchem.1c00504.

(129) Sarott, R. C.; Viray, A. E. G.; Pfaff, P.; Sadybekov, A.; Rajic, G.; Katritch, V.; Carreira, E. M.; Frank, J. A. Optical Control of Cannabinoid Receptor 2-Mediated Ca2+ Release Enabled by Synthesis of Photoswitchable Probes. *J Am Chem Soc* **2021**, *143* (2), 736–743. https://doi.org/10.1021/jacs.0c08926.

(130) Steinmüller, S. A. M.; Tutov, A.; Hislop, J. N.; Decker, M. Bridging the Binding Sites 2.0: Photoswitchable Dualsteric Ligands for the Cannabinoid 2 Receptor. *ACS Chem Neurosci* **2023**, *14* (20), 3737–3744. https://doi.org/10.1021/acschemneuro.3c00509.

(131) Hauwert, N. J.; Mocking, T. A. M.; Da Costa Pereira, D.; Lion, K.; Huppelschoten, Y.; Vischer, H. F.; De Esch, I. J. P.; Wijtmans, M.; Leurs, R. A Photoswitchable Agonist for the Histamine H3 Receptor, a Prototypic Family A G Protein-Coupled Receptor. *Angewandte Chemie International Edition* **2019**, *58* (14), 4531–4535. https://doi.org/10.1002/anie.201813110.

(132) Roche, O.; Nettekoven, M.; Vifian, W.; Sarmiento, R. M. R. Refinement of Histamine H3 Ligands Pharmacophore Model Leads to a New Class of Potent and Selective Naphthalene Inverse Agonists. *Bioorg Med Chem Lett* **2008**, *18* (15), 4377–4379. https://doi.org/10.1016/j.bmcl.2008.06.062.

(133) Hauwert, N. J.; Mocking, T. A. M.; Da Costa Pereira, D.; Kooistra, A. J.; Wijnen, L. M.; Vreeker, G. C. M.; Verweij, E. W. E.; De Boer, A. H.; Smit, M. J.; De Graaf, C.; Vischer, H. F.; de Esch, I. J. P.; Wijtmans, M.; Leurs, R. Synthesis and Characterization of a Bidirectional Photoswitchable Antagonist Toolbox for Real-Time GPCR Photopharmacology. *J Am Chem Soc* **2018**, *140* (12), 4232–4243. https://doi.org/10.1021/jacs.7b11422.

(134) Gómez-Santacana, X.; de Munnik, S. M.; Vijayachandran, P.; Da Costa Pereira, D.; Bebelman, J. P. M.; de Esch, I. J. P.; Vischer, H. F.; Wijtmans, M.; Leurs, R. Photoswitching the Efficacy of a Small-Molecule Ligand for a Peptidergic GPCR: From Antagonism to Agonism. *Angewandte Chemie International Edition* **2018**, *57* (36), 11608–11612. https://doi.org/10.1002/anie.201804875.

(135) Mori, S.; Arella, D.; Decker, M. Photoswitchable Allosteric and Dualsteric Ligands in GPCR Pharmacology. *Trends Pharmacol Sci* **2025**, *0* (0). https://doi.org/10.1016/j.tips.2025.05.009.

(136) Donthamsetti, P.; Konrad, D. B.; Hetzler, B.; Fu, Z.; Trauner, D.; Isacoff, E. Y. Selective Photoswitchable Allosteric Agonist of a G Protein-Coupled Receptor. *J Am Chem Soc* **2021**, *143* (24), 8951–8956. https://doi.org/10.1021/jacs.1c02586.

(137) Broichhagen, J.; Johnston, N. R.; Von Ohlen, Y.; Meyer-Berg, H.; Jones, B. J.; Bloom, S. R.; Rutter, G. A.; Trauner, D.; Hodson, D. J. Allosteric Optical Control of a Class B G-Protein-Coupled Receptor. *Angewandte Chemie - International Edition* **2016**, *55* (19), 5865–5868. https://doi.org/10.1002/anie.201600957.

(138) Pupo, A. S.; Duarte, D. A.; Lima, V.; Teixeira, L. B.; Parreiras-e-Silva, L. T.; Costa-Neto, C. M. Recent Updates on GPCR Biased Agonism. *Pharmacol Res* **2016**, *112*, 49–57. https://doi.org/10.1016/j.phrs.2016.01.031.

(139) Sink, A.; Pottie, E.; Carter, S. J.; Tombari, R. J.; Weber, V.; Carloni, P.; Rossetti, G.; Olson, D. E.; Stove, C. P.; Decker, M. Design, Synthesis, and In Vitro Characterization of a

Tryptamine-Based Visible-Light Photoswitchable 5-HT2AR Ligand Showing Efficacy Preference for β-Arrestin over Mini-Gq. *J Med Chem* **2025**, *68* (13), 13628–13639. https://doi.org/10.1021/acs.jmedchem.5c00442.

(140) Esmaeili, A. J.; Montazeri, P.; Gomez, J. C.; Dumervil, D. J.; Nezhad, F. S.; Steinhardt, R. C. Photoswitchable TCB-2 for Control of the 5-HT2A Receptor and Analysis of Biased Agonism. *Chemical Communications* **2024**, *60* (83), 11956–11959. https://doi.org/10.1039/d4cc03892d.

(141) Broichhagen, J.; Podewin, T.; Meyer-Berg, H.; Von Ohlen, Y.; Johnston, N. R.; Jones, B. J.; Bloom, S. R.; Rutter, G. A.; Hoffmann-Röder, A.; Hodson, D. J.; Trauner, D. Optical Control of Insulin Secretion Using an Incretin Switch. *Angewandte Chemie - International Edition* **2015**, *54* (51), 15565–15569. https://doi.org/10.1002/anie.201506384.

(142) Steinmüller, S. A. M.; Fender, J.; Deventer, M. H.; Tutov, A.; Lorenz, K.; Stove, C. P.; Hislop, J. N.; Decker, M. Visible-Light Photoswitchable Benzimidazole Azo-Arenes as β-Arrestin2-Biased Selective Cannabinoid 2 Receptor Agonists. *Angewandte Chemie - International Edition* **2023**, *62* (49). https://doi.org/10.1002/anie.202306176.

(143) Volarić, J.; Szymanski, W.; Simeth, N. A.; Feringa, B. L. Molecular Photoswitches in Aqueous Environments. *Chem Soc Rev* **2021**, *50* (22), 12377–12449. https://doi.org/10.1039/d0cs00547a.

(144) Greenfield, J. L.; Gerkman, M. A.; Gibson, R. S. L.; Han, G. G. D.; Fuchter, M. J. Efficient Electrocatalytic Switching of Azoheteroarenes in the Condensed Phases. *J Am Chem Soc* **2021**, *143* (37), 15250–15257. https://doi.org/10.1021/jacs.1c06359.

Chapter 2

A radiolabeled photoswitchable G protein-coupled receptor antagonist enlightens ligand binding kinetics associated with photoswitching

Lars C.P. Binkhorst,[1,#] Ivana Josimovic,[1,#] Bas De Boer,[1] Icaro A. Simon,[1] Frank Van Der Aa,[2] Barbara A. Zarzycka,[1] Iwan J.P. De Esch,[1] Henry F. Vischer,[1] Albert D. Windhorst,[2] Maikel Wijtmans,[1] Rob Leurs[1]

Adapted from: *J. Am. Chem. Soc.* **2025**, 147, 27, 23991–24000

[1] Amsterdam Institute of Molecular and Life Sciences, Division of Medicinal Chemistry, Faculty of Science, Vrije Universiteit Amsterdam, De Boelelaan 1083, 1081 HV Amsterdam, the Netherlands.

[2]Department of Radiology and Nuclear Medicine, Amsterdam UMC, location Vrije Universiteit, De Boelelaan 1117, 1081 HV Amsterdam, the Netherlands

[#] Authors contributed equally to this manuscript.

Abstract

Photopharmacology offers powerful opportunities to control protein signaling using photoresponsive ligands. Despite the vast potential of photoswitchable ligands for spatio-temporal target protein control, research on ligand-protein binding kinetics of these ligands remains limited. Herein, we describe the discovery of the first radiolabeled photoswitchable ligand, [^{3}H]VUF26063 ([^{3}H]**3f**), to assess light-dependent ligand-protein binding kinetics in real time. The key compound (**3f**) is an arylazopyrazole-based antagonist targeting a prototypic family A GPCR, the histamine H_3 receptor (H_3R), and enabled convenient radiolabeling via a growth vector on the pyrazole. Its photochemical properties, sub-nanomolar affinity of the *trans* isomer and a 50-fold decrease in affinity upon switching, allowed for reversible photochemical control of H_3R binding kinetics in real time. The kinetic binding data obtained with this radiolabeled ligand indicate that **3f** isomerizes in the H_3R extended binding pocket upon illumination. Our results shed light on the binding kinetics of photoswitchable ligands and will have relevance beyond GPCRs as targets.

Introduction

Photopharmacology offers a powerful approach to regulate protein function with high spatial and temporal precision through the use of photoresponsive ligands (e.g., photocaging and photoswitching).[1–3] A variety of photoswitchable small-molecule ligands have been developed for various signaling proteins or enzymes, and are designed to reversibly isomerize between two distinct photostationary states (PSS) upon illumination, each capable of differentially modulating biology.[4,5] While equilibrium properties such as PSS composition and target affinity have been the primary focus of most studies with photoswitchable ligands, kinetic parameters and particularly ligand-protein binding kinetics have received comparatively little attention.[6–8]

In this study, we addressed this gap using the histamine H_3 receptor (H_3R), an archetypal class A G protein-coupled receptor (GPCR), as a model system. The photopharmacology of GPCRs, one of the most extensively studied protein families and the target of approximately 36% of approved therapeutics,[9] has seen remarkable advances in recent years and therefore these targets constitute an excellent model protein family.[10–13] The H_3R is predominantly expressed in the central nervous system, where it modulates the release of histamine and other key neurotransmitters.[14] It is implicated in various neuropathologies, including Parkinson's and Alzheimer's diseases, neuropsychiatric conditions such as Tourette's syndrome and schizophrenia, and sleep disorders like narcolepsy.[15–17] Its therapeutic importance is evident from the approval of inverse agonist pitolisant for the treatment of narcolepsy.[18–20]

We have previously developed first-generation azobenzene-based H_3R antagonists (e.g. VUF14862)[21] and agonists (e.g. VUF15000).[22] Indeed, our 2021 in-depth analysis of the chemical diversity of photoswitchable ligands for class A GPCRs showed that azobenzenes were predominantly used as photoswitchable moieties (84%).[12] Yet, azobenzenes exhibit

well-described drawbacks, such as low aqueous solubility, dependence on UV light for *trans*/*cis* isomerization, and sub-optimal PSS_{trans} values. Hence, improved tools for advanced studies are eagerly awaited and the photopharmacology field at large has shifted towards next-generation photoswitch moieties to improve PSS_{trans} values, increase solubility and enable photoisomerization at longer wavelengths for better tissue penetration and lower tissue damage.[23–25] Among these, arylazopyrazoles have recently emerged as superior alternatives to azobenzenes, offering highly efficient and reversible switching at longer wavelengths, greater PSS percentages in both directions, and enhanced aqueous solubility owing to their heteroatom-rich structure.[5,26–29]

Using these recent advancements in the field, we developed an arylazopyrazole-based second-generation series of photoswitchable H_3R ligands with improved physicochemical, photochemical, and pharmacological properties compared to our earlier H_3R antagonist[22] series. Key compound (**3f**) binds H_3R with sub-nanomolar affinity, undergoes efficient and quantitative photoisomerization between *trans* and *cis* states and exhibits a 50-fold decrease in H_3R affinity upon switching. Importantly, the pyrazole growth vector enabled straightforward radiolabeling of **3f**, yielding [^{3}H]**3f** which is, to our knowledge, the first radiolabeled photoswitchable ligand. This unique and novel tool allowed us to probe the role of ligand-protein binding kinetics in light-mediated regulation of GPCR function and provided compelling evidence that photoisomerization can occur within the binding pocket of a target protein.

Results and discussion

Design

Compound **1**[21] was chosen as a starting point (Figure 1, Table 1). The generally accepted pharmacophore model for non-imidazole H_3R antagonists entails a basic *N,N*-dialkylamino moiety separated by an aliphatic linker to an aromatic core decorated with additional substituents.[30,31] Indeed, **1** comprises a piperidine bound to an unsubstituted azobenzene with a classical aminopropyloxy linker.[30–34] To increase the affinity for H_3R, the propyloxy sidechain was rigidified through a *trans*-cyclobutyl group (**2**). Rigidification is a general strategy to improve target binding affinity[35] and has proven to be successful in the H_3R field.[21,36–39] The azobenzene was subsequently replaced by a trimethylarylazopyrazole moiety (**3a**). In addition to its known benefits (*vide supra*), the pyrazole has the additional advantage of potentially improving the required molecular recognition event between ligand and protein, as heteroatoms are often involved in productive interactions with proteins, and presenting a synthetically tractable growth vector for appending additional protein recognition elements.[5] We pursued growing from the nitrogen atom of the pyrazole with specific groups (**3b-f**), aiming to further improve solubility by increasing the dipole moment,[40] probe additional molecular interactions within the H_3R pocket,[41,42] and potentially increase the affinity shift by inducing clashes between one of the photochemical isomers and the protein.

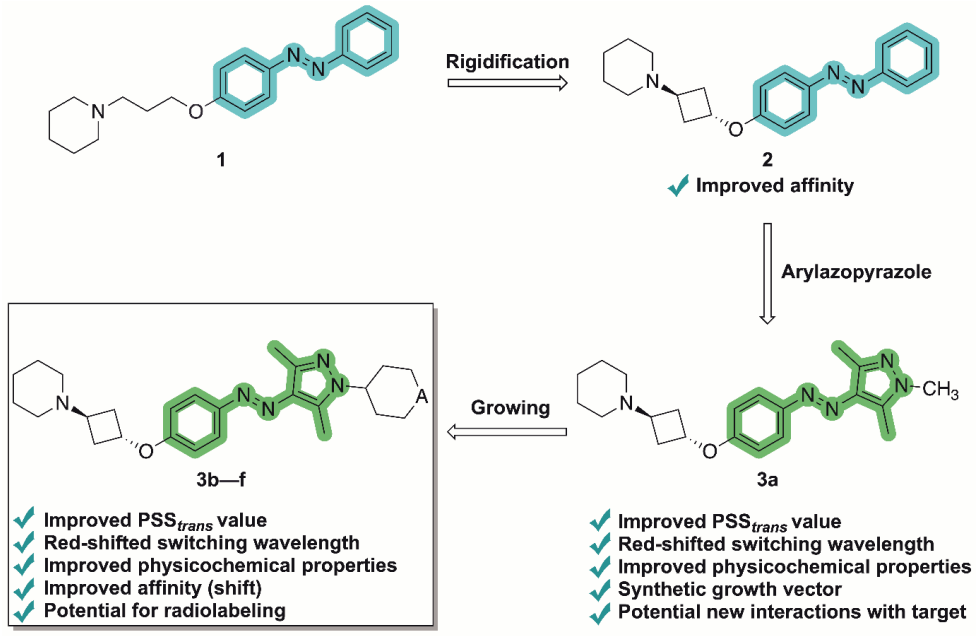

Figure 1. Design strategy towards high-affinity arylazopyrazole-based H_3R antagonists. Improvements listed are relative to azobenzene ligand **1**.

To achieve this, relatively large and rigid substituents, i.e., six-membered rings, were chosen. A substituent without a hydrogen bond donor or acceptor in the six-membered ring (cyclohexyl analogue **3b**) and substituents with hydrogen bond donors and/or acceptors such as a tetrahydropyran, piperidine and *N*-methylpiperidine moiety (**3c**,**e**,**f** respectively) were introduced. The secondary amine in **3e** also provided a vector that could be used for radiolabeling. For the synthesis of **3a-f**, 4-aminophenol (**4**) was converted by a diazonium coupling with acetylacetone to give **5** (Scheme 1).[43] This intermediate was heated under reflux with substituted hydrazines to give phenols **6a–d**,**f**. Subsequent coupling with *cis*-tosylate **7**[39] gave compounds **3a–d**,**f** with the expected *trans* configuration of the 3-piperidino-cyclobutoxy motif as confirmed with 1D NOESY. Compound **3d** was deprotected under acidic conditions to give **3e**.

Scheme 1. General synthetic route for arylazopyrazoles **3a-f.**[a]

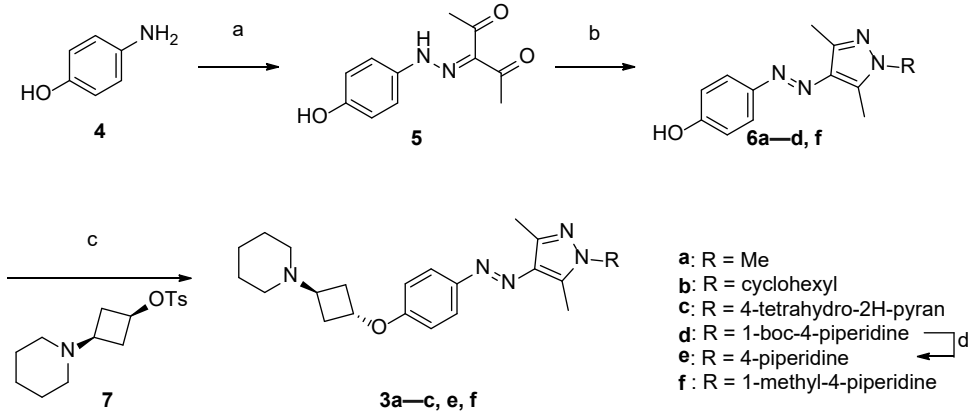

[a]Reagents and conditions used: (a) (i) $NaNO_2$, HCl, H_2O/AcOH, 0 °C, 30 min; (ii) acetylacetone, NaOAc, EtOH/H_2O, 0 °C, 30 min, 58%; (b) $RNHNH_2$, TEA, EtOH, reflux, 17 h, 57-96%; (c) (i) NaH, DMF, r.t., 30 min; (ii) **7**, 75 °C, DMF, 17 h, 24-52%; (d) HCl, dioxane, rt, 17 h, 70%;

Structure-photochemistry and structure-activity relationships

Photochemical properties and target binding affinities were monitored in parallel to guide the design and synthesis cycles (Table 1). As expected, rigidification of the sidechain of **1** improves target interaction, with **2** having nanomolar affinity and a 4-fold difference in affinity between *trans*-**2** and **2** at PSS_{cis} ('*cis*-on'). Replacing the azobenzene in **2** with a trimethylarylazopyrazole (**3a**) results in a more than 10-fold improved K_i value for *trans*-**3a** compared to *trans*-**2**. Since **3a** at PSS_{cis} shows reduced affinity compared to **2** at PSS_{cis}, **3a** has an improved photochemically induced affinity shift but, interestingly, with a *trans*-on profile. Next to sub-nanomolar H_3R affinity, **3a** also shows improved (photo)chemical properties compared to **2** and these were, as expected, also observed for its analogues **3b**,**c**,**e**,**f**. Firstly, as reported for many arylazopyrazole-based photoswitchable ligands,[26,27] the *trans*-arylazopyrazole moiety in **3a-c**,**e**,**f** can be efficiently isomerized upon illumination (PSS_{cis} = 88-99%). Secondly, the estimated thermal half-life of PSS_{cis} states of **3a-c**,**e**,**f** at 20 °C in HBSS buffer (1% DMSO) is increased from 2 days for **2** up to at least a week (Figure S1-6, Table 1). Thirdly, the enhanced band separation of the arylazopyrazoles[26,27] allows the use of 506 nm (green light) for **3b**,**c**,**e**,**f** instead of 434 nm (blue light) required for **2**, to more efficiently (92-95% versus 74% for **2**) switch the arylazopyrazole-based ligands back from the PSS_{cis} state to the PSS_{trans} state. This observation is in line with previously reported differences in the efficiency of back-switching of azobenzene- and arylazopyrazole-based photoswitchable ligands.[27]

While, as expected, the photochemical properties of **3a-c**,**e**,**f** are not greatly affected by substitution on the pyrazole, the molecular interaction with the H_3R binding pocket is sensitive to *N*-substitution of the pyrazole (Table 1). Introducing a lipophilic cyclohexyl ring (**3b**) results in a 30-fold decrease in H_3R affinity compared to **3a**. Interestingly, incorporating

an oxygen or nitrogen atom in the cyclohexyl ring (**3c**,**e**,**f**) restores high-affinity target binding in combination with an improved light-induced affinity shift of 20-50 fold (Table 1). As mentioned, (substituted) arylazopyrazole moieties potentially also improve solubility compared to azobenzene-based ligands. Therefore, nephelometry[44,45] was used to qualitatively compare the solubility of arylazopyrazole **3f** to our first-generation azobenzene-based antagonist VUF14862[21] (Figure S7). Neither of these compounds form aggregates[46] nor precipitate at concentrations of relevance in our pharmacology assays (*vide infra*). However, *trans*-VUF14862 shows a relatively high tendency to aggregate/precipitate at high concentrations (> $10^{-4.5}$ M), while this was not observed for **3f** in either state, suggesting an improved solubility profile of **3f**.

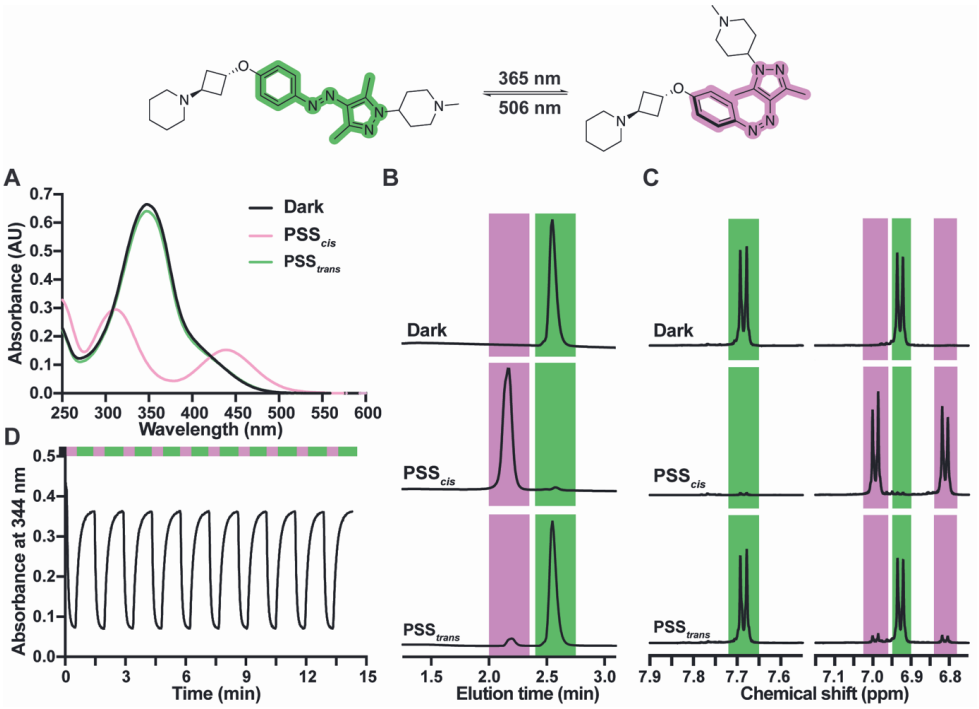

Figure 2. Photochemical properties of **3f**. (A) UV-vis spectra of 25 µM **3f** in HBSS buffer containing 1% DMSO in the dark, after illumination to PSS_{cis} with 365 ± 10 nm for 2 min and after subsequent illumination to PSS_{trans} with 506 ± 20 nm for 2 min. (B) Representative parts of LC–MS chromatograms of **3f** in the dark, after illumination with 365 ± 10 nm for 300 s to reach PSS_{cis} and subsequently with 506 ± 20 nm for 300 s to reach PSS_{trans}. (C) Part of ^{1}H NMR spectra of 10 mM **3f** in DMSO-d_6 (representing the two aromatic signals) in the dark, after illumination with 365 ± 10 nm for 600 s to reach PSS_{cis} and subsequently 506 ± 20 nm for 900 s to reach PSS_{trans}. (D) Reversible isomerization cycles of 25 µM **3f** in HBSS buffer containing 1% DMSO, repeatedly illuminated for 30 s with 365 ± 10 nm to reach PSS_{cis} and subsequently for 60 s with 506 ± 20 nm to reach PSS_{trans}. The y-axis shows the absorbance at 344 nm.

Ligand **3f** was selected for in-depth studies given its excellent switching properties (PSS_{cis} = 98%, PSS_{trans} = 93%), improved solubility, sub-nanomolar H_3R affinity (pK_i = 9.3 ± 0.1) of the *trans* isomer, and the 50-fold difference in affinity between *trans* and PSS_{cis} states. Its clean and robust photoswitching was further confirmed by LC-MS, NMR and UV studies. Ligand **3f** shows a good band separation of the n–π* transition bands of the *trans* and PSS_{cis} states in the 400-550 nm area (Figure 2A). This allows efficient *trans*-PSS_{cis} photoswitching in HBSS buffer using UV light (365 nm) and PSS_{cis}-PSS_{trans} back-switching with green light (506 nm). LC-MS analysis (Figure 2B) and, more quantitively, ^{1}H NMR analysis (Figure 2C) reveal high PSS_{cis} and PSS_{trans} values for **3f** (98% and >95% *cis* isomer for PSS_{cis} by LC-MS and ^{1}H NMR analysis, respectively; 93% and 93% *trans* isomer for PSS_{trans} by LC-MS and ^{1}H NMR analysis, respectively). These analyses also confirmed that no photodecomposition occurs upon illumination with either 365 or 506 nm. Reversible isomerization cycles could be conducted in HBSS buffer without any photobleaching (Figure 2D). After irradiation for 30 s with 365 nm, the PSS_{cis} state was reached. Subsequently, the PSS_{trans} state was obtained after irradiation for 60 s with 506 nm. This indicates that the switching processes from *trans* to PSS_{cis} states and from PSS_{cis} to PSS_{trans} states are fast, with half-lives of 3.1 and 7.3 s, respectively.

Table 1. Photochemical parameters, H_3R affinity (pK_i) values and corresponding affinity shifts between PSS_{cis} and *trans* states.

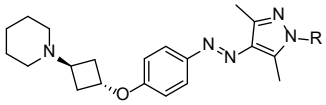

Compound number	R	λ_{max} *trans*[a] (nm)	λ_{max} *cis*[a] (nm)	PSS_{cis} (area %*cis*)[b]	PSS_{trans} (area %*trans*)[b]	Half-life[c] (days)	pK_i *trans* ± SEM[d]	pK_i PSS_{cis} ± SEM[d]	Fold K_i shift[e]
1[f]	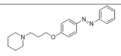	344	432	97	68	11	7.3 ± 0.1	8.1 ± 0.1	6.3 ↑
2	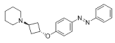	350	425	97	74	2	8.0 ± 0.1	8.6 ± 0.2	4.0 ↑
3a		347	439	95	93	18	9.1 ± 0.1	8.2 ± 0.1	7.9 ↓
3b		351	440	88	94	7	7.7 ± 0.2	6.6 ± 0.1	12.6 ↓
3c		349	440	94	95	25	8.6 ± 0.1	7.3 ± 0.1	20.0 ↓
3e		346	434	99	92	29	9.3 ± 0.2	7.9 ± 0.1	25.1 ↓
3f		348	439	98	93	13	9.3 ± 0.1	7.6 ± 0.2	50.1 ↓

[a]Determined at 25 µM in HBSS buffer containing 1% DMSO. [b]Photostationary state area percentages after illumination of *trans* isomer with 365 ± 10 nm at 1 mM in DMSO for 10 min as determined by LC-MS analysis at the isosbestic point, or PSS_{cis} states with 506 ± 20 nm (for **3**) or 434 ± 20 nm (for **1** and **2**) at 1 mM in DMSO for 10 min as determined by LCMS analysis at the isosbestic point. [c]Approximate thermal relaxation half-life times of PSS_{cis} states in HBSS buffer + 1 % DMSO, as estimated by the method of Ahmed *et al*.[47] by extrapolating to 20 °C. Arrhenius plots are available in Figure S1-6. [d]Affinity (pK_i) values as obtained from [^{3}H]NAMH

competition experiments on cell homogenates overexpressing H_3R. Values are means of *n* = 3 experiments, performed in triplicate ± SEM [e]Fold shift calculated as (high-affinity state)/(low-affinity state), with the arrow indicating lower (↓) or higher (↑) affinity of the PSS_{cis} state in comparison to the *trans* state. [f]Data reported by Hauwert *et al*.[21]

*Binding mode of **3f***

Molecular modeling studies were performed to rationalize the observed affinities of the different isomers of **3f**. Both isomers were docked in the crystal structure of the human H_3R in complex with antagonist PF03654746 (PDB: 7F61).[41] Four independent 1 µs all-atom molecular dynamics (MD) simulations were performed for each complex, to validate predicted binding poses. The predicted pose of *trans*-**3f** (Figure 3A, B) is located within the orthosteric pocket with its aromatic photoswitchable moiety extending into the extended binding pocket (EBP) formed by TM2, TM7 and ECL2. This region forms a tight aromatic cluster surrounded by residues $Y91^{2.61}$, $Y94^{2.64}$, $W110^{3.28}$, $Y189^{ECL2}$, $F193^{ECL2}$, and $F398^{7.39}$. Notably, the predicted binding pose of *trans*-**3f** indicates a substantial overlap with the pose of PF03654746 in the H_3R X-ray structure (Figure S8). In contrast, the folded conformation of the *cis* isomer does not fit within the EBP and needs an enlarged binding pocket to be accommodated, where the arylazopyrazole moiety is located towards TM5 and 6 moving away from the EBP and its key aromatic cluster residues $Y91^{2.61}$, $Y94^{2.64}$, $W110^{3.28}$ (Figure 3C, D). Thus, this binding pose does not overlap well with the crystallographic binding mode of PF03654746 (Figure S8). Both *trans*- and *cis*-**3f** form an ionic interaction with $D114^{3.32}$, that anchors the piperidine in a similar position, deep inside the orthosteric binding pocket (Figure 3B and D, respectively). In the MD trajectories, the more extended, linear shape of *trans*-**3f** reaches the EBP, which results in a binding pose making increased contact with the extracellular loop region, with the *N*-methylpiperidine group being solvent exposed (Figure 3A, B). This solvent exposure can explain the structure-activity relationship (SAR) listed in Table 1 for the arylazopyrazole-based *trans* isomers. While the small *N*-methyl group (**3a**) likely experiences minimal desolvation costs near the entrance of the binding pocket, the larger and apolar cyclohexyl group (**3b**) will experience a greater desolvation penalty. In contrast, more polar substituents (**3c**,**e,f**) are better accommodated in a solvent-exposed environment and can maintain favorable interaction with surrounding water molecules. *Trans*-**3f** also engages in aromatic interactions with $Y189^{ECL2}$, $F193^{ECL2}$, $F398^{7.39}$, an additional salt bridge with $D391^{7.32}$ and a transient H-bond interaction with $Y394^{7.35}$ (Figure 3B). While the folded conformation of *cis*-**3f** (Figure 3C) also engages in aromatic interactions with $F193^{ECL2}$, it further forms a secondary salt bridge with $E395^{7.36}$ and occasional cation-π interactions with $R381^{6.58}$ and $F398^{7.39}$ (Figure 3D). The conformational differences between the isomers also induce a 90-degree rotation of the cyclobutyl linker. For *trans*-**3f**, the oxygen atom in the linker is directed toward $Y115^{3.33}$, while for *cis*-**3f**, the oxygen atom is oriented toward $W110^{3.28}$, contributing to distinct spatial arrangements of the isomers within the H_3R binding site (Figure 3B, D). In all, the linear shape of *trans*-**3f** demonstrates an improved fit in

the H_3R binding pocket compared to *cis*-**3f,** potentially explaining the observed higher binding affinity of *trans*-**3f** compared to **3f** at PSS_{cis}.

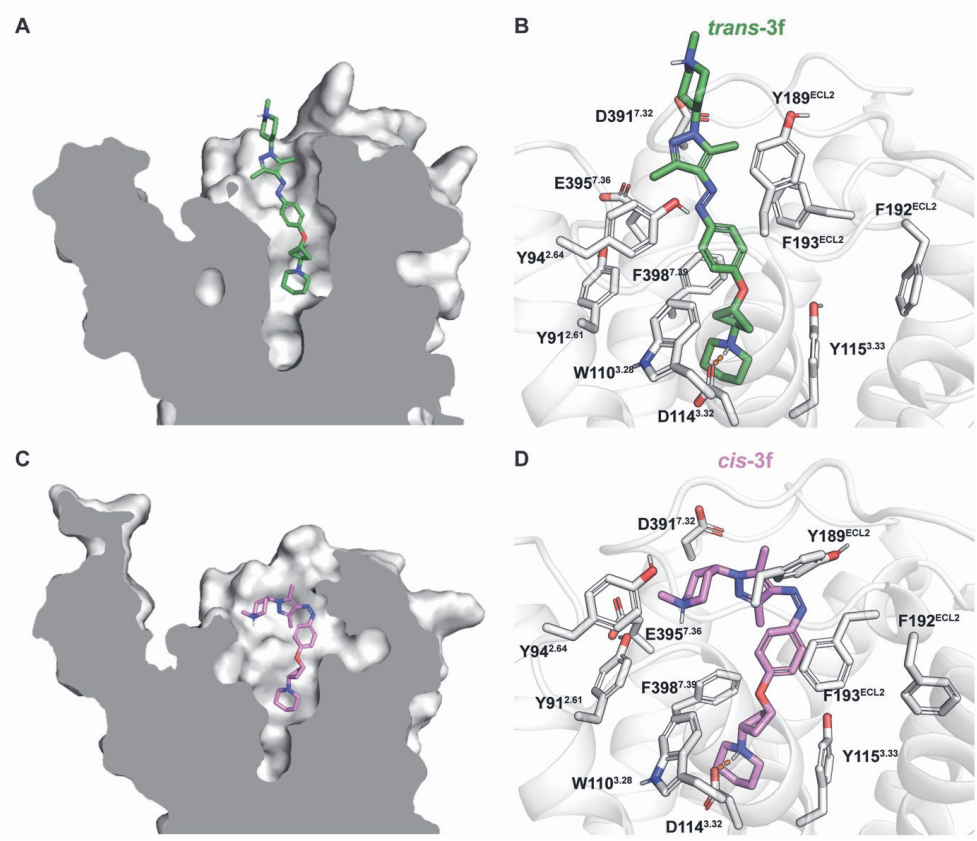

Figure 3. (A) Slice-through depiction of H_3R pocket formed by *trans*-**3f**. (B) Predicted binding pose of *trans*-**3f** (green carbon atoms). (C) Slice-through depiction of H_3R pocket formed by *cis*-**3f**. (D) Predicted binding pose of *cis*-**3f** (pink carbon atoms). Poses are based on representative MD snapshots. Ionic interactions are shown in orange dashed lines in Figures B and D.

*Photopharmacological evaluation of **3f***

Arylazopyrazole **3f** is a H_3R ligand with sub-nanomolar affinity and excellent selectivity over the other three histamine receptor proteins (Table 1, Figure 4A). Competition binding experiments reveal that *trans*-**3f** does not bind to any of the other three histamine receptor subtypes at concentrations lower than 1 µM. Moreover, *trans*-**3f** binds with high affinity to the mouse H_3R (pK_i = 8.8 ± 0.2) and maintains a 42-fold shift in affinity upon photoisomerization to **3f**-PSS_{cis}.

The ability of **3f** to modulate H_3R signaling in living cells was evaluated. H_3R is coupled to $G\alpha_i$ proteins both in native tissues and transfected cells.[48,49] The canonical inhibition of forskolin-

stimulated adenylate cyclase activity following H_3R activation with the high-affinity H_3R-specific agonist immethridine[50] (pEC_{50} = 9.1 ± 0.1, Figure 4B) was measured in transiently transfected HEK293T cells co-expressing H_3R and a NanoBiT-based cAMP sensor, measuring cAMP-dependent subunit disassembly of protein kinase A.[51] Both *trans*-**3f** and pre-irradiated *trans*-**3f** (i.e. to afford **3f**-PPS_{cis}) show concentration-dependent antagonism of 10 nM immethridine-induced H_3R activation (Figure 4B). Reminiscent of the pattern observed for **3f** in radioligand binding, *trans*-**3f** shows a significantly higher antagonistic potency (pIC_{50} = 7.5 ± 0.1) in this functional assay, compared to **3f**-PPS_{cis} (pIC_{50} = 6.4 ± 0.1). The affinity determined in radioligand binding experiments shows a larger shift between *trans*-**3f** and **3f**-PPS_{cis} (50-fold, Table 1) in comparison to the observed potency shift with the live cell cAMP sensor (12.6-fold). This difference most likely reflects the difference in assay conditions (membranes versus live cells, different buffers). Also, bioluminescence stemming from light-based assays is known to potentially interfere with the isomeric ratio of photoswitchable ligands.[12,52,53] With nanoluciferase emitting light with a peak around 460 nm[54] and the possibility of some **3f**-PSS_{cis} back-switching to **3f**-PSS_{trans} between 430 – 500 nm (Figure 2A) during the time of data collection, the observed potency shift between *trans*-**3f** and **3f**-PPS_{cis} might be underestimated.

Ligand **3f** was investigated in an *in situ* dynamic photopharmacology assay using transiently transfected HEK293T cells, expressing H_3R and the cAMP sensor. Pre-incubation of 100 nM of *trans*-**3f** with 10 nM immethridine blocked the H_3R agonist response for approximately 80% (Figure 4C). Subsequent illumination with 365 nm LED light (10 min, 2 mW) results in the reversal of the response up to approximately 80% of the maximal agonist response, indicative of *in situ* switching of *trans*-**3f** to **3f**-PSS_{cis} and a concomitant loss of H_3R blockade. *In situ* back-switching with 500 nm LED light (10 min, 1.5 mW) restored H_3R blockade, confirming successful **3f**-PSS_{cis} to **3f**-PSS_{trans} conversion. An additional 365-500 nm illumination cycle results in a similar modulation of the H_3R activity (Figure 4C).

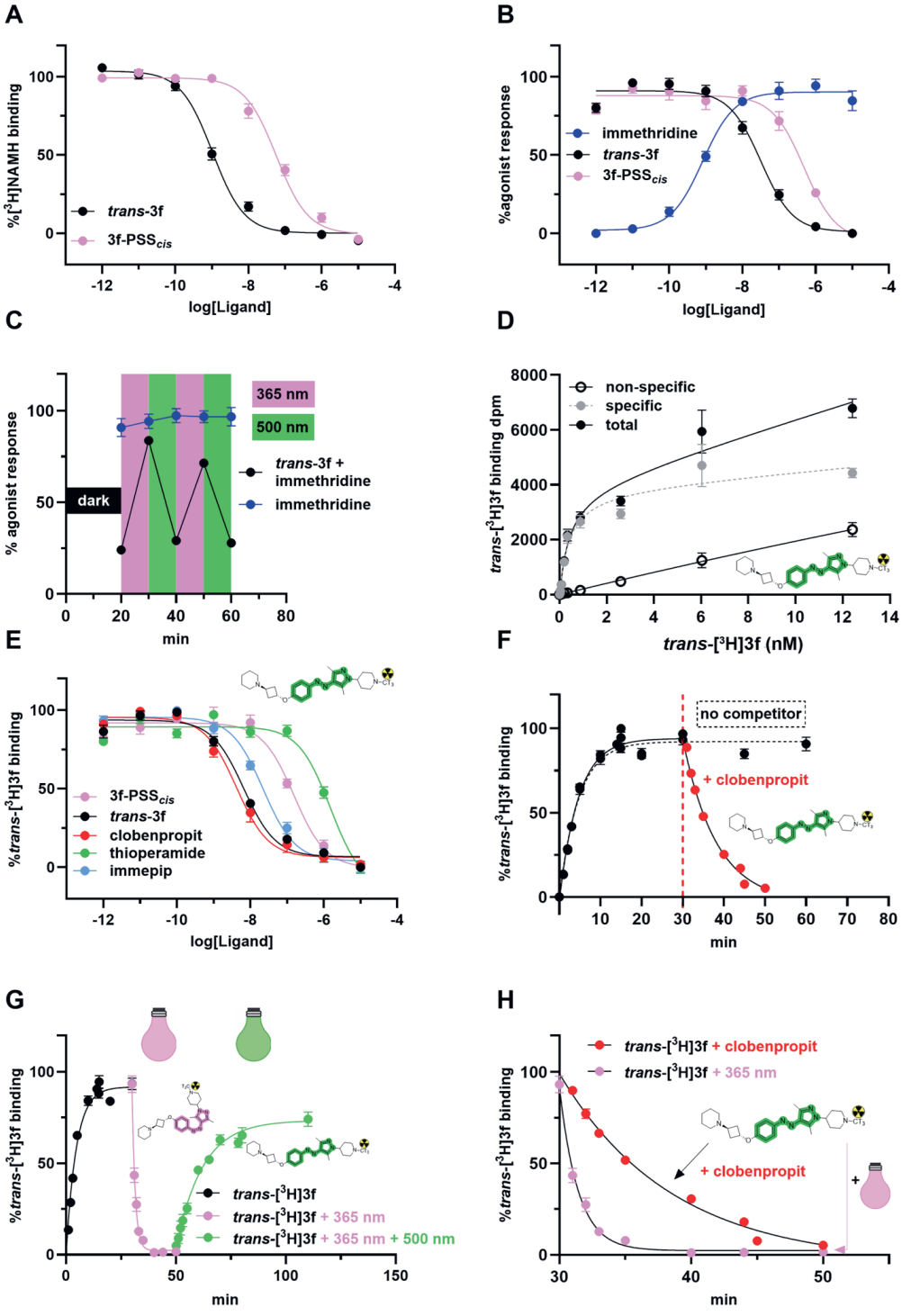

Figure 4. Photopharmacological characterization of **3f** and its radiolabeled analogue [^{3}H]**3f**.

(A) Concentration-response curves of **3f** obtained in radioligand H_3R binding assays in competition with 1.6 nM [^{3}H]NAMH. (B) Concentration-response curves of immethridine alone and 10 nM immethridine in competition with *trans*-**3f** or **3f**-PPS_{cis} in a functional H_3R-NanoBit-PKA assay after 15 min of incubation. (C) Dynamic alterations in functional H_3R-dependent nBit-cAMP sensor activity, caused by competition of 10 nM immethridine with 100 nM *trans*-**3f** and subsequent switching thereof, in comparison with immethridine activity over switching cycles. Dark indicates the pre-incubation time of *trans*-**3f** before immethridine stimulation and subsequent switching, magenta stripes indicate irradiation with 365 nm light, and green stripes indicate irradiation with 500 nm light. (D) Saturation binding experiments with *trans*-[^{3}H]**3f** indicative of total, specific and non-specific binding on cell homogenates expressing H_3R. (E) Displacement of *trans*-[^{3}H]**3f** with H_3R-specific unlabeled ligands in radioligand binding assays. (F) Association and dissociation binding curves of *trans*-[^{3}H]**3f** (0.5 nM). A 60 min association was performed with no competitor present. Dissociation from H_3R was initiated with 10 µM clobenpropit after 30 min of pre-incubation with *trans*-[^{3}H]**3f**. (G) Light-dependent modulation of *trans*-[^{3}H]**3f** (0.5 nM) H_3R binding and kinetics without antagonist present. (H) Dissociation of *trans*-[^{3}H]**3f** (0.5 nM) from H_3R initiated either with 10 µM clobenpropit, or without competitor but using 365 nm light. Data represent mean ± SEM of at least *n* = 3 experiments, performed in triplicate. Curves are normalized to their own plateaus.

*Synthesis and application of [^{3}H]**3f***

The kinetics of the molecular recognition events underlying photoswitchable ligands remain poorly understood.[6–8] Therefore, we used the desmethyl analogue **3e** to prepare radiolabeled **3f** (i.e. [^{3}H]**3f**) as a means to directly study H_3R-ligand binding kinetics. Specifically, the availability of **3e** allowed the use of a previously described CT_3 incorporation using CT_3-nosylate[55,56] (Scheme 2) to prepare [^{3}H]**3f.** To our knowledge, *trans*-[^{3}H]**3f** is the first radiolabeled photoswitchable ligand ever reported. Purity and light-dependent switching of the radiolabeled compound were confirmed by liquid chromatography and the recording of [^{3}H]-chromatograms using a β-scintillation HPLC detector. *Trans*-[^{3}H]**3f** contained 2% *cis* isomer, while after 10 min of irradiation with 365 nm LED light (10 V, 2 mW), 96% *cis* isomer was obtained (Figure S9), yielding similarly high PSS_{cis} values as observed for non-labeled **3f** (Table 1).

Scheme 2. Synthesis of [^{3}H]**3f.** [a]

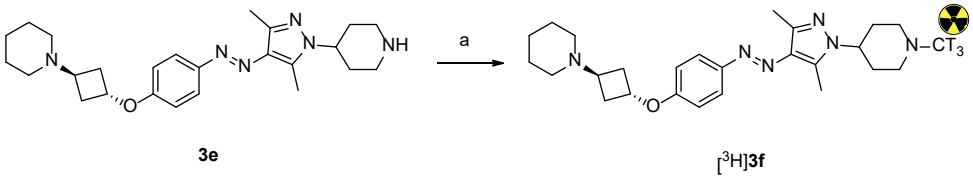

3e [^{3}H]**3f**

[a]Reagents and conditions used: (a) [^{3}H]methyl nosylate, MeCN, 70 °C, 15 min.

In saturation binding studies, *trans*-[^{3}H]**3f** binds H_3R with sub-nanomolar affinity (pK_d = 9.2 ± 0.0, Figure 4D, Table 2) and exhibits low non-specific binding. The binding of *trans*-[^{3}H]**3f** to H_3R is effectively abrogated by the reference H_3R ligands clobenpropit, thioperamide and immepip (Figure 4E). Both unlabeled **3f** isomers also fully abrogate *trans*-[^{3}H]**3f** binding to H_3R, with *trans*-**3f** (pK_i = 9.0 ± 0.1) being considerably more effective than **3f**-PSS_{cis} (pK_i = 7.7 ± 0.0, Figure 4E). In kinetic experiments, the binding of 0.5 nM *trans*-[^{3}H]**3f** to H_3R reaches equilibrium at 15 min (Figure 4F). Bound *trans*-[^{3}H]**3f** dissociates from H_3R with a dissociation half-life ($t_{½}$) of 4.9 ± 0.4 min upon addition of an excess of clobenpropit (10 µM). This results in k_{off} = 0.15 ± 0.02 min^{-1} and k_{on} = 129 ± 28 10^6 M^{-1} min^{-1} for *trans*-[^{3}H]**3f**. Compared to *trans*-[^{3}H]**3f**, kinetic H_3R binding experiments with [^{3}H]**3f**-PSS_{cis} (obtained by pre-illuminating *trans*-[^{3}H]**3f**) revealed a 10-fold lower k_{on} value (13 ± 6 10^6 M^{-1} min^{-1}) but a similar k_{off} (0.11 ± 0.00 min^{-1}) value (Table 2). The calculated kinetic affinities for *trans*-[^{3}H]**3f** and [^{3}H]**3f**-PSS_{cis} (pK_{dkin} = k_{off}/k_{on} = 8.9 ± 0.2 and 7.9 ± 0.3, respectively) correspond well to the affinities obtained in equilibrium saturation and competition binding assays (pK_d = 9.2 ± 0.0 and pK_i = 7.6 ± 0.2, respectively; Table 2).

Table 2. Kinetic parameters of [^{3}H]**3f** binding to H_3R as determined in association and dissociation radioligand binding experiments, calculated kinetic affinities and affinities obtained from binding experiments.

State	k_{on} (10^6 M^{-1} min^{-1})	k_{off} (min^{-1})	$t_{½}$ (min)[a]	$pK_{d(kin)}$[b]	pK_d or pK_i
Trans	129 ± 28	0.15 ± 0.02 (clobenpropit)	4.9 ± 0.4	8.9 ± 0.2	9.2 ± 0.0[c]
		1.12 ± 0.28 (365 nm light)	0.8 ± 0.2		
PSS_{cis}	13 ± 6	0.11 ± 0.00 (clobenpropit)	6.2 ± 0.2	7.9 ± 0.3	7.6 ± 0.2[d]

Data are mean ± SEM of at least *n* = 3 independent experiments. [a]Dissociation $t_{1/2}$ = ln 2/k_{off} [b]$pK_{d(kin)}$ = k_{off}/k_{on} [c]pK_d obtained in saturation binding experiments [d]pK_i of unlabeled PSS_{cis}.

Next, we probed if H_3R binding of *trans*-[^{3}H]**3f** could be modulated by illumination by *in situ* photoswitching (Figure 4G). Exposure of pre-bound *trans*-[^{3}H]**3f** to 365 nm light resulted in a rapid dissociation from H_3R to approximately 0% (Figure 4G, magenta), even though no competitor is present. This is consistent with fast quantitative photoswitching of *trans*-[^{3}H]**3f**

to [^{3}H]**3f**-PSS$_{cis}$, which will not bind H_3R at this concentration due to its lower affinity. Subsequent exposure to 500 nm green light re-established H_3R binding of *trans*-[^{3}H]**3f** over time (Figure 4G, green), confirming successful back-switching of the low-affinity [^{3}H]**3f**-PSS$_{cis}$ state to high-affinity *trans*-[^{3}H]**3f**. Comparing the kinetics of clobenpropit-induced dissociation of *trans*-[^{3}H]**3f** and [^{3}H]**3f**-PSS$_{cis}$ as well as the 365 nm light-induced dissociation of *trans*-[^{3}H]**3f** reveals a remarkable difference in dissociation kinetics (Figure 4H, Table 2). Photoswitching of pre-bound *trans*-[^{3}H]**3f** by 365 nm illumination results in 6.2-fold faster dissociation kinetics ($t_{½}$ = 0.8 ± 0.2 min) as compared to the dissociation of dark *trans*-[^{3}H]**3f** ($t_{½}$ = 4.9 ± 0.4 min) and [^{3}H]**3f**-PSS$_{cis}$ ($t_{½}$ = 6.2 ± 0.4 min) (Table 2). Similar findings concerning light-dependent dissociation rates of photoswitchable negative allosteric modulators of the Class C GPCR $mGlu_5$ have been reported using a mass spectrometry binding assay.[6] Our kinetic data exclude the dissociation process from being governed by photoswitching of unbound *trans*-[^{3}H]**3f** in solution and subsequent readjustment of the binding equilibrium.

This photochemically induced kinetic pattern is reminiscent of the known effects of retinal confinement within a photoresponsive protein.[57–60] Retinal is a naturally occurring photoswitchable chromophore that is covalently linked to opsin proteins via a Schiff's base to a lysine residue in TM7. Upon illumination retinal is switched from its 11-*cis*-retinal configuration to an all-*trans*-retinal form. This configurational change of the chromophore subsequently results in GPCR protein activation and triggers a cascade of biochemical events that convert light into electrical signals for vision.[61] Retinal isomerization occurs more rapidly and with greater stereoselectivity within the binding pocket of the protein host, achieving a higher quantum yield compared to when it occurs in solution.[58,59] However, for synthetic photoswitchable compounds, including azobenzene-based ones, confinement can affect their photochemical behavior less advantegously.[60,62] As suggested for azobenzene-based ligands for an allosteric site of $mGluR_5$,[6] our kinetic data provide evidence that **3f** is switching when bound to H_3R. Specifically, our modeling studies (Figure 3) suggest that the photoswitchable moiety of **3f** sits within the EBP surrounded by flexible extracellular loops, indicating sufficient conformational flexibility to allow for this switching to occur, although the constraints of the interactions of **3f** within the protein likely still reduce the efficiency of **3f** to undergo a *trans-cis* isomerization compared to in solution. For an azobenzene-based A_{2A} receptor ligand, it has been proposed based on detailed spectroscopy studies that the overall outcome (efficiency and rate) of switching in the protein pocket depends on the isomerization of the azo moiety, reorientation of the phenyl group, and the potential for longer-lived excited states due to protein-coupled motion.[7] It was also recently shown, using time-resolved crystallography, that related photoswitchable A_{2A} receptor ligands can be switched in the protein binding pocket and that intermediate states of ligand dissociation can be resolved.[63] In this system, confinement of photoswitchable ligands by protein binding reduces the quantum efficiency of photoisomerization.[63] Although we focused on binding kinetics and not on photoswitching kinetics, it is likely that the factors uncovered in the A_{2A} studies will also be involved in our case and will collectively manifest themselves in different binding kinetics. Indeed, the same

A_{2A} study[63] highlighted that photoswitching of a bound ligand can lead to conformational changes in the protein and, in line with this finding, we hypothesize that photoswitching of **3f** in the protein binding pocket provides a metastable *cis*-**3f**/H_3R complex from which *cis*-**3f** is expelled faster than pre-formed *cis*-**3f** is expelled in the dark. As such, our data contribute to the emerging conceptual framework on the effect of protein confinement on photoswitchable ligand behavior, that is needed for the future design of optimal photoswitchable ligands.

Conclusion

We have designed and synthesized a second-generation photoswitchable antagonist series for an archetypical GPCR (H_3R), incorporating the arylazopyrazole as a photoswitchable moiety. Classical limitations of azobenzene-based photoswitchable ligands were efficiently addressed with the new series enhancing aqueous solubility, enabling the use of green light to reach PSS_{trans}, and boosting high PSS values both ways. Pharmacological parameters such as the overall affinity and the affinity shift were improved from template **1** to key compound VUF26063 (**3f**). Ligand **3f** exhibits a 50-fold affinity shift between its isomers and is a high-affinity, sub-nanomolar *trans*-on antagonist for H_3R that can reversibly modulate H_3R-dependent signaling in living cells in a light-dependent manner. Capitalizing on a readily accessible synthetic growth vector in **3f**, we prepared the first radiolabeled photoswitchable ligand [^{3}H]VUF26063 ([^{3}H]**3f**). This compound was used to characterize the kinetic aspects of receptor-ligand binding events underlying the dynamic modulation of receptor signaling and indicated that the *trans* isomer undergoes light-induced isomerization in the H_3R EBP. Our study highlights the potential of detailed kinetic characterization of the binding process for photoswitchable ligands and could aid in a better prediction of the spatiotemporal effects of protein modulation by photoswitchable small molecules.

Acknowledgements

We thank Hans Custers for acquiring HRMS analyses, Elwin Janssen for NMR assistance, Andrea van de Stolpe for support with the photochemistry equipment, and Maurice Buzink for help with culturing of Nluc-H_2R stable cell lines.

References

(1) Velema, W. A.; Szymanski, W.; Feringa, B. L. Photopharmacology: Beyond Proof of Principle. *J. Am. Chem. Soc.* 2**014**, *136* (6), 2178–2191. https://doi.org/10.1021/ja413063e.

(2) Fuchter, M. J. On the Promise of Photopharmacology Using Photoswitches: A Medicinal Chemist's Perspective. *J. Med. Chem.* **2020**, *63* (20), 11436–11447. https://doi.org/10.1021/acs.jmedchem.0c00629.

(3) Liu, Y.; Wang, T.; Wang, W. Photopharmacology and Photoresponsive Drug Delivery. *Chem. Soc. Rev.* **2025**, ASAP. https://doi.org/10.1039/d5cs00125k.

(4) Hüll, K.; Morstein, J.; Trauner, D. In Vivo Photopharmacology. *Chem. Rev.* **2018**, *118* (21), 10710–10747. https://doi.org/10.1021/acs.chemrev.8b00037.

(5) Kobauri, P.; Dekker, F. J.; Szymanski, W.; Feringa, B. L. Rational Design in Photopharmacology with Molecular Photoswitches. *Angew. Chem. Int. Ed.* **2023**, *62* (30), e202300681. https://doi.org/10.1002/anie.202300681.

(6) Ricart-Ortega, M.; Berizzi, A. E.; Pereira, V.; Malhaire, F.; Catena, J.; Font, J.; Gómez-Santacana, X.; Munõz, L.; Zussy, C.; Serra, C.; Rovira, X.; Goudet, C.; Llebaria, A. Mechanistic Insights into Light-Driven Allosteric Control of GPCR Biological Activity. *ACS Pharmacol. Transl. Sci.* **2020**, *3* (5), 883–895. https://doi.org/10.1021/acsptsci.0c00054.

(7) Saßmannshausen, T.; Glover, H.; Trabuco, M.; Neidhart, W.; Cheng, R.; Hennig, M.; Slavov, C.; Standfuss, J.; Wachtveitl, J. Kinetic Basis for the Design of Azobenzene-Based Photoswitchable A2a Adenosine Receptor Ligands. *J. Am. Chem. Soc.* **2024**, *146* (47), 32670–32677. https://doi.org/10.1021/jacs.4c11995.

(8) Gu, X.; Yuan, H.; Zhao, W.; Sun, N.; Yan, W.; Jiang, C.; He, Y.; Liu, H.; Cheng, J.; Guo, D. Optical-Controlled Kinetic Switch: Fine-Tuning of the Residence Time of an Antagonist Binding to the Vasopressin V2 Receptor in In Vitro, Ex Vivo, and In Vivo Models of ADPKD. *J. Med. Chem.* **2023**, *66* (2), 1454–1466. https://doi.org/10.1021/acs.jmedchem.2c01625.

(9) Lorente, J. S.; Sokolov, A. V; Ferguson, G.; Schiöth, H. B.; Hauser, A. S.; Gloriam, D. E. GPCR Drug Discovery: New Agents, Targets and Indications. *Nat. Rev. Drug Discov.* **2025**, ASAP. https://doi.org/10.1038/s41573-025-01139-y.

(10) Ricart-Ortega, M.; Font, J.; Llebaria, A. GPCR Photopharmacology. *Mol. Cell. Endocrinol.* **2019**, *488*, 36–51. https://doi.org/10.1016/j.mce.2019.03.003.

(11) Panarello, S.; Rovira, X.; Llebaria, A.; Gómez-Santacana, X. Photopharmacology of G - Protein-Coupled Receptors. In *Molecular Photoswitches*; John Wiley & Sons, Ltd, **2022**; Vol. 2–2, pp 921–944. https://doi.org/10.1002/9783527827626.ch37.

(12) Wijtmans, M.; Josimovic, I.; Vischer, H. F.; Leurs, R. Optical Control of Class A G Protein-Coupled Receptors with Photoswitchable Ligands. *Curr. Opin. Pharmacol.* **2022**, *63*, 102192. https://doi.org/10.1016/j.coph.2022.102192.

(13) Berizzi, A. E.; Goudet, C. Strategies and Considerations of G-Protein-Coupled Receptor Photopharmacology. *Adv. Pharmacol.* **2020**, *88*, 143–172. https://doi.org/10.1016/bs.apha.2019.12.001.

(14) Leurs, R.; Bakker, R. A.; Timmerman, H.; de Esch, I. J. P. The Histamine H3 Receptor: From Gene Cloning to H3 Receptor Drugs. *Nat. Rev. Drug Discov.* **2005**, *4* (2), 107–120. https://doi.org/10.1038/nrd1631.
(15) Panula, P.; Chazot, P. L.; Cowart, M.; Gutzmer, R.; Leurs, R.; Liu, W. L. S.; Stark, H.; Thurmond, R. L.; Haas, H. L. International Union of Basic and Clinical Pharmacology. XCVIII. Histamine Receptors. *Pharmacol. Rev.* **2015**, *67* (3), 601–655. https://doi.org/10.1124/pr.114.010249.
(16) Cheng, L.; Liu, J.; Chen, Z. The Histaminergic System in Neuropsychiatric Disorders. *Biomolecules* **2021**, *11* (9), 1345. https://doi.org/10.3390/biom11091345.
(17) Harwell, V.; Fasinu, P. S. Pitolisant and Other Histamine-3 Receptor Antagonists—An Update on Therapeutic Potentials and Clinical Prospects. *Medicines* **2020**, *7* (9), 55. https://doi.org/10.3390/medicines7090055.
(18) Sarfraz, N.; Okuampa, D.; Hansen, H.; Alvarez, M.; Cornett, E. M.; Kakazu, J.; Kaye, A. M.; Kaye, A. D. Pitolisant, a Novel Histamine-3 Receptor Competitive Antagonist, and Inverse Agonist, in the Treatment of Excessive Daytime Sleepiness in Adult Patients with Narcolepsy. *Health Psychol. Res.* **2022**, *10* (2), 34222. https://doi.org/10.52965/001c.34222.
(19) Thorpy, M. J.; Bogan, R. K. Update on the Pharmacologic Management of Narcolepsy: Mechanisms of Action and Clinical Implications. *Sleep Med.* **2020**, *68*, 97–109. https://doi.org/10.1016/j.sleep.2019.09.001.
(20) Meskill, G. J.; Davis, C. W.; Zarycranski, D.; Doliba, M.; Schwartz, J. C.; Dayno, J. M. Clinical Impact of Pitolisant on Excessive Daytime Sleepiness and Cataplexy in Adults With Narcolepsy: An Analysis of Randomized Placebo-Controlled Trials. *CNS Drugs* **2022**, *36* (1), 61–69. https://doi.org/10.1007/s40263-021-00886-x.
(21) Hauwert, N. J.; Mocking, T. A. M.; Da Costa Pereira, D.; Kooistra, A. J.; Wijnen, L. M.; Vreeker, G. C. M.; Verweij, E. W. E.; De Boer, A. H.; Smit, M. J.; De Graaf, C.; Vischer, H. F.; De Esch, I. J. P.; Wijtmans, M.; Leurs, R. Synthesis and Characterization of a Bidirectional Photoswitchable Antagonist Toolbox for Real-Time GPCR Photopharmacology. *J. Am. Chem. Soc.* **2018**, *140* (12), 4232–4243. https://doi.org/10.1021/jacs.7b11422.
(22) Hauwert, N. J.; Mocking, T. A. M.; Da Costa Pereira, D.; Lion, K.; Huppelschoten, Y.; Vischer, H. F.; De Esch, I. J. P.; Wijtmans, M.; Leurs, R. A Photoswitchable Agonist for the Histamine H3 Receptor, a Prototypic Family A G-Protein-Coupled Receptor. *Angew. Chem. Int. Ed.* **2019**, *58* (14), 4531–4535. https://doi.org/10.1002/anie.201813110.
(23) Bléger, D.; Hecht, S. Visible-Light-Activated Molecular Switches. *Angew. Chem. Int. Ed.* **2015**, *54* (39), 11338–11349. https://doi.org/10.1002/anie.201500628.
(24) Stolik, S.; Delgado, J. A.; Pérez, A.; Anasagasti, L. Measurement of the Penetration Depths of Red and near Infrared Light in Human "Ex Vivo" Tissues. *J. Photochem. Photobiol. B* **2000**, *57* (2–3), 90–93. https://doi.org/10.1016/S1011-1344(00)00082-8.
(25) Kunzi-Rapp, K. Photodynamic Therapy in Dermatology. *J. Am. Acad. Dermatol.* **2000**, *42* (3), 389–413. https://doi.org/10.1016/S0190-9622(00)90209-3.
(26) Calbo, J.; Weston, C. E.; White, A. J. P.; Rzepa, H. S.; Contreras-García, J.; Fuchter, M. J. Tuning Azoheteroarene Photoswitch Performance through Heteroaryl Design. *J. Am. Chem. Soc.* **2017**, *139* (3), 1261–1274. https://doi.org/10.1021/jacs.6b11626.
(27) Weston, C. E.; Richardson, R. D.; Haycock, P. R.; White, A. J. P.; Fuchter, M. J. Arylazopyrazoles: Azoheteroarene Photoswitches Offering Quantitative Isomerization

and Long Thermal Half-Lives. *J. Am. Chem. Soc.* **2014**, *136* (34), 11878–11881. https://doi.org/10.1021/ja505444d.

(28) Mukherjee, A.; Seyfried, M. D.; Ravoo, B. J. Azoheteroarene and Diazocine Molecular Photoswitches: Self-Assembly, Responsive Materials and Photopharmacology. *Angew. Chem. Int. Ed.* **2023**, *62* (42), e202304437. https://doi.org/10.1002/anie.202304437.

(29) Dang, T.; Zhang, Z. Y.; Li, T. Visible-Light-Activated Heteroaryl Azoswitches: Toward a More Colorful Future. *J. Am. Chem. Soc.* **2024**, *146* (29), 19609–19620. https://doi.org/10.1021/jacs.4c03135.

(30) Berlin, M.; Boyce, C. W.; De Lera Ruiz, M. Histamine H3 Receptor as a Drug Discovery Target. *J. Med. Chem.* **2011**, *54* (1), 26–53. https://doi.org/10.1021/jm100064d.

(31) Celanire, S.; Wijtmans, M.; Talaga, P.; Leurs, R.; De Esch, I. J. P. Keynote Review: Histamine H3 Receptor Antagonists Reach out for the Clinic. *Drug Discov. Today* **2005**, *10* (23–24), 1613–1627. https://doi.org/10.1016/S1359-6446(05)03625-1.

(32) Hancock, A. A.; Diehl, M. S.; Faghih, R.; Bush, E. N.; Krueger, K. M.; Krishna, G.; Miller, T. R.; Wilcox, D. M.; Nguyen, P.; Pratt, J. K.; Cowart, M. D.; Esbenshade, T. A.; Jacobson, P. B. In Vitro Optimization of Structure Activity Relationships of Analogues of A-331440 Combining Radioligand Receptor Binding Assays and Micronucleus Assays of Potential Antiobesity Histamine H3 Receptor Antagonists. *Basic Clin. Pharmacol. Toxicol.* **2004**, *95* (3), 144–152. https://doi.org/10.1111/j.1742-7843.2004.950307.x.

(33) Roche, O.; Rodríguez Sarmiento, R. M. A New Class of Histamine H3 Receptor Antagonists Derived from Ligand Based Design. *Bioorg. Med. Chem. Lett.* **2007**, *17* (13), 3670–3675. https://doi.org/10.1016/j.bmcl.2007.04.056.

(34) Apodaca, R.; Dvorak, C. A.; Xiao, W.; Barbier, A. J.; Boggs, J. D.; Wilson, S. J.; Lovenberg, T. W.; Carruthers, N. I. A New Class of Diamine-Based Human Histamine H3 Receptor Antagonists: 4-(Aminoalkoxy)Benzylamines. *J. Med. Chem.* **2003**, *46* (18), 3938–3944. https://doi.org/10.1021/jm030185v.

(35) Tang, K.; Wang, S.; Gao, W.; Song, Y.; Yu, B. Harnessing the Cyclization Strategy for New Drug Discovery. *Acta Pharm. Sin. B* **2022**, *12* (12), 4309–4326. https://doi.org/10.1016/j.apsb.2022.09.022.

(36) Dvorak, C. A.; Apodaca, R.; Barbier, A. J.; Berridge, C. W.; Wilson, S. J.; Boggs, J. D.; Xiao, W.; Lovenberg, T. W.; Carruthers, N. I. 4-Phenoxypiperidines: Potent, Conformationally Restricted, Non-Imidazole Histamine H3 Antagonists. *J. Med. Chem.* **2005**, *48* (6), 2229–2238. https://doi.org/10.1021/jm049212n.

(37) Black, L. A.; Liu, H.; Diaz, G. J.; Fox, G. B.; Browman, K. E.; Wetter, J.; Marsh, K. C.; Miller, T. R.; Esbenshade, T. A.; Brioni, J.; Cowart, M. D. Minimization of Potential HERG Liability in Histamine H3 Receptor Antagonists. *Inflammation Research* **2008**, *57* (Suppl 1), 45–46. https://doi.org/10.1007/s00011-007-0622-2.

(38) Medhurst, A. D.; Atkins, A. R.; Beresford, I. J.; Brackenborough, K.; Briggs, M. A.; Calver, A. R.; Cilia, J.; Cluderay, J. E.; Crook, B.; Davis, J. B.; Davis, R. K.; Davis, R. P.; Dawson, L. A.; Foley, A. G.; Gartlon, J.; Gonzalez, M. I.; Heslop, T.; Hirst, W. D.; Jennings, C.; Jones, D. N. C.; Lacroix, L. P.; Martyn, A.; Ociepka, S.; Ray, A.; Regan, C. M.; Roberts, J. C.; Schogger, J.; Southam, E.; Stean, T. O.; Trail, B. K.; Upton, N.; Wadsworth, G.; Wald, J. A.; White, T.; Witherington, J.; Woolley, M. L.; Worby, A.; Wilson, D. M. GSK189254, a Novel H3 Receptor Antagonist That Binds to Histamine H3 Receptors in Alzheimer's Disease Brain and Improves Cognitive Performance in

Preclinical Models. *J. Pharmacol. Exp. Ther.* **2007**, *321* (3), 1032–1045. https://doi.org/10.1124/jpet.107.120311.

(39) Wijtmans, M.; Denonne, F.; Célanire, S.; Gillard, M.; Hulscher, S.; Delaunoy, C.; Van Houtvin, N.; Bakker, R. A.; Defays, S.; Gérard, J.; Grooters, L.; Hubert, D.; Timmerman, H.; Leurs, R.; Talaga, P.; De Esch, I. J. P.; Provins, L. Histamine H 3 Receptor Ligands with a 3-Cyclobutoxy Motif: A Novel and Versatile Constraint of the Classical 3-Propoxy Linker. *Medchemcomm* **2010**, *1* (1), 39–44. https://doi.org/10.1039/C0MD00056F.

(40) Volarić, J.; Szymanski, W.; Simeth, N. A.; Feringa, B. L. Molecular Photoswitches in Aqueous Environments. *Chem. Soc. Rev.* **2021**, *50* (22), 12377–12449. https://doi.org/10.1039/d0cs00547a.

(41) Peng, X.; Yang, L.; Liu, Z.; Lou, S.; Mei, S.; Li, M.; Chen, Z.; Zhang, H. Structural Basis for Recognition of Antihistamine Drug by Human Histamine Receptor. *Nature Communications 2022 13:1* **2022**, *13* (1), 1–9. https://doi.org/10.1038/s41467-022-33880-y.

(42) Zhang, X.; Liu, G.; Zhong, Y.-N.; Zhang, R.; Yang, C.-C.; Niu, C.; Pu, X.; Sun, J.; Zhang, T.; Yang, L.; Zhang, C.; Li, X.; Shen, X.; Xiao, P.; Sun, J.-P.; Gong, W. Structural Basis of Ligand Recognition and Activation of the Histamine Receptor Family. *Nat. Commun.* **2024**, *15* (1), 1–16. https://doi.org/10.1038/s41467-024-52585-y.

(43) Stricker, L.; Fritz, E. C.; Peterlechner, M.; Doltsinis, N. L.; Ravoo, B. J. Arylazopyrazoles as Light-Responsive Molecular Switches in Cyclodextrin-Based Supramolecular Systems. *J. Am. Chem. Soc.* **2016**, *138* (13), 4547–4554. https://doi.org/10.1021/jacs.6b00484.

(44) Hoelke, B.; Gieringer, S.; Arlt, M.; Saal, C. Comparison of Nephelometric, UV-Spectroscopic, and HPLC Methods for High-Throughput Determination of Aqueous Drug Solubility in Microtiter Plates. *Anal. Chem.* **2009**, *81* (8), 3165–3172. https://doi.org/10.1021/ac9000089.

(45) Bevan, C. D.; Lloyd, R. S. A High-Throughput Screening Method for the Determination of Aqueous Drug Solubility Using Laser Nephelometry in Microtiter Plates. *Anal. Chem.* **2000**, *72* (8), 1781–1787. https://doi.org/10.1021/ac9912247.

(46) Sassano, M. F.; Doak, A. K.; Roth, B. L.; Shoichet, B. K. Colloidal Aggregation Causes Inhibition of G Protein-Coupled Receptors. *J. Med. Chem.* **2013**, *56* (6), 2406–2414. https://doi.org/10.1021/jm301749y.

(47) Ahmed, Z.; Siiskonen, A.; Virkki, M.; Priimagi, A. Controlling Azobenzene Photoswitching through Combined Ortho-Fluorination and -Amination. *Chemical Communications* **2017**, *53* (93), 12520–12523. https://doi.org/10.1039/C7CC07308A.

(48) Wieland, K.; Bongers, G.; Yamamoto, Y.; Hashimoto, T.; Yamatodani, A.; Menge, W. M. B. P.; Timmerman, H.; Lovenberg, T. W.; Leurs, R. Constitutive Activity of Histamine H 3 Receptors Stably Expressed in SK-N-MC Cells: Display of Agonism and Inverse Agonism by H 3 Antagonists ABSTRACT Agonist-Independent Activity of G-Protein-Coupled Receptor. *J. Pharmacol. Exp. Ther.* **2001**, *299* (3), 908–914. https://doi.org/10.1016/S0022-3565(24)29209-0.

(49) Clark, E. A.; Hill, S. J. Sensitivity of Histamine H3 Receptor Agonist-Stimulated [35S]GTPγ[S]Binding to Pertussis Toxin. *Eur. J. Pharmacol.* **1996**, *296* (2), 223–225. https://doi.org/10.1016/0014-2999(95)00800-4.

(50) Kitbunnadaj, R.; Zuiderveld, O. P.; Christophe, B.; Hulscher, S.; Menge, W. M. P. B.; Gelens, E.; Snip, E.; Bakker, R. A.; Celanire, S.; Gillard, M.; Talaga, P.; Timmerman, H.;

Leurs, R. Identification of 4-(1H-Imidazol-4(5)-Ylmethyl)Pyridine (Immethridine) as a Novel, Potent, and Highly Selective Histamine H3 Receptor Agonist. *J. Med. Chem.* **2004**, *47* (10), 2414–2417. https://doi.org/10.1021/jm049932u.

(51) Dixon, A. S.; Schwinn, M. K.; Hall, M. P.; Zimmerman, K.; Otto, P.; Lubben, T. H.; Butler, B. L.; Binkowski, B. F.; MacHleidt, T.; Kirkland, T. A.; Wood, M. G.; Eggers, C. T.; Encell, L. P.; Wood, K. V. NanoLuc Complementation Reporter Optimized for Accurate Measurement of Protein Interactions in Cells. *ACS Chem. Biol.* **2016**, *11* (2), 400–408. https://doi.org/10.1021/acschembio.5b00753.

(52) Kolarski, D.; Miró-Vinyals, C.; Sugiyama, A.; Srivastava, A.; Ono, D.; Nagai, Y.; Iida, M.; Itami, K.; Tama, F.; Szymanski, W.; Hirota, T.; Feringa, B. L. Reversible Modulation of Circadian Time with Chronophotopharmacology. *Nat. Commun.* **2021**, *12* (1), 1–12. https://doi.org/10.1038/s41467-021-23301-x.

(53) Wirth, U.; Erl, J.; Azzam, S.; Höring, C.; Skiba, M.; Singh, R.; Hochmuth, K.; Keller, M.; Wegener, J.; König, B. Monitoring the Reversibility of GPCR Signaling by Combining Photochromic Ligands with Label-Free Impedance Analysis. *Angew. Chem. Int. Ed.* **2023**, *135* (21), e202215547. https://doi.org/10.1002/anie.202215547.

(54) England, C. G.; Ehlerding, E. B.; Cai, W. NanoLuc: A Small Luciferase Is Brightening Up the Field of Bioluminescence. *Bioconjug. Chem.* **2016**, *27* (5), 1175–1187. https://doi.org/10.1021/acs.bioconjchem.6b00112.

(55) Pounds, S.; Hickey, M. J.; Kingston, L. P.; Mather, A. N.; Wilkinson, D. J.; Sidorov, G. V.; Zverkov, Yu. B.; Myasoedov, N. F.; Karpenko, I. L.; Shirokova, E. A.; Yanvarev, D. M.; Yasko, M. V.; Skoblov, Yu. S.; Susan, A. B.; Myasoedov, N. F.; Nagaev, I. Y.; Shevchenko, V. P.; Susan, A. B.; Rotert, G.; Krüger, J.; Fels, G.; Wuest, F.; Mäding, P.; Zessin, J.; Pleiß, U.; Wüst, F.; Bloom, A. J.; Derdau, V.; Oekonomopulos, R.; Schubert, G.; Andres, H.; Burtscher, P.; Metz, Y.; Moenius, Th.; Kaegi, F.; Metz, Y.; Rodriguez, I.; Ruetsch, R.; Janssen, C. G. M.; Verreet, B.; Lenoir, H. A. C.; Thijssen, J. B. A.; Stuerm, R. P.; Krins, A.; Rausch, E.; Breyer, M.; Hucke, K.; Gaefke, D.; Schmeer, K. 11th Conference of the Central European Division e.V. of the International Isotope Society. *J. Labelled Comp. Radiopharm.* **2004**, *47* (4), 243–288. https://doi.org/10.1002/jlcr.814.

(56) Filer, C. N. Synthesis and Characterization of Tritium-Labelled Substances. *Applied Radiation and Isotopes* **2018**, *137*, 261–272. https://doi.org/10.1016/j.apradiso.2018.02.029.

(57) Nogly, P.; Weinert, T.; James, D.; Carbajo, S.; Ozerov, D.; Furrer, A.; Gashi, D.; Borin, V.; Skopintsev, P.; Jaeger, K.; Nass, K.; Båth, P.; Bosman, R.; Koglin, J.; Seaberg, M.; Lane, T.; Kekilli, D.; Brünle, S.; Tanaka, T.; Wu, W.; Milne, C.; White, T.; Barty, A.; Weierstall, U.; Panneels, V.; Nango, E.; Iwata, S.; Hunter, M.; Schapiro, I.; Schertler, G.; Neutze, R.; Standfuss, J. Retinal Isomerization in Bacteriorhodopsin Captured by a Femtosecond X-Ray Laser. *Science.* **2018**, *361* (6398). https://doi.org/10.1126/science.aat0094.

(58) Freedman, K. A.; Becker, R. S. Comparative Investigation of the Photoisomerization of the Protonated and Unprotonated N-Butylamine Schiff Bases of 9-Cis-, 11-Cis-, 13-Cis-, and All-Trans-Retinals. *J. Am. Chem. Soc.* **1986**, *108* (6), 1245–1251. https://doi.org/10.1021/ja00266a020.

(59) Hamm, P.; Zurek, M.; Röschinger, T.; Patzelt, H.; Oesterhelt, D.; Zinth, W. Femtosecond Spectroscopy of the Photoisomerisation of the Protonated Schiff Base

of All-Trans Retinal. *Chem. Phys. Lett.* **1996**, *263* (5), 613–621. https://doi.org/10.1016/s0009-2614(96)01269-9.

(60) Grommet, A. B.; Lee, L. M.; Klajn, R. Molecular Photoswitching in Confined Spaces. *Acc. Chem. Res.* **2020**, *53* (11), 2600–2610. https://doi.org/10.1021/acs.accounts.0c00434.

(61) Hofmann, K. P.; Lamb, T. D. Rhodopsin, Light-Sensor of Vision. *Prog. Retin. Eye Res.* **2023**, *93*, 101116. https://doi.org/10.1016/j.preteyeres.2022.101116.

(62) Gemen, J.; Church, J. R.; Ruoko, T. P.; Durandin, N.; Białek, M. J.; Weißenfels, M.; Feller, M.; Kazes, M.; Odaybat, M.; Borin, V. A.; Kalepu, R.; Diskin-Posner, Y.; Oron, D.; Fuchter, M. J.; Priimagi, A.; Schapiro, I.; Klajn, R. Disequilibrating Azobenzenes by Visible-Light Sensitization under Confinement. *Science.* **2023**, *381* (6664). https://doi.org/10.1126/science.adh9059.

(63) Glover, H.; Saßmannshausen, T.; Bertrand, Q.; Trabuco, M.; Slavov, C.; Bacchin, A.; Andres, F.; Kondo, Y.; Stipp, R.; Wranik, M.; Khusainov, G.; Carrillo, M.; Kekilli, D.; Nan, J.; Gonzalez, A.; Cheng, R.; Neidhart, W.; Weinert, T.; Leonarski, F.; Dworkowski, F.; Kepa, M.; Wachtveitl, J.; Hennig, M.; Standfuss, J. Photoswitch Dissociation from a G Protein-Coupled Receptor Resolved by Time-Resolved Serial Crystallography. *Nat. Commun.* **2024**, *15* (1), 10837. https://doi.org/10.1038/s41467-024-55109-w.

(64) Peng, X.; Yang, L.; Liu, Z.; Lou, S.; Mei, S.; Li, M.; Chen, Z.; Zhang, H. Structural Basis for Recognition of Antihistamine Drug by Human Histamine Receptor. *Nat. Commun.* **2022**, *13* (1), 1–9. https://doi.org/10.1038/s41467-022-33880-y.

(65) Grätz, L.; Tropmann, K.; Bresinsky, M.; Müller, C.; Bernhardt, G.; Pockes, S. NanoBRET Binding Assay for Histamine H2 Receptor Ligands Using Live Recombinant HEK293T Cells. *Sci. Rep.* **2020**, *10* (1), 1–10. https://doi.org/10.1038/s41598-020-70332-3.

(66) Bosma, R.; Wang, Z.; Kooistra, A. J.; Bushby, N.; Kuhne, S.; Van Den Bor, J.; Waring, M. J.; De Graaf, C.; De Esch, I. J.; Vischer, H. F.; Sheppard, R. J.; Wijtmans, M.; Leurs, R. Route to Prolonged Residence Time at the Histamine H1 Receptor: Growing from Desloratadine to Rupatadine. *J. Med. Chem.* **2019**, *62* (14), 6630–6644. https://doi.org/10.1021/acs.jmedchem.9b00447.

(67) Dixon, A. S.; Schwinn, M. K.; Hall, M. P.; Zimmerman, K.; Otto, P.; Lubben, T. H.; Butler, B. L.; Binkowski, B. F.; MacHleidt, T.; Kirkland, T. A.; Wood, M. G.; Eggers, C. T.; Encell, L. P.; Wood, K. V. NanoLuc Complementation Reporter Optimized for Accurate Measurement of Protein Interactions in Cells. *ACS Chem. Biol.* **2016**, *11* (2), 400–408. https://doi.org/10.1021/acschembio.5b00753.

(68) Yung-Chi, C.; Prusoff, W. H. Relationship between the Inhibition Constant (KI) and the Concentration of Inhibitor Which Causes 50 per Cent Inhibition (I50) of an Enzymatic Reaction. *Biochem. Pharmacol.* **1973**, *22* (23), 3099–3108. https://doi.org/10.1016/0006-2952(73)90196-2.

(69) Webb, B.; Sali, A. Comparative Protein Structure Modeling Using MODELLER. *Curr. Protoc. Bioinformatics* **2016**, *54* (1), 5.6.1-5.6.37. https://doi.org/10.1002/cpbi.3.

(70) Shen, Q.; Tang, X.; Wen, X.; Cheng, S.; Xiao, P.; Zang, S. K.; Shen, D. D.; Jiang, L.; Zheng, Y.; Zhang, H.; Xu, H.; Mao, C.; Zhang, M.; Hu, W.; Sun, J. P.; Zhang, Y.; Chen, Z. Molecular Determinant Underlying Selective Coupling of Primary G-Protein by Class A GPCRs. *Advanced Science* **2024**, *11* (23), 2310120. https://doi.org/10.1002/advs.202310120.

(71) Miller-Gallacher, J. L.; Nehmé, R.; Warne, T.; Edwards, P. C.; Schertler, G. F. X.; Leslie, A. G. W.; Tate, C. G. The 2.1 Å Resolution Structure of Cyanopindolol-Bound B1-

Adrenoceptor Identifies an Intramembrane Na+ Ion That Stabilises the Ligand-Free Receptor. *PLoS One* **2014**, *9* (3), e92727. https://doi.org/10.1371/journal.PONE.0092727.

(72) Abagyan, R.; Totrov, M.; Kuznetsov, D. ICM—A New Method for Protein Modeling and Design: Applications to Docking and Structure Prediction from the Distorted Native Conformation. *J. Comput. Chem.* **1994**, *15* (5), 488–506. https://doi.org/10.1002/jcc.540150503.

(73) Lee, J.; Cheng, X.; Swails, J. M.; Yeom, M. S.; Eastman, P. K.; Lemkul, J. A.; Wei, S.; Buckner, J.; Jeong, J. C.; Qi, Y.; Jo, S.; Pande, V. S.; Case, D. A.; Brooks, C. L.; MacKerell, A. D.; Klauda, J. B.; Im, W. CHARMM-GUI Input Generator for NAMD, GROMACS, AMBER, OpenMM, and CHARMM/OpenMM Simulations Using the CHARMM36 Additive Force Field. *J. Chem. Theory Comput.* **2016**, *12* (1), 405–413. https://doi.org/10.1021/acs.jctc.5b00935.

(74) Vanommeslaeghe, K.; Hatcher, E.; Acharya, C.; Kundu, S.; Zhong, S.; Shim, J.; Darian, E.; Guvench, O.; Lopes, P.; Vorobyov, I.; Mackerell, A. D. CHARMM General Force Field: A Force Field for Drug-like Molecules Compatible with the CHARMM All-Atom Additive Biological Force Fields. *J. Comput. Chem.* **2010**, *31* (4), 671–690. https://doi.org/10.1002/jcc.21367.

(75) Klaja, O.; Frank, J. A.; Trauner, D.; Bondar, A. N. Potential Energy Function for a Photo-Switchable Lipid Molecule. *J. Comput. Chem.* **2020**, *41* (27), 2336–2351. https://doi.org/10.1002/jcc.26387.

(76) Huang, J.; Rauscher, S.; Nawrocki, G.; Ran, T.; Feig, M.; De Groot, B. L.; Grubmüller, H.; MacKerell, A. D. CHARMM36m: An Improved Force Field for Folded and Intrinsically Disordered Proteins. *Nat. Methods* **2016**, *14* (1), 71–73. https://doi.org/10.1038/nmeth.4067.

(77) Páll, S.; Zhmurov, A.; Bauer, P.; Abraham, M.; Lundborg, M.; Gray, A.; Hess, B.; Lindahl, E. Heterogeneous Parallelization and Acceleration of Molecular Dynamics Simulations in GROMACS. *Journal of Chemical Physics* **2020**, *153* (13), 134110. https://doi.org/10.1063/5.0018516.

(78) Bouysset, C.; Fiorucci, S. ProLIF: A Library to Encode Molecular Interactions as Fingerprints. *J. Cheminform.* **2021**, *13* (1), 1–9. https://doi.org/https://doi.org/10.1186/s13321-021-00548-6.

Supplementary information

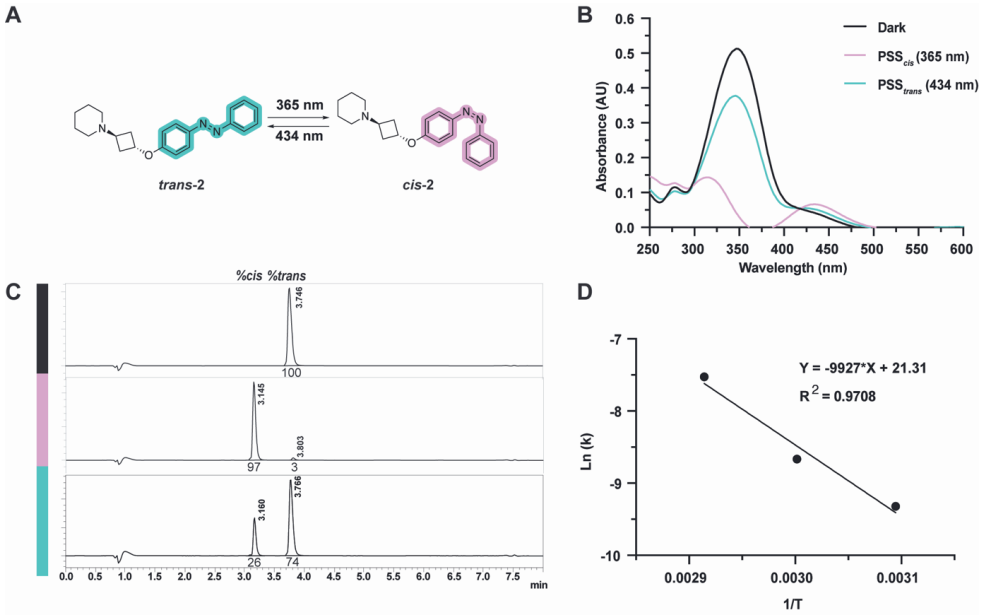

Figure S1. (A) Chemical structures of the *trans* and *cis* isomers of **2**. (B) UV-vis spectra of 25 µM of **2** in HBSS buffer containing 1% DMSO as the *trans* isomer (black), after illumination with 365 ± 11 nm for 2 min to PSS$_{cis}$ (magenta) and after subsequent illumination with 434 ± 9 nm for 4 min to PSS$_{trans}$ (cyan). (C) *Trans*-**2** (upper panel) and photostationary state (PSS) area percentages after illumination with 365 ± 11 nm for 10 min to reach PSS$_{cis}$ (middle panel) and after subsequent illumination with 434 ± 9 nm for 10 min to reach PSS$_{trans}$ (lower panel) at 10 mM in DMSO as determined by LC-MS analysis at the isosbestic point (295 nm). (D) Arrhenius fit for the thermal relaxation of **2** at three different temperatures (50 °C, 60 °C, 70 °C), as measured at 25 µM in HBSS buffer containing 1% DMSO.

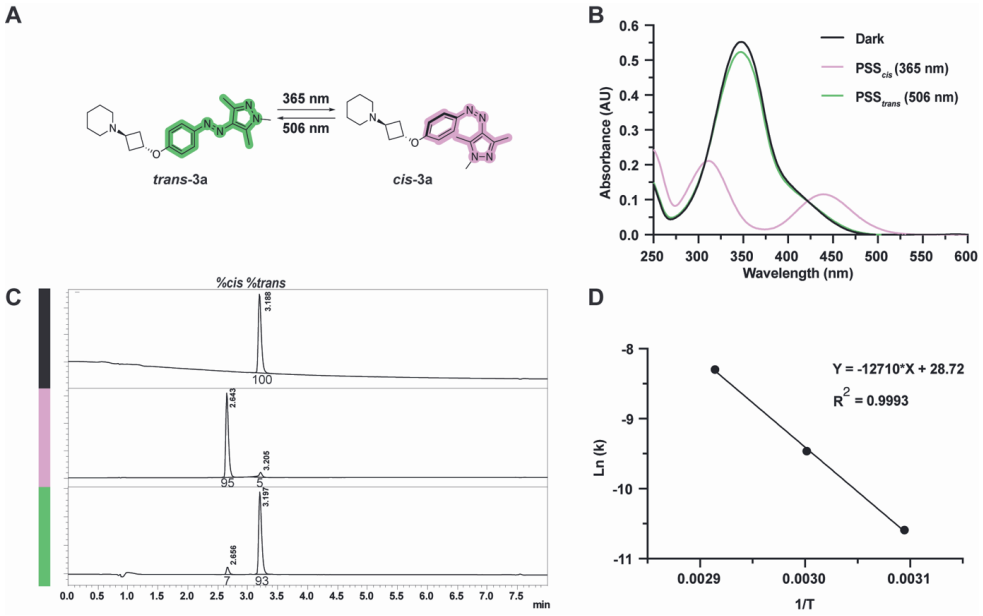

Figure S2. (A) Chemical structures of the *trans* and *cis* isomers of **3a**. (B) UV-vis spectra of 25 µM of **3a** in HBSS buffer containing 1% DMSO as the *trans* isomer (black), after illumination with 365 ± 11 nm for 2 min to PSS$_{cis}$ (magenta) and after subsequent illumination with 506 ± 18 nm for 4 min to PSS$_{trans}$ (green). (C) *Trans*-**3a** (upper panel) and photostationary state (PSS) area percentages after illumination with 365 ± 11 nm for 5 min to reach PSS$_{cis}$ (middle panel) and after subsequent illumination with 506 ± 18 nm for 10 min to reach PSS$_{trans}$ (lower panel) at 10 mM in DMSO as determined by LC-MS analysis at the isosbestic point (305 nm). (D) Arrhenius fit for the thermal relaxation of **3a** at three different temperatures (50 °C, 60 °C, 70 °C), as measured at 25 µM in HBSS buffer containing 1% DMSO.

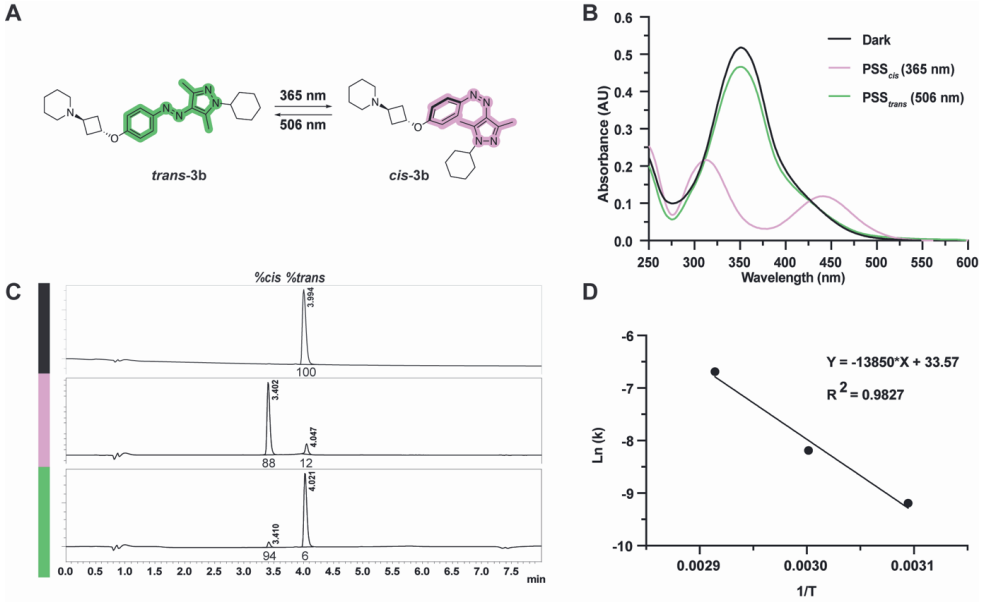

Figure S3. (A) Chemical structures of the *trans* and *cis* isomers of **3b**. (B) UV-vis spectra of 25 µM of **3b** in HBSS buffer containing 1% DMSO as the *trans* isomer (black), after illumination with 365 ± 11 nm for 2 min to PSS$_{cis}$ (magenta) and after subsequent illumination with 506 ± 18 nm for 4 min to PSS$_{trans}$ (green). (C) *Trans*-**3b** (upper panel) and photostationary state (PSS) area percentages after illumination with 365 ± 11 nm for 5 min to reach PSS$_{cis}$ (middle panel) and after subsequent illumination with 506 ± 18 nm for 10 min to reach PSS$_{trans}$ (lower panel) at 10 mM in DMSO as determined by LC-MS analysis at the isosbestic point (310 nm). (D) Arrhenius fit for the thermal relaxation of **3b** at three different temperatures (50 °C, 60 °C, 70 °C), as measured at 25 µM in HBSS buffer containing 1% DMSO.

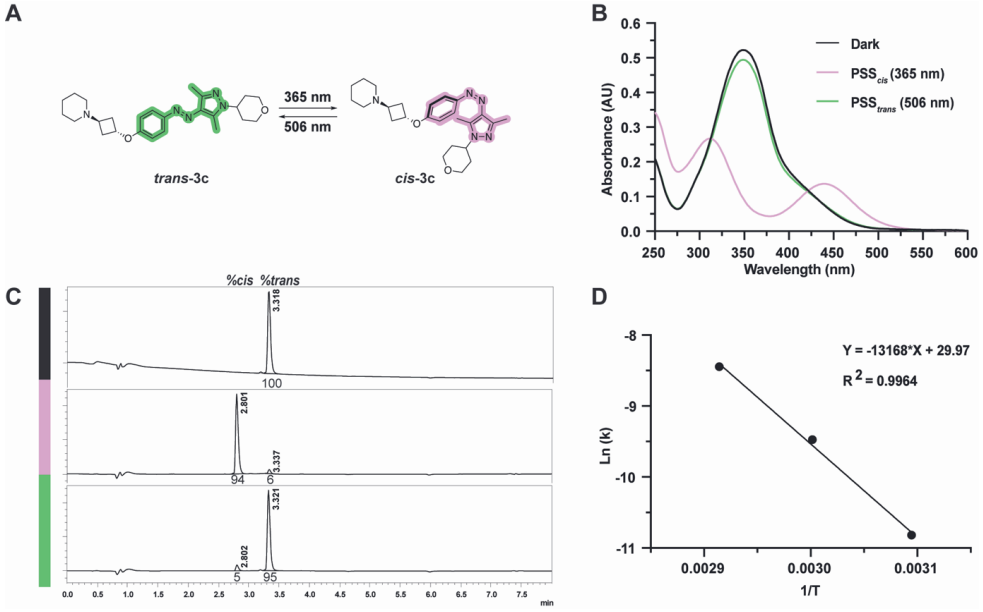

Figure S4. (A) Chemical structures of the *trans* and *cis* isomers of **3c**. (B) UV-vis spectra of 25 µM of **3c** in HBSS buffer containing 1% DMSO as the *trans* isomer (black), after illumination with 365 ± 11 nm for 2 min to PSS_{cis} (magenta) and after subsequent illumination with 506 ± 18 nm for 4 min to PSS_{trans} (green). (C) *Trans*-**3c** (upper panel) and photostationary state (PSS) area percentages after illumination with 365 ± 11 nm for 5 min to reach PSS_{cis} (middle panel) and after subsequent illumination with 506 ± 18 nm for 10 min to reach PSS_{trans} (lower panel) at 10 mM in DMSO as determined by LC-MS analysis at the isosbestic point (310 nm). (D) Arrhenius fit for the thermal relaxation of **3c** at three different temperatures (50 °C, 60 °C, 70 °C), as measured at 25 µM in HBSS buffer containing 1% DMSO.

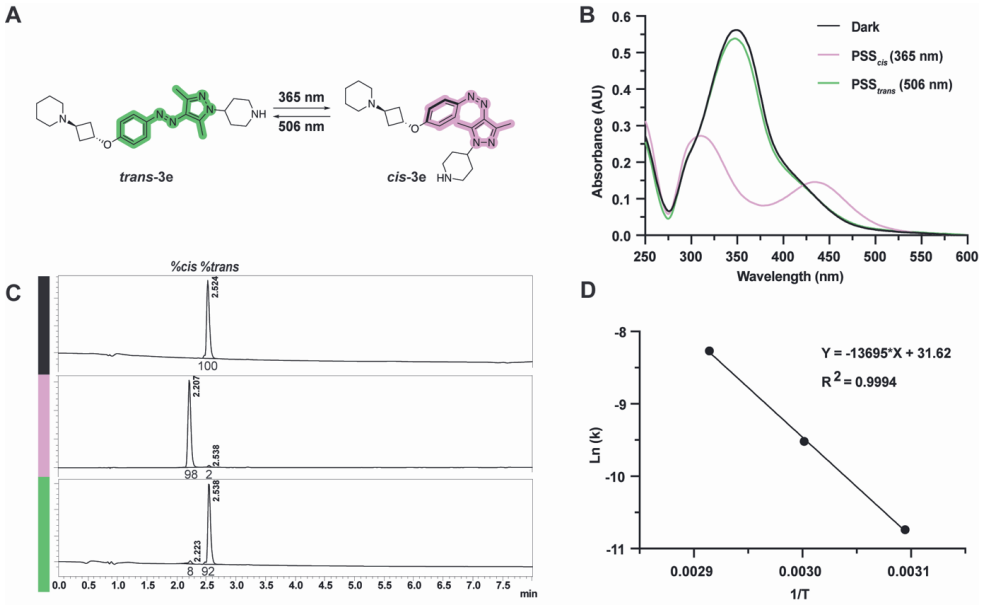

Figure S5. (A) Chemical structures of the *trans* and *cis* isomers of **3e**. (B) UV-vis spectra of 25 µM of **3e** in HBSS buffer containing 1% DMSO as the *trans* isomer (black), after illumination with 365 ± 11 nm for 2 min to PSS$_{cis}$ (magenta) and after subsequent illumination with 506 ± 18 nm for 4 min to PSS$_{trans}$ (green). (C) *Trans*-**3e** (upper panel) and photostationary state (PSS) area percentages after illumination with 365 ± 11 nm for 5 min to reach PSS$_{cis}$ (middle panel) and after subsequent illumination with 506 ± 18 nm for 10 min to reach PSS$_{trans}$ (lower panel) at 10 mM in DMSO as determined by LC-MS analysis at the isosbestic point (305 nm). (D) Arrhenius fit for the thermal relaxation of **3e** at three different temperatures (50 °C, 60 °C, 70 °C), as measured at 25 µM in HBSS buffer containing 1% DMSO.

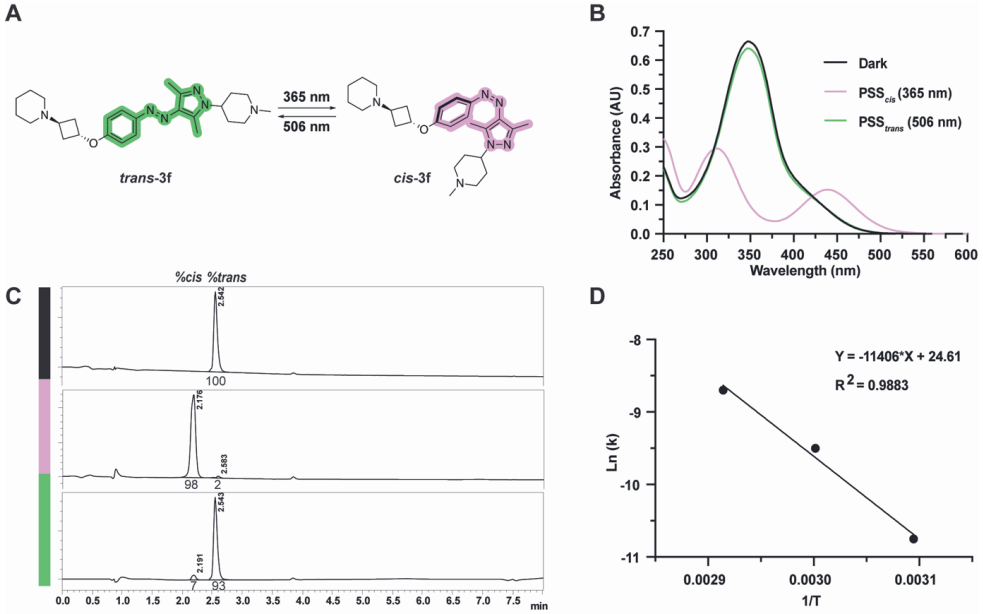

Figure S6. (A) Chemical structures of the *trans* and *cis* isomers of **3f**. (B) UV-vis spectra of 25 µM of **3f** in HBSS buffer containing 1% DMSO as the *trans* isomer (black), after illumination with 365 ± 11 nm for 2 min to PSS$_{cis}$ (magenta) and after subsequent illumination with 506 ± 18 nm for 4 min to PSS$_{trans}$ (green). (C) *Trans*-**3f** (upper panel) and photostationary state (PSS) area percentages after illumination with 365 ± 11 nm for 5 min to reach PSS$_{cis}$ (middle panel) and after subsequent illumination with 506 ± 18 nm for 10 min to reach PSS$_{trans}$ (lower panel) at 10 mM in DMSO as determined by LC-MS analysis at the isosbestic point (305 nm). (D) Arrhenius fit for the thermal relaxation of **3f** at three different temperatures (50 °C, 60 °C, 70 °C), as measured at 25 µM in HBSS buffer containing 1% DMSO.

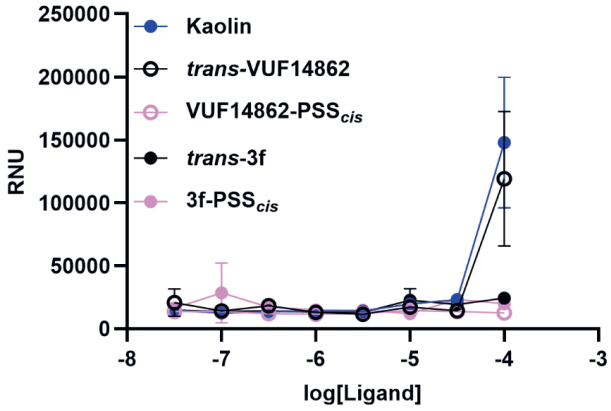

Figure S7. Nephelometry data for **3f**, VUF14862 (first-generation H_3R photoswitchable antagonist[21]) and the kaolin control. Mean of triplicates ± SD shown.

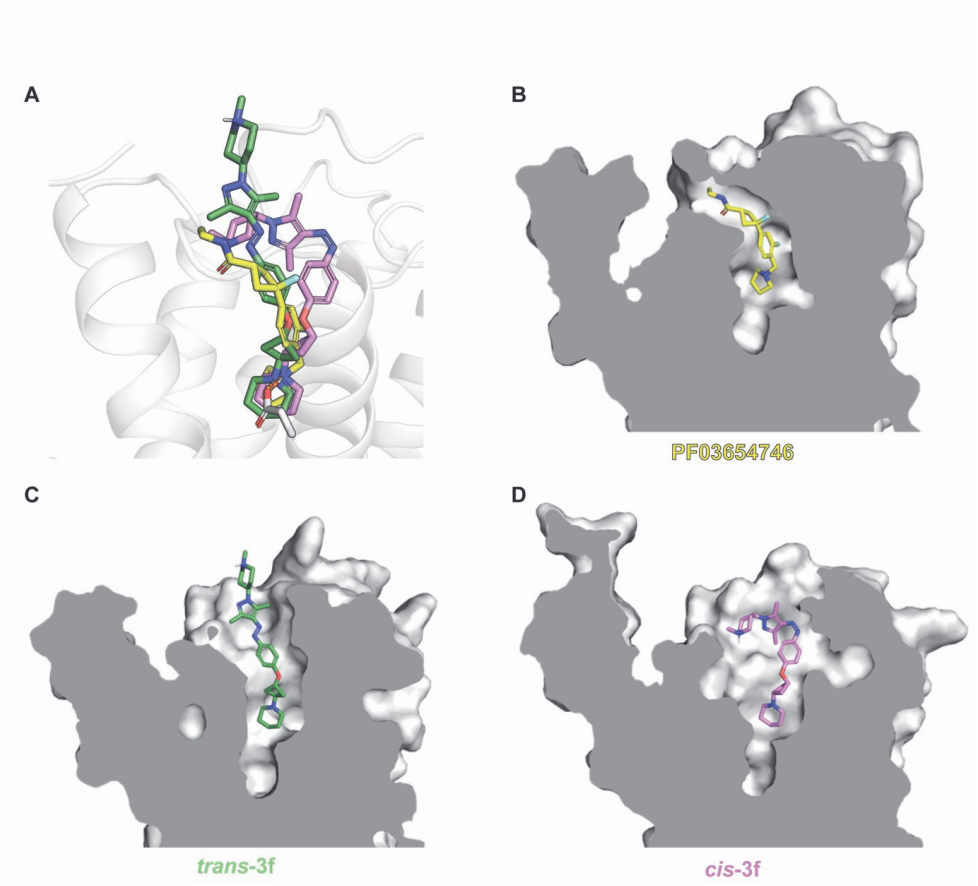

Figure S8. (A) Overlay of the binding pose of PF03654746 taken from its X-ray crystal structure (PDB: 7F61[64]) and representative snapshots of **3f** isomers from MD simulations. (B-D) Comparison of ligand binding pocket sizes for (B) PF03654746 (yellow carbon atoms, X-ray pose), (C) *trans*-**3f** (green carbon atoms, representative MD snapshot), and (D) *cis*-**3f** (magenta carbon atoms, representative MD snapshot).

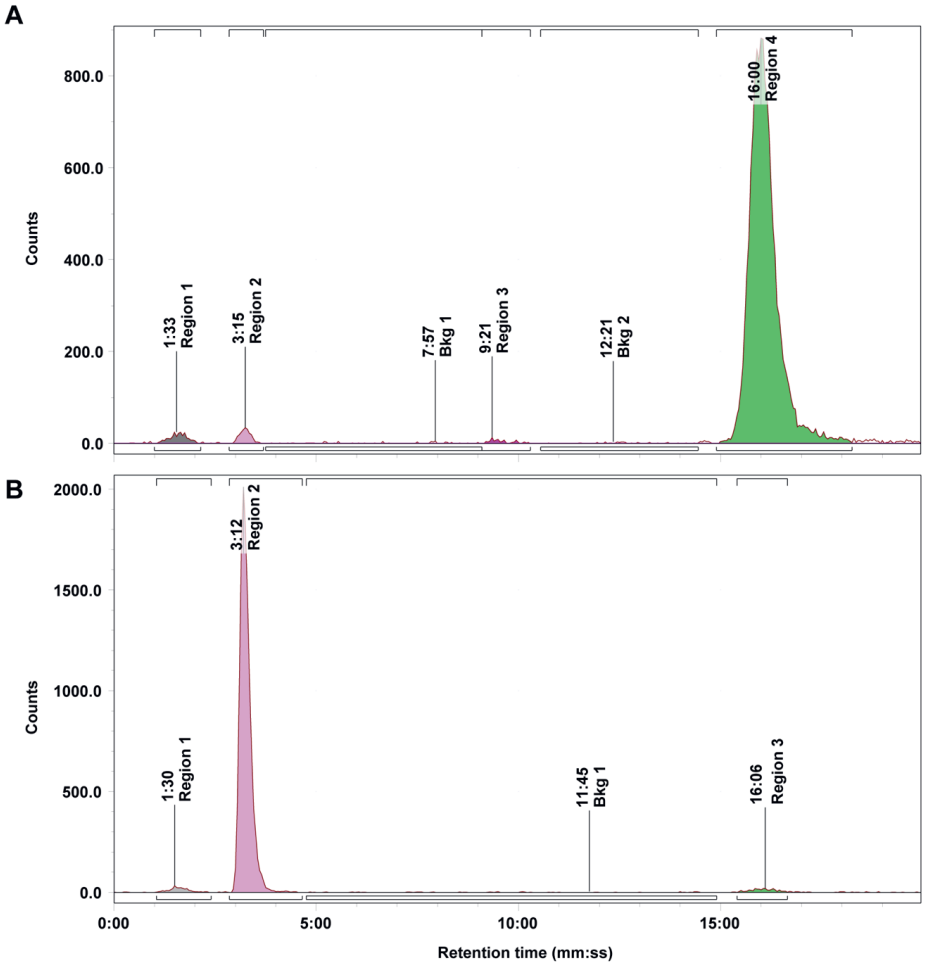

Figure S9. ^{3}H-chromatogram of (A) *trans*-[^{3}H]**3f** containing 96% of the *trans* isomer and 2% of the *cis* isomer and (B) [^{3}H]**3f** at PSS_{cis} containing 2% of the *trans* isomer and 96% of the *cis* isomer. Photoswitching was performed in EtOH with a 100-fold dilution of the stock shown in Figure S10. The products were analyzed with HPLC (Jasco PU-2080 Pump, Jasco UV-2075 UV detector, Lablogic β-RAM Scintillation detector, XBridge C18, 4.6x100 mm, 100Å, 5µm, 45% acetonitrile, 55% water, 0.2% DIPEA, 1 ml/min, 254 nm).

A

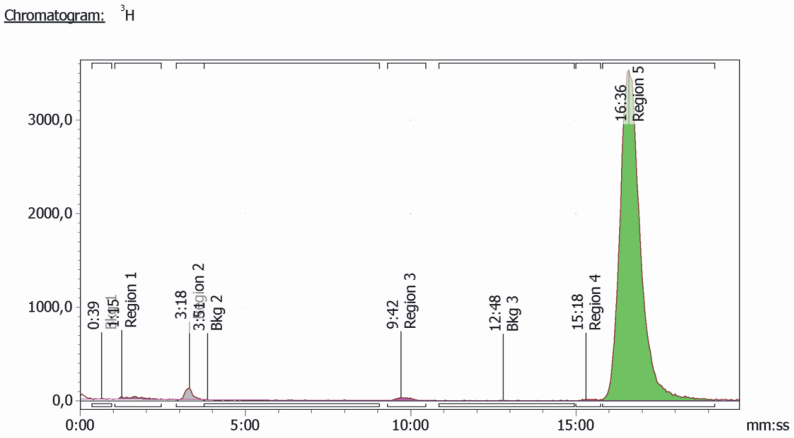

Regions: ³H Detector: ß-RAM

Name	Start (mm:ss)	End (mm:ss)	Retention (mm:ss)	Height (Counts)	Area (Counts)	%ROI (%)
Bkg 1	0:21	0:57	0:39	26,0		
Region 1	1:03	2:27	1:15	48,0	339,4	0,66
Region 2	2:54	3:45	3:18	140,0	649,3	1,25
Bkg 2	3:45	9:03	3:51	15,0		
Region 3	9:18	10:27	9:42	37,0	316,2	0,61
Bkg 3	10:51	14:57	12:48	8,0		
Region 4	15:00	15:45	15:18	20,0	125,9	0,24
Region 5	15:48	19:12	16:36	3534,0	50336,8	97,24
5 Peaks					51767,6	100,00

B

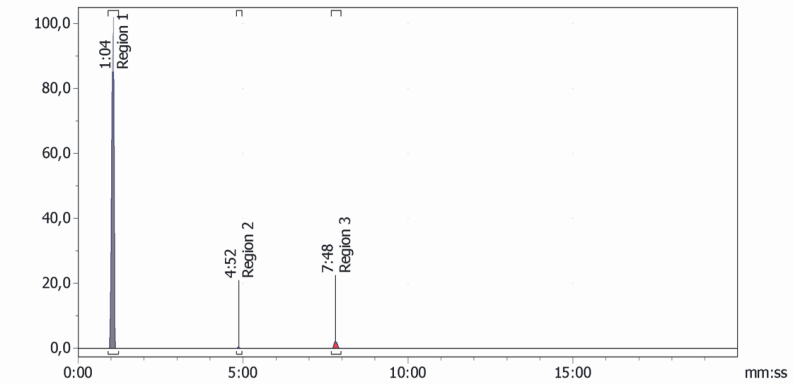

Regions: UV Detector:

Name	Start (mm:ss)	End (mm:ss)	Retention (mm:ss)	Height (mAU)	Area (mAU·s)	%ROI (%)
Region 1	0:54	1:13	1:04	101,8	503,1	96,99
Region 2	4:48	4:58	4:52	0,6	1,4	0,27
Region 3	7:40	7:58	7:48	2,1	14,2	2,74
3 Peaks					518,7	100,00

Figure S10. (A) ^{3}H-chromatogram and (B) UV chromatogram of the *trans*-[^{3}H]**3f** stock. The products were analyzed with HPLC (Jasco PU-2080 Pump, Jasco UV-2075 UV detector, Lablogic β-RAM Scintillation detector, XBridge C18, 4.6x100 mm, 100Å, 5µm, 45% acetonitrile,

55% water, 0.2% DIPEA, 1 ml/min, 254 nm). The peak at 1.0 min is the solvent front. A minor UV impurity was observed at 7.48 min.

Experimental procedures - Pharmacology

Materials

All radioligands mentioned in this paper (except [^{3}H]**3f**) were purchased from Perkin Elmer. UR-KAT478[65] was a kind gift from the Pockes group, University of Regenburg, Germany. All other chemicals were of analytical grade and obtained from commercial sources. HA-tagged wild-type human H_1R, and H_4R, and non-tagged H_3R (full-length isoform 445), mouse H_3R, all expressed in pcDEF$_3$ were made in-house and described previously[66] pcDEF$_3$, SmBiT-PRKACA, LgBiT-PRKAR2A[67] in plasmid DNA, encoding for a NanoBit cAMP sensor were purchased from Promega.

Cell culture, transfection and preparation of cell homogenates

HEK293T cells were cultured in DMEM supplemented with 10% FBS and Penicillin (100 IU/ml) and Streptomycin (100 µg/ml) at 37° C, 5% CO_2. HEK293T cells stably expressing N-terminally tagged Nluc-hH_2R were a kind gift from the Pockes lab, University of Regensburg, Germany, and were cultured as described previously. [65]

To transiently overexpress the H_3R, 2 million HEK293T cells were seeded in a 10 cm petri dish. On the following day, cells were transfected with 2.5 µg hH_3R in pcDEF$_3$, 2.5 µg pcDEF$_3$ and 20 µg PEI per dish and cultured as described above. 48 hours post transfection, the medium was aspirated and transfected cells were collected in a 50 ml falcon, using 5 ml ice cold PBS per dish. The cell homogenate suspension was spun down at 3000 rpm, for 10 minutes at 4° C. Supernatant was aspirated, the pellet resuspended in 1 ml ice-cold PBS per dish and centrifuged again. The pellets were stored at -20° C until use. Mouse H_3R, human H_1R and H_4R were similarly overexpressed in HEK293T cells.

[^{3}H]**3f** binding experiments

For use in *trans*-[^{3}H]**3f** saturation binding experiments H_3R-expressing cell homogenates were resuspended in 50 mM Tris-HCl buffer (pH 7.4 at 4º C) and homogenized by sonication (Sonifier Branson). *Trans*-[^{3}H]**3f** was dissolved in 50 mM Tris-HCl (pH 7.4 at RT) containing 0.8% ethanol. A concentration range from 0.2 – 15.9 nM of *trans*-[^{3}H]**3f** was incubated in the dark with H_3R-expressing cell homogenates (7.5 µg protein in 50 µl) in a total volume of 100 µl for 2 hours at RT on a shaker at 300 rpm. The incubation was terminated by filtration of all samples on a GF/C plate (Perkin Elmer) using the FilterMate 96 harvester (Perkin Elmer). GF/C plates were dried (45 minutes at 60° C), whereafter Microscint-O (25 µl/well) was added. Radioactivity was measured after a 2-hour incubation period with Microscint-O, using the MicroBeta plate reader (Perkin Elmer). To determine non-specific binding, the binding of each *trans*-[^{3}H]**3f** concentration to H_3R was also determined after co-incubation with 10 µM clobenpropit. Specific binding was determined by subtracting the non-specific binding from the total binding.

For association experiments, *trans*-[^{3}H]**3f** (0.5 nM) was incubated with H_3R-expressing cell homogenates (7.5 µg protein in 50 µl) at RT for different time intervals, ranging from 0-60 minutes. For dissociation experiments, 0.5 nM *trans*-[^{3}H]**3f** was incubated with H_3R-

expressing cell homogenates at RT for at least 20 minutes to reach equilibrium, after which dissociation was started with addition of 10 µM clobenpropit and remaining *trans*-[^{3}H]**3f** binding was determined after different time intervals (0-20 min) as described above.

To investigate the binding kinetics of [^{3}H]**3f** PSS$_{cis}$, *trans*-[^{3}H]**3f** (7.93 µM) was irradiated with 365 nm (10 V, 2 mW, constant mode, consistently used for this wavelength) light (96 LED array plates, LAD-1, LEDA-x, Bio Research Center Co., Ltd. Izumi, Japan) for 10 min in a black 96 well plate (Greiner), after which it was diluted to an end concentration of 25 nM. The association-dissociation experiments were performed as for *trans*-[^{3}H]**3f** but the Tris-HCl binding buffer was supplemented with 0.1 % BSA to improve solubility.

For competition binding studies ligands (10 µM to 1 pM) were incubated with [^{3}H]NAMH (2 nM), or *trans*-[^{3}H]**3f** (3.7-4.5 nM), and H_3R-expressing cell homogenates (7.5 µg protein in 50 ul) for 2 hours at 25° C.

Dynamic kinetic radioligand binding experiments with *trans*-[^{3}H]3f

After equilibration of *trans*-[^{3}H]**3f** (0.5 nM) with H_3R-expressing cell homogenates in a black 96 well plate, the mixture was irradiated with 365 nm at RT during different time intervals ranging from 0-20 minutes. The incubations were terminated by filtration and binding was measured as described above.

In another set of experiments *trans*-[^{3}H]**3f (**0.5 nM) was equilibrated with hH_3R-expressing cell homogenates and subsequently switched to PSS$_{cis}$ by 365 nm light illumination at RT for 20 minutes. Thereafter, the mixture was irradiated with 500 nm LED (7.5 V, 1.5 mW, constant mode, consistently used for this wavelength) at RT for different time intervals ranging from 0-60 minutes. The incubations were terminated by filtration and binding was measured as described above.

Binding studies to determine receptor selectivity of 3f

Radioligand competition binding experiments to investigate receptor selectively of **3f** were performed as described before[2,3] with slightly altered incubation times (2 hours), using cell homogenates expressing either human H_1R, H_3R or H_4R and the subtype specific radioligands [^{3}H]mepyramine (1.9 – 2.4 nM), [^{3}H]N-alpha-methyl-histamine ([^{3}H]NAMH) (1.4 – 1.7 nM) or [^{3}H]histamine (4.0 – 4.8 nM), respectively. H_2R selectivity was assessed using a NanoBRET binding assay as published[4] with minor modifications. The assay was performed with HEK293T cells stably expressing Nluc-H_2R. Cells were incubated with ligands and the fluorescent H_2R tracer UR-KAT478 for 2 hours at 25 °C. Thereafter, Nano-Glo® (Promega, catalog number N2011) (3.2 µL/ml), the substrate of Nluc, was added and BRET signal generated due to the close proximity of Nluc and Nano-Glo® and UR-KAT478 was measured using CLARIOstar (BMG, Germany), separating luminescence bands at 470 nm and 640 nm (80 nm bandwitdh each).

NanoBiT– protein kinase A (PKA) assays

HEK293T cells were transfected in suspension with 0.3 µg of SmBiT-PRKACA, 0.3 µg LgBiT-PRKAR2A[6] and 1.4 µg hH_3R per million cells in a 1:6 DNA to linear PEI ratio and immediately seeded in white 96-well plates (Greiner) in a density of 60 000 cells per well. Post transfection (24 hours), DMEM was exchanged for 60 µL HBSS, after which 10 µL antagonists (10 µM – 1 pM) were added, and subsequently 10 µL of 10 nM immethridine and 10 µL of 10 µM forskolin were added. Thereafter, 10 µL Nano-Glo® in an end dilution of 3.2 µL/mL was added and luminescence was measured over time in the CLARIOstar (BMG, Germany) at 470 nm (80 nm bandwith).

To dynamically photoswitch **3f** during the assay, the plate was taken out of CLARIOstar following a kinetic cycle of 20 min. The plate was covered with a transparent lid and irradiated from the top with 365 nm light for 10 min at RT followed by an endpoint measurement in the CLARIOstar. Next, the plate was irradiated as described above with 500 nm light for 10 min at RT followed by measurement in the CLARIOstar. This process was repeated as described for an additional irradiation-measurement cycle.

Data analysis

GraphPad Prism 10 was used for all data analysis and visualization. Functional data were fitted using the non-linear regression "three parameter dose-response curve" to obtain pEC_{50} and pIC_{50} values. Saturation binding data were analyzed using the "one-site binding" model to obtain K_d values. Competition binding data was fitted using a "one-site binding" model to obtain pIC_{50} values, which were converted into pK_i values using the Cheng-Prusoff equation.[68]

Association and dissociation binding data were analyzed using a "one-site association model for one radioligand concentration" and "one-phase exponential decay" model, respectively.

Experimental procedures – Computational chemistry

Preparation of receptor structure

The crystal structure of inactive histamine H_3R bound to PF-03654746 (PDB: 7F61)[64] was used as the starting point of our molecular modeling studies. Using MODELER[69], ICL3 was remodeled and the S121$^{3.39}$K mutation in the sodium binding pocket was reverted to the wild-type. To allow docking of the photoswitchable compounds, the rotamer of Y189^{ECL2} within the EBP was adjusted to enlarge the pocket. Y189^{ECL2} thus adopts a rotamer similar to that observed in the cryo-EM structures of H_3R in active state (PDB: 8YUU and 8YUV).[70] Additionally, a sodium ion was placed in the sodium binding site based on the sodium-bound β_1-adrenoreceptor crystal structure (PDB: 4BVN).[71]

Molecular docking

Molecular docking was performed using ICM-Pro (v3.9-3a) molecular modeling and drug discovery suite (Molsoft).[72] During docking, ligands were treated as flexible, with binding poses and internal torsions sampled using the biased probability Monte Carlo (BPMC) procedure.[72] This process included local energy minimization after each random move. Comprehensive sampling of the ligand conformational space was performed with effort parameter was set to 30 with 30 conformations scored with the ICM VLS score. To not interconvert isomers during the docking process, the option “relax covalent geometry” was not selected. Binding poses with the lowest score and interaction with D114$^{3.32}$ of each compound and isomer were selected for further analysis. The selected binding poses were further optimized in a postprocessing step using BPMC sampling, which optimized the ligand conformation and side-chain residues located within 5 Å of the ligand.

Molecular dynamics simulation

The H_3R complexes obtained from docking were prepared for molecular dynamics simulations with the CHARMM-GUI web server.[73] As terminal group patching, the N-terminus was acetylated, the C-terminus was methylamidated. The disulfide bonds between residues C107$^{3.25}$-188^{ECL2} and C384$^{6.61}$-C388^{ECL3} were checked for proper linkage. The complexes were embedded in a box of approximately 80x80x120 Å containing a POPC membrane bilayer, TIP3 water molecules, and a 150 mM concentration of NaCl. Ligands were parameterized using CGenFF.[74] Parameters of the azobond dihedral with a minimum of 180° for *cis* isomers were adjusted from 63.60 to 75.73 kJ/mol and azobond dihedrals with a minimum of 0° for *cis* isomers were adjusted from 2.09 to 1.26 kJ/mol in line with parameters reported by Klaja et al.[75] The CHARMM36m force field[76] was applied for the rest of the system.

All simulations were performed using GROMACS 2023.1.[77] The system was first minimized by a 5000-step steepest descent minimization using periodic boundary conditions. Subsequently, the system was equilibrated in multiple steps, following the default CHARMM equilibration protocol with only the simulation time doubled. After equilibration, a 1000 ns production run in the NPT ensemble was performed using a time step integration of 4 fs with hydrogen mass repartitioning. LINCS constraints were applied to the hydrogen covalent

bonds. The electrostatic interactions were calculated with the particle-mesh Ewald (PME) algorithm with a cutoff of 1.2 nm. The v-rescale algorithm was used to maintain a temperature of 310.15 K and the pressure was kept at 1 bar by semi-isotropic coupling to c-rescale barostat (τp = 5.0 ps, compressibility = $4.5*10^{-5}$ bar). Atomic positions were saved every 100 ps.

Frequencies of ligand-protein and water-mediated interactions were calculated with ProLIF[78] and the use of in-house Python scripts. To ensure proper equilibration, the initial 500 ns of each simulation were excluded from the analysis. Representative binding modes from MD simulation of the *cis* and *trans* isomers of **3f** were obtained by using the Gromacs clustering command (*gmx cluster*). The first 500 ns of the 1000 ns simulations was discarded and the remaining 500 ns of each of the four independent simulations were concatenated. Gromacs clustering of the H_3R pocket residues (residue IDs: 27, 91, 94, 95, 98, 110, 111, 114, 115, 118, 187, 188, 189, 190, 193, 374, 378, 391, 394, 395, 398, 401, 402) was performed and the highest populated cluster was deemed as representative for the average binding mode of the ligand.

Experimental procedures – Photochemistry

UV−Vis spectra were recorded using a Thermo-scientific Evolution 201 PC spectrophotometer equipped with a thermostated cell holder set at 20 °C. Fits of UV−vis spectroscopy data were generated using Prism 10.1.0. Illumination for almost all photochemical experiments was executed using a Sutter instruments Lambda LS with a 300 W full-spectrum lamp connected to a Sutter instruments Lambda 10-3 optical filter changer equipped with 360 ± 10 nm, 434 ± 9 nm 494 ± 9 nm, or a Lambda 721 optical beam combiner system equipped with 365 ± 11 nm and 506 ± 14 nm filter. The light intensity used for the lambda 10-3 optical filter is 0.93 mW/mm^2 using the 360 ± 20 nm filter, 0.79 mW/mm^2 for the 434 ± 9 nm filter, 0.77 mW/mm^2 for the 494 ± 9 nm filter as measured using a Thorlabs PM16−401 power meter. The light intensity used for the lambda 721 optical beam combiner is 200 mW using the 365 ± 11 nm filter and 60 mW for the 506 ± 12 nm filter. For photochemical analyses, illuminations were performed in Hellma Suprasil quartz 114QS cuvettes. For the dynamic illuminations, a 4-way cuvette holder (Avantes) was used. The left outlet of the holder is connected to an Avantes AvaLight-DH-S-BAL Deuterium lamp. The right outlet is connected through a fiber to an AvaSpec UV/Vis spectrometer. The lower outlet is connected to a Lambda 721 optical beam combiner system equipped with 365 ± 11 nm and 506 ± 14 nm filter illumination means. The upper outlet is covered with a black cap. The temperature of the solution in the cuvette (20 °C) is controlled by Q-blue Wireless Temperature Control software. Thermal relaxation experiments and Arrhenius extrapolations were performed according to Priimagi *et al*[47], using a compound concentration of 25 µM in HBSS +1% DMSO and temperatures of 50, 60, and 70 °C. Illuminations for pharmacological experiments were performed in cylindrical clear glass vials with a volume of 4.5 mL. The typical distance between light source and vial or cuvette was 2 cm.

Experimental procedures - Synthesis

All chemicals and solvents were obtained from commercial suppliers (primarily Sigma-Aldrich, BLD pharma and Combi-Blocks) and used without purification. DCM, DMF, THF and Et_2O were dried by passing through a PureSolv solvent purification system. All reactions with photoresponsive compounds were carried out in the dark or under red light. IUPAC names were adapted from ChemDraw Professional 21.0 (PerkinElmer). Reactions were monitored by thin layer chromatography (Merck Silicagel 60 F254) by visualization under 254 nm lamp. Flash column chromatography was performed with Screening Devices 40-63 µm (Biotage) or GraceResolv (Büchi) cartridges on Isolera One with UV-Vis detection (Biotage). Nuclear magnetic resonance (NMR) spectra were determined with a Bruker Avance II 500 MHz or a Bruker Avance III HD 600 MHz spectrometer. Chemical shifts are reported in parts per million (ppm) against the reference compound using the signal of the residual non-deuterated solvent ($CDCl_3$ δ = 7.26 ppm (^{1}H), δ = 77.16 ppm (^{13}C); DMSO-d_6 δ = 2.50 ppm (^{1}H), δ = 39.52 ppm (^{13}C)). NMR spectra were processed using MestReNova 14.0 software. The peak multiplicities are defined as follows: s, singlet; d, doublet; t, triplet; q, quartet; dd, doublet of doublets; ddd, doublet of doublets of doublets; dt, doublet of triplets; dq, doublet of quartets; td, triplet of doublets; tt, triplet of triplets; qd, quartet of doublets; p, pentet; dp, doublet of pentets; br, broad signal; m, multiplet. For NMR listings, in addition to specific instructions that are given by the journal in the guidelines for authors the following additional procedures were used: 1) Multiplicity is not solely reported based on peak shapes, but also distinguishes the coupling to all non-equivalent protons that have similar J values; 2) If additional smaller couplings are observed but are too small for accurate quantitation because the precision is smaller than the digital resolution, a symbol $^{\Delta}$ will be used; 3) The notation 'm' is used in case of obscured accurate interpretation as a result of (i) overlapping signals for different protons, or (ii) a result of overlapping signal lines within the same proton signal; 4) For any rotamers or diastereomers, signals will be listed separately; 5) NMR signals that could only be detected with HSQC analysis are denoted with a $^{\#}$ symbol; 6) NMR signals that could only be detected with HMBC analysis are denoted with a * symbol; 7) If one or more signals remain undetected after extensive 1D and 2D NMR analyses, this will be mentioned. 8) Signals for exchangeable proton atoms (such as NH and OH groups) are only listed if clearly visible (excluding e.g. the use of D_2O or CD_3OD) and if confirmed by a D_2O shake and/or HSQC. Purity determination was performed with Liquid Chromatography using a Shimadzu LC-20AD liquid chromatography pump system with a Shimadzu SPDM20A photodiode array detector and MS detection with a Shimadzu LCMS-2010EV mass spectrometer operating in both positive and negative ionization mode. A Waters XBridge C18 column 5 µm 4.6 x 50 mm was used at 40 °C. The mobile phase used was a mixture of A = Water + 0.1% HCO_2H and B = acetonitrile (MeCN) + 0.1% HCO_2H. The eluent program 'acidic mode' used is as follows: flow rate: 1.0 mL/min, start 95% A in a linear gradient to 10% A over 4.5 min, hold 1.5 min at 10% A, in 0.5 min in a linear gradient to 95% A, hold 1.5 min at 95% A, total runtime: 8.0 min. Compound purities were calculated as the percentage peak area of the analysed compound by UV detection at 254 nm. Unless mentioned otherwise, all compounds have a LC purity of >95 %.

High-resolution mass spectra (HRMS) were recorded on a Bruker micrOTOF mass spectrometer using ESI in positive ion mode (HRMS).

General procedure A

To a solution of 3-(2-(4-hydroxyphenyl)hydrazineylidene)pentane-2,4-dione (**5**) in EtOH (0.12 M) was added the respective hydrazine (1.0 eq) and Et_3N (2.0 eq). The reaction mixture was heated at reflux for 17 h. The reaction mixture was cooled to rt and concentrated under reduced pressure. Where indicated, the obtained crude product was purified by flash column chromatography to give phenols **6a–d,f**.

General procedure B

To a solution of phenol **6** (1.5 eq) in DMF (0.25 M) was added NaH (60% dispersion in mineral oil, 2.0 eq). The reaction mixture was stirred for 30 min at rt. Subsequently, tosylate **7**[39] (1.0 eq) was added. The reaction mixture was heated at 75 °C for 17 h. The reaction mixture was cooled to rt, poured in ice-water and extracted thrice with EtOAc. The combined organic layers were washed with brine, dried over Na_2SO_4 and concentrated under reduced pressure. The crude product was purified using reverse phase (MPLC). The desired fractions were combined, made basic using satd. aq. $NaHCO_3$ and extracted using EtOAc. The combined organic layers were washed with brine, dried over Na_2SO_4 and concentrated *in vacuo*. The products were lyophilised to give compounds **3a–d,f.**

3-(2-(4-hydroxyphenyl)hydrazineylidene)pentane-2,4-dione (5)

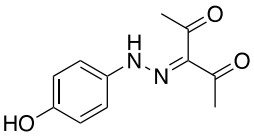

A solution of 4-aminophenol (**4**, 5.0 g, 46 mmol, 1.0 eq) in AcOH (70 mL) and conc. aq. HCl (11 mL) was cooled to 0 °C. A solution of $NaNO_2$ (3.8 g, 55 mmol, 1.2 eq) in water (10 mL) was added drop-wise. After stirring for 45 min at 0 °C, the resulting solution containing the diazonium salt was added drop-wise to another flask cooled to 0 °C containing a suspension of pentane-2,4-dione (6.1 mL, 60 mmol, 1.3 eq) and NaOAc (11.3 g, 137 mmol, 3.0 eq) in EtOH (46 mL) and water (28 mL). The mixture was stirred for 1 h at 0 °C. The resulting brown precipitate was collected via vacuum filtration. After washing with water, water/EtOH (1:1) and *c*Hex the obtained solid was dried under vacuum affording the product as a dark yellow solid (5.8 g, 58% yield). **^{1}H NMR** (600 MHz, DMSO-d_6) δ 14.49 (s, 1H), 9.63 (s, 1H), 7.44 (d, J = 8.9 Hz, 2H), 6.83 (d, J = 8.9 Hz, 2H), 2.46 (s, 3H), 2.38 (s, 3H). **^{13}C NMR** (151 MHz, DMSO-d_6) δ 196.0, 195.9, 155.9, 133.7, 132.1, 118.1, 116.1, 31.0, 26.4. **LCMS** (acidic)**:** t_r: 3.49 min, purity: 96% (254 nm).

(*E*)-4-((1,3,5-trimethyl-1*H*-pyrazol-4-yl)diazenyl)phenol (**6a**)

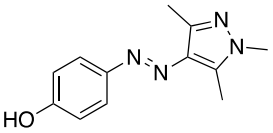

General procedure A was followed, using dione **5** (400 mg, 1.8 mmol), $MeHNNH_2$ (143 µL, 2.7 mmol) and EtOH (15 mL). Concentration *in vacuo* gave compound **3a** (411 mg, 98% yield). **^{1}H NMR** (600 MHz, DMSO-d_6) δ 9.93 (s, 1H), 7.61 (d, *J* = 8.7 Hz, 2H), 6.87 (d, *J* = 8.9 Hz, 2H), 3.71 (s, 3H), 2.51 (s, 3H), 2.34 (s, 3H). **^{13}C NMR** (151 MHz, DMSO-d_6) δ 159.1, 146.1, 139.9, 138.1, 134.0, 123.1, 115.6, 35.9, 13.7, 9.4. **LCMS** (acidic)**:** t_r: 3.67 min, purity: 99% (254 nm), λ_{max}: 345 nm, $[M+H]^+$ m/z calc. 231.12, found 231.10.

(*E*)-4-((1-cyclohexyl-3,5-dimethyl-1*H*-pyrazol-4-yl)diazenyl)phenol (**6b**)

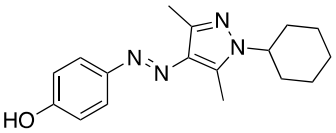

General procedure A was followed, using dione **5** (500 mg, 2.3 mmol), cyclohexylhydrazine hydrochloride (342 mg, 2.3 mmol), Et_3N (0.63 mL, 4.5 mmol) and EtOH (19 mL). Purification by column chromatography (0 -> 50% 90:5:5 EtOAc:MeOH:TEA in cHex) gave the title compound as a yellow solid (497 mg, 73% yield). **^{1}H NMR** (500 MHz, $CDCl_3$) δ 7.71 (d, J = 9.0 Hz, 2H), 6.90 (d, J = 8.7 Hz, 2H), 6.76 (s, 1H), 4.00 (dddd, J = 11.7, 11.7, 3.8, 3.8 Hz, 1H), 2.58 (s, 3H), 2.50 (s, 3H), 2.05 – 1.95 (m, 2H), 1.95 – 1.85 (m, 4H), 1.74 – 1.71 (m, 1H), 1.44 – 1.35 (m, 2H), 1.29 (dddd, J = 11.9, 11.9, 2.5, 2.5 Hz, 1H). **^{13}C NMR** (126 MHz, $CDCl_3$) δ 157.6, 148.0, 142.0, 137.3, 134.7, 123.6, 115.8, 57.9, 32.6, 25.9, 25.3, 14.0, 9.8. **LCMS** (acidic)**:** t_r: 4.95 min, purity: 99% (254 nm), λ_{max}: 349 nm, $[M+H]^+$ m/z calc. 299.19, found 299.15.

(*E*)-4-((3,5-dimethyl-1-(tetrahydro-2*H*-pyran-4-yl)-1*H*-pyrazol-4-yl)diazenyl)phenol (**6c**)

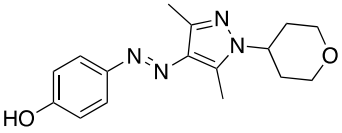

General procedure A was followed, using dione **5** (300 mg, 1.4 mmol), (tetrahydro-2H-pyran-4-yl)hydrazine hydrochloride (311 mg, 1.4 mmol), Et_3N (0.38 mL, 2.8 mmol) and EtOH (11 mL). Purification by column chromatography (0 -> 50% 90:5:5 EtOAc:MeOH:TEA in cHex) gave the title compound as a yellow solid (170 mg, 42% yield). **^{1}H NMR** (600 MHz, $CDCl_3$) δ 7.72 (d, 2H), 6.90 (d, 2H), 5.69 (s, 1H), 4.24 (dddd, *J* = 11.6, 11.6, 4.1, 4.1 Hz, 1H), 4.15 (dd$^{\triangle}$, *J* = 11.4, 4.5 Hz, 2H), 3.55 (ddd, *J* = 12.2, 12.1, 1.9 Hz, 2H), 2.61 (s, 3H), 2.50 (s, 3H), 2.37 (dddd, *J* = 12.3, 12.0, 12.0, 4.6 Hz, 2H), 1.84 (ddd$^{\triangle}$, *J* = 13.0, 4.3, 2.0 Hz, 2H). **^{13}C NMR** (151 MHz, $CDCl_3$) δ 157.2, 148.2, 142.2, 137.4, 135.0, 123.7, 115.7, 67.3, 54.9, 32.5, 14.2, 9.8. **LCMS** (acidic)**:** t_r: 3.84 min, purity: 96% (254 nm), λ_{max}: 345 nm, $[M+H]^+$ m/z calc. 301.17, found 301.15.

tert-butyl (_E_)-4-(4-((4-hydroxyphenyl)diazenyl)-3,5-dimethyl-1H-pyrazol-1-yl)piperidine-1-carboxylate (6d)

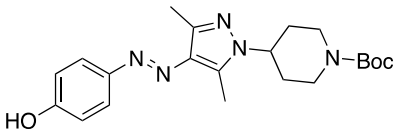

General procedure A was followed, using dione **5** (350 mg, 1.6 mmol), *tert-butyl* 4-hydrazineylpiperidine-1-carboxylate oxalate (485 mg, 1.6 mmol), Et_3N (0.44 mL, 3.2 mmol) and EtOH (11 mL). Purification by column chromatography (30 -> 70% EtOAc in cHex) and additional co-evaporation of the concentrated desired fractions with Et_2O, gave the title compound as a fluffy yellow solid (363 mg, 57% yield). **^{1}H NMR** (500 MHz, $CDCl_3$) δ 7.72 (d, *J* = 8.8 Hz, 2H), 6.90 (d, *J* = 8.8 Hz, 2H), 4.44 – 4.20 (m, 2H), 4.15 (dddd, *J* = 11.6, 11.6, 4.1, 4.1 Hz, 1H), 2.96 – 2.77 (m, 2H), 2.59 (s, 3H), 2.48 (s, 3H), 2.25 – 2.11 (m, 2H), 1.91 – 1.83 (m, 2H), 1.48 (s, 9H). **^{13}C NMR** (126 MHz, $CDCl_3$) δ 157.3, 154.6, 148.2, 142.2, 137.4, 135.0, 123.7, 115.7, 80.1, 77.4, 77.2, 76.9, 55.9, 42.9#, 31.6, 28.6, 14.2, 9.8. **LCMS** (acidic)**:** t_r: 4.83, purity: 91%, λ_{max}: 345 nm, $[M+H]^+$ m/z calc. 400.23, found 400.25.

(_E_)-4-((3,5-dimethyl-1-(1-methylpiperidin-4-yl)-1_H_-pyrazol-4-yl)diazenyl)phenol (6f)

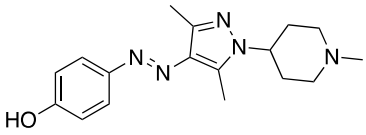

General procedure A was followed, using dione **5** (500 mg, 2.3 mmol), 4-hydrazineyl-1-methylpiperidine dihydrochloride (459 mg, 2.3 mmol), Et_3N (0.63 mL, 4.6 mmol) and EtOH (19 mL). Purification by column chromatography (50 -> 100% 90:5:5 EtOAc:MeOH:TEA in cHex) gave the title compound as a yellow solid (551 mg, 77% yield). **^{1}H NMR** (500 MHz, DMSO-d_6) δ 9.91 (s, 1H), 7.61 (d, *J* = 8.8 Hz, 2H), 6.86 (d, *J* = 8.9 Hz, 2H), 4.12 (dddd, *J* = 10.9, 5.1 Hz, 1H), 2.92 – 2.82 (m, 2H), 2.55 (s, 3H), 2.35 (s, 3H), 2.21 (s, 3H), 2.12 – 2.00 (m, 4H), 1.84 – 1.75 (m, 2H). **^{13}C NMR** (126 MHz, DMSO-d_6) δ 159.0, 146.1, 139.7, 137.8, 133.9, 123.1, 115.6, 54.5, 54.3, 45.9, 31.1, 14.2, 9.0. **LCMS** (acidic)**:** t_r: 2.69 min, purity: >99% (254 nm), λ_{max}: 345 nm, $[M+H]^+$ m/z calc. 314.20, found 314.20.

1-((1_r_,3_r_)-3-(4-((_E_)-(1,3,5-trimethyl-1_H_-pyrazol-4-yl)diazenyl)phenoxy)cyclobutyl)piperidine fumarate (3a)

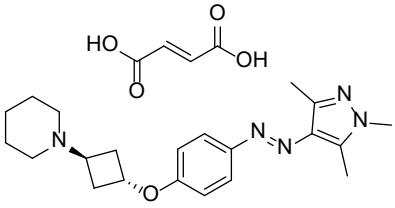

General procedure B was followed, using phenol **6a** (179 mg, 0.78 mmol), NaH (31 mg, 0.78 mmol), and tosylate **7** (105 mg, 0.39 mmol). The crude product was purified by reverse phase column chromatography (5 -> 95% MeCN + 0.1% HCO_2H in H_2O + 0.1% HCO_2H). Desired fractions were combined, made basic using aq. satd. $NaHCO_3$ and extracted with EtOAc thrice. The combined organic layers were dried over Na_2SO_4, filtered and concentrated to give the free base as a

yellow oil. The free base was converted to the fumarate salt by recrystallization from IPA to give the title compound as yellow crystals (34 mg, 24%).
^{1}H NMR (600 MHz, CD_3OD) δ 7.79 – 7.70 (m, 2H), 6.96 – 6.88 (m, 2H), 6.71 (s, 2H), 4.93 (ddd, *J* = 7.0, 4.7, 2.1 Hz, 1H), 3.92 – 3.84 (m, 1H), 3.77 (s, 3H), 2.85 – 2.73 (m, 2H), 2.62 – 2.52 (m, 5H), 2.43 (s, 3H), 1.99 – 1.55 (m, 6H). **^{13}C NMR** (151 MHz, CD_3OD) δ 171.4, 159.7, 149.5, 142.8, 140.4, 136.3, 135.7, 124.4, 116.3, 68.9, 58.6, 51.7, 36.0, 33.3, 24.2, 22.9, 13.8, 9.7. **LCMS** (acidic)**:** t_r: 3.17 min, purity: 99% (254 nm), λ_{max}: 344 nm, $[M+H]^+$ m/z calc. 368.24, found 368.25. **HRMS**: $[M+H]^+$ calc. for $C_{21}H_{30}N_5O$: 368.2445, found 368.2441.

1-((1*r*,3*r*)-3-(4-((*E*)-(1-cyclohexyl-3,5-dimethyl-1*H*-pyrazol-4-yl)diazenyl)phenoxy)cyclobutyl) piperidine fumarate (**3b**)

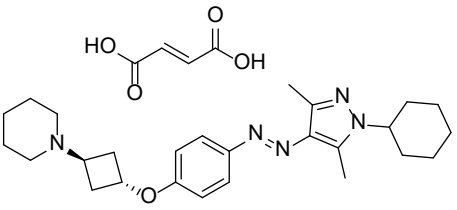

General procedure B was followed, using phenol **6b** (159 mg, 0.53 mmol), NaH (28 mg, 0.71 mmol), and tosylate **7** (110 mg, 0.39 mmol). The crude product was purified by reverse phase column chromatography (5 -> 95% MeCN + 0.1% HCO_2H in H_2O + 0.1% HCO_2H). Desired fractions were combined, made basic using aq. satd. $NaHCO_3$ and extracted with EtOAc thrice. The combined organic layers were dried over Na_2SO_4, filtered and concentrated to give the free base as a yellow oil. The free base was converted to a fumarate salt by recrystallization from IPA to give the title compound as yellow crystals (80 mg, 52%).
^{1}H NMR (500 MHz, CD_3OD) δ 7.74 (d, *J* = 9.5 Hz, 2H), 6.93 (d, *J* = 9.5 Hz, 2H), 6.71 (s, 2H), 4.94 (tt, *J* = 6.9, 2.2 Hz, 1H), 4.21 – 4.10 (m, 1H), 3.92 (tt, *J* = 8.0, 8.0 Hz, 1H), 3.18 – 3.02 (m, 2H), 2.80 (ddd, *J* = 11.2, 9.1, 5.2 Hz, 2H), 2.63 – 2.55 (m, 5H), 2.44 (s, 3H), 1.97 – 1.79 (m, 10H), 1.79 – 1.60 (m, 3H), 1.55 – 1.45 (m, 2H), 1.32 (dddd, *J* = 16.6, 13.1, 8.1, 4.7 Hz, 2H). **^{13}C NMR** (126 MHz, CD_3OD) δ 169.6, 158.2, 148.2, 141.2, 138.2, 134.7, 134.1, 123.0, 114.9, 67.5, 57.3, 57.3, 50.3, 48.1, 47.9, 47.8, 47.6, 47.4, 47.3, 47.1, 32.1, 31.9, 25.2, 25.0, 22.8, 21.4, 12.7, 8.1. **LCMS** (acidic)**:** t_r: 3.99 min, purity: 98% (254 nm), λ_{max}: 349 nm, $[M+H]^+$ m/z calc. 436.31, found 436.35. **HRMS**: $[M+H]^+$ calc. for $C_{26}H_{38}N_5O$: 436.3071, found 436.3064.

1-((1*r*,3*r*)-3-(4-((*E*)-(3,5-dimethyl-1-(tetrahydro-2*H*-pyran-4-yl)-1*H*-pyrazol-4-yl)diazenyl) phenoxy)cyclobutyl)piperidine fumarate (**3c**)

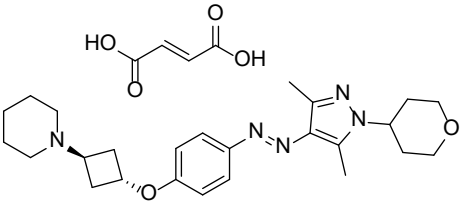

General procedure B was followed, using phenol **6c** (152 mg, 0.51 mmol), NaH (27 mg, 0.68 mmol), and tosylate **7** (105 mg, 0.34 mmol). The crude product was purified by reverse phase column chromatography (5 -> 95% MeCN + 0.1% HCO_2H in H_2O + 0.1% HCO_2H). Desired fractions were combined, basified using satd. aq. $NaHCO_3$ and extracted with

EtOAc thrice. The combined organic layers were dried over Na_2SO_4, filtered and concentrated to give the free base as a yellow oil. The free base was converted to a fumarate salt by recrystallization from IPA to give the title compound as yellow crystals (43 mg, 29%).
^{1}H NMR (500 MHz, CD_3OD) δ 7.65 (d, *J* = 9.0 Hz, 2H), 6.83 (d, *J* = 9.0 Hz, 2H), 6.61 (s, 2H), 4.84 (tt, *J* = 7.0, 2.2 Hz, 1H), 4.35 (tt, *J* = 11.6, 4.1 Hz, 1H), 3.98 (dd, *J* = 11.4, 4.7 Hz, 2H), 3.88 – 3.79 (m, 1H), 3.51 (ddd, *J* = 12.1, 2.0, 2.0 Hz, 2H), 3.18 – 2.79 (m, 4H), 2.76 – 2.68 (m, 2H), 2.57 – 2.45 (m, 5H), 2.35 (s, 3H), 2.20 – 2.08 (m, 2H), 1.85 – 1.70 (m, 6H), 1.65 – 1.48 (m, 2H). **^{13}C NMR** (126 MHz, CD_3OD) δ 169.3, 158.3, 148.2, 141.5, 138.5, 134.7, 134.3, 123.0, 114.9, 67.5, 66.6, 57.3, 54.2, 50.3, 32.0, 31.9, 22.7, 21.4, 12.7, 8.0. **LCMS** (acidic)**:** t_r: 3.29 min, purity: 96% (254 nm), λ_{max}: 349 nm, $[M+H]^+$ m/z calc. 438.29, found 438.35. **HRMS**: $[M+H]^+$ calc. for $C_{25}H_{36}N_5O_2$: 438.2864, found 436.3064.

***tert*-butyl 4-(3,5-dimethyl-4-((*E*)-(4-((1*r*,3*r*)-3-(piperidin-1-yl)cyclobutoxy)phenyl)diazenyl)-1*H*-pyrazol-1-yl)piperidine-1-carboxylate (3d)**

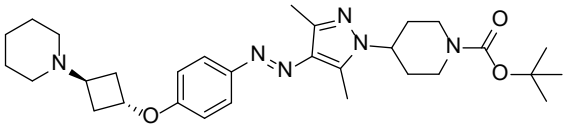

General procedure B was followed, using phenol **6d** (152 mg, 0.49 mmol), NaH (26 mg, 0.65 mmol), and tosylate **7** (100 mg, 0.32 mmol). The crude compound was purified by column chromatography (20 -> 70% 90:5:5 EtOAc:MeOH:TEA in cHex) to give the Boc-protected intermediate **3d** as a yellow solid (72 mg, 42%). **^{1}H NMR** (600 MHz, CD_3OD) δ 7.72 (d, *J* = 8.9 Hz, 2H), 6.88 (d, *J* = 8.9 Hz, 2H), 4.84 – 4.81 (m, 1H), 4.38 (tt, *J* = 11.6, 4.1 Hz, 1H), 4.23 (d, *J* = 13.5 Hz, 2H), 3.20 – 3.09 (m, 1H), 3.04 – 2.82 (m, 2H), 2.61 (s, 3H), 2.58 – 2.19 (m, 11H), 2.04 (ddd, *J* = 12.6, 12.4, 4.3 Hz, 2H), 1.95 – 1.83 (m, 2H), 1.72 – 1.61 (m, 4H), 1.60 – 1.42 (m, 11H). **^{13}C NMR** (151 MHz, CD_3OD) δ 160.3, 156.3, 149.2, 142.9, 139.8, 135.6, 135.6, 124.4, 116.2, 81.3, 70.3, 58.7, 56.4, 51.9, 34.2, 32.5, 28.7, 25.9, 24.8, 14.1, 9.4. **LCMS** (acidic)**:** t_r: 4.01 min, purity: 95% (254 nm), λ_{max}: 345 nm, $[M+H]^+$ m/z calc. 537.35, found 537.45.

1-((1*r*,3*r*)-3-(4-((*E*)-(3,5-dimethyl-1-(piperidin-4-yl)-1*H*-pyrazol-4-yl)diazenyl)phenoxy) cyclobutyl)piperidine (3e)

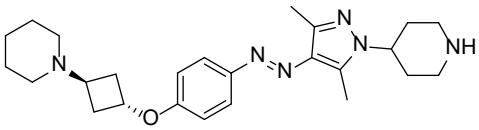

Compound **3d** (72 mg, 0.13 mmol) was dissolved in dioxane (1 mL) and 4M HCl in dioxane (1 mL) was added. The reaction mixture was stirred overnight at rt. The reaction mixture was concentrated to give a yellow solid, which was mixed with satd. aq. $NaHCO_3$. Extraction was performed with EtOAc thrice. The combined organic layers were washed with water and brine, dried over Na_2SO_4, filtered and concentrated. The crude product was purified by reverse phase column chromatography (5 -> 95% MeCN + 0.1% HCO_2H in H_2O + 0.1% HCO_2H). Desired fractions were combined, made basic using aq. sat. $NaHCO_3$ and extracted with EtOAc thrice. The combined organic layers were dried over

Na_2SO_4, filtered and concentrated to give the free base as a yellow solid (41 mg, 70%). **^{1}H NMR** (600 MHz, CD_3OD) δ 7.73 (d, *J* = 9.2 Hz, 2H), 6.89 (d, *J* = 8.9 Hz, 2H), 4.83 (tt, *J* = 4.1, 2.7 Hz, 2H), 4.34 (tt, *J* = 11.7, 4.0 Hz, 1H), 3.26 – 3.17 (m, 2H), 3.04 (tt, *J* = 7.5, 7.5 Hz, 1H), 2.80 (dd△, *J* = 13.0, 2.6 Hz, 2H), 2.62 (s, 3H), 2.48 – 2.40 (m, 6H), 2.53 – 2.22 (m, 11H), 2.27 (d, *J* = 0.8 Hz, 3H), 2.10 (ddd, *J* = 12.7, 12.6, 4.2 Hz, 2H), 1.95 – 1.88 (m, 2H), 1.64 (tt, *J* = 5.7, 5.7 Hz, 4H), 1.56 – 1.44 (m, 2H). **^{13}C NMR** (151 MHz, CD_3OD) δ 160.3, 149.2, 142.7, 139.7, 135.6, 124.3, 116.2, 70.5, 58.7, 56.5, 52.0, 46.0, 34.4, 33.2, 26.1, 25.1, 14.2, 9.4. **LCMS** (acidic)**:** t_r: 2.45 min, purity: 97% (254 nm), λ_{max}: 338 nm, $[M+H]^+$ m/z calc. 437.30, found 437.30. **HRMS**: $[M+H]^+$ calc. for $C_{25}H_{37}N_6O_2$: 437.3023, found 437.3022.

4-(3,5-dimethyl-4-((*E*)-(4-((1*r*,3*r*)-3-(piperidin-1-yl)cyclobutoxy)phenyl)diazenyl)-1*H*-pyrazol-1-yl)-1-methylpiperidine (**3f**)

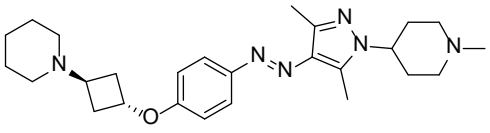

General procedure B was followed, using phenol **6f** (152 mg, 0.49 mmol), NaH (26 mg, 0.65 mmol), and tosylate **7** (100 mg, 0.32 mmol). The crude product was purified by reverse phase column chromatography (5 -> 95% MeCN + 0.1% HCO_2H in H_2O + 0.1% HCO_2H). Desired fractions were combined, made basic using aq. satd. $NaHCO_3$ and extracted with EtOAc thrice. The combined organic layers were dried over Na_2SO_4, filtered and concentrated to give the free base as a yellow solid (31 mg, 21%). **^{1}H NMR** (600 MHz, CD_3OD) δ 7.72 (d, *J* = 8.9 Hz, 2H), 6.89 (d, *J* = 8.9 Hz, 2H), 4.83 (tt, *J* = 6.8, 3.4 Hz, 1H), 4.20 (ddd△, *J* = 11.1, 7.8, 4.2 Hz, 1H), 3.09 – 2.99 (m, 3H), 2.61 (s, 3H), 2.55 – 2.14 (m, 18H), 1.97 – 1.82 (m, 2H), 1.63 (tt, *J* = 5.7, 5.7 Hz, 4H), 1.57 – 1.40 (m, 2H). **^{13}C NMR** (151 MHz, CD_3OD) δ 160.3, 149.2, 142.6, 139.8, 135.8, 124.3, 116.2, 70.5, 58.7, 56.3, 55.7, 52.0, 46.1, 34.4, 32.2, 26.1, 25.1, 14.2, 9.4. **LCMS** (acidic)**:** t_r: 2.47 min, purity: 99% (254 nm), λ_{max}: 343 nm, $[M+H]^+$ m/z calc. 451.32, found 451.30. **HRMS**: $[M+H]^+$ calc. for $C_{26}H_{39}N_6O_2$: 451.3180, found 451.3184.

Radiolabeling of 3f with [^{3}H]methyl nosylate

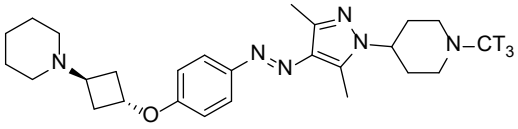

Compound **3e** (0.22 mg, 0.55 µmol) was dissolved in 117 µL of [^{3}H]methyl nosylate (Perkin Elmer, 827 MBq/mL in MeCN). The reaction mixture was heated for 15 min at 70 °C. Next, the reaction mixture was allowed to cool to rt, diluted with 2 mL eluent and injected onto a HPLC system (Jasco PU-2080 Pump, Jasco UV-2075 UV detector, Luna C18, 10x250 mm, 100 Å, 10µm, 60% acetonitrile, 40% water, 0.2% DIPEA, 5 ml/min, 254 nm) for purification. The product eluted between 38 and 44 min and was collected in a solution of 80 mL water. The total mixture was purged over a Sep-Pak tC18 (Waters, Milford, USA) which was pre-washed with 10 mL of EtOH and 10 mL of water, successively. After trapping of [^{3}H]**3f**, the Sep-Pak was washed with 20 mL of water and [^{3}H]**3f** was obtained with elution of the Sep-

Pak with 2 mL of EtOH. The concentration of [^{3}H]**3f** in EtOH was determined using beta counting (Hidex 300 SL, Turku, Finland) and found to be 22.3 MBq/mL. The product was analyzed with HPLC (Jasco PU-2080 Pump, Jasco UV-2075 UV detector, Lablogic β-RAM Scintilation detector, XBridge C18, 4.6x100 mm, 100Å, 5µm, 45% MeCN, 55% water, 0.2% DIPEA, 1 ml/min, 254 nm) and found to be of 97.2% radiochemical purity. A small UV trace impurity was observed at 7.48 min (Figure S21), which was not the precursor. The molar activity was 2.8 MBq/nmol and the molar concentration was 7.93 nmol/mL, based on the applied [^{3}H]methyl nosylate.

Chapter 3

‘Photoswitch hopping’ in Photopharmacology: A Comparative Study on Photochemical and Pharmacological Properties

Lars C.P. Binkhorst,[#] Ivana Josimovic,[#] Tess H. Stepek, Samu Kovács, Henry F. Vischer, Maikel Wijtmans and Rob Leurs

Manuscript in preparation

Division of Medicinal Chemistry, Amsterdam Institute of Molecular and Life Sciences, Faculty of Science, Vrije Universiteit Amsterdam, De Boelelaan 1108, 1081 HZ Amsterdam, The Netherlands

[#] Authors contributed equally to this manuscript.

Abstract

Azobenzenes are widely used in photoresponsive systems due to their robust *trans* to *cis* isomerization. Recently, heteroaryl azo (HAA) switches, in which a heteroaromatic moiety replaces one phenyl ring in an azobenzene, have received attention due to their improved photoswitching properties. Despite their potential advantages, HAA-based photoswitchable moieties remain underexplored in photopharmacology, an area that uses small-molecule photoswitchable protein ligands and light to control protein activity. This study describes a 'photoswitch hop' approach resulting in twelve photoswitchable ligands with known and new HAA moieties, as applied to an archetypical G protein-coupled receptor (GPCR) protein, the histamine H_3 (H_3R) receptor. HAA building blocks were synthesized using five different approaches, requiring tailored diazotization conditions for unstable heterocyclic diazonium salts. Physicochemical, photochemical, glutathione (GSH) stability, and pharmacological properties of the HAA-based photoswitchable ligands were systematically compared to their azobenzene counterpart. Diverse photochemical profiles were observed among the ligands, with multiple ligands showing red-shifted λ_{max} *trans* values but at the cost of reduced PSS_{cis} values compared to the parent azobenzene. Notably, all ligands show higher PSS_{trans} values and at least one improved switching wavelength (green light) compared to the azobenzene (blue light). The ligands display a wide variety of thermal half-lives in the PSS_{cis} state, ranging from minutes to days, and do not show aggregation/precipitation at relevant concentrations. Specific ligands were susceptible to degradation in the presence of GSH, particularly in the PSS_{cis} state. In the biochemical case study using H_3R, several ligands show an improved affinity of the *trans* isomer compared to the azobenzene template, but in some cases, this is accompanied by a diminished affinity shift between states. As an illustration of the potential of a 'photoswitch hop', isoxazole **3k** (VUF26257) was discovered to have a picomolar affinity (K_i *trans* = 158 pM) and appropriate affinity shift (13-fold). Identifying a compound that performs optimally across all properties will retain a case-by-case character based on the application, but this work provides a blueprint for future exploration of HAA photoswitches in photopharmacology. Equally importantly, our findings may also extend to other chemistry areas that use light-responsive systems.

Introduction

Azobenzenes represent the most widely used class of molecular photoswitches in various chemistry fields, such as supramolecular chemistry, imaging, metal catalysis, materials science, and photopharmacology.[1–5] This is because of their well-studied isomerization, robust photoswitching properties and ease of synthesis.[6,7] A key photopharmacology approach entails the use of small-molecule photoswitchable ligands (often azobenzenes) that reversibly isomerise upon illumination ('photoswitching'), giving distinctly different biological properties to the two isomers.[8] However, incorporating azobenzenes in bioactive ligands poses several limitations. Their hydrophobic nature often results in limited solubility of the ensuing ligand in aqueous environments[9,10] and ultraviolet (UV) light is required to switch the thermodynamically stable *trans* isomer to the metastable *cis* isomer. Switching the *cis* isomer

back to the *trans* isomer often requires blue light (400-450 nm) and overlapping absorption bands of the two isomers in this spectral region lead to low photostationary states (PSS) values.[6] Importantly, the use of UV light is far from biocompatible in light of its potential cell toxicity and limited tissue penetration. Recent efforts in the field have therefore aimed to achieve switching both ways with visible light ('red-shifting').[11,12] For example, tetra-*ortho*-substituted azobenzenes are known for their ability to switch using visible light.[12] However, especially larger *ortho* substituents (e.g., chlorine or methoxy) may for steric reasons significantly alter protein binding of the ligand compared to its unsubstituted azobenzene counterpart. Another red-shifting strategy, which is perhaps sterically less invasive, is the incorporation of heteroarylazo (HAA) switches, in which one of the phenyl rings in azobenzene has been replaced by a heteroaromatic moiety. Some HAA moieties are known for decades but only recently have HAA switches received attention in photopharmacology, given their excellent switching properties.[10,13–16] Most particularly, arylazopyrazoles have rapidly become a mainstay in the photopharmacology field, [17–25] but photoswitchable protein ligands based on many other HAA switches remain underexplored in photopharmacology. This seems somewhat unexpected, as photoswitches containing heteroaromatic rings should be particularly interesting given the high prevalence of heteroaromatic moieties among small-molecule drugs.[26] Replacing benzene rings with heteroaromatic rings is a common strategy to enhance solubility,[10] and the incorporation of heteroatoms can facilitate productive molecular recognition events with the protein target (e.g., hydrogen bonding or metal coordination), allowing tuning of both the photochemical and pharmacological properties simultaneously.[10,27]

Despite the potential advantages of HAA-containing photoswitchable ligands, there is a lack of comparative studies on their various properties (including photochemical and pharmacological) in photopharmacology. This may partly be attributed to the limited availability of synthetic methodologies for incorporating HAA scaffolds in drug-like structures.[14,27] Computational approaches have been used to correlate theoretical and experimental half-lives[28] of many HAA switches and to propose ideal photoswitches with red-shifted wavelengths and long half-lives.[29] However, none of the latter were taken forward for photopharmacology approaches. Here, to provide the field with a systematic comparison, we explore known and underexplored five-membered HAA switches in a "photoswitch hop" (akin to the "scaffold hop" in medicinal chemistry).[30,31] We systematically compare twelve ligands with HAA photoswitches to the corresponding azobenzene in terms of key physicochemical and photochemical properties. For advanced biochemical use such as *in vivo*, the chemical stability in the presence of GSH is emerging as a relevant property of photoswitches[11,32–35] and we explored this property for both configurational states of the ligands. For pharmacological proof of concept, we selected a G protein-coupled receptor (GPCR). GPCRs are one of the most extensively studied protein classes targeted by approximately 36% of all marketed drugs.[36] GPCRs have also been successfully used in photopharmacology studies with a range of photoswitchable ligands disclosed.[37–40] However, our 2022 review shows that

at the time, only 5 % of photoswitchable GPCR ligands contain a HAA, compared to 84 % of azobenzenes,[38] making a comparative study on an exemplary GPCR both timely and relevant.

Results and discussion

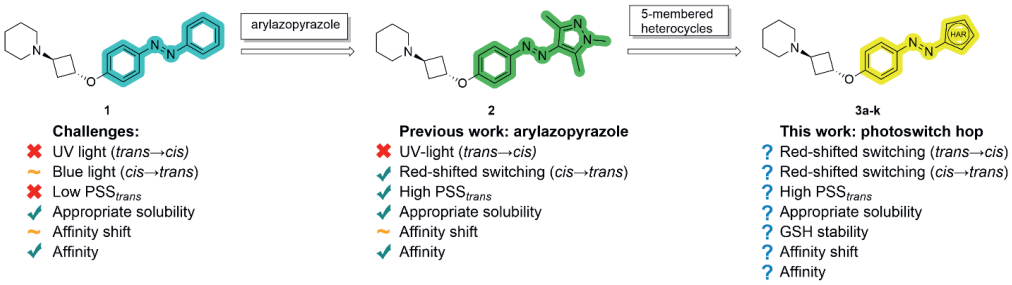

Figure 1. Design towards HAA-containing photoswitchable ligands based on previously published H_3R antagonists.[41]

Design

For the pharmacological proof of concept, we used the archetypical H_3R. The H_3R is primarily expressed in the central nervous system and has been linked to various neurological and psychiatric disorders, including Parkinson's and Alzheimer's disease, Tourette's and schizophrenia, as well as sleep disorders, such as narcolepsy.[42–44] Currently, one drug, Pitolisant (Wakix® and Ozawade®), is marketed targeting the H_3R for the treatment of narcolepsy as well as obstructive sleep apnea. Additionally, the medicinal chemistry of H_3R ligands has been well documented.[45] In previous research,[41] we showed that replacing the azobenzene photoswitch of H_3R ligand **1** with an arylazopyrazole (i.e., **2**; Figure 1) provides a compound with appropriate solubility, better PSS_{trans} value of 93 % (Table 1), high H_3R affinity for *trans*-**2** (pK_i = 9.1) and an 8-fold affinity shift between *trans*-**2** and **2**-PSS_{cis} (Table 2). In the current study, we built upon this work by exploring additional ligands with eleven additional five-membered heterocycles (**3a-k**, Figure 1). The set comprises a variety of sulphur-, oxygen- and/or nitrogen-containing heteroaromatics. Our set includes several previously reported nitrogen-containing HAA switches.[18] Likewise, photoswitches such as the 2-aryl-3,5-dimethylisoxazole,[19] 2-arylazoimidazole[20] and 2-arylazothiazole[21] have already been extensively characterized in terms of their photochemistry properties and have also been incorporated into various photoswitchable protein ligands.[46–49] Others (e.g., thiadiazole[50]) have been studied for their photochemical switching properties, but not in the photopharmacology field. Most notably, heteroaromatic rings such as isoxazole (e.g., 3-arylazoisoxazole and 5-arylazoisoxazole) and sulphur-containing photoswitches (e.g., 5-arylazothiazole) remain, to the best of our knowledge, mostly unexplored in photoswitching chemistry, and thus in the photopharmacology field as well. Introducing a variety of established and underexplored switches into H_3R template ligand **2** in a comparative fashion will provide better insight into how these heteroaromatic rings affect the photochemical, physicochemical, GSH stability and pharmacological properties of these ligands.

Synthesis

The synthesis of compound **3a-k** commenced with the preparation of phenol intermediates **5b-k** and 4-fluorobenzene **10** (Scheme 1) as building blocks. Phenols **5b-i** were synthesized using four different conditions, generally involving heterocyclic anilines **4** being converted to their diazonium salt, followed by coupling to PhOH. Thiazol-4-amine hydrochloride (**4f**) was made *in situ* from Boc-precursor **6** due to the presumed instability of the amine and reacted with NO^+ BF_4^- to provide the corresponding diazonium salt. Most other intermediate diazonium salts were prepared by standard diazotization conditions with dilute aq. HCl and $NaNO_2$. However, several heterocyclic anilines (i.e., **4h-i**) decomposed under these conditions. Alternative diazotization conditions using *tert*-butyl nitrite in polar aprotic solvents (THF and MeCN) were also unsuccessful, as no conversion of the starting material was observed. Based on a literature procedure, use of $NaNO_2$ and concentrated H_3PO_4 followed by the addition of PhOH in MeOH, resulted in the successful formation of phenol intermediates **5h-i**.[51] Furthermore, 4-aminophenol (**7**) underwent diazonium coupling with acetylacetone to give **8**, which was heated with H_2NOH and Na_2CO_3 to yield isoxazole **5k**.[52] The synthesis of 4-fluorophenyl intermediate **10** was based on a procedure by Heindl *et al*.[53] using a Turbo-Grignard reagent (made from **9**) and 4-fluorobenzenediazonium tetrafluoroborate. Using this method, compound **10** was obtained successfully. It is of interest to point out that efforts to synthesize the phenol intermediates from two attempted additional heteroaromatics, i.e. oxazol-2-amine and 1,3,4-oxadiazol-2-amine, were unsuccessful using any of the diazonium-based approaches described here.

Scheme 1. Synthesis of heteroaryl photoswitchable building blocks **6a, c-k** and **10**.[a]

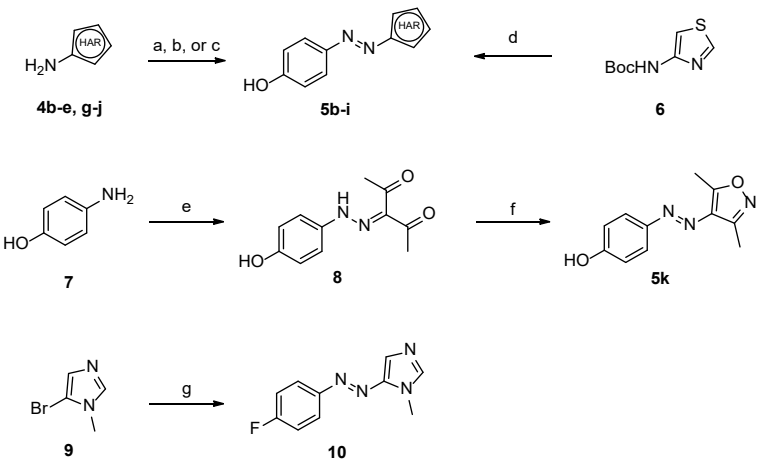

[a]**Reagents and conditions:** (a) For **5b,c**: (i) $NaNO_2$, HCl, H_2O, 0°C, 1 h (ii) PhOH, NaOH, H_2O, 0°C to rt, 1.5 h, 20-95%; (b) For **5d, e, g:** (i) HCl, H_2O (ii) $NaNO_2$, PhOH, NaOH, 0°C to rt, 2h, 26-87%; (c) For **5h-j:** (i) $NaNO_2$, H_3PO_4, 0°C, 30 min (ii) PhOH, MeOH, 0°C to rt, 30 min, 27-85%; (d) For **5f**: (i) 4M HCl in 1,4-dioxane, MeOH, rt, 18 h (ii) NO^+ BF_4^-, TFA, MeCN, 0°C, 30 min (iii) PhOH, K_2CO_3, H_2O, 0°C to rt, 30 min, 42%; (e) (i) $NaNO_2$, aq. HCl, H_2O/AcOH, 0°C, 45 min; (ii) Acetylacetone, NaOAc, H_2O/EtOH, 0°C, 1 h, 44%; (f) NH_2OH·HCl, Na_2CO_3, EtOH, reflux, 18 h, 51%; (g) (i) ^{i}PrMgCl·LiCl, THF, rt, 45 min (ii) $ZnBr_2$, THF, -20 °C to rt, 30 min (iii) 4-$FPhN_2^+$ BF_4^-, NMP/THF, -40 °C to -20 °C, 22 h, 20%;

The *trans*-3-piperidino-cyclobutoxy linker was installed via two distinctly different routes. The first route involved coupling phenols **5b, c, k** with previously reported[54] *cis*-tosylate **11** to yield compound **3b, c, k**. The second route delivered **14a, d-i**, starting with either a Mitsunobu reaction using phenols **4e-i** and commercially available *cis*-alcohol **12,** or a nucleophilic aromatic substitution on **10** with commercially available *trans*-alcohol **13**. Intermediates **15a, d-i** were obtained by removing the Boc protecting group of **14a, d-i** using 4M HCl in dioxane. The final step involved the formation of the piperidine ring using 1,5-dibromopentane to give ligands **3a, d-i**.

Scheme 2. Synthesis of heteroaryl-containing photoswitchable ligands **3a-k**.[a]

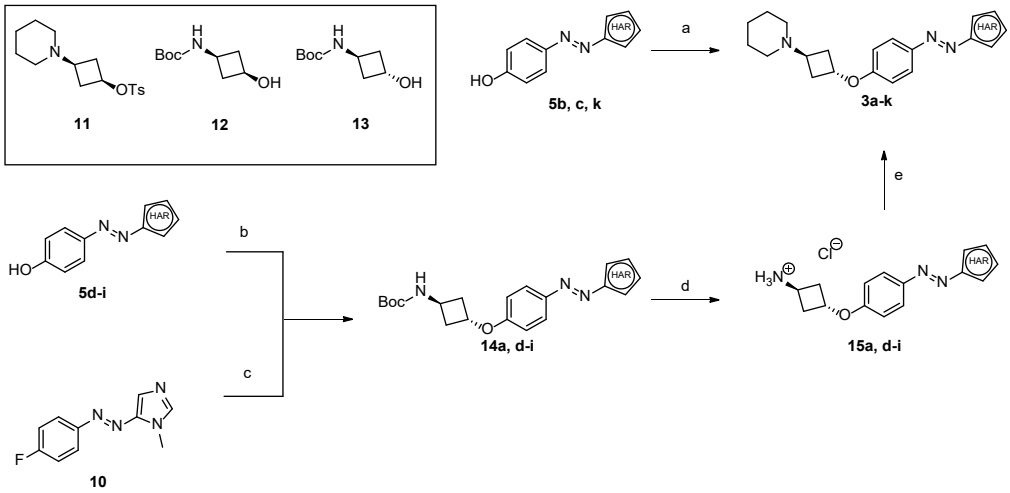

[a]**Reagents and conditions:** (a) (i) NaH, DMF, rt (ii) **11**, DMF, 70-90°C, 20-22 h, 6-9%; (b) **12**, PPh_3, DIAD, THF, 0°C to 50 °C, 17 h, 26-90%; (c) (i) **13**, NaH, DMF, 1.5 h, 0°C (ii) **10,** 0°C to rt, 12h, 40%; (d) 4 M HCl in 1,4-dioxane, MeOH, rt, 1-4 h, 53-93%; (e) 1,5-dibromopentane, DIPEA, MeCN, reflux, 17 h, 41-74%;

Structure-Photochemistry Relationship

The comparison of the photochemistry properties of the photoswitchable ligands **3a-k** with azobenzene **1** reveals several qualitative trends (Figure 2, Table 1). Compounds **2** and **3c, d, f, i, k** show absorption features resembling those of azobenzene **1**, and their λ_{max} *trans* values (π-π*) are comparable to the λ_{max} *trans* value (π-π*) of azobenzene **1**. Consequently, a wavelength of 360 nm (UV light) was used for the *trans-cis* switching of these compounds. The PSS value for the *trans-cis* switching (PSS_{cis}) of **2** and **3c,d,f,i, k** upon illumination with 360 nm is >= 87%. In contrast, the λ_{max} *trans* values (π-π*) for **3a,b,e,g,h,j** are more red-shifted compared to that of azobenzene **1**, mostly allowing the use of wavelengths into the visible range for the *trans-cis* switching (i.e., 400 nm for **3b,g,h,j** or 434 nm for **3e**). However, the associated PSS_{cis} values are reduced (52-80%), with **3g** having the lowest PSS_{cis} value (64%).

Table 1. Photochemical parameters of photoswitchable ligands **3a-k.**

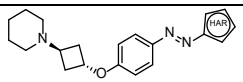

Compound	HAR	λ_{max} π-π* *trans*[a] (nm)	λ_{max} n-π* *trans*[a] *(nm)*[f]	λ_{max} π-π* *cis*[a] (nm)	λ_{max} n-π* *cis*[a] (nm)	Illumination wavelength for PSS_{cis} (nm)	PSS_{cis} (area %*cis*) ± SD[b]	Illumination wavelength for PSS_{trans} (nm)	PSS_{trans} (area %*trans*) ± SD[c]	$t_{1/2}$[d]
1[e]		344	~434	312	432	360	97 ± 0	434	68 ± 0	11 d
2[e]		347	~430	315	439	360	95 ± 0	494	93 ± 0	7 d
3a		372	-	315	~434[f]	360	80 ± 0	494	74 ± 0	109 min
3b		391	-	340	450	400	n.d.[g]	560	n.d.[g]	10 min
3c		349	-	~325[f]	428	360	97 ± 0	494	87 ± 1	30 d
3d		351	-	336	436	360	90 ± 0	494	87 ± 0	16 d
3e		390	-	-[f]	~383[f]	434	n.d.[g]	520	n.d.[g]	7 min
3f		352	-	333	437	360	93 ± 0	494	85 ± 0	182 min
3g		380	-	346	~459[f]	400	64 ± 4[h]	520	93 ± 1[h]	44 min
3h		390	-	363	~464[f]	400	n.d.[g]	520	n.d.[g]	22 min
3i		352	-	334	430	360	87 ± 0	494	85 ± 1	52 min
3j		372	~464	346	451	400	81 ± 1	520	92 ± 0	45 min
3k		339	~430	318	432	360	95 ± 0	494	92 ± 0	21 d

[a]Determined at 25 µM in HBSS buffer containing 1% DMSO.

[b]Photostationary state area percentages after illumination of *trans* isomer with the indicated illumination wavelength to PSS_{cis} at 10 mM in DMSO as determined by acidic LC-MS analysis at the isosbestic point. Values are means of experiments ± SD, performed in duplicate.

[c]Photostationary state area percentages after illumination of PSS_{cis} states with the indicated illumination wavelength for PSS_{trans} at 10 mM in DMSO as determined by acidic LC-MS analysis at the isosbestic point. Values are means of experiments ± SD, performed in duplicate.

[d]Thermal relaxation ($t_{1/2}$) of PSS_{cis} states in HBSS buffer containing 1% DMSO. For compounds with $t_{1/2}$ > 1 day, the thermal relaxation was estimated by the method of Ahmed *et al*.[55] and extrapolated to 20°C. Arrhenius plots are available in the SI.

[e]Previously published data.[41]

[f]No distinct absorption band could be identified. An approximate value is provided where reasonably possible.

[g]Photostationary state area percentages could not be accurately determined by LC-MS analysis due to short $t_{1/2}$.
[h]Photostationary state area percentages were determined by basic LC-MS analysis instead of acidic LC-MS analysis.

In all cases, there is sufficient to good separation between the *trans* n-π* and *cis* n-π* bands, which allows for generally high PSS_{trans} values with, importantly, all of these being higher than that of **1** (68 %). Although the absorption spectra of **3a,b,e,g,h** show insufficiently distinct or broad n-π* absorption bands for the *cis* isomer (Figure S3B, S4B, S7B, S8B, S10B), the absorption features of the *trans* and *cis* isomers are sufficiently resolved at wavelengths > 500 nm. Thus, all compounds could be switched from the *cis* isomer to the *trans* isomer with wavelengths of 494 nm (green light, **2** and **3a,c,d,f,i,k**), 520 nm (green light**, 3e**,**g**,**h**,**j**) or 560 nm (yellow-green light, **3b**). Noteworthy, heteroaryls **2** and **3g,j,k** have very high PSS_{trans} values of >=92 %. Compounds **3c,d,f,h,i** on the other hand, have PSS_{trans} values between 85-89%, while **3a** exhibits the lowest but still appreciable PSS_{trans} value of 74%. Even though *cis-trans* switching sometimes requires illumination in the tail of a band with the associated risk of (too) long illumination times,[56] the approximate illumination times shown in Figure 2 are still acceptable, which we attribute to the generally high intensity of the n-π* band of the heteroaryl switches.

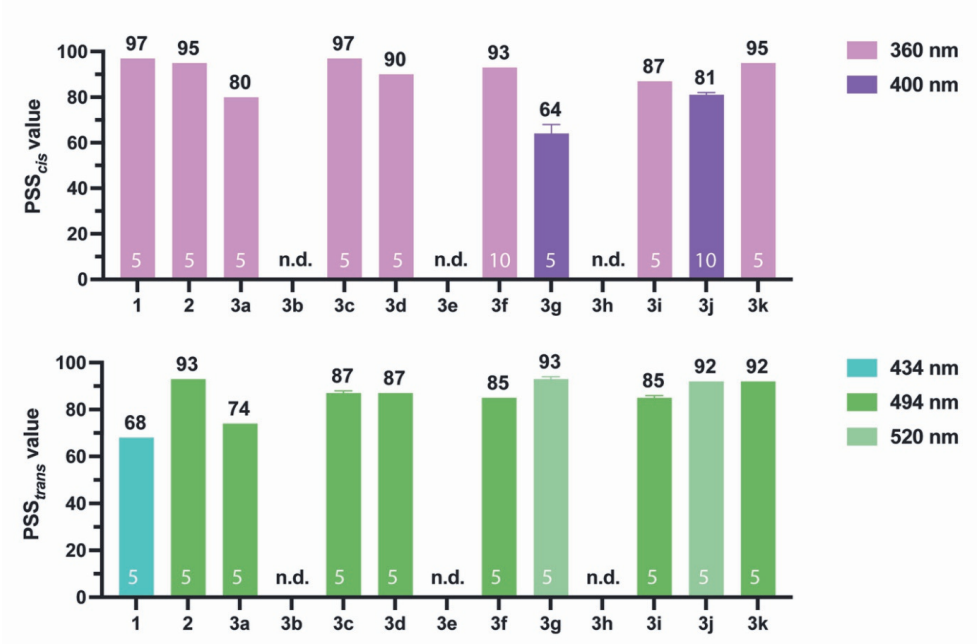

Figure 2. Overview of PSS_{cis} and PSS_{trans} values for compounds **1, 2, 3a-k** as determined by LC-MS (See Table 1) in HBSS buffer containing 1% DMSO. The colors of the bars indicate the wavelength used to achieve PSS. The approximated time needed to achieve the PSS is given in minutes (white numbers), with the PSS being checked in time intervals of 5 minutes.

The half-lives of the *cis* isomers for **2**,**3a-k** at 20°C vary widely. Compared to azobenzene **1**, which has a half-life of 7 days, **2** and **3c,d,k** have similar half-lives in the range of days. In contrast, the other photoswitchable ligands studied show much shorter half-lives. Compounds **3a,f** have half-lives of approximately 2 and 3 h, respectively, while **3g,i,j** have a half-life of approximately 45 min. The very short half-life of **3b,e,h** (7-22 min) prevented reliable quantification of both PSS_{cis} and PSS_{trans} values by LC-MS analysis. Switching for these compounds, however, was confirmed by UV analysis (Figures S4, S7 and S10).

Physicochemical properties

Key physicochemical properties (Table S1, Figure S14) were calculated (using CDD software).[57] These include the molecular weight (MW), the number of hydrogen bond donors (HBD) and hydrogen bond acceptors (HBA), the partition coefficient (cLogP), the distribution coefficient at pH 7.4 ($cLogD_{7.4}$), calculated solubility (LogS), and the topological polar surface area (TPSA). The number of HBD and HBA can be important for molecular recognition and binding affinity to the protein target. Notably, by design the HAA switches exhibit a higher number of HBAs (5-7) compared to azobenzene **1** (4). This increase offers opportunities for productive hydrogen bonding interactions with the target protein. In terms of lipophilicity, most HAA compounds show a decrease in cLogP (4.0-5.2) and cLogD values (2.1-3.6) relative to azobenzene **1** (cLogP = 5.9, cLogD = 4.4), indicating lower hydrophobicity. Interestingly, **3c** and **3e** exhibit the highest lipophilicity among the heterocycles studied (5.2 and 5.0). The TPSA of azobenzene **1** is relatively low (37.2 Å²), while HAA switches show increased TPSA values (50.1-67.9 Å²). Calculated solubility (LogS) values suggest improved aqueous solubility for the HAA ligands compared to azobenzene **1**. While azobenzene **1** shows a LogS value of -6.5, the HAA switches have logS values between -5.1 and -6.0. We investigated the approximate solubility in HBSS buffer containing 1% DMSO by nephelometry (Table S2).[58,59] We define a solubility as appropriate if no precipitation and/or aggregation[60] is observed at 10^{-4} M, a common highest concentration in pharmacological assays. Only two compounds do not adhere to this cutoff. Specifically, we found that the *trans* isomers of arylazothiadiazole **3h** and arylazoisoxazole **3k** show significant precipitation at 10^{-4} M, while other ligands, including azobenzene ligand **1**, do not show precipitation and/or aggregation up to 10^{-4} M. For photoswitchable ligands with thermal half-lives of >7 days, the approximate solubility was also studied at PSS_{cis}. As expected, none of the compounds show aggregation up to 10^{-4} M when switched to PSS_{cis}.[9] Importantly, because of the high affinity of the ligands, no compounds show aggregation/precipitation at concentrations relevant for assay conditions.

Aqueous chemical stability in the absence and presence of GSH

Inherent buffer stability of ligands was investigated PBS buffer containing 1% DMSO (37 °C, pH 7.4) for 12 h in both the *trans* and PSS_{cis} states. We found that all compounds were stable in the *trans* configuration. However, when switched to the PSS_{cis} state degradation could be observed for compound **1, 2,** and **3c**. (Figure S15). In a similar setup, we also investigated the stability of the photoswitchable ligands in the presence of glutathione (GSH). GSH, a reducing and nucleophilic agent present in cells at high concentrations (0.5 mM – 10 mM),[61] is known

to have the potential to reduce the azo bond, which can compromise photoswitching under physiological conditions.[8,9] Some HAA switches have been shown to be stable against GSH,[34] although others are not,[62] highlighting the importance of systematic evaluation of this property. The stability of the photoswitchable ligands was monitored in PBS buffer using LC-MS for 12 h at intervals of approximately 1 h. Most ligands, including the parent azobenzene **1**, are stable in the *trans* configuration. However, imidazoles **3a** and **3b**, thiazole **3f** and isoxazole **3j** (Figure 3) are susceptible to GSH decomposition. Indeed, it has previously been shown that 2-arylazoimidazoles undergo decomposition induced by GSH.[62]

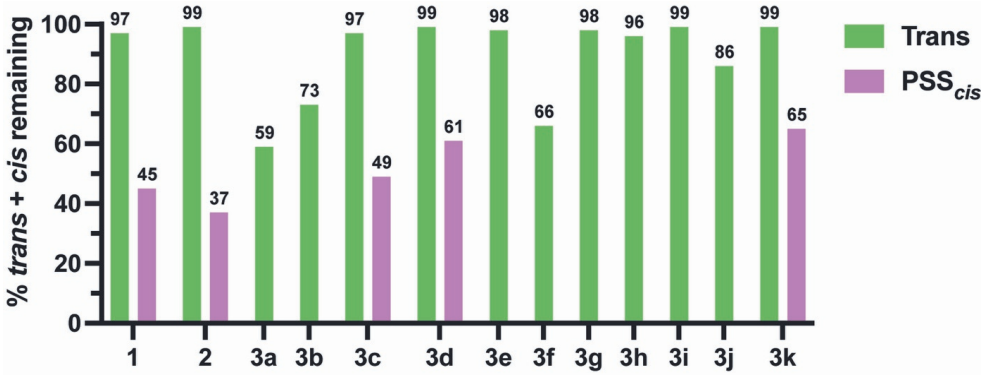

Figure 3. Percentage of compound (*trans* and *cis* combined) remaining after 12 h incubation of *trans* (green) or PSS_{cis} (purple) in the dark with 4.6 mM GSH at 37 °C in PBS buffer.[63] For **3a,b,e,f,g,h,j** no data for PSS_{cis} stability could be measured because of its too fast relaxation.

When investigating the GSH stability of compounds, the focus has often been on the stability of the *trans* isomer. Only occasionally has the stability of the PSS_{cis} state toward GSH been reported.[46,62,64] However, the stability of the *cis* isomer in the presence of GSH is at least as important as that of the *trans* isomer, for example, when the *cis* isomer is the more active isomer of the ligand. For compounds with thermal half-lives greater than 7 d at 20 °C (i.e., **1, 2, 3c, 3d** and **3k**), the stability of the PSS_{cis} state was tested. When adding GSH to compounds at PSS_{cis}, at least two processes can occur simultaneously, i.e., reaction of the compound with GSH and thermal relaxation of the *cis* isomer to the *trans* isomer. Compounds **1, 2, 3c, 3d** and **3k**, which are all stable as the *trans* isomer, are more prone to reaction with GSH at PSS_{cis}, with 37-65 % of the compound (*trans* and *cis* isomers combined) remaining after 12 h. While *trans*-arylazopyrazoles are known for their stability against GSH,[34] we found that arylazopyrazole **2** also reacts as PSS_{cis}. Additionally, we observed that GSH significantly accelerates the dark *cis* to *trans* conversion for **1, 2, 3c, 3d** and **3k** (Figure S16). Specifically, 4 out of 5 compounds completely revert from the *cis* to the *trans* isomer in the dark with GSH present. These findings are qualitatively in agreement with Park *et al*. and Moroder *et al*.,[65,66] who previously reported the accelerated *cis* to *trans* isomerization of azobenzenes by GSH.[58,59]

Pharmacology

Table 2. Human H_3R binding affinity values and affinity shifts of **1, 2, 3a-k**.

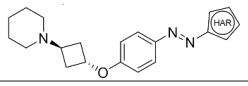

Compound	HAR	pK_i *trans* ± SEM[a]	pK_i PSS$_{cis}$ ± SEM[a]	pK_i shift[b]	Compound	HAR	pK_i *trans* ± SEM[a]	pK_i PSS$_{cis}$ ± SEM[a]	pK_i shift[b]
1[c]		8.0 ± 0.1	8.6 ± 0.2	0.6	**3f**		8.3 ± 0.1	8.4 ± 0.1[d]	0.1
2[c]		9.1 ± 0.1	8.2 ± 0.1	-0.9	**3g**		8.6 ± 0.1	8.4 ± 0.1[e]	-0.2
3a		9.2 ± 0.2	8.6 ± 0.1[d]	-0.6	**3h**		8.4 ± 0.1	8.4 ± 0.2[e]	0.0
3b		9.2 ± 0.1	8.7 ± 0.1[e]	-0.5	**3i**		8.1 ± 0.1	8.0 ± 0.1[d]	-0.1
3c		8.4 ± 0.1	8.2 ± 0.1	-0.2	**3j**		8.1 ± 0.0	8.0 ± 0.1[e]	-0.1
3d		8.1 ± 0.0	7.6 ± 0.0	-0.5	**3k**		9.8 ± 0.1	8.7 ± 0.0	-1.1
3e		8.4 ± 0.0	8.2 ± 0.0[e]	-0.2					

[a]Affinity (pK_i) values obtained from radioligand competition experiments with 1.6 nM [^{3}H]NAMH. Values are means of n = 3 experiments ± SEM, performed in triplicate. Full dose-response curves are available in SI.

[b]Affinity shifts between PSS$_{cis}$ and *trans* states are defined as p$K_{i,PSScis}$-p$K_{i,trans}$.

[c]Previously published data.[41]

[d]Continuous illumination at 365 nm at 25°C during the experiment.

[e]Continuous illumination at 400 nm at 25°C during the experiment.

The affinities (pK_i) of HAA ligands for the H_3R were evaluated by competition radioligand-binding experiments with [^{3}H]*N*-α-methylhistamine (Table 2). For compounds with relatively short thermal half-lives of the *cis* isomer (**3a,b,e-j**, Table 1), continuous illumination was used to measure the pK_i value at PSS$_{cis}$. In a previous study, we showed that replacing the phenyl ring of azobenzene **1** with an arylazopyrazole moiety yields high-affinity ligand *trans*-**2** (pK_i = 9.1) with an 8-fold affinity shift between *trans*-**2** and **2**-PSS$_{cis}$.

Similarly, the incorporation of imidazole rings (**3a** and **3b**) results in an improved *trans* affinity (pK_i = 9.2) compared to that of **1** (pK_i = 8.0) with an affinity shift of 0.6 log units. While azobenzene **1** is a *cis*-on compound (i.e., the affinity of PSS_{cis} is higher than that of the *trans* state), imidazoles **3a** and **3b** and also pyrazole **2** are *trans*-on compounds. Isomeric pyrazole **3c** has a lower affinity than pyrazole **2** and imidazoles **3a** and **3b**, and reduced affinity shift (-0.2 log units). Addition of an extra nitrogen atom (triazole **3d**) show slower affinities for both the *trans* (pK_i = 8.1) and PSS_{cis} (pK_i = 7.6) states compared to the imidazoles and pyrazoles. Replacement of the phenyl ring in **1** with five-membered heterocycles that contain both sulfur and nitrogen atom (thiazoles **3e** and **3f**, thiadiazoles **3g** and **3h**) exhibit similar or slight higher affinities of the *trans* isomers (pK_i = 8.3 – 8.6) compared to that of azobenzene **1** (pK_i = 8.0), but similar or lower affinity at PSS_{cis} (pK_i = 8.2 – 8.4) compared to that of **1** (pK_i = 8.6). Consequently, affinity shifts were minimal (-0.2 – 0.0). Of the heterocycles containing one oxygen and one nitrogen atom (isoxazoles **3i-3k**), the *trans* isomer of **3i** and **3j** display a similar affinity (pK_i = 8.1) compared to *trans*-**1**. However, no affinity shift was observed for either compound because of the lower affinity at PSS_{cis} (pK_i = 8.0). Remarkably, dimethyl-substituted regioisomeric isoxazole **3k** shows a more than 50-fold increase in affinity of the *trans* isomer to the pM range (pK_i = 9.8) compared to those of azobenzene **1** and other isoxazoles. The affinity at PSS_{cis} remains comparable to that of **1**, resulting in an appreciable 13-fold affinity shift (-1.1 log units).

The findings described here highlight the potential of known and underexplored HAA photoswitches as alternatives to azobenzenes, as exemplified by tunable ligands in photopharmacology. But several important factors should be considered. As highlighted by Crespi *et al*. and Dang *et al.,*[27,67] the synthesis of HAA switches remains a significant challenge with a clear need for improved synthetic procedures. In this work, we used five different conditions for the synthesis of the HAA intermediates (**5b-k**, **10**). Careful adjustment of diazotization conditions, especially for unstable heteroaryl amines, was essential to access these building blocks. Despite these efforts, we were unable to obtain the phenol intermediates from oxazol-2-amine and 1,3,4-oxadiazol-2-amine using any of these routes, emphasizing the need for improved synthetic methodologies.

Although the photochemical properties of several HAA switches have been previously reported,[13,20,50,52,62,68] most studies have focused on measurements in organic solvents such as MeCN or DMSO. These conditions often do not reflect the aqueous environment key in many uses of photoswitches, where solvent effects, such as hydrogen bonding can significantly alter photochemical properties.[9,38,69,70] A comparison between our ligands **2/3** and available reported MeO analogues (i.e. with the alkoxy unit in **2/3** replaced by a MeO moiety) can be made. For instance, Dolai *et al*.[62] reported high PSS values (>94% for both PSS_{cis} and PSS_{trans}) and a half-life of ~1 h for the *p*-OMe analog of **3b** in MeCN. In contrast, we observe a much shorter half-life of approximately 10 min in buffer and were unable to quantify the PSS values of **3b**, due to the fast thermal relaxation. Despite solvent differences affecting the thermal relaxation, the λ_{max} values of reported MeO-compounds in MeCN show

similar values to those of **2/3** in buffer.[52,68,71] When compared to parent azobenzene **1**, ligands **2, 3c, 3d, 3f, 3i** and **3k** exhibit similar absorption features and λ_{max} *trans* values, resulting in PSS_{cis} values >= 87% upon illumination. However, the use of UV light (360 nm) is still required for optimal *trans* to *cis* switching. In contrast, **3a, 3b, 3e, 3g, 3h,** and **3j** show more red-shifted λ_{max} *trans* values, allowing for higher wavelengths for *trans* to *cis* switching (i.e., 400 nm for **3b,g,h**,**j** or 434 nm for **3e**) but with reduced PSS_{cis} values. This highlights the challenges of balancing red-shifted switching wavelengths and suitable PSS values. Importantly, for all the HAA switches, the wavelengths for *cis* to *trans* isomerization are red-shifted (494-560 nm) compared to that of **1** and higher PSS_{trans} values are obtained, demonstrating the photochemical potential of these HAA switches. As a representative example, the key compound **3k** was subjected to in-depth photochemical analysis. The UV-Vis spectra of 25 µM **3k** in HBSS buffer exhibit good band separation of the n–π* transition bands of the *trans* and PSS_{cis} states (Figure 4A). Isomerisation was analysed using both LC-MS (Figure 4B) and ^{1}H NMR analysis (Figure 4C). After illumination with 365 nm light for 5 min PSS_{cis} was achieved, with 97% and >95% *cis* isomer PSS_{cis} values obtained by LC-MS and ^{1}H NMR analysis, respectively. Subsequent illumination with 506 nm light for 15-20 min resulted in a high PSS_{trans} value of 93% and 91% *trans* isomer by LC-MS and ^{1}H NMR analysis, respectively. Dynamic photoswitching of 25 µM **3k** in HBSS buffer monitored by absorbance at 340 nm confirmed fast *trans* to PSS_{cis} isomerisation with a half-life of 1.4 s and slower PSS_{cis} to PSS_{trans} isomerisation with a half-life of 40 s.

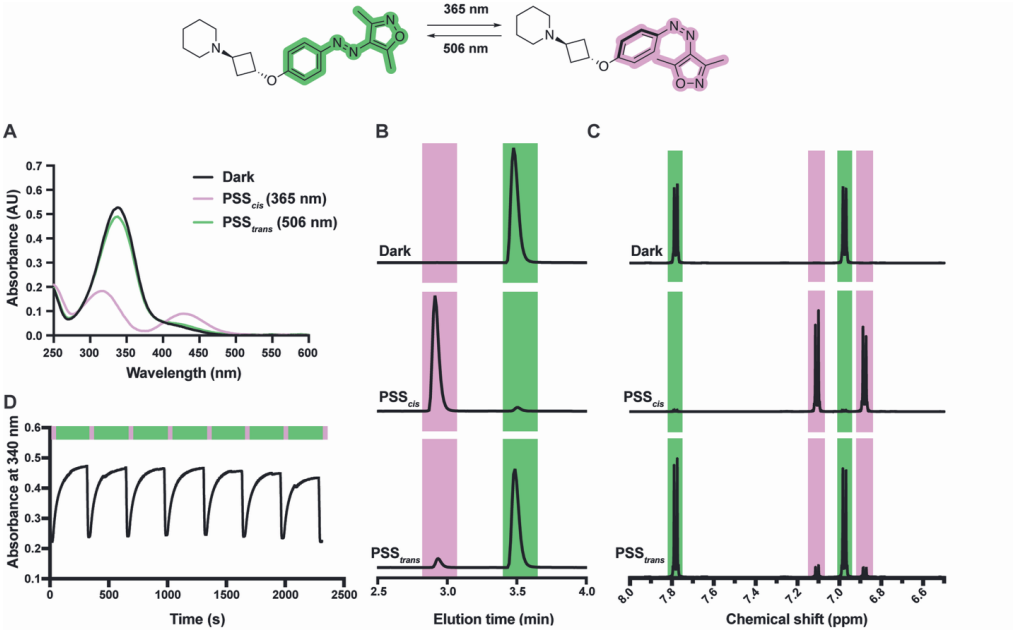

Figure 4. Photochemical properties of **3k**. (A) UV-Vis spectra of **3k** (25 µM, HBSS buffer containing 1% DMSO-d_6) in the dark, after illumination to PSS$_{cis}$ with 365 ± 11 nm for 2 min and after subsequent illumination to PSS$_{trans}$ with 506 ± 18 nm for 8 min. (B) Representative parts of LC–MS chromatograms of **3k** (10 mM, DMSO-d_6) in the dark, after illumination with 365 ± 11 nm for 10 min to reach PSS$_{cis}$ and subsequently with 506 ± 18 nm for 20 min to reach PSS$_{trans}$ as determined by LC-MS analysis at the isosbestic point (290 nm). (C) Part of the ^{1}H NMR spectra representing the two aromatic signals of **3k** (10 mM, DMSO-d_6) in the dark, after illumination with 365 ± 11 nm for 10 min to reach PSS$_{cis}$ and subsequently 506 ± 18 nm for 15 min to reach PSS$_{trans}$. (D) Reversible isomerisation cycles of **3k** (25 µM, HBSS buffer containing 1% DMSO), repeatedly illuminated for 20 s with 365 ± 11 nm to reach PSS$_{cis}$ and subsequently for 300 s with 506 ± 18 nm to reach PSS$_{trans}$. The y-axis shows the absorbance at 340 nm.

Aqueous solubility of photoswitches tends to be underestimated as a key parameter.[9] Most HAA switches show improved calculated solubility values (cLogS) compared to that of **1** and demonstrate suitable aqueous solubility in nephelometry experiments (up to at least $10^{-4.5}$ M). However, despite the presence of additional heteroatoms, no significant improvements in experimentally determined solubility were found compared to **1**. In fact, thiadiazole **3h** and isoxazole **3k** show precipitation/aggregation at $10^{-4.5}$ M, while for **1** this was not observed. Chemical stability of all *trans*-ligands in buffer was good, but with GSH present imidazole **3a** and **3b**, thiazole **3f**, and isoxazole **3j** are susceptible to decomposition. The limited GSH stability of *cis* isomers (not only of all measured HAA switches, but also of **1**) may need to be addressed for successful *in vivo* applications in photopharmacology. The notion of photoswitchable ligands being more prone to GSH-based decomposition in the PSS$_{cis}$ state is

particularly relevant when applications of HAA switches in the presence of reducing agents such as alkylthiols are used. Previously, Schehr *et al.* [46] and Kolarski *et al*.[72] have shown examples where dithiothreitol significantly affected experiments.

The pharmacological evaluation of the ligands at the H_3R revealed that all HAA ligands in the *trans* configuration were at least equipotent and, in many cases, more potent than azobenzene **1**. In essence, this shows the beneficial effects heteroatoms can have om molecular recognition with proteins. Interestingly, while azobenzene **1** is more potent in the *cis* configuration, HAA switches afford compounds that are more potent in the *trans* configuration. This may be the result of the spatial features of the *cis* conformation that HAA switches adopt and that are known to be different than that of *cis*-azobenzenes.[13,27,73] Perhaps as a result, many HAA switches have a lower affinity shift. However, our HAA scan was able to capture nuances in the ligand-H_3R molecular recognition events, leading to one compound (**3k**) exhibiting a good affinity shift (13-fold) and picomolar affinity (pK_i = 9.8) in the *trans* configuration. To our knowledge, this represents the highest absolute affinity for a small-molecule photoswitchable GPCR ligand.

Our study presents limitations and opportunities alike. An important consideration is that the H_3R, while being an informative model protein, does not fully represent the diversity of class A GPCRs or other protein targets. Therefore, extrapolation to other systems should be done with caution. Additionally, the specific decoration of the photoswitchable moieties (i.e. in our case with H_3R recognition features) can strongly affect any of the properties reported in our study, and the ligands studied here are therefore not necessarily representative of other molecules in the same class of HAA photoswitches. On the other hand, while the focus of this research was on photopharmacology, the properties reported for the HAA switches may also extend to other fields that rely on light-responsive systems, e.g., materials science and solar energy storage, supramolecular chemistry, imaging, and metal catalysis.[1,3–5] The success of 'photoswitch hopping' in any area depends heavily on the specific requirements for application. For example, we demonstrate that by varying the heterocycles the thermal half-life can be tuned from minutes to one month. Depending on the application, a suitable HAA can be introduced to modify its half-life, as well as preferred wavelengths and switching properties. Collectively, this research provides a blueprint for rational design and future implementation of HAA photoswitches.

Conclusions

Using a 'photoswitch hop' we explored five-membered HAA photoswitchable moieties through their incorporation in ligands for a hallmark GPCR protein (histamine H_3). Twelve HAA photoswitchable ligands were prepared and systematically compared to their azobenzene counterpart in terms of their physicochemical, photochemical, GSH stability, and pharmacological properties. Importantly, compared to the azobenzene parent **1**, all HAA ligands show higher PSS_{trans} values and allow red-shifting of at least one but sometimes both switching wavelength(s). The thermal relaxation of the *cis* isomers varies widely among the

HAAs, highlighting the diverse thermal stability profiles of these HAA switches. All compounds show appropriate buffer solubility, but GSH compromises the stability of some *trans* and all measured *cis* states. The 'photoswitch hop' gave several ligands with an improved H_3R affinity of the *trans* isomer. Affinity shifts vary, but a profile with excellent molecular recognition (K_i = 158 pM) and sufficient affinity shift (13-fold) is harbored in isoxazole **3k** (VUF26257). Ligand **3k** is, to our knowledge, the small-molecule ligand with the highest affinity in the GPCR photopharmacology field reported to date. The properties disclosed herein can aid in future applications of HAA photoswitches in photopharmacology and other areas that rely on photoresponsive systems, and demonstrate the importance of finely balancing the properties of the photoresponsive molecules for their broader use.

Acknowledgments

We acknowledge The Dutch Research Council (NWO) for financial support (OCENW.KLEIN.532, "Towards the next frontiers in GPCR photopharmacology"). We thank, Hans Custers for acquiring HRMS analyses, Elwin Janssen for NMR assistance, and Andrea van de Stolpe for setting up the photochemistry equipment.

References

(1) Mukherjee, A.; Seyfried, M. D.; Ravoo, B. J. Azoheteroarene and Diazocine Molecular Photoswitches: Self-Assembly, Responsive Materials and Photopharmacology. *Angewandte Chemie - International Edition* **2023**, *62* (42), e202304437. https://doi.org/10.1002/anie.202304437.

(2) Kobauri, P.; Dekker, F. J.; Szymanski, W.; Feringa, B. L. Rational Design in Photopharmacology with Molecular Photoswitches. *Angewandte Chemie - International Edition* **2023**, *62* (30), e202300681. https://doi.org/10.1002/anie.202300681.

(3) Olesińska-Mönch, M.; Deo, C. Small-Molecule Photoswitches for Fluorescence Bioimaging: Engineering and Applications. *Chemical Communications* **2023**, *59* (6), 660–669. https://doi.org/10.1039/d2cc05870g.

(4) Jerca, F. A.; Jerca, V. V.; Hoogenboom, R. Advances and Opportunities in the Exciting World of Azobenzenes. *Nature Reviews Chemistry 2021 6:1* **2021**, *6* (1), 51–69. https://doi.org/10.1038/s41570-021-00334-w.

(5) Thaggard, G. C.; Haimerl, J.; Park, K. C.; Lim, J.; Fischer, R. A.; Maldeni Kankanamalage, B. K. P.; Yarbrough, B. J.; Wilson, G. R.; Shustova, N. B. Metal-Photoswitch Friendship: From Photochromic Complexes to Functional Materials. *J Am Chem Soc* **2022**, *144* (51), 23249–23263. https://doi.org/10.1021/jacs.2C09879.

(6) Tavassoli, A.; Hamilton, A. D.; Spring, D. R.; Beharry, A. A.; Woolley, G. A. Azobenzene Photoswitches for Biomolecules. *Chem Soc Rev* **2011**, *40* (8), 4422–4437. https://doi.org/10.1039/c1cs15023e.

(7) Küllmer, F.; Gregor, L.; Arndt, H. D. Systematic Modifications of Substitution Patterns for Property Tuning of Photoswitchable Asymmetric Azobenzenes. *Org Biomol Chem* **2022**, *20* (20), 4204–4214. https://doi.org/10.1039/d2ob00214k.

(8) Velema, W. A.; Szymanski, W.; Feringa, B. L. Photopharmacology: Beyond Proof of Principle. *J Am Chem Soc* **2014**, *136* (6), 2178–2191. https://doi.org/10.1021/ja413063e.

(9) Volarić, J.; Szymanski, W.; Simeth, N. A.; Feringa, B. L. Molecular Photoswitches in Aqueous Environments. *Chem Soc Rev* **2021**, *50* (22), 12377–12449. https://doi.org/10.1039/d0cs00547a.

(10) Fuchter, M. J. On the Promise of Photopharmacology Using Photoswitches: A Medicinal Chemist's Perspective. *J Med Chem* **2020**, *63* (20), 11436–11447. https://doi.org/10.1021/acs.jmedchem.0c00629.

(11) Dong, M.; Babalhavaeji, A.; Samanta, S.; Beharry, A. A.; Woolley, G. A. Red-Shifting Azobenzene Photoswitches for in Vivo Use. *Acc Chem Res* **2015**, *48* (10), 2662–2670. https://doi.org/10.1021/ACS.ACCOUNTS.5b00270.

(12) Cardano, F.; Márquez García, R.; Szymanski, W. Manipulation of Chemistry and Biology with Visible Light Using Tetra-ortho-Substituted Azobenzenes and Azonium Ions. *Angewandte Chemie International Edition* **2025**. https://doi.org/10.1002/anie.202423506.

(13) Calbo, J.; Weston, C. E.; White, A. J. P.; Rzepa, H. S.; Contreras-García, J.; Fuchter, M. J. Tuning Azoheteroarene Photoswitch Performance through Heteroaryl Design. *J Am Chem Soc* **2017**, *139* (3), 1261–1274. https://doi.org/10.1021/jacs.6b11626.

(14) Dang, T.; Zhang, Z. Y.; Li, T. Visible-Light-Activated Heteroaryl Azoswitches: Toward a More Colorful Future. *J Am Chem Soc* **2024**, *146* (29), 19609–19620. https://doi.org/10.1021/jacs.4c03135.

(15) Greenfield, J. L.; Gerkman, M. A.; Gibson, R. S. L.; Han, G. G. D.; Fuchter, M. J. Efficient Electrocatalytic Switching of Azoheteroarenes in the Condensed Phases. *J Am Chem Soc* **2021**, *143* (37), 15250–15257. https://doi.org/10.1021/jacs.1c06359.

(16) Weston, C. E.; Richardson, R. D.; Haycock, P. R.; White, A. J. P.; Fuchter, M. J. Arylazopyrazoles: Azoheteroarene Photoswitches Offering Quantitative Isomerization and Long Thermal Half-Lives. *J Am Chem Soc* **2014**, *136* (34), 11878–11881. https://doi.org/10.1021/ja505444d.

(17) Matsuo, K.; Ogawa, H.; Yamaoka, S.; Waku, T.; Kobori, A. A Chemical Platform for the Efficient Screening of Arylazopyrazole-Based Photoswitchable CENP-E Inhibitors Using Mild Cyclization Reactions. *Bioorg Med Chem Lett* **2024**, *111*, 129892. https://doi.org/10.1016/j.mbcl.2024.129892.

(18) Wirth, U.; Raabe, K.; Kalaba, P.; Keimpema, E.; Muttenthaler, M.; König, B. Photoswitchable Probes of Oxytocin and Vasopressin. *J Med Chem* **2023**, *66* (21), 14853–14865. https://doi.org/10.1021/acs.jmedchem.3c01415.

(19) Kolarski, D.; Miró-Vinyals, C.; Sugiyama, A.; Srivastava, A.; Ono, D.; Nagai, Y.; Iida, M.; Itami, K.; Tama, F.; Szymanski, W.; Hirota, T.; Feringa, B. L. Reversible Modulation of Circadian Time with Chronophotopharmacology. *Nature Communications 2021 12:1* **2021**, *12* (1), 1–12. https://doi.org/10.1038/s41467-021-23301-x.

(20) Sink, A.; Gerwe, H.; Hübner, H.; Boivin-Jahns, V.; Fender, J.; Lorenz, K.; Gmeiner, P.; Decker, M. "Photo-Adrenalines": Photoswitchable B2-Adrenergic Receptor Agonists as Molecular Probes for the Study of Spatiotemporal Adrenergic Signaling. *Chemistry – A European Journal* **2024**, *30* (11), e202303506. https://doi.org/10.1002/chem.202303506.

(21) Wirth, U.; Erl, J.; Azzam, S.; Höring, C.; Skiba, M.; Singh, R.; Hochmuth, K.; Keller, M.; Wegener, J.; König, B. Monitoring the Reversibility of GPCR Signaling by Combining Photochromic Ligands with Label-Free Impedance Analysis. *Angewandte Chemie* **2023**, *135* (21), e202215547. https://doi.org/10.1002/ange.202215547.

(22) Aguirre, T.; Teichmann, E.; Römpp, F. Q.; Vivier, R.; Bryant, C.; Hulverson, M. A.; Van Voorhis, W. C.; Ojo, K. K.; Doggett, J. S.; Fiedler, D.; Hecht, S. Photoswitchable Inhibitors to Optically Control Specific Kinase Activity. *ACS Chem Biol* **2023**, *18* (6), 1378–1387. https://doi.org/10.1021/acschembio.3c00119.

(23) Sarkar, H. S.; Mashita, T.; Kowada, T.; Hamaguchi, S.; Sato, T.; Kasahara, K.; Matubayasi, N.; Matsui, T.; Mizukami, S. Arylazopyrazole-Based Photoswitchable Inhibitors Selective for Escherichia Coli Dihydrofolate Reductase. *ACS Chem Biol* **2023**, *18* (2), 340–346. https://doi.org/10.1021/acschembio.2c00749.

(24) Schulte, A. M.; Kolarski, D.; Sundaram, V.; Srivastava, A.; Tama, F.; Feringa, B. L.; Szymanski, W. Light-Control over Casein Kinase 1δ Activity with Photopharmacology: A Clear Case for Arylazopyrazole-Based Inhibitors. *Int J Mol Sci* **2022**, *23* (10), 5326. https://doi.org/10.3390/ijms23105326.

(25) Lahmy, R.; Hübner, H.; Lachmann, D.; Gmeiner, P.; König, B. Development of Photoswitchable Tethered Ligands That Target the μ-Opioid Receptor. *ChemMedChem* **2023**, *18* (23), e202300228. https://doi.org/10.1002/cmdc.202300228.

(26) Gomtsyan, A. Heterocycles in Drugs and Drug Discovery. *Chem Heterocycl Comp* **2012**, *48* (1), 7–10. https://doi.org/10.1007/s10593-012-0960-z.

(27) Crespi, S.; Simeth, N. A.; König, B. Heteroaryl Azo Dyes as Molecular Photoswitches. *Nature Reviews Chemistry*. Nature Publishing Group March 1, 2019, pp 133–146. https://doi.org/10.1038/s41570-019-0074-6.

(28) Adrion, D. M.; Kaliakin, D. S.; Neal, P.; Lopez, S. A. Benchmarking of Density Functionals for Z-Azoarene Half-Lives via Automated Transition State Search. *Journal of Physical Chemistry A* **2021**, *125* (29), 6474–6485. https://doi.org/10.1021/acs.jpca.1c01695.

(29) Mukadum, F.; Nguyen, Q.; Adrion, D. M.; Appleby, G.; Chen, R.; Dang, H.; Chang, R.; Garnett, R.; Lopez, S. A. Efficient Discovery of Visible Light-Activated Azoarene Photoswitches with Long Half-Lives Using Active Search. *J Chem Inf Model* **2021**, *61* (11), 5524–5534. https://doi.org/10.1021/acs.jcim.1c00954.

(30) Acharya, A.; Yadav, M.; Nagpure, M.; Kumaresan, S.; Guchhait, S. K. Molecular Medicinal Insights into Scaffold Hopping-Based Drug Discovery Success. *Drug Discov Today* **2024**, *29* (1), 103845. https://doi.org/10.1016/j.drudis.2023.103845.

(31) Sun, H.; Tawa, G.; Wallqvist, A. Classification of Scaffold-Hopping Approaches. *Drug Discov Today* **2012**, *17* (7–8), 310–324. https://doi.org/10.1016/j.drudis.2011.10.024.

(32) Lützel, K.; Laqua, H.; Sathian, M. B.; Nißl, B.; Szántó, J. K.; Senser, C.-A.; Savasci, G.; Allmendinger, L.; Kicin, B.; Ruf, V.; Kammerer, D.; Lohmüller, T.; Karaghiosoff, K.; Ali, A. M.; Storch, U.; Schnitzler, M. M. y; Ochsenfeld, C.; Konrad, D. A Platform for the Development of Highly Red-Shifted Azobenzene-Based Optical Tools. *Angewandte Chemie International Edition* **2025**, e202501779. https://doi.org/10.1002/anie.202501779.

(33) Volarić, J.; Buter, J.; Schulte, A. M.; Van Den Berg, K. O.; Santamaría-Aranda, E.; Szymanski, W.; Feringa, B. L. Design and Synthesis of Visible-Light-Responsive Azobenzene Building Blocks for Chemical Biology. *Journal of Organic Chemistry* **2022**, *87* (21), 14319–14333. https://doi.org/10.1021/acs.joc.2c01777.

(34) Stricker, L.; Böckmann, M.; Kirse, T. M.; Doltsinis, N. L.; Ravoo, B. J. Arylazopyrazole Photoswitches in Aqueous Solution: Substituent Effects, Photophysical Properties, and Host–Guest Chemistry. *Chemistry – A European Journal* **2018**, *24* (34), 8639–8647. https://doi.org/10.1002/chem.201800587.

(35) Kerckhoffs, A.; Christensen, K. E.; Langton, M. J. Fast Relaxing Red and Near-IR Switchable Azobenzenes with Chalcogen and Halogen Substituents: Periodic Trends, Tuneable Thermal Half-Lives and Chalcogen Bonding. *Chem Sci* **2022**, *13* (39), 11551–11559. https://doi.org/10.1039/d2sc04601f.

(36) Lorente, J. S.; Sokolov, A. V.; Ferguson, G.; Schiöth, H. B.; Hauser, A. S.; Gloriam, D. E. GPCR Drug Discovery: New Agents, Targets and Indications. *Nature Reviews Drug Discovery 2025* **2025**, 1–22. https://doi.org/10.1038/s41573-025-01139-y.

(37) Panarello, S.; Rovira, X.; Llebaria, A.; Gómez-Santacana, X. Photopharmacology of G - Protein-Coupled Receptors. In *Molecular Photoswitches*; John Wiley & Sons, Ltd, 2022; Vol. 2–2, pp 921–944. https://doi.org/10.1002/9783527827626.ch37.

(38) Wijtmans, M.; Josimovic, I.; Vischer, H. F.; Leurs, R. Optical Control of Class A G Protein-Coupled Receptors with Photoswitchable Ligands. *Curr Opin Pharmacol* **2022**, *63*, 102192. https://doi.org/10.1016/j.coph.2022.102192.

(39) Ricart-Ortega, M.; Font, J.; Llebaria, A. GPCR Photopharmacology. *Mol Cell Endocrinol* **2019**, *488*, 36–51. https://doi.org/10.1016/j.mce.2019.03.003.

(40) Berizzi, A. E.; Goudet, C. Strategies and Considerations of G-Protein-Coupled Receptor Photopharmacology. *Adv Pharmacol* **2020**, *88*, 143–172. https://doi.org/10.1016/bs.apha.2019.12.001.

(41) Binkhorst, L. C. P.; Josimovic, I.; Boer, B. De; Simon, I. A.; Aa, F. Van Der; Zarzycka, B. A.; Esch, I. J. P. De; Vischer, H. F.; Windhorst, A. D.; Wijtmans, M.; Leurs, R. A

Radiolabeled Photoswitchable G Protein-Coupled Receptor Antagonist Enlightens Ligand Binding Kinetics Associated with Photoswitching. *J Am Chem Soc* **2025**. https://doi.org/10.1021/jacs.5c07349.

(42) Panula, P.; Chazot, P. L.; Cowart, M.; Gutzmer, R.; Leurs, R.; Liu, W. L. S.; Stark, H.; Thurmond, R. L.; Haas, H. L. International Union of Basic and Clinical Pharmacology. XCVIII. Histamine Receptors. *Pharmacol Rev* **2015**, *67* (3), 601–655. https://doi.org/10.1124/pr.114.010249.

(43) Cheng, L.; Liu, J.; Chen, Z. The Histaminergic System in Neuropsychiatric Disorders. *Biomolecules* **2021**, *11* (9), 1345. https://doi.org/10.3390/biom11091345.

(44) Harwell, V.; Fasinu, P. S. Pitolisant and Other Histamine-3 Receptor Antagonists—An Update on Therapeutic Potentials and Clinical Prospects. *Medicines* **2020**, *7* (9), 55. https://doi.org/10.3390/medicines7090055.

(45) Berlin, M.; Boyce, C. W.; De Lera Ruiz, M. Histamine H3 Receptor as a Drug Discovery Target. *J Med Chem* **2011**, *54* (1), 26–53. https://doi.org/10.1021/jm100064d.

(46) Schehr, M.; Ianes, C.; Weisner, J.; Heintze, L.; Müller, M. P.; Pichlo, C.; Charl, J.; Brunstein, E.; Ewert, J.; Lehr, M.; Baumann, U.; Rauh, D.; Knippschild, U.; Peifer, C.; Herges, R. 2-Azo-, 2-Diazocine-Thiazols and 2-Azo-Imidazoles as Photoswitchable Kinase Inhibitors: Limitations and Pitfalls of the Photoswitchable Inhibitor Approach. *Photochemical and Photobiological Sciences* **2019**, *18* (6), 1398–1407. https://doi.org/10.1039/c9pp00010k.

(47) Matsuo, K.; Thayyil, S.; Kawaguchi, M.; Nakagawa, H.; Tamaoki, N. A Visible Light-Controllable Rho Kinase Inhibitor Based on a Photochromic Phenylazothiazole. *Chemical Communications* **2021**, *57* (93), 12500–12503. https://doi.org/10.1039/d1cc04905d.

(48) Dolai, A.; Bhunia, S.; Jana, S. K.; Bera, S.; Mandal, S.; Samanta, S. Photoisomerization and Light-Controlled Antibacterial Activity of Fluoroquinolone-Azoisoxazole Hybrids. *ChemBioChem* **2024**, *25* (8), e202300851. https://doi.org/10.1002/cbic.202300851.

(49) Prischich, D.; Gomila, A. M. J.; Milla-Navarro, S.; Sangüesa, G.; Diez-Alarcia, R.; Preda, B.; Matera, C.; Batlle, M.; Ramírez, L.; Giralt, E.; Hernando, J.; Guasch, E.; Meana, J. J.; de la Villa, P.; Gorostiza, P. Adrenergic Modulation With Photochromic Ligands. *Angewandte Chemie International Edition* **2021**, *60* (7), 3625–3631. https://doi.org/10.1002/anie.202010553.

(50) Cheruthu, N. M.; Hashim, P. K.; Sahu, S.; Takahashi, K.; Nakamura, T.; Mitomo, H.; Ijiro, K.; Tamaoki, N. Azophotoswitches Containing Thiazole, Isothiazole, Thiadiazole, and Isothiadiazole. *Org Biomol Chem* **2024**, *23* (1), 207–212. https://doi.org/10.1039/d4Ob01573h.

(51) Pratt, D.; Nojiri, M.; Kawagishi, T. Method Effecting a Reversible Colour Change of Dyed Hair. EP1535599A1, 2005.

(52) Kumar, P.; Srivastava, A.; Sah, C.; Devi, S.; Venkataramani, S. Arylazo-3,5-Dimethylisoxazoles: Azoheteroarene Photoswitches Exhibiting High Z-Isomer Stability, Solid-State Photochromism, and Reversible Light-Induced Phase Transition. *Chemistry – A European Journal* **2019**, *25* (51), 11924–11932. https://doi.org/10.1002/chem.201902150.

(53) Heindl, A. H.; Wegner, H. A. Rational Design of Azothiophenes—Substitution Effects on the Switching Properties. *Chemistry – A European Journal* **2020**, *26* (60), 13730–13737. https://doi.org/10.1002/chem.202001148.

(54) Celanire, S.; Provins, L.; Denonne, F.; Valade, A. Compounds Comprising a Cyclobutoxy Group. WO2009147149A1, 2009.

(55) Ahmed, Z.; Siiskonen, A.; Virkki, M.; Priimagi, A. Controlling Azobenzene Photoswitching through Combined Ortho-Fluorination and -Amination. *Chemical Communications* **2017**, *53* (93), 12520–12523. https://doi.org/10.1039/c7cc07308a.

(56) Lameijer, L. N.; Budzak, S.; Simeth, N. A.; Hansen, M. J.; Feringa, B. L.; Jacquemin, D.; Szymanski, W. General Principles for the Design of Visible-Light-Responsive Photoswitches: Tetra-Ortho-Chloro-Azobenzenes. *Angewandte Chemie - International Edition* **2020**, *59* (48), 21663–21670. https://doi.org/10.1002/anie.202008700

(57) *The Collaborative Drug Discovery database (Burlingame, CA. www.collaborativedrug.com) was used in this study.* https://www.collaborativedrug.com/ (accessed 2025-07-09).

(58) Bevan, C. D.; Lloyd, R. S. A High-Throughput Screening Method for the Determination of Aqueous Drug Solubility Using Laser Nephelometry in Microtiter Plates. *Anal Chem* **2000**, *72* (8), 1781–1787. https://doi.org/10.1021/ac9912247.

(59) Hoelke, B.; Gieringer, S.; Arlt, M.; Saal, C. Comparison of Nephelometric, UV-Spectroscopic, and HPLC Methods for High-Throughput Determination of Aqueous Drug Solubility in Microtiter Plates. *Anal Chem* **2009**, *81* (8), 3165–3172. https://doi.org/10.1021/ac9000089.

(60) Sassano, M. F.; Doak, A. K.; Roth, B. L.; Shoichet, B. K. Colloidal Aggregation Causes Inhibition of G Protein-Coupled Receptors. *J Med Chem* **2013**, *56* (6), 2406–2414. https://doi.org/10.1021/jm301749y.

(61) Meister, A.; Anderson, M. E. Glutathione. *Annu Rev Biochem* **1983**, *Vol. 52* (Volume 52, 1983), 711–760. https://doi.org/10.1146/annurev.bi.52.070183.003431.

(62) Dolai, A.; Box, S. M.; Bhunia, S.; Bera, S.; Das, A.; Samanta, S. Photoisomerization of 2-Arylazoimidazoles under Visible Light: Identifying a Predictive Tool to Anticipate and

Tune Likely Photoswitching Performance and Cis Half-Life. *Journal of Organic Chemistry* **2023**, *88* (13), 8236–8247. https://doi.org/10.1021/acs.joc.3c00211.

(63) Ward, R. A.; Anderton, M. J.; Ashton, S.; Bethel, P. A.; Box, M.; Butterworth, S.; Colclough, N.; Chorley, C. G.; Chuaqui, C.; Cross, D. A. E.; Dakin, L. A.; Debreczeni, J. É.; Eberlein, C.; Finlay, M. R. V.; Hill, G. B.; Grist, M.; Klinowska, T. C. M.; Lane, C.; Martin, S.; Orme, J. P.; Smith, P.; Wang, F.; Waring, M. J. Structure- and Reactivity-Based Development of Covalent Inhibitors of the Activating and Gatekeeper Mutant Forms of the Epidermal Growth Factor Receptor (EGFR). *J Med Chem* **2013**, *56* (17), 7025–7048. https://doi.org/10.1021/jm400822z.

(64) Sheldon, J. E.; Dcona, M. M.; Lyons, C. E.; Hackett, J. C.; Hartman, M. C. T. Photoswitchable Anticancer Activity via Trans – Cis Isomerization of a Combretastatin A-4 Analog. *Org Biomol Chem* **2015**, *14* (1), 40–49. https://doi.org/10.1039/c5Ob02005k.

(65) Standaert, R. F.; Park, S. B. Abc Amino Acids: Design, Synthesis, and Properties of New Photoelastic Amino Acids. *Journal of Organic Chemistry* **2006**, *71* (21), 7952–7966. https://doi.org/10.1021/jo060763q.

(66) Boulègue, C.; Löweneck, M.; Renner, C.; Moroder, L. Redox Potential of Azobenzene as an Amino Acid Residue in Peptides. *ChemBioChem* **2007**, *8* (6), 591–594. https://doi.org/10.1002/cbic.200600495.

(67) Dang, T.; Zhang, Z. Y.; Li, T. Visible-Light-Activated Heteroaryl Azoswitches: Toward a More Colorful Future. *J Am Chem Soc* **2024**, *146* (29), 19609–19620. https://doi.org/10.1021/jacs.4c03135.

(68) Lin, R.; Hashim, P. K.; Sahu, S.; Amrutha, A. S.; Cheruthu, N. M.; Thazhathethil, S.; Takahashi, K.; Nakamura, T.; Kikukawa, T.; Tamaoki, N. Phenylazothiazoles as Visible-Light Photoswitches. *J Am Chem Soc* **2023**, *145* (16), 9072–9080. https://doi.org/10.1021/jacs.3C00609.

(69) Bandara, H. M. D.; Burdette, S. C. Photoisomerization in Different Classes of Azobenzene. *Chem Soc Rev* **2012**, *41* (5), 1809–1825. https://doi.org/10.1039/c1cs15179g.

(70) Broichhagen, J.; Frank, J. A.; Trauner, D. A Roadmap to Success in Photopharmacology. *Acc Chem Res* **2015**, *48* (7), 1947–1960. https://doi.org/10.1021/acs.accounts.5b00129.

(71) Dolai, A.; Box, S. M.; Bhunia, S.; Bera, S.; Das, A.; Samanta, S. Photoisomerization of 2-Arylazoimidazoles under Visible Light: Identifying a Predictive Tool to Anticipate and Tune Likely Photoswitching Performance and Cis Half-Life. *Journal of Organic Chemistry* **2023**, *88* (13), 8236–8247. https://doi.org/10.1021/acs.joc.3c00211.

(72) Kolarski, D.; Sugiyama, A.; Rodat, T.; Schulte, A.; Peifer, C.; Itami, K.; Hirota, T.; Feringa, B. L.; Szymanski, W. Reductive Stability Evaluation of 6-Azopurine Photoswitches for the Regulation of CKIα Activity and Circadian Rhythms. *Org Biomol Chem* **2021**, *19* (10), 2312–2321. https://doi.org/10.1039/d1Ob00014d.

(73) Wendler, T.; Schütt, C.; Näther, C.; Herges, R. Photoswitchable Azoheterocycles via Coupling of Lithiated Imidazoles with Benzenediazonium Salts. *Journal of Organic Chemistry* **2012**, *77* (7), 3284–3287. https://doi.org/10.1021/jo202688x.

Supplementary information

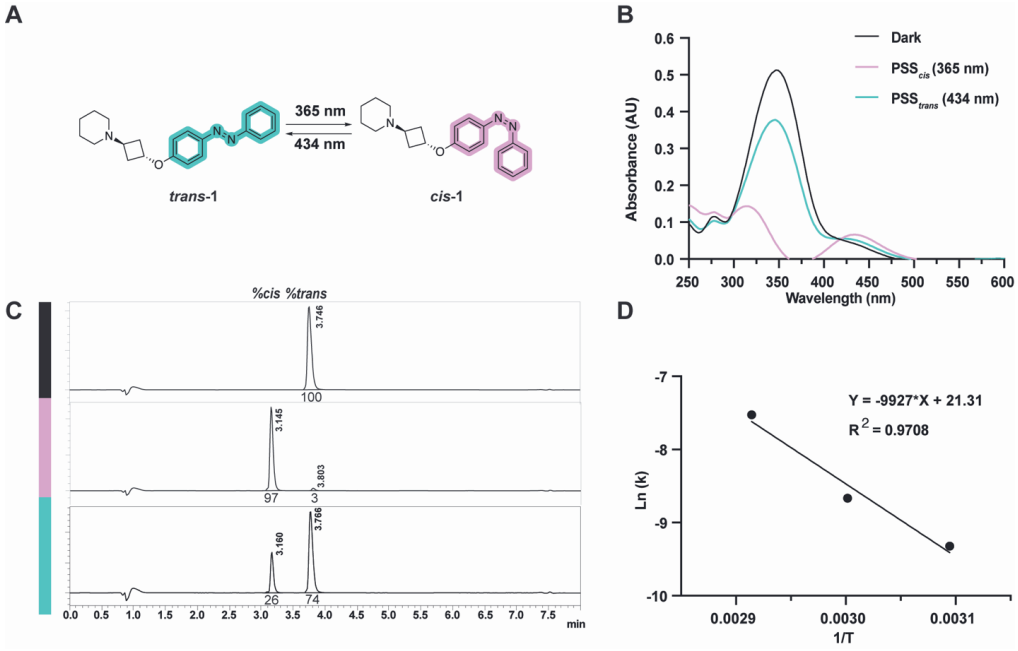

Figure S1. (A) Chemical structures of the *trans* and *cis* isomers of **1**. (B) UV-vis spectra of 25 µM of **1** in HBSS buffer containing 1% DMSO as the *trans* isomer (black), after illumination with 365 ± 11 nm for 2 min to PSS$_{cis}$ (magenta) and after subsequent illumination with 434 ± 9 nm for 4 min to PSS$_{trans}$ (cyan). (C) *Trans*-**1** (upper panel) and photostationary state (PSS) area percentages after illumination with 365 ± 10 nm for 5 min to reach PSS$_{cis}$ (middle panel) and after subsequent illumination with 434 ± 9 nm for 5 min to reach PSS$_{trans}$ (lower panel) at 10 mM in DMSO as determined by LC-MS analysis at the isosbestic point (295 nm). (D) Arrhenius fit for the thermal relaxation of **1** at three different temperatures (50 °C, 60 °C, 70 °C), as measured at 25 µM in HBSS buffer containing 1% DMSO.

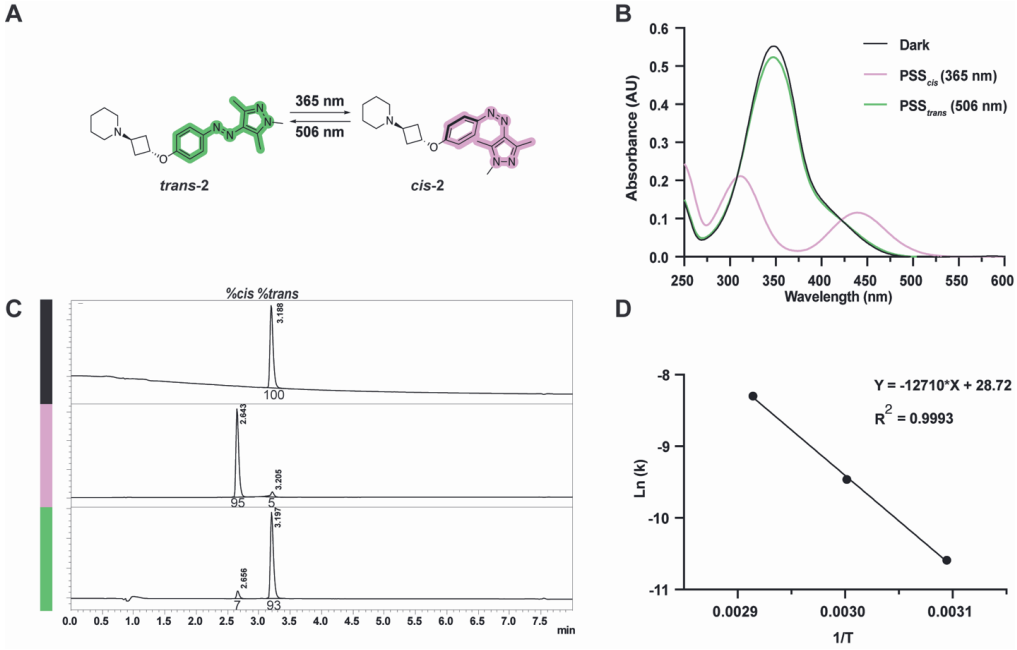

Figure S2. (A) Chemical structures of the *trans* and *cis* isomers of **2**. (B) UV-vis spectra of 25 µM of **2** in HBSS buffer containing 1% DMSO as the trans isomer (black), after illumination with 365 ± 11 nm for 2 min to PSS$_{cis}$ (magenta) and after subsequent illumination with 506 ± 18 nm for 4 min to PSS$_{trans}$ (green). (C) *Trans*-**2** (upper panel) and photostationary state (PSS) area percentages after illumination with 365 ± 11 nm for 5 min to reach PSS$_{cis}$ (middle panel) and after subsequent illumination with 506 ± 18 nm for 5 min to reach PSS$_{trans}$ (lower panel) at 10 mM in DMSO as determined by LC-MS analysis at the isosbestic point (305 nm). (D) Arrhenius fit for the thermal relaxation of **2** at three different temperatures (50 °C, 60 °C, 70 °C), as measured at 25 µM in HBSS buffer containing 1% DMSO.

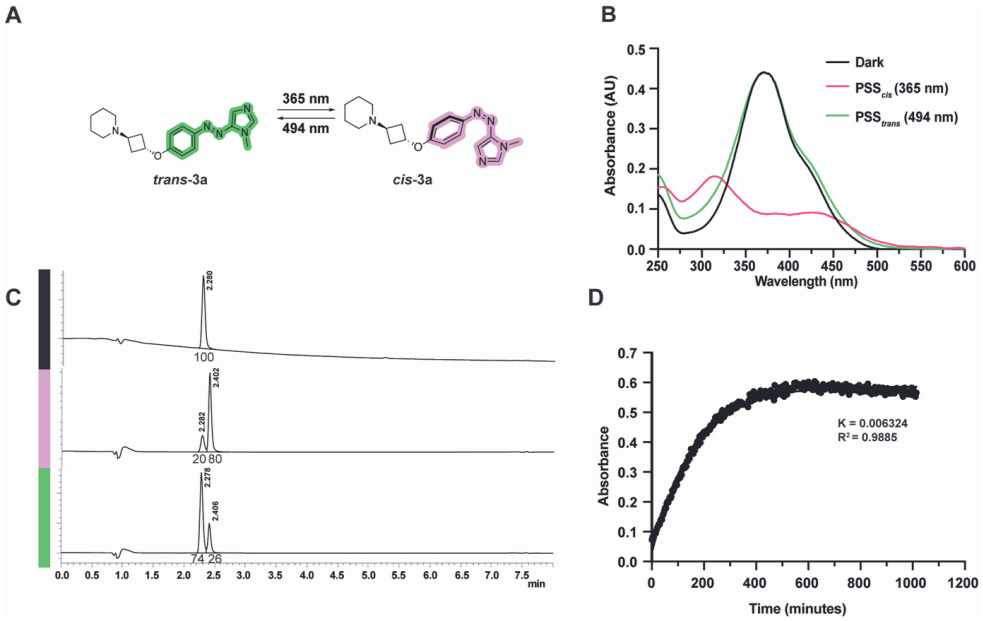

Figure S3. (A) Chemical structures of the *trans* and *cis* isomers of **3a**. (B) UV-vis spectra of 25 µM of **3a** in HBSS buffer containing 1% DMSO as the trans isomer (black), after illumination with 365 ± 11 nm for 2 min to PSS$_{cis}$ (magenta) and after subsequent illumination with 494 ± 9 nm for 2 min to PSS$_{trans}$ (green). (C) *Trans*-**3a** (upper panel) and photostationary state (PSS) area percentages after illumination with 360 ± 20 nm for 5 min to reach PSS$_{cis}$ (middle panel) and after subsequent illumination with 494 ± 9 nm for 5 min to reach PSS$_{trans}$ (lower panel) at 10 mM in DMSO as determined by LC-MS analysis at the isosbestic point (320 nm). (D) Thermal relaxation of *cis*-**3a** at 20°C, as measured at 25 µM in HBSS buffer containing 1% DMSO by UV absorbance at 360 nm.

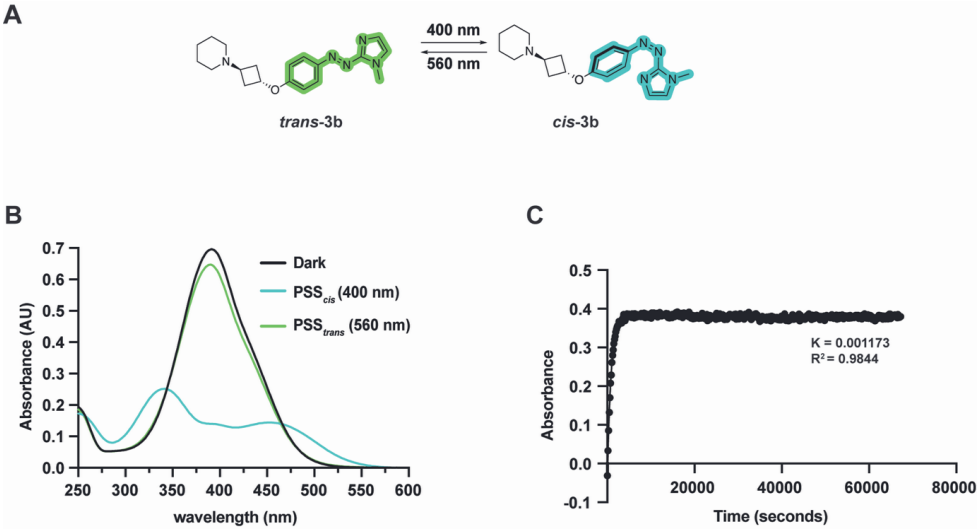

Figure S4. (A) Chemical structures of the *trans* and *cis* isomers of **3b**. (B) UV-vis spectra of 25 µM of **3b** in HBSS buffer containing 1% DMSO as the trans isomer (black), after illumination with 400 ± 5 nm for 2 min to PSS_{cis} (cyan) and after subsequent illumination with 560 ± 5 nm for 18 min to PSS_{trans} (green). (C) Thermal relaxation of *cis*-**3b** at 20°C, as measured at 25 µM in HBSS buffer containing 1% DMSO by UV absorbance at 360 nm.

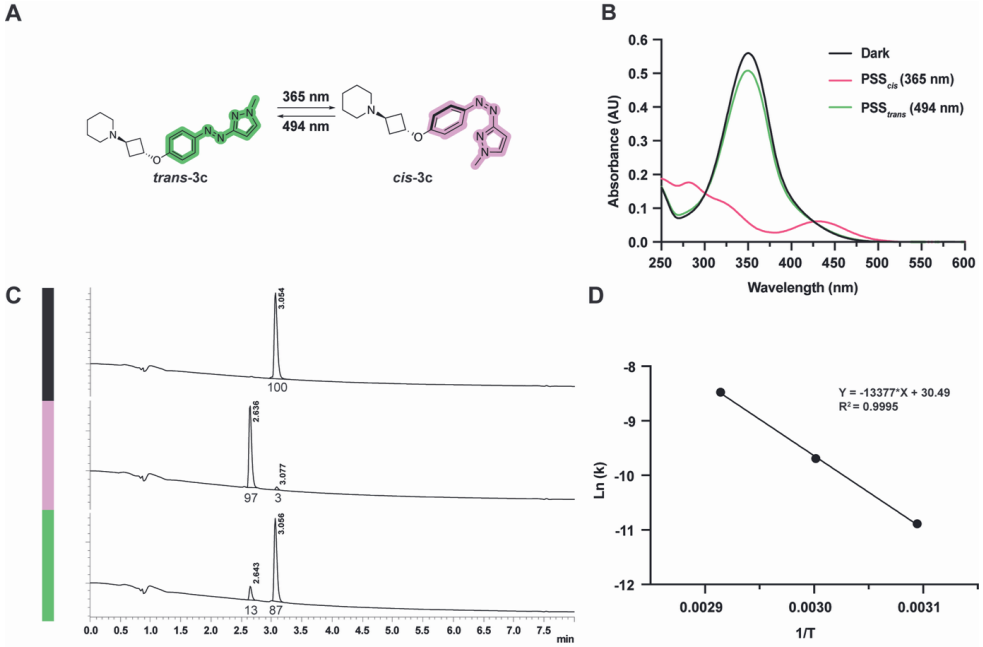

Figure S5. (A) Chemical structures of the *trans* and *cis* isomers of **3c**. (B) UV-vis spectra of 25 µM of **3c** in HBSS buffer containing 1% DMSO as the trans isomer (black), after illumination with 365 ± 11 nm for 2 min to PSS_{cis} (magenta) and after subsequent illumination with 494 ± 9 nm for 4 min to PSS_{trans} (green). (C) *Trans*-**3c** (upper panel) and photostationary state (PSS) area percentages after illumination with 360 ± 20 nm for 5 min to reach PSS_{cis} (middle panel) and after subsequent illumination with 494 ± 9 nm for 5 min to reach PSS_{trans} (lower panel) at 10 mM in DMSO as determined by LC-MS analysis at the isosbestic point (320 nm). (D) Arrhenius fit for the thermal relaxation of **3c** at three different temperatures (50 °C, 60 °C, 70 °C), as measured at 25 µM in HBSS buffer containing 1% DMSO.

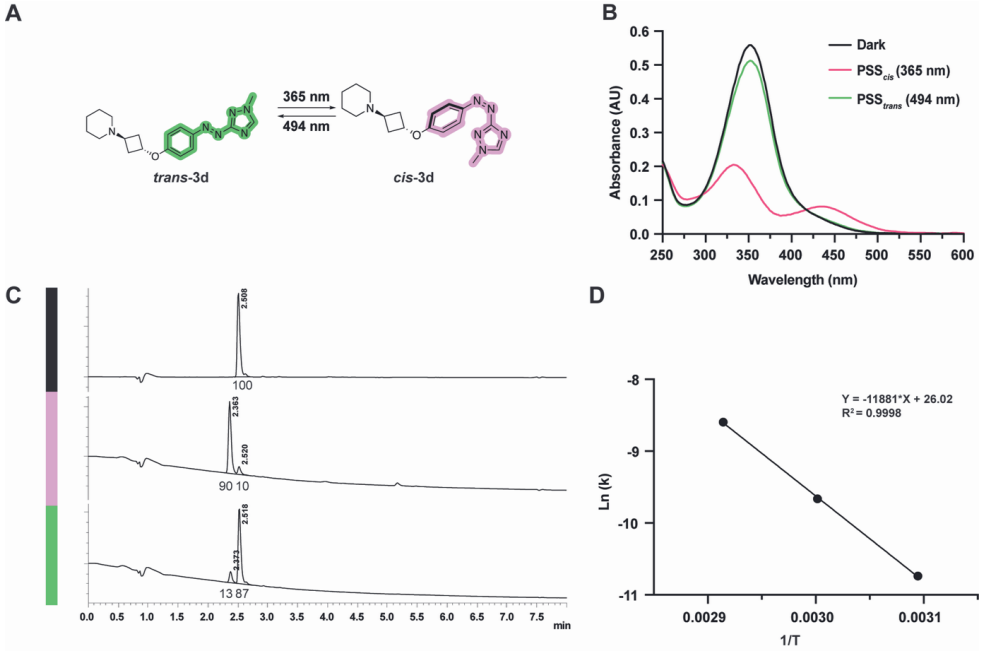

Figure S6. (A) Chemical structures of the *trans* and *cis* isomers of **3d**. (B) UV-vis spectra of 25 µM of **3d** in HBSS buffer containing 1% DMSO as the trans isomer (black), after illumination with 365 ± 11 nm for 4 min to PSS$_{cis}$ (magenta) and after subsequent illumination with 494 ± 9 nm for 4 min to PSS$_{trans}$ (green). (C) *Trans*-**3d** (upper panel) and photostationary state (PSS) area percentages after illumination with 360 ± 20 nm for 5 min to reach PSS$_{cis}$ (middle panel) and after subsequent illumination with 494 ± 9 nm for 5 min to reach PSS$_{trans}$ (lower panel) at 10 mM in DMSO as determined by LC-MS analysis at the isosbestic point (295 nm). (D) Arrhenius fit for the thermal relaxation of **3d** at three different temperatures (50 °C, 60 °C, 70 °C), as measured at 25 µM in HBSS buffer containing 1% DMSO.

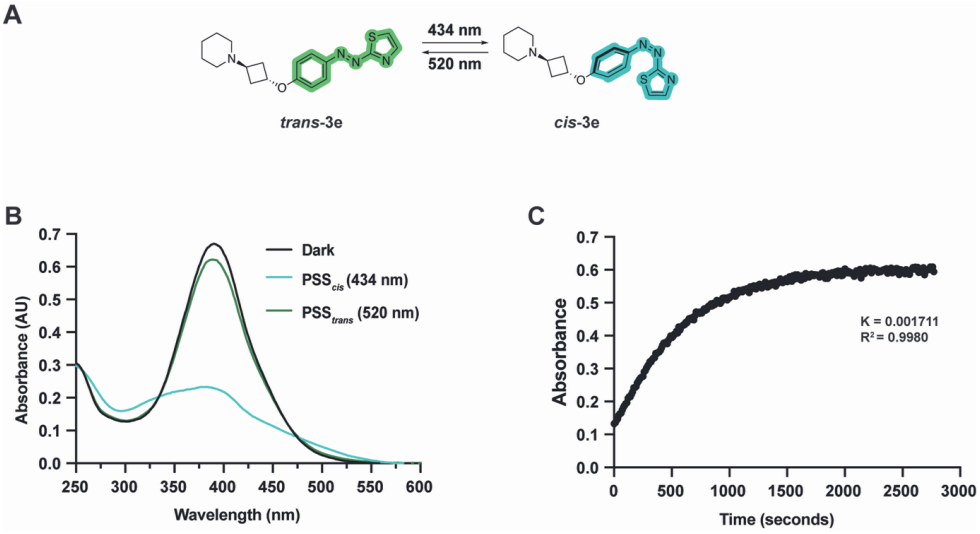

Figure S7. (A) Chemical structures of the *trans* and *cis* isomers of **3e**. (B) UV-vis spectra of 25 µM of **3e** in HBSS buffer containing 1% DMSO as the trans isomer (black), after illumination with 400 ± 5 nm for 2 min to PSS$_{cis}$ (cyan) and after subsequent illumination with 520 ± 12 nm for 4 min to PSS$_{trans}$ (green). (C) Thermal relaxation of *cis*-**3e** at 20°C, as measured at 25 µM in HBSS buffer containing 1% DMSO.

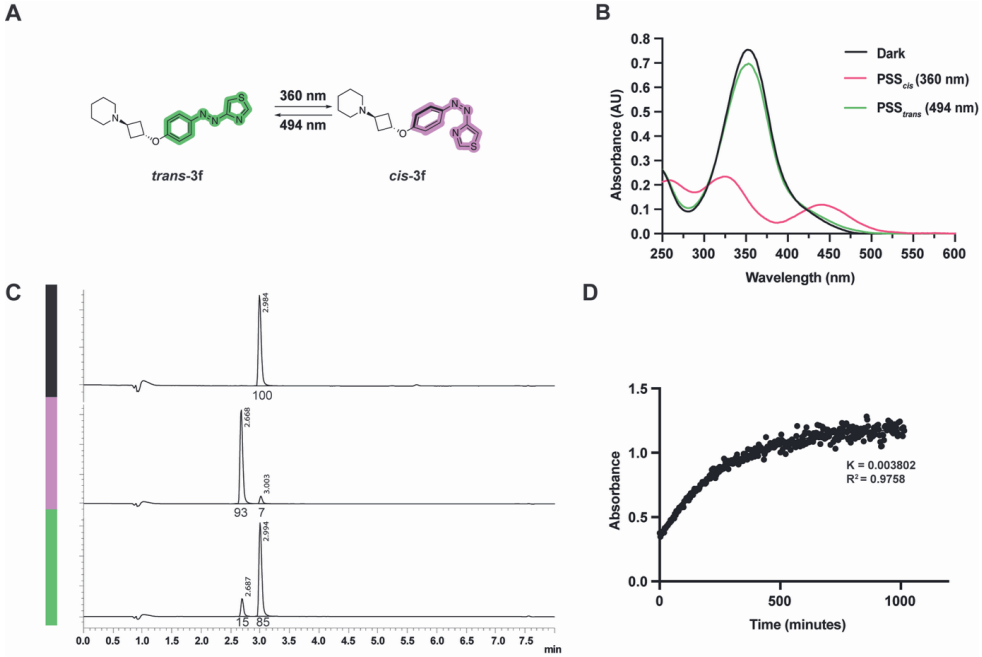

Figure S8. (A) Chemical structures of the *trans* and *cis* isomers of **3f**. (B) UV-vis spectra of 25 µM of **3f** in HBSS buffer containing 1% DMSO as the *trans* isomer (black), after illumination with 400 ± 5 nm for 2 min to PSS$_{cis}$ (cyan) and after subsequent illumination with 520 ± 12 nm for 2 min to PSS$_{trans}$ (green). (C) *Trans*-**3f** (upper panel) and photostationary state (PSS) area percentages after illumination with 360 ± 20 nm for 5 min to reach PSS$_{cis}$ (middle panel) and after subsequent illumination with 494 ± 9 nm for 5 min to reach PSS$_{trans}$ (lower panel) at 10 mM in DMSO as determined by LC-MS analysis at the isosbestic point (305 nm). (D) Thermal relaxation of *cis*-**3f** at 20°C, as measured at 25 µM in HBSS buffer containing 1% DMSO.

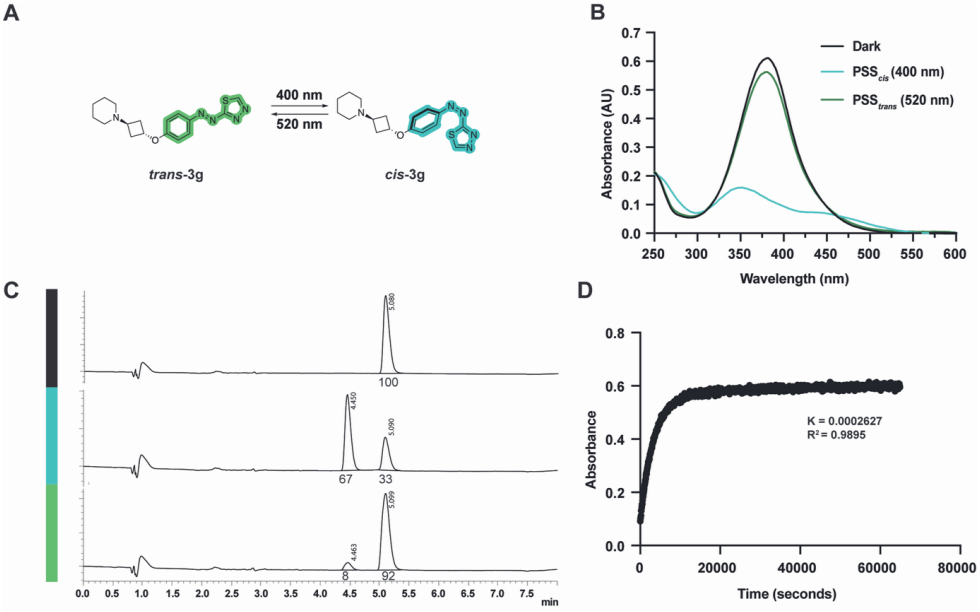

Figure S9. (A) Chemical structures of the *trans* and *cis* isomers of **3g**. (B) UV-vis spectra of 25 µM of **3g** in HBSS buffer containing 1% DMSO as the *trans* isomer (black), after illumination with 400 ± 5 nm for 2 min to PSS_{cis} (cyan) and after subsequent illumination with 520 ± 12 nm for 2 min to PSS_{trans} (green). (C) *Trans*-**3g** (upper panel) and photostationary state (PSS) area percentages after illumination with 400 ± 5 nm for 10 min to reach PSS_{cis} (middle panel) and after subsequent illumination with 520 ± 12 nm for 5 min to reach PSS_{trans} (lower panel) at 10 mM in DMSO as determined by LC-MS analysis at the isosbestic point (314 nm). (D) Thermal relaxation of *cis*-**3g** at 20°C, as measured at 25 µM in HBSS buffer containing 1% DMSO.

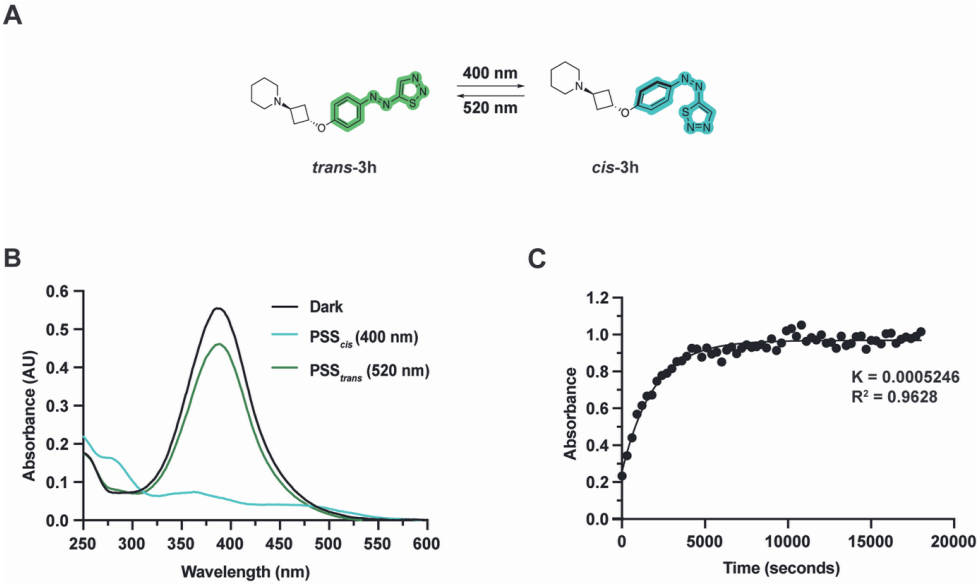

Figure S10. (A) Chemical structures of the *trans* and *cis* isomers of **3h**. (B) UV-vis spectra of 25 µM of **3h** in HBSS buffer containing 1% DMSO as the *trans* isomer (black), after illumination with 400 ± 5 nm for 2 min to PSS_{cis} (cyan) and after subsequent illumination with 520 ± 12 nm for 2 min to PSS_{trans} (green). (C) Thermal relaxation of *cis*-**3h** at 20°C, as measured at 25 µM in HBSS buffer containing 1% DMSO by UV absorbance at 360 nm.

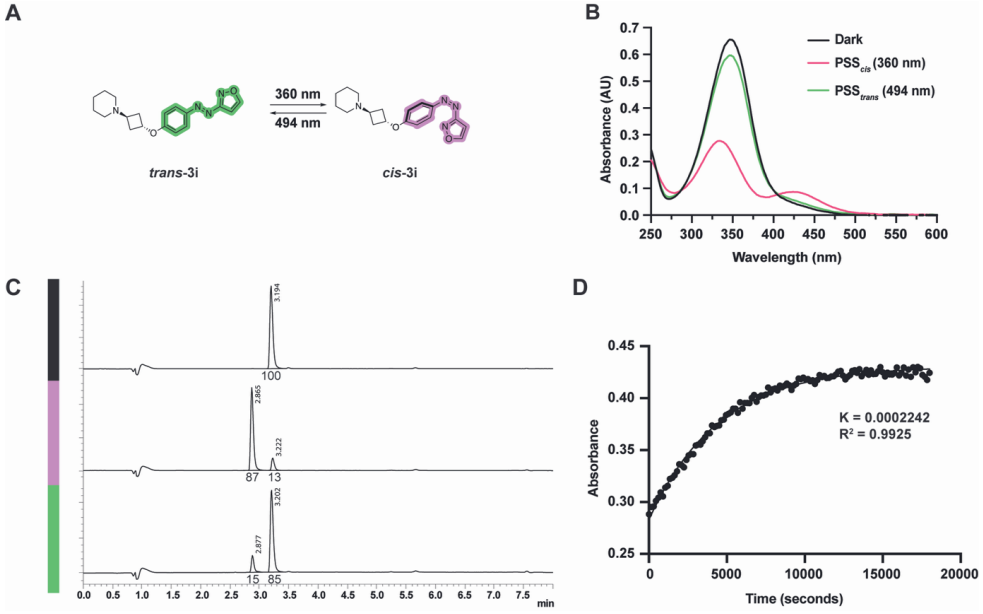

Figure S11. (A) Chemical structures of the *trans* and *cis* isomers of **3i**. (B) UV-vis spectra of 25 µM of **3i** in HBSS buffer containing 1% DMSO as the *trans* isomer (black), after illumination with 400 ± 5 nm for 2 min to PSS$_{cis}$ (cyan) and after subsequent illumination with 520 ± 12 nm for 2 min to PSS$_{trans}$ (green). (C) *Trans*-**3i** (upper panel) and photostationary state (PSS) area percentages after illumination with 360 ± 20 nm for 5 min to reach PSS$_{cis}$ (middle panel) and after subsequent illumination with 494 ± 9 nm for 5 min to reach PSS$_{trans}$ (lower panel) at 10 mM in DMSO as determined by LC-MS analysis at the isosbestic point (314 nm). (D) Thermal relaxation of *cis*-**3i** at 20°C, as measured at 25 µM in HBSS buffer containing 1% DMSO by UV absorbance at 320 nm.

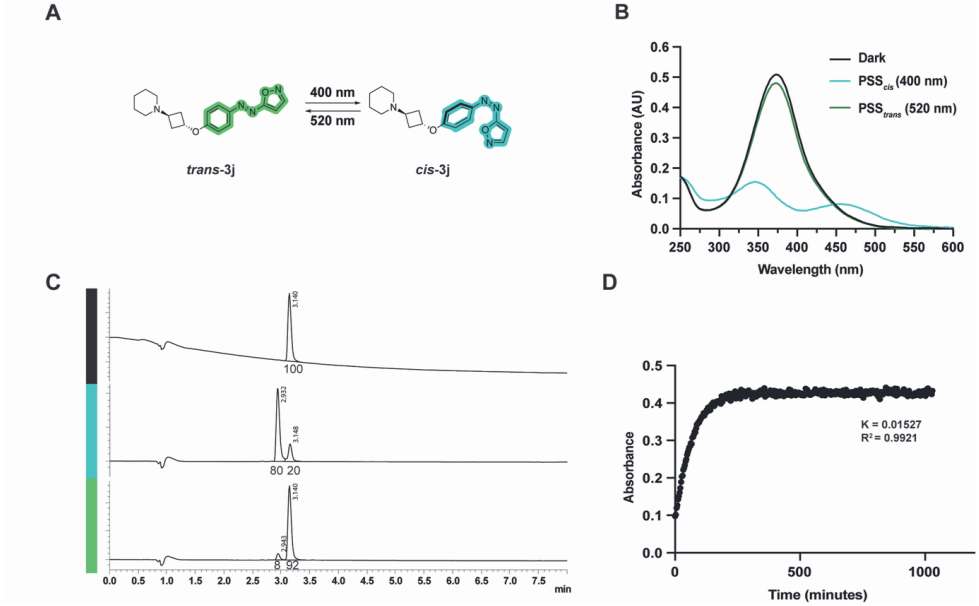

Figure S12. (A) Chemical structures of the *trans* and *cis* isomers of **3j**. (B) UV-vis spectra of 25 µM of **3j** in HBSS buffer containing 1% DMSO as the *trans* isomer (black), after illumination with 400 ± 5 nm for 2 min to PSS_{cis} (cyan) and after subsequent illumination with 520 ± 12 nm for 2 min to PSS_{trans} (green). (C) *Trans*-**3j** (upper panel) and photostationary state (PSS) area percentages after illumination with 360 ± 20 nm for 10 min to reach PSS_{cis} (middle panel) and after subsequent illumination with 494 ± 9 nm for 5 min to reach PSS_{trans} (lower panel) at 10 mM in DMSO as determined by LC-MS analysis at the isosbestic point (314 nm). (D) Thermal relaxation of *cis*-**3j** at 20°C, as measured at 25 µM in HBSS buffer containing 1% DMSO by UV absorbance at 360 nm.

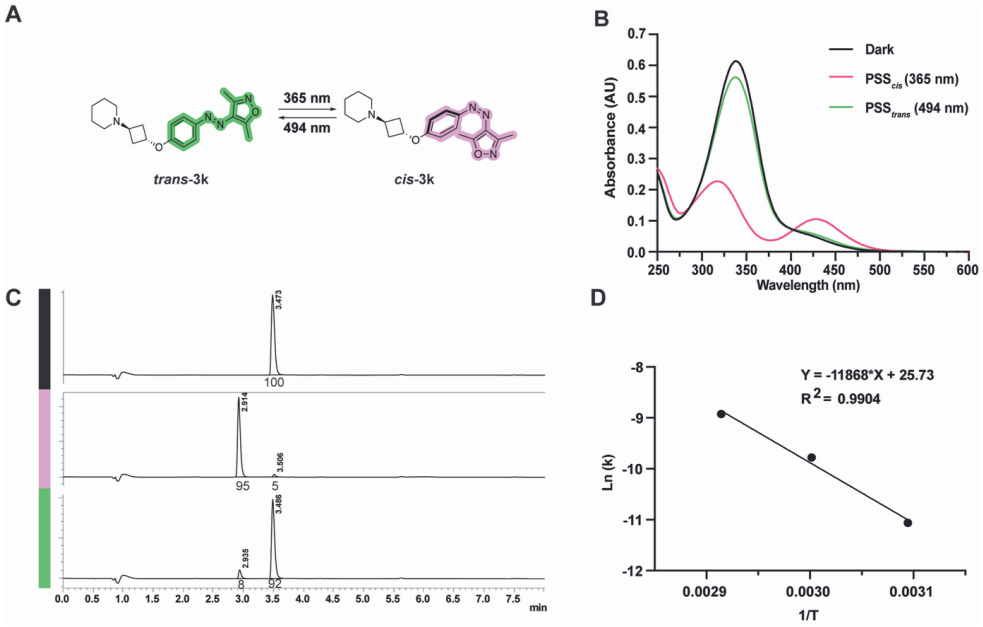

Figure S13. (A) Chemical structures of the *trans* and *cis* isomers of **3k**. (B) UV-vis spectra of 25 µM of **3k** in HBSS buffer containing 1% DMSO as the trans isomer (black), after illumination with 365 ± 11 nm for 2 min to PSS$_{cis}$ (magenta) and after subsequent illumination with 494 ± 9 nm for 6 min to PSS$_{trans}$ (green). (C) *Trans*-**3k** (upper panel) and photostationary state (PSS) area percentages after illumination with 360 ± 20 nm for 5 min to reach PSS$_{cis}$ (middle panel) and after subsequent illumination with 494 ± 9 nm for 5 min to reach PSS$_{trans}$ (lower panel) at 10 mM in DMSO as determined by LC-MS analysis at the isosbestic point (290 nm). (D) Arrhenius fit for the thermal relaxation of **3k** at three different temperatures (50 °C, 60 °C, 70 °C), as measured at 25 µM in HBSS buffer containing 1% DMSO.

Table S1. Calculated physicochemical properties for compounds **1,2,3a-k.**

Compound		MW	HBD	HBA	Log P	log $D_{7.4}$	Log S	TPSA
1[e]		335.45	0	4	5.9	4.4	-6.5	37.2 Å^2
2[e]		367.50	0	6	4.5	3.5	-5.7	55.0 Å^2
3a		339.44	0	6	4.4	2.7	-5.4	55.0 Å^2
3b		339.44	0	6	4.1	2.8	-5.2	55.0 Å^2
3c		339.44	0	6	4.5	3.6	-5.5	55.0 Å^2
3d		340.43	0	7	4.0	2.1	-5.1	67.9 Å^2
3e		342.46	0	5	5.2	3.6	-6.0	50.1 Å^2
3f		342.46	0	5	5.0	3.6	-5.9	50.1 Å^2
3g		343.45	0	6	4.7	3.0	-5.7	63.0 Å^2
3h		343.45	0	6	4.8	3.1	-5.7	63.0 Å^2
3i		326.40	0	6	4.8	3.3	-5.6	63.2 Å^2
3j		326.40	0	6	4.2	3.3	-5.2	63.2 Å^2
3k		354.45	0	6	4.8	3.6	-5.8	63.2 Å^2

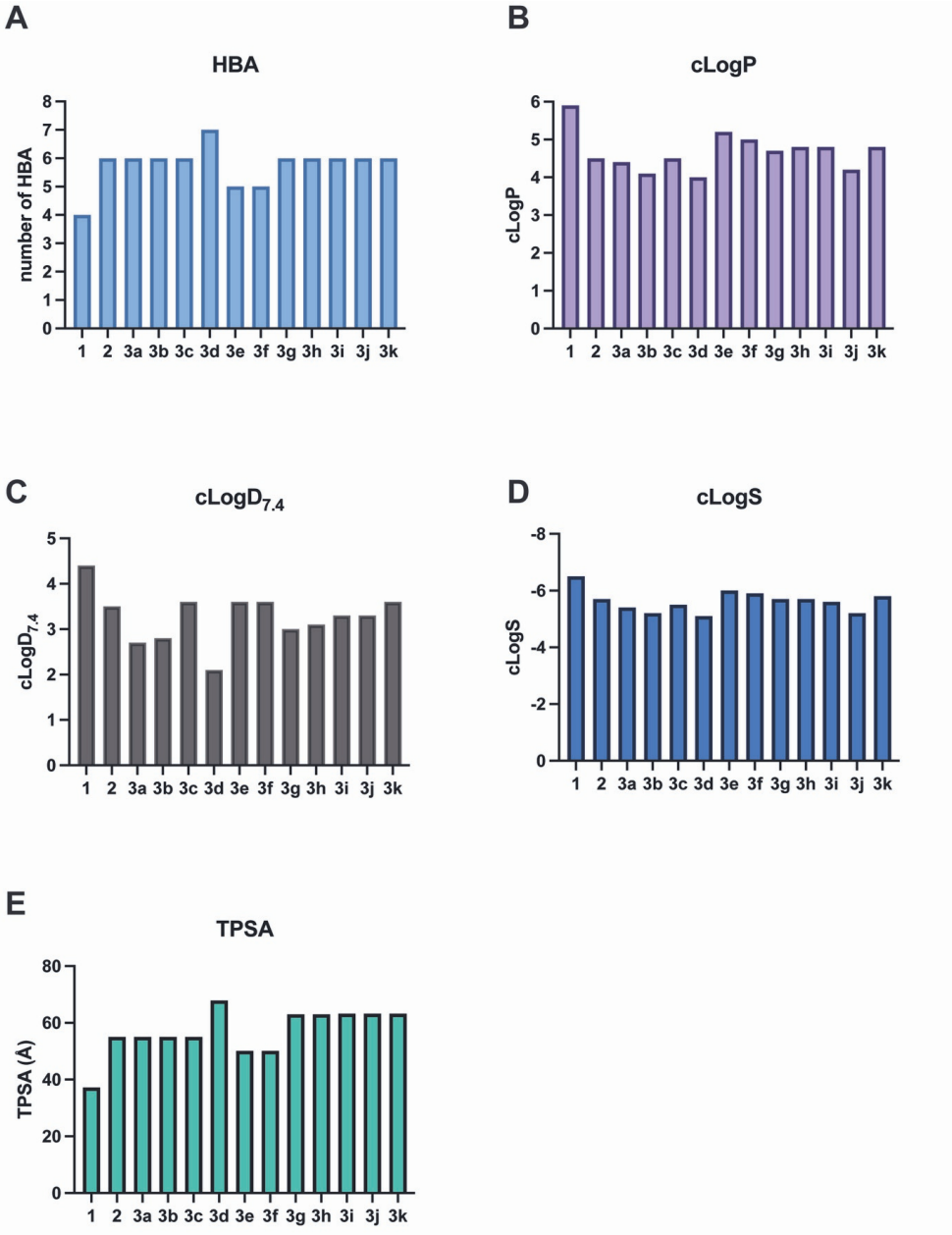

Figure S14. Calculated physicochemical properties (A) HBA, (B) cLogP, (C) cLogD$_{7.4}$, (D) cLogS, and (E) TPSA for compounds **1,2,3a-k**.

Table S2. Approximate solubility of HAA photoswitchable ligands **1**, **2**, **3a-k.**

Compound	HAR	Minimum concentration of aggregation[a]	Compound	HAR	Minimum concentration of aggregation[a]
1		> $10^{-4.0}$ M (*trans*) > $10^{-4.0}$ M (PSS_{cis})	**3f**[b]		> $10^{-4.0}$ M
2		> $10^{-4.0}$ M (*trans*) > $10^{-4.0}$ M (PSS_{cis})	**3g**[b]		> $10^{-4.0}$ M
3a[b]		> $10^{-4.0}$ M	**3h**[b]		> $10^{-4.5}$ M
3b[b]		> $10^{-4.0}$ M	**3i**[b]		> $10^{-4.0}$ M
3c		> $10^{-4.0}$ M (*trans*) > $10^{-4.0}$ M (PSS_{cis})	**3j**[b]		> $10^{-4.0}$ M
3d		> $10^{-4.0}$ M (*trans*) > $10^{-4.0}$ M (PSS_{cis})	**3k**		> $10^{-4.5}$ M (*trans*) > $10^{-4.0}$ M (PSS_{cis})
3e[b]		> $10^{-4.0}$ M			

[a]The highest concentration at which no scattering was observed in nephelometry analysis.[58,59]

[b]Approximate solubility for PSScis could not be measured due to fast thermal relaxtion. Measurements were taken with intervals of $10^{-4.0}$ up to $10^{-7.5}$.

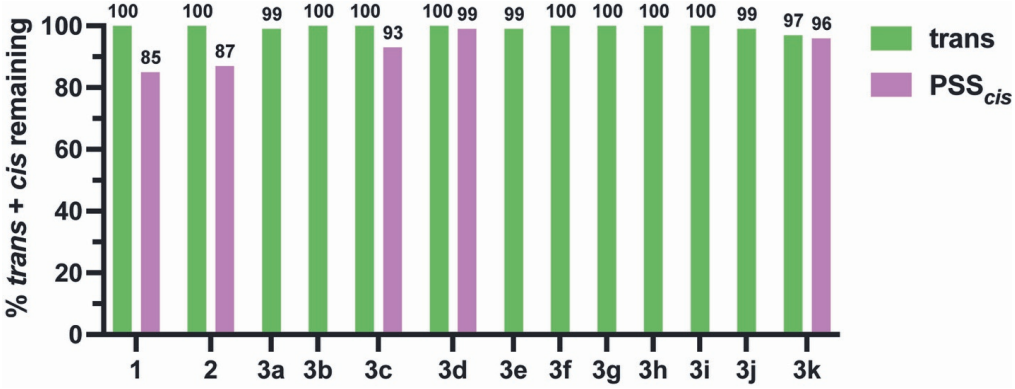

Figure S15. Chemical stability of compounds after 12h incubation at 37 ºC in PBS buffer.

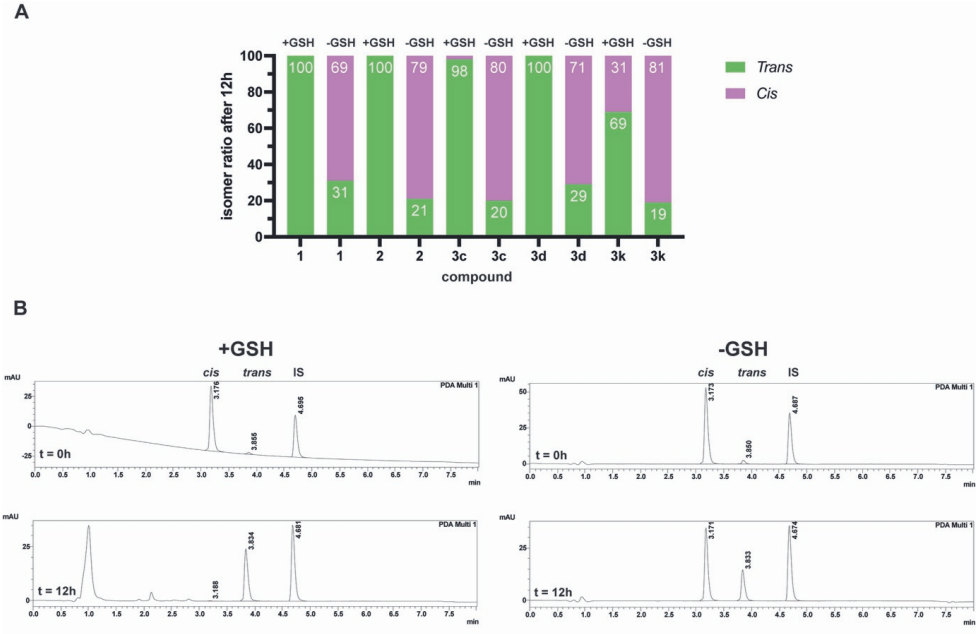

Figure S16. (A) *Trans*/*cis* ratio of ligands **1**, **2**, **3c**, **3d** and **3k** upon incubation of PSS_{cis} for 12 h in the dark with GSH (+GSH) and without GSH present (-GSH) at 37ºC in PBS. (B) Representative LC chromatograms of **1**-PSS_{cis} with GSH and without GSH present at two different time points (t = 0h and t = 12h). IS refers to the internal standard used (diclofenac).

Experimental procedures - Photochemistry

UV−Vis spectra were recorded using a Thermo-scientific Evolution 201 PC spectrophotometer equipped with a thermostated cell holder set at 20 °C. Fits of UV−vis spectroscopy data were generated using Prism 10.1.0. Illumination for almost all photochemical experiments was executed using a Sutter instruments Lambda LS with a 300 W full-spectrum lamp connected to a Sutter instruments Lambda 10-3 optical filter changer equipped with 360 ± 20 nm, 434 ± 9 nm 494 ± 9 nm, with the remaining illuminations performed with a Lambda 721 optical beam combiner system equipped with 365 ± 11 nm and 506 ± 18 nm filter. The light intensity used for the lambda 10-3 optical filter is 0.93 mW/mm^2 using the 360 ± 20 nm filter, 0.79 mW/mm^2 for the 434 ± 9 nm filter, 0.77 mW/mm^2 for the 494 ± 9 nm filter as measured using a Thorlabs PM16−401 power meter. The light intensity used for the lambda 721 optical beam combiner is 200 mW using the 365 ± 11 nm filter and 60 mW for the 506 ± 18 nm filter. For photochemical analyses, illuminations were performed in Hellma Suprasil quartz 114QS cuvettes. For the dynamic illuminations, a 4-way cuvette holder (Avantes) was used. The left outlet of the holder is connected to an Avantes AvaLight-DH-S-BAL Deuterium lamp. The right outlet is connected through a fiber to an AvaSpec UV/Vis spectrometer. The lower outlet is connected to a Lambda 721 optical beam combiner system equipped with 365 ± 11 nm and 506 ± 18 nm filter illumination means. The upper outlet is covered with a black cap. The temperature of the solution in the cuvette (20 °C) is controlled by Q-blue Wireless Temperature Control software. Thermal relaxation experiments and Arrhenius extrapolations were performed according to Priimagi *et al*,[74] using a compound concentration of 25 µM in HBSS +1% DMSO and temperatures of 50, 60, and 70 °C. Illuminations for pharmacological experiments were performed in cylindrical clear glass vials with a volume of 4.5 mL. The typical distance between light source and vial or cuvette was 2 cm.

Experimental procedures - Chemistry

All chemicals and solvents were obtained from commercial suppliers (primarily Sigma-Aldrich, BLD pharma and Combi-Blocks) and used without purification. DCM, DMF, THF and Et_2O were dried by passing through a PureSolv solvent purification system. All reactions were carried out under N_2 atmosphere unless mentioned otherwise. All reactions with photoresponsive compounds were carried out in the dark or under red light. IUPAC names were adapted from Chemdraw Professional 21.0 (PerkinElmer). Reactions were monitored by thin layer chromatography (Merck Silicagel 60 F254) by visualization under 254 nm lamp. Flash column chromatography was performed with Screening Devices 40-63 µm (Biotage) or GraceResolv (Büchi) cartridges on Isolera One with UV-Vis detection (Biotage). Nuclear magnetic resonance (NMR) spectra were determined with a Bruker Avance II 500 MHz or a Bruker Avance III HD 600 MHz spectrometer. Chemical shifts are reported in parts per million (ppm) against the reference compound using the signal of the residual non-deuterated solvent ($CDCl_3$ δ = 7.26 ppm (^{1}H), δ = 77.16 ppm (^{13}C); DMSO-d_6 δ = 2.50 ppm (^{1}H), δ = 39.52 ppm (^{13}C)). NMR spectra were processed using MestReNova 14.1 software. The peak multiplicities are defined as follows: s, singlet; d, doublet; t, triplet; q, quartet; dd, doublet of doublets; ddd, doublet of doublets of doublets; dt, doublet of triplets; dq, doublet of quartets; td, triplet of doublets; tt, triplet of triplets; qd, quartet of doublets; p, pentet; dp, doublet of pentets; br, broad signal; m, multiplet. For NMR listings, in addition to specific instructions that are given by the journal in the guidelines for authors the following additional procedures were used: 1) Multiplicity is not solely reported based on peak shapes, but also distinguishes the coupling to all non-equivalent protons that have similar J values; 2) If additional smaller couplings are observed but are too small for accurate quantitation because the precision is smaller than the digital resolution, a symbol $^{\Delta}$ will be used; 3) The notation 'm' is used in case of obscured accurate interpretation as a result of (i) overlapping signals for different protons, or (ii) a result of overlapping signal lines within the same proton signal; 4) For any rotamers or diastereomers, signals will be listed separately; 5) NMR signals that could only be detected with HSQC analysis are denoted with a $^{\#}$ symbol; 6) NMR signals that could only be detected with HMBC analysis are denoted with a * symbol; 7) If one or more signals remain undetected after extensive 1D and 2D NMR analyses, this will be mentioned. 8) Signals for exchangeable proton atoms (such as NH and OH groups) are only listed if clearly visible (excluding e.g. the use of D_2O or CD_3OD) and if confirmed by a D_2O shake and/or HSQC. Analytical HPLC analyses were performed using a Shimadzu LC-20AD liquid chromatography pump system, equipped with a Waters XBridge C18 column 5 µm 4.6 x 50 mm (used at 40 °C), connected to a Shimadzu SPDM20A photodiode array detector. MS detection was performed using Shimadzu LCMS-2010EV mass spectrometer operating in both positive and negative ionization mode. The mobile phase used for acidic mode was a mixture of A = H_2O + 0.1% HCO_2H and B = MeCN + 0.1% HCO_2H. The mobile phase used for basic mode was a mixture of A = H_2O and B = MeCN + 0.4% w/v NH_4HCO_3. The method used is as follows: flow rate: 1.0 mL/min, start 95% A in a linear gradient to 10% A over 4.5 min, hold 1.5 min at 10% A, in 0.5 min in a linear gradient to 95% A, hold 1.5 min at 95% A, total runtime: 8.0 min. Analytical UPLC analyses were

performed using a Shimadzu LC-40D liquid chromatograph pump system, equipped with an Xbridge (BEH C18) 2.5 µm column (50 mm, 2.1 mm), connected to a Shimadzu SPD-M40 diode array detector. MS detection was performed using a Shimadzu LCMS-2020 EV mass spectrometer. The mobile phase used for acidic mode was a mixture of A = H_2O + 0.1% HCO_2H and B = MeCN + 0.1% HCO_2H, The method used is as follows: flow rate: flow rate: 0.4 mL/min, start 95% A in a linear gradient to 10% A over 1.75 min, hold 0.2tab5 min at 10% A, in 0.25 min in a linear gradient to 95% A, hold 0.75 min at 95% A, total run time: 3 min. Compound purities were calculated as the percentage peak area of the analysed compound by UV detection at 254 nm. Unless mentioned otherwise, all compounds have a LC purity of >95 %. High-resolution mass spectra (HRMS) were recorded on a Bruker micrOTOF mass spectrometer using ESI in positive ion mode (HRMS). λ_{max} values provided in the procedures are those extracted from the LC analysis.

General procedure A

Aniline **7** was dissolved in H_2O (0.40 M). Conc. aq. HCl (4.1 eq) was added. The solution was cooled to 0°C, after which a solution of $NaNO_2$ (1.1 eq) in H_2O (0.67 M) was added dropwise between 0-4°C. The solution was stirred at 0°C for 30 min. This diazonium salt solution was added dropwise to a solution of PhOH (1.1 eq) and NaOH (3.3 eq) in H_2O (0.50 M) while keeping the temperature between 0-4°C. The resulting mixture was stirred at 0°C. Upon completion (TLC/LC), the solution was made basic with satd. aq. $NaHCO_3$ and extracted thrice with EtOAc (except for **6d**, where the mixture was acidified). The combined organic layers were washed with satd. aq. $NaHCO_3$ and brine, dried over Na_2SO_4 and concentrated under reduced pressure to afford **6**. Where indicated, the obtained crude product was purified for subsequent reactions.

General procedure B

Aniline **7** was dissolved in H_2O (1.12 M). Conc. aq. HCl (3.5 eq) was added. The solution was cooled to 0°C, after which a solution of $NaNO_2$ (1.1 eq), PhOH (1.0-1.5 eq), and NaOH (2.1 eq) in H_2O (0.67 M) was added dropwise while keeping the temperature between 0-4°C. The resulting suspension was stirred at rt for the indicated time and filtered to afford **6**. Where indicated, the obtained crude product was purified for subsequent reactions.

General procedure C

Tert-butyl ((1s,3s)-3-hydroxycyclobutyl)carbamate (**12**), phenol **6** (1.1 eq), and Ph_3P (1.6 eq) were dissolved in THF (0.06 M). DIAD (40% w/w in PhMe, 1.4 eq) was added dropwise to this solution at 0°C during 5 min. The reaction mixture was stirred for the indicated time. The reaction mixture was concentrated under reduced pressure. The resulting crude product was dissolved in EtOAc and washed with water. The aq. layer was extracted thrice with EtOAc. The combined organic layers were washed with brine, dried over Na_2SO_4, filtered, and concentrated under reduced pressure to afford **14**. Where indicated, the obtained crude product was purified for subsequent reactions.

General procedure D

Compound **14** was dissolved in MeOH (0.10 M). HCl (4 M in dioxane, 10 eq) was added. The reaction mixture was stirred at rt for the indicated time. The reaction mixture was concentrated under reduced pressure. Trituration with acetone afforded **15**.

General procedure E

Phenol **6** was dissolved in DMF (0.94 M) and NaH (60% dispersion in mineral oil, 1.6 eq) was added. The resulting solution was stirred at rt for 45 min, after which **11** (1.3 eq) was added. The reaction mixture was stirred for the indicated time at the indicated temperature. The reaction mixture was cooled to rt, diluted with ice water, and extracted thrice with EtOAc. The combined organic layers were washed with water:brine (1:1) and brine, dried over Na_2SO_4,

filtered, and concentrated under reduced pressure to afford **3**. Where indicated, the obtained crude product was purified for subsequent reactions.

General procedure F

DIPEA (3 eq) and 1,5-dibromopentane (1.1 eq) were added to a solution of **15** in anhydrous MeCN (0.20 M). The reaction mixture was stirred at reflux for the indicated time. The reaction mixture was cooled to rt, concentrated under reduced pressure and extracted thrice with EtOAc/water. The combined organic layers were extracted with brine, dried over Na_2SO_4, filtered, and concentrated under reduced pressure to afford **3**. Where indicated, the obtained crude product was purified for subsequent reactions.

***(E)*-4-((1-methyl-1H-imidazol-2-yl)diazenyl)phenol (5b)**

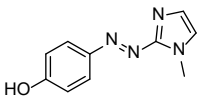

This compound was synthetised according to general procedure **A**, using 2-amino-1-methylimidazole hydrochloride (**4b**, 503 mg, 3.77 mmol) in H_2O (9.4 mL), conc. aq. HCl (1.3 mL, 15 mmol), $NaNO_2$ (286 mg, 4.14 mmol) in H_2O (5.7 mL), PhOH (390 mg, 4.14 mmol) and NaOH (503 mg, 12.6 mmol) in H_2O (7.5 mL). The crude product was purified using normal-phase column chromatography (55-100% EtOAc in cHex). This yielded the title compound as a gold-colored solid (155 mg, 20%). **^{1}H NMR** (500 MHz, DMSO-d_6) δ 10.35 (s, 1H), 7.80 (d, J = 8.8 Hz, 2H), 7.47 (d^{Δ}, 1H), 7.14 (d^{Δ}, 1H), 6.93 (d, J = 8.8 Hz, 2H), 3.95 (s, 3H). **^{13}C NMR** (126 MHz, DMSO-d_6) δ 161.1, 152.0, 146.0, 129.2, 124.8, 124.5, 116.0, 32.7. **LC-MS** (HPLC, acidic): t_r: 2.18 min, purity: 96% (254 nm), λ_{max}: 423 nm, $[M+H]^+$ m/z calculated (calc.): 203.09, found 203.05.

***(E)*-4-((1-methyl-1*H*-pyrazol-3-yl)diazenyl)phenol (5c)**

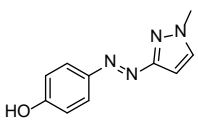

This compound was synthetised according to general procedure **A**, using 1-methyl-1*H*-pyrazol-3-amine (**4c**, 400 mg, 4.12 mmol) in H_2O (10.3 mL), conc. aq. HCl (1.5 mL, 18 mmol), $NaNO_2$ (313 mg, 4.53 mmol) in H_2O (6.2 mL), PhOH (426 mg, 4.53 mmol) and NaOH (544 mg, 13.6 mmol) in H_2O (8.2 mL). The reaction mixture was acidified using 1M aq. HCl, filtered, and dried under vacuum. This yielded the title compound as a bright yellow solid (794 mg, 95%). **^{1}H NMR** (500 MHz, DMSO-d_6) δ 10.27 (s, 1H), 7.78 (d, *J* = 2.4 Hz, 1H), 7.73 (d, *J* = 8.9 Hz, 2H), 6.93 (d, *J* = 8.9 Hz, 2H), 6.46 (d, *J* = 2.4 Hz, 1H), 3.95 (s, 3H). **^{13}C NMR** (126 MHz, DMSO-d_6) δ 163.6, 161.2, 145.8, 133.3, 124.9, 116.4, 94.6, 39.7[#]. **LC-MS** (HPLC, acidic): t_r: 3.23 min, purity: >99% (254 nm), λ_{max}: 349 nm, $[M+H]^+$ m/z calc.: 203.09, found 203.00.

***(E)*-4-((1-methyl-1H-1,2,4-triazol-3-yl)diazenyl)phenol (5d)**

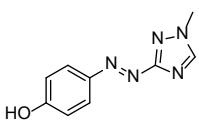

This compound was synthetised according to general procedure **B**, using 1-methyl-1H-1,2,4-triazol-3-amine (**4d**, 302 mg, 3.08 mmol) in H_2O (2.7 mL), conc. aq. HCl (0.9 mL, 0.01 mol), $NaNO_2$ (225 mg, 3.26 mmol), PhOH (288 mg, 3.06 mmol), and NaOH (257 mg, 6.43 mmol) in H_2O (4.6 mL). The resulting suspension was stirred at rt for 30 min and filtered. This yielded the title compound as a yellow solid (543 mg, 87%). **^{1}H NMR** (500 MHz, DMSO-d_6) δ 10.45 (s, 1H), 8.58 (s, 1H), 7.81 (d, *J* = 8.8 Hz, 2H), 6.95 (d, *J* = 8.9 Hz, 2H), 3.97 (s, 3H). **^{13}C NMR** (126 MHz, DMSO-d_6) δ 168.8, 161.8, 145.8, 145.5, 125.2, 116.1, 36.5. **LC-MS** (UPLC, acidic): t_r: 1.08 min, purity: 96% (254 nm), λ_{max}: 353 nm, $[M+H]^+$ m/z calc.: 204.09, found 204.05.

***(E)*-4-(thiazol-2-yldiazenyl)phenol (5e)**

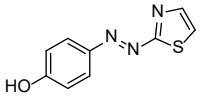

This compound was synthetised according to general procedure **B**, using 2-aminothiazole (**4e**, 2.001 g, 19.98 mmol) in H_2O (17.8 mL), conc. aq. HCl (6.1 mL, 69 mmol), $NaNO_2$ (1.461 g, 21.17 mmol), PhOH (1.880 g, 19.97 mmol), and NaOH (1.679 g, 41.98 mmol) in H_2O (30 mL). The resulting suspension was

stirred at rt for 20 h and filtered. The residue was purified using normal-phase column chromatography (20-60% EtOAc in cHex) followed by reverse-phase column chromatography (10-90% MeCN + 0.1% HCO_2H in H_2O + 0.1% HCO_2H). The desired fractions were combined, made basic using satd. aq. $NaHCO_3$ and extracted using EtOAc. The combined organic layers were washed with brine, dried over $MgSO_4$, and concentrated under reduced pressure. This yielded the title compound as dark red brown solid (1.079 g, 26%). **^{1}H NMR** (500 MHz, DMSO-d_6) δ 8.01 (d, *J* = 3.3 Hz, 1H), 7.84 (d, *J* = 9.0 Hz, 2H), 7.78 (d, *J* = 3.3 Hz, 1H), 6.93 (d, *J* = 8.9 Hz, 2H). **^{13}C NMR** (126 MHz, DMSO-d_6) δ 177.0, 164.3, 143.8, 143.5, 126.4, 121.4, 116.9. **LC-MS** (UPLC, acidic): t_r: 1.68 min, purity: 98% (254 nm), λ_{max}: 390 nm, $[M+H]^+$ m/z calc.: 206.04, found 205.95.

***(E)*-4-((1,3,4-thiadiazol-2-yl)diazenyl)phenol (5f)**

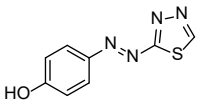

This compound was synthetised according to general procedure **B**, using 1,3,4-thiadiazol-2-amine (**4f**, 1.000 g, 9.89 mmol) in H_2O (8.8 mL), conc. aq. HCl (3.0 mL, 34 mmol), $NaNO_2$ (723 mg, 10.5 mmol), PhOH (1.40 g, 14.83 mmol), and NaOH (831 mg, 20.8 mmol) in H_2O (14.8 mL). The resulting suspension was stirred at rt for 2 h and filtered. The residue was purified using normal-phase column chromatography (20-100% EtOAc in cHex followed by 0-10% MeOH in DCM). This yielded the title compound as a black solid (576 mg, 28%). **^{1}H NMR** (500 MHz, DMSO-d_6) δ 9.60 (s, 1H), 7.98 – 7.88 (m, 2H), 7.05 – 6.96 (m, 2H). **^{13}C NMR** (126 MHz, DMSO-d_6) δ 179.8, 164.3, 154.4, 144.6, 127.0, 116.8. **LC-MS** (HPLC, acidic): t_r: 3.15 min, purity: 85% (254 nm), λ_{max}: 383 nm, $[M+H]^+$ m/z calc.: 207.03, found 206.95.

(*E*)-4-(thiazol-4-yldiazenyl)phenol (5g)

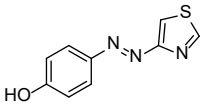

To a solution of *tert*-butyl thiazol-4-ylcarbamate (**6**, 2.00 g, 9.99 mmol, 1.0 eq) in DCM was added HCl (4.0 M in dioxane, 10 mL, 4.0 eq). The reaction mixture was stirred at rt for 18 h. The reaction mixture was filtered and washed with Et_2O twice to give thiazol-4-amine hydrochloride as a white solid, which was directly used in the next step. To a solution of this thiazol-4-amine hydrochloride (500 mg, 3.66 mmol, 1.0 eq) in TFA (1.5 mL) and MeCN (5 mL) at 0°C was added $NO^+BF_4^-$ (428 mg, 3.66 mmol, 1.0 eq) portion-wise. The mixture was stirred for 30 min and subsequently added dropwise to a solution of PhOH (344 mg, 3.66 mmol, 1.0 eq) and K_2CO_3 (2.53 g, 18.3 mmol, 5.0 eq) in H_2O (10 mL). The resulting reaction mixture was stirred for 30 min, after which it was extracted using EtOAc thrice. The combined organic layers were washed with water, brine, dried over Na_2SO_4, filtered and concentrated. The crude product was purified using normal-phase column chromatography (1-6% MeOH + NH_3 in DCM) to give the title product as an orange crystalline solid (315 mg, 42%). **^{1}H NMR** (600 MHz, DMSO-d_6) δ 10.38 (s, 1H), 9.23 (d, *J* = 2.2 Hz, 1H), 8.09 (d, *J* = 2.1 Hz, 1H), 7.79 (d, *J* = 8.9 Hz, 2H), 6.95 (d, *J* = 8.8 Hz, 2H). **^{13}C NMR** (151 MHz, DMSO-d_6) δ 165.6, 161.3, 154.8, 145.3, 124.9, 116.0, 113.0. **LC-MS**

(HPLC, acidic): t_r: 3.23 min, purity: >99% (254 nm), λ_{max}: 354 nm, $[M+H]^+$ m/z calc.: 206.04, found 206.00.

(*E*)-4-((1,2,3-thiadiazol-5-yl)diazenyl)phenol (5h)

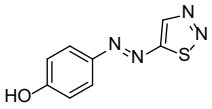

To a solution of 1,2,3-thiadiazol-5-amine (**4h**, 101 mg, 1.00 mmol, 1.0 eq) in conc. aq. H_3PO_4 (5 mL) at 0°C was added $NaNO_2$ (138 mg, 2.00 mmol, 2.0 eq). PhOH (94 mg) in MeOH (3 mL) was added dropwise. After complete addition, the reaction mixture was slowly warmed to rt and stirred for an additional 30 min. The reaction mixture was poured in H_2O (50 mL) and extracted using EtOAc thrice. The combined organic layers were washed with water, brine, dried over Na_2SO_4, filtered and concentrated. The crude product was purified using reverse-phase column chromatography (5-90% MeCN + 0.1% HCO_2H in H_2O + 0.1% HCO_2H) to give the title compound as an orange solid (55 mg, 27%). **^{1}H NMR** (600 MHz, DMSO-d_6) δ 11.13 (s, 1H), 9.56 (s, 1H), 7.87 (d, *J* = 8.9 Hz, 2H), 7.02 (d, *J* = 8.9 Hz, 2H). **^{13}C NMR** (151 MHz, DMSO-d_6) δ 171.4, 164.0, 145.9, 145.1, 126.6, 116.7. **LC-MS** (HPLC, acidic): t_r: 3.89 min, purity: 98% (254 nm), λ_{max}: 399 nm, $[M+H]^+$ m/z calc.: 207.03, found 206.95.

(*E*)-4-(isoxazol-3-yldiazenyl)phenol (5i)

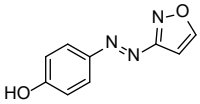

To a solution of isoxazol-3-amine (**4i**, 200 mg, 2.38 mmol, 1.0 eq) in conc. aq. H_3PO_4 (10 mL) at 0°C was added $NaNO_2$ (164 mg, 2.38 mmol, 1.0 eq). PhOH (224 mg, 2.8 mmol, 1.0 eq) in MeOH (3 mL) was added dropwise. After complete addition, the reaction mixture was slowly warmed to rt and stirred for an additional 30 min. The reaction mixture was poured in H_2O (50 mL) and extracted with EtOAc thrice. The combined organic layers were washed with water, brine, dried over Na_2SO_4, filtered and concentrated to give the title compound as a yellow solid (381 mg, 85%). ^{1}H NMR (500 MHz, DMSO-d_6) δ 10.69 (s, 1H), 9.04 (d, *J* = 1.8 Hz, 1H), 7.88 (d, *J* = 8.7 Hz, 2H), 6.99 (d, *J* = 8.8 Hz, 2H), 6.83 (d, *J* = 1.8 Hz, 1H). ^{13}C NMR (126 MHz, DMSO) δ 172.7, 162.9, 162.1, 145.2, 126.0, 116.3, 95.3. **LC-MS** (HPLC, acidic): t_r: 3.65 min, purity: 98% (254 nm), λ_{max}: 353 nm, $[M+H]^+$ m/z calc.: 190.06, found 190.00.

(*E*)-4-(isoxazol-5-yldiazenyl)phenol (5j)

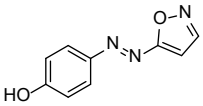

To a solution of isoxazol-5-amine (**4j**, 200 mg, 2.38 mmol, 1.0 eq) in conc. aq. H_3PO_4 (10 mL) at 0°C was added $NaNO_2$ (164 mg, 2.38 mmol, 1.0 eq). PhOH (224 mg, 2.8 mmol, 1.0 eq) in MeOH (3 mL) was added dropwise. After complete addition, the reaction mixture was slowly warmed to rt and stirred for an additional 30 min. The reaction mixture was poured in water (50 mL) and extracted with EtOAc thrice. The combined organic layers were washed with water, brine, dried over Na_2SO_4, filtered and concentrated to give the title compound as a yellow solid (62 mg, 14%). **^{1}H NMR** (600 MHz, DMSO) δ 10.82 (s, 1H), 8.76 (d, *J* = 1.9 Hz, 1H), 7.87 (d, *J* = 9.0 Hz, 2H), 6.99 (d, *J* = 8.9 Hz, 2H), 6.91 (d, *J* = 1.9 Hz, 1H). **^{13}C NMR** (151 MHz, DMSO) δ 173.2,

163.4, 153.0, 145.5, 126.3, 116.5, 96.5. **LC-MS** (HPLC, acidic): t_r: 3.57 min, purity: >99% (254 nm), λ_{max}: 375 nm, $[M+H]^+$ m/z calc.: 190.06, found 189.95.

***(E)*-3-((4-hydroxyphenyl)diazenyl)pentane-2,4-dione (8)**

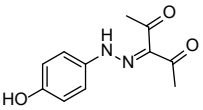

A solution of $NaNO_2$ (2.28 g, 33.0 mmol, 1.2 eq) in H_2O (5 mL) was added dropwise to a solution of 4-aminophenol (**7**, 3.00 g, 27.5 mmol) in AcOH (41 mL) and conc. aq. HCl (6.3 mL) that was cooled at 0-4°C. The resulting suspension was stirred at 0°C for 45 min. The diazonium salt solution was added to a suspension of pentane-2,4-dione (3.7 mL, 36.0 mmol, 1.3 eq) and NaOAc (6.76 g, 82.5 mmol, 3.0 eq) in EtOH (28 mL) and H_2O (17 mL). The mixture was stirred at 0°C for 1 h and filtered. The residue was washed with water, water:EtOH (1:1), and cHex. This yielded the title compound as a pale brown solid (2.33 g, 39%). **^{1}H NMR** (600 MHz, DMSO-d_6) δ 14.49 (s, 1H), 9.65 (s, 1H), 7.44 (d, *J* = 8.9 Hz, 2H), 6.83 (d, *J* = 8.9 Hz, 2H), 2.46 (s, 3H), 2.38 (s, 3H). **^{13}C NMR** (151 MHz, DMSO-d_6) δ 196.0, 196.0, 155.9, 133.7, 132.1, 118.1, 116.1, 31.1, 26.5. **LC-MS** (HPLC, acidic): t_r: 3.64 min, purity: >99% (254 nm), λ_{max}: 398 nm, $[M+H]^+$ m/z calc.: 221.09, found 221.05.

***(E)*-4-((3,5-dimethylisoxazol-4-yl)diazenyl)phenol (5k)**

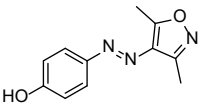

A solution of **5** (300 mg, 1.36 mmol, 1.0 eq), $H_2NOH.HCl$ (50% w/w in H_2O, 142 mg, 2.04 mmol, 1.5 eq), and Na_2CO_3 (217 mg, 2.04 mmol, 1.5 eq) in EtOH (13.6 mL) was heated at reflux for 18 h. The solution was concentrated under reduced pressure. The crude product was purified using normal-phase column chromatography (0-40% EtOAc in cHex) to give the title compound as a yellow solid (150 mg, 51%). **^{1}H NMR** (600 MHz, DMSO-d_6) δ 10.25 (s, 1H), 7.71 (d, *J* = 9.0 Hz, 2H), 6.91 (d, *J* = 8.7 Hz, 2H), 2.70 (s, 3H), 2.43 (s, 3H). **^{13}C NMR** (151 MHz, DMSO-d_6) δ 168.1, 160.6, 153.1, 145.5, 131.5, 124.1, 115.9, 11.7, 11.3. **LC-MS** (UPLC, acidic): t_r: 1.85 min, purity: 98% (254 nm), λ_{max}: 343 nm, $[M+H]^+$ m/z calc.: 218.09, found 218.00.

(*E*)-5-((4-fluorophenyl)diazenyl)-1-methyl-1*H*-imidazole (10)

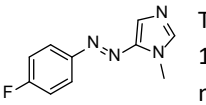

To a solution of 5-bromo-1-methyl-1*H*-imidazole (**9**, 742 mg, 4.61 mmol, 1.5 eq) in THF (3.1 mL) was added *i*PrMgCl·LiCl (1.3 M in THF, 893 mg, 6.15 mmol, 2.0 eq) dropwise at rt over 10 min. After full consumption of the starting material (LC analysis), $ZnBr_2$ (554 mg, 2.46 mmol, 0.8 eq) in THF (2.5 mL) was added at -20 °C. The solution was stirred for 1 h at rt and was added dropwise to a suspension of 4-$FPhN_2^+$ BF_4^- (645 mg, 3.07 mmol, 1.0 eq) in a mixture of NMP (3.1 mL) and THF (3.1 mL) at −78 °C over 25 min. After complete addition, the suspension was allowed to warm to rt and was stirred for 22 h. The reaction mixture was quenched with satd. aq. NH_4Cl (5 mL) and water (5 mL). The mixture was extracted with Et_2O thrice. The combined organic phases were dried over Na_2SO_4, filtered and concentrated. The crude product was purified using reverse-phase

column chromatography (5 -55 % MeCN + 0.1% HCO_2H in H_2O + 0.1% HCO_2H). The desired fractions were combined, made basic using satd. aq. $NaHCO_3$ and extracted using EtOAc. The combined organic layers were washed with brine, dried over $MgSO_4$, and concentrated under reduced pressure. This yielded the title compound as a red solid (86 mg, 14%). **^{1}H NMR** (500 MHz, $CDCl_3$) δ 7.87 – 7.80 (m, 2H), 7.60 (s, 1H), 7.57 (d, *J* = 0.9 Hz, 1H), 7.20 – 7.12 (m, 2H), 3.96 (s, 3H). **^{13}C NMR** (126 MHz, $CDCl_3$) δ 164.2 (d, *J* = 252.3 Hz), 149.7 (d, *J* = 3.2 Hz), 145.3, 140.6, 124.4 (d, *J* = 8.6 Hz), 123.4, 116.2 (d, *J* = 22.8 Hz), 32.6. **^{19}F NMR** (471 MHz, $CDCl_3$) δ -109.7. **LC-MS** (HPLC, acidic): t_r: 2.90 min, purity: 92% (254 nm), λ_{max}: 352 nm, $[M+H]^+$ m/z calc.: 205.09, found 205.00.

tert-butyl ((1r,3r)-3-(4-((E)-(1-methyl-1H-imidazol-5-yl)diazenyl)phenoxy)cyclobutyl)carbamate (14a)

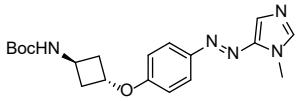

To a solution of **13** (161 mg, 0.86 mmol, 1.3 eq) in DMF (1.7 mL) was added NaH (48 mg, 1.19 mmol, 1.8 eq) at 0 °C. The mixture was stirred for 1.5 h. Fluoride **10** (135 mg, 0.66 mmol, 1.0 eq) in DMF (0.37 mL) was added at 0 °C. The reaction mixture was warmed to rt and stirred for 12 h. The reaction mixture was diluted with satd. aq. NH_4Cl and extracted using EtOAc thrice. The combined organic layers were washed with water, brine, dried over Na_2SO_4, filtered and concentrated. The crude product was purified using reverse-phase column chromatography (5-55 % MeCN + 0.1% HCO_2H in H_2O + 0.1% HCO_2H) to give the title compound as a yellow solid (98 mg, 40%). **^{1}H NMR** (500 MHz, DMSO-d_6) δ 7.95 – 7.90 (m, 1H), 7.82 – 7.76 (m, 2H), 7.39 (d, *J* = 0.9 Hz, 1H), 7.33 (d, *J* = 7.3 Hz, 1H), 6.99 – 6.93 (m, 2H), 4.94 – 4.85 (m, 1H), 4.16 – 4.06 (m, 1H), 3.90 (s, 3H), 2.47 – 2.31 (m, 4H), 1.39 (s, 9H). **^{13}C NMR** (126 MHz, DMSO) δ 159.4, 154.8, 146.8, 144.9, 141.1, 123.9, 120.8, 115.4, 69.6, 41.7, 36.6, 31.8, 28.2. **LC-MS** (HPLC, acidic): t_r: 3.59 min, purity: 99% (254 nm), λ_{max}: 366 nm, $[M+H]^+$ m/z calc.: 372.20, found 372.20.

tert-butyl ((1r,3r)-3-(4-(*(E)*-(1-methyl-1H-1,2,4-triazol-3-yl)diazenyl)phenoxy)cyclobutyl)carbamate (14d)

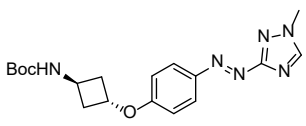

This compound was synthetised according to general procedure **C**, using **12** (250 mg, 1.34 mmol), **5d** (297 mg, 1.46 mmol), Ph_3P (560 mg, 2.14 mmol) in THF (22.3 mL), and DIAD (40% w/w in PhMe, 1.0 mL, 1.4 mmol). The reaction mixture was stirred at 0°C for 10 min and at rt for 22 h. The crude product was purified using normal-phase column chromatography (0 -100% EtOAc in cHex), followed by reverse-phase column chromatography (5-55 % MeCN + 0.1% HCO_2H in H_2O + 0.1% HCO_2H). The desired fractions were combined, made basic using satd. aq. $NaHCO_3$ and extracted using EtOAc. The combined organic layers were washed with brine, dried over $MgSO_4$, and concentrated under reduced pressure. This yielded the title compound as a yellow solid (222 mg, 45%). **^{1}H NMR** (600 MHz, DMSO-d_6) δ 8.61 (s, 1H), 7.90 (d, *J* = 9.0 Hz, 2H), 7.36 (d, *J* = 7.4 Hz, 1H), 7.02 (d, *J* = 9.0 Hz, 2H), 4.97 – 4.89 (m, 1H), 4.17 – 4.07 (m, 1H), 3.99 (s, 3H), 2.47 – 2.33 (m, 4H), 1.40 (s, 9H). **^{13}C NMR**

(151 MHz, DMSO-d_6) δ 168.7, 160.8, 154.8, 146.4, 146.0, 125.0, 115.6, 77.8, 69.8, 41.6, 36.6, 36.6, 28.3. **LC-MS** (HPLC, acidic): t_r: 4.08 min, purity: 99% (254 nm), λ_{max}: 355 nm, $[M+H]^+$ m/z calc.: 373.20, found 373.10.

***tert*-butyl ((1r,3r)-3-(4-(*(E)*-thiazol-2-yldiazenyl)phenoxy)cyclobutyl)carbamate (14e)**

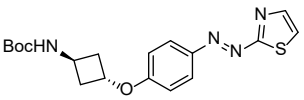

This compound was synthetised according to general procedure **C**, using **12** (470 mg, 2.51 mmol), **5e** (560 mg, 2.73 mmol), Ph_3P (1.045 g, 3.984 mmol) in THF (41.3 mL), and DIAD (40% w/w in PhMe, 1.8 mL, 3.4 mmol). The crude product was purified using reverse-phase column chromatography (5-90 % MeCN + 0.1% HCO_2H in H_2O + 0.1% HCO_2H). The desired fractions were combined, made basic using satd. aq. $NaHCO_3$ and extracted using EtOAc. The combined organic layers were washed with brine, dried over $MgSO_4$, and concentrated under reduced pressure. This yielded the title product as an orange solid (839 mg, 90%). **^{1}H NMR** (600 MHz, DMSO-d_6) δ 8.09 (d, *J* = 3.3 Hz, 1H), 7.94 (d, *J* = 9.0 Hz, 2H), 7.88 (d, *J* = 3.3 Hz, 1H), 7.35 (d, *J* = 7.4 Hz, 1H), 7.05 (d, *J* = 9.1 Hz, 2H), 5.00 – 4.92 (m, 1H), 4.17 – 4.06 (m, 1H), 2.47 – 2.30 (m, 4H), 1.39 (s, 9H). **^{13}C NMR** (151 MHz, DMSO-d_6) δ 176.5, 161.7, 154.8, 145.3, 144.0, 125.9, 122.4, 116.0, 77.8, 70.1, 41.6, 36.6, 28.3. **LC-MS** (HPLC, acidic): t_r: 5.07 min, purity: 95% (254 nm), λ_{max}: 388 nm, $[M+H]^+$ m/z calc.: 375.15, found 375.10.

***tert*-butyl ((1r,3r)-3-(4-(*(E)*-(1,3,4-thiadiazol-2-yl)diazenyl)phenoxy)cyclobutyl)carbamate (14f)**

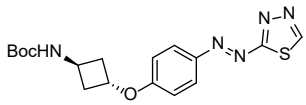

This compound was synthetised according to general procedure **C**, using **12** (462 mg, 2.47 mmol), **5f** (559 mg, 2.71 mmol), Ph_3P (1.037 g, 3.954 mmol) in THF (41 mL), and DIAD (40% w/w in PhMe, 1.8 mL, 1.4 mmol). The reaction mixture was stirred at 0°C for 10 min, then at rt for 21 h. The crude product was purified using reverse-phase column chromatography (5-90% MeCN + 0.1% HCO_2H in H_2O + 0.1% HCO_2H). The desired fractions were combined, made basic using satd. aq. $NaHCO_3$ and extracted using EtOAc. The combined organic layers were washed with brine, dried over $MgSO_4$, and concentrated under reduced pressure. This yielded the title compound as a yellow/gold solid (243 mg, 26%). **^{1}H NMR** (500 MHz, DMSO-d_6) δ 9.64 (s, 1H), 8.04 – 7.98 (m, 2H), 7.34 (d, *J* = 7.4 Hz, 1H), 7.12 – 7.04 (m, 2H), 4.98 (tt, *J* = 6.5, 4.3 Hz, 1H), 4.20 – 3.95 (m, 1H), 2.48 – 2.27 (m, 4H), 1.39 (s, 9H). **^{13}C NMR** (126 MHz, DMSO-d_6) δ 179.6, 162.7, 154.84, 154.79, 145.5, 126.6, 116.1, 77.8, 70.3, 41.6, 36.5, 28.2. **LC-MS** (HPLC, acidic): t_r: 4.65 min, purity: 95% (254 nm), λ_{max}: 377 nm, $[M+H]^+$ m/z calc.: 376.14, found 376.10.

tert-butyl ((1_r_,3_r_)-3-(4-((_E_)-thiazol-4-yldiazenyl)phenoxy)cyclobutyl)carbamate (14g)

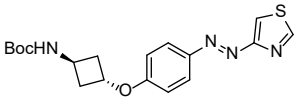

This compound was synthetised according to general procedure **C**, using **12** (166 mg, 0.89 mmol), **5g** (200 mg, 0.98 mmol), Ph_3P (349 mg, 1.33 mmol) in THF (3 mL), and DIAD (262 µL, 1.33 mmol). The reaction mixture was stirred at 0°C for 10 min and at 50 °C for 2 h. The crude product was purified using reverse-phase column chromatography (5-90% MeCN + 0.1% HCO_2H in H_2O + 0.1% HCO_2H).The desired fractions were combined, made basic using satd. aq. $NaHCO_3$ and extracted using EtOAc. The combined organic layers were washed with brine, dried over $MgSO_4$, and concentrated under reduced pressure. This yielded the title compound as an orange solid (311 mg, 94%). **^{1}H NMR** (600 MHz, DMSO-d_6) δ 9.25 (d, *J* = 2.1 Hz, 1H), 8.17 (d, *J* = 2.2 Hz, 1H), 7.87 (d, *J* = 8.9 Hz, 2H), 7.33 (d, *J* = 7.4 Hz, 1H), 7.01 (d, *J* = 8.9 Hz, 2H), 4.96 – 4.89 (m, 1H), 4.11 (m, 1H), 2.47 – 2.33 (m, 4H), 1.39 (s, 9H). **^{13}C NMR** (151 MHz, DMSO-d_6) δ 165.9, 160.8, 155.4, 155.3, 146.8, 125.2, 116.0, 114.7, 70.2, 42.1, 37.1, 28.7. **LC-MS** (HPLC, acidic): t_r: 4.71 min, purity: 98% (254 nm), λ_{max}: 352 nm, $[M+H]^+$ m/z calc.: 375.14, found 375.15.

tert-butyl ((1_r_,3_r_)-3-(4-((_E_)-(1,2,3-thiadiazol-5-yl)diazenyl)phenoxy)cyclobutyl)carbamate (14h)

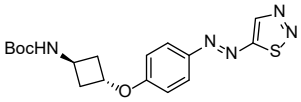

This compound was synthetised according to general procedure **C**, using **12** (99 mg, 0.53 mmol), **5h** (120 mg, 0.58 mmol), Ph_3P (208 mg, 0.79 mmol) in THF (1.8 mL), and DIAD (156 µL, 0.79 mmol). The reaction mixture was stirred at 0°C for 10 min and at 50 °C for 2 h. The crude product was purified using normal-phase column chromatography (0-5% MeOH + NH_3 in DCM). This gave the title compound as a red solid (83 mg, 42%). **^{1}H NMR** (600 MHz, $CDCl_3$) δ 9.15 (s, 1H), 7.91 (d, *J* = 8.9 Hz, 2H), 6.89 (d, *J* = 8.8 Hz, 2H), 4.93 – 4.87 (m, 1H), 4.80 (s, 1H), 4.34 (s, 1H), 2.65 – 2.56 (m, 2H), 2.51 – 2.41 (m, 2H), 1.46 (s, 9H). **^{13}C NMR** (151 MHz, CDCl3) δ 171.6, 162.3, 155.1, 146.7, 145.6, 126.2, 115.7, 70.0, 42.7, 37.4, 28.4**. LC-MS** (HPLC, acidic): t_r: 5.25 min, purity: 94% (254 nm), λ_{max}: 387 nm, $[M+H]^+$ m/z calc.: 376.14, found 376.15.

tert-butyl ((1_r_,3_r_)-3-(4-((_E_)-isoxazol-3-yldiazenyl)phenoxy)cyclobutyl)carbamate (14i)

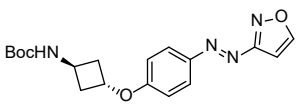

This compound was synthetised according to general procedure **C**, using **12** (180 mg, 0.96 mmol), **5i** (200 mg, 1.06 mmol), Ph_3P (378 mg, 1.44 mmol) in THF (3.2 mL), and DIAD (284 µL, 1.44 mmol). The reaction mixture was stirred at 0°C for 10 min and at 50 ℃ for 2 h. The crude product was purified using normal-phase column chromatography (10-60% EtOAc in cHex) followed by reverse-phase column chromatography (20-90% MeCN+0.1% HCO2H in H_2O+0.1% HCO_2H). The desired fractions were combined,

made basic using satd. aq. $NaHCO_3$ and extracted using EtOAc. The combined organic layers were washed with brine, dried over Na_2SO_4, and concentrated under reduced pressure. This yielded the title compound as yellow solid (231 mg, 67%). **^{1}H NMR** (500 MHz, DMSO-d_6) δ 9.07 (d, *J* = 1.8 Hz, 1H), 7.95 (d, *J* = 8.9 Hz, 2H), 7.34 (d, *J* = 7.1 Hz, 1H), 7.05 (d, *J* = 8.8 Hz, 2H), 6.85 (d, *J* = 1.8 Hz, 1H), 4.95 (m, 1H), 4.20 – 4.06 (m, 1H), 2.49 – 2.30 (m, 4H), 1.39 (s, 9H). **^{13}C NMR** (126 MHz, DMSO-d_6) δ 172.7, 162.3, 161.7, 154.8, 146.1, 125.7, 115.8, 95.3, 77.8, 70.0, 41.6, 36.5, 28.2. **LC-MS** (HPLC, acidic): t_r: 5.05 min, purity: 99% (254 nm), λ_{max}: 377 nm, $[M+H]^+$ m/z calc.: 359.17, found 359.15.

tert-butyl ((1*r*,3*r*)-3-(4-((*E*)-isoxazol-5-yldiazenyl)phenoxy) cyclobutyl)carbamate (14j)

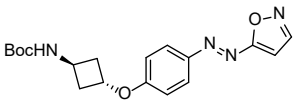

This compound was synthetised according to general procedure **C**, using **12** (90 mg, 0.48 mmol), **5j** (100 mg, 0.53 mmol), Ph_3P (189 mg, 0.72 mmol) in THF (1.6 mL), and DIAD (142 µL, 0.72 mmol). The reaction mixture was stirred at 0°C for 10 min and at 50 °C for 2 h. The crude product was purified using normal-phase column chromatography (10-60% EtOAc in cHex). This yielded the title compound as an orange solid (70 mg, 40%). **^{1}H NMR** (600 MHz, DMSO-d_6) δ 8.79 (d, *J* = 1.9 Hz, 1H), 7.95 (d, *J* = 8.9 Hz, 2H), 7.33 (d, *J* = 7.4 Hz, 1H), 7.05 (d, *J* = 8.9 Hz, 2H), 6.99 (d, *J* = 1.9 Hz, 1H), 5.00 – 4.91 (m, 1H), 4.19 – 4.06 (m, 1H), 2.47 – 2.33 (m, 4H), 1.39 (s, 9H). **^{13}C NMR** (151 MHz, DMSO- d_6) δ 173.4, 162.5, 155.3, 153.6, 146.9, 126.4, 115.7, 97.9, 78.3, 70.6, 42.1, 37.0, 29.1. **LC-MS** (HPLC, acidic): t_r: 5.02 min, purity: 95% (254 nm), λ_{max}: 363 nm, $[M+H]^+$ m/z calc.: 359.17, found 359.15.

(1*r*,3*r*)-3-(4-((*E*)-(1-methyl-1*H*-imidazol-5-yl)diazenyl)phenoxy)cyclobutan-1-amine hydrochloride (15a)

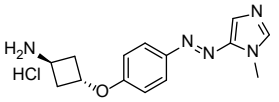

This compound was synthetised according to general procedure **D**, using **14a** (67 mg, 0.18 mmol), MeOH (1.8 mL) and HCl (4 M in dioxane, 0.45 mL, 1.8 mmol). This yielded the title compound as a yellow solid (42 mg, 76%). **^{1}H NMR** (500 MHz, CD_3OD) δ 8.97 (s, 1H), 8.01 – 7.94 (m, 2H), 7.85 (d, J = 1.5 Hz, 1H), 7.07 – 6.98 (m, 2H), 5.12 (tt, J = 7.1, 3.9 Hz, 1H), 4.20 (s, 3H), 4.03 (tt, J = 8.4, 5.8 Hz, 1H), 2.80 – 2.62 (m, 4H). **^{13}C NMR** (126 MHz, CD_3OD) δ 161.4, 147.2, 145.3*, 136.3, 125.4, 115.5, 108.9, 69.1, 42.3, 33.9, 32.8. **LCMS** (HPLC, acidic): t_r: 1.90 min, purity: 84% (254 nm), λ_{max}: 356 nm, $[M+H]^+$ m/z calc.: 272.15, found 272.10.

(1r,3r)-3-(4-((*E*)-(1-methyl-1H-1,2,4-triazol-3-yl)diazenyl)phenoxy)cyclobutan-1-amine hydrochloride (15d)

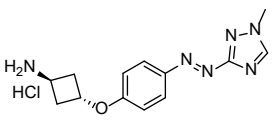

This compound was synthetised according to general procedure **D**, using **14d** (143 mg, 0.384 mmol), MeOH (3.8 mL) and HCl (4 M in dioxane, 1.0 mL, 3.8 mmol). This yielded the title compound as yellow crystals (110 mg, 93%). **^{1}H NMR** (600 MHz, DMSO-d_6) δ

8.62 (s, 1H), 8.54 – 8.42 (m, 3H), 7.91 (d, *J* = 8.9 Hz, 2H), 7.02 (d, *J* = 9.0 Hz, 2H), 5.20 – 5.13 (m, 1H), 3.98 (s, 3H), 3.89 – 3.81 (m, 1H), 2.74 – 2.65 (m, 2H), 2.49 – 2.44 (m, 2H). **^{13}C NMR** (151 MHz, DMSO-d_6) δ 168.7, 160.3, 146.6, 146.0, 125.1, 115.6, 69.3, 41.3, 36.6, 33.9. **LC-MS** (HPLC, acidic): t_r: 2.18 min, purity: 97% (254 nm), λ_{max}: 355 nm, $[M+H]^+$ m/z calc.: 273.15, found 273.10.

(1r,3r)-3-(4-(*(E)*-thiazol-2-yldiazenyl)phenoxy)cyclobutan-1-amine hydrochloride (15e)

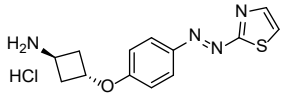

This compound was synthetised according to general procedure **D**, using **14e** (815 mg, 2.18 mmol), MeOH (21.8 mL) and HCl (4 M in dioxane, 5.4 mL, 1.4 mmol). This yielded the title compound as orange crystals (498 mg, 74%). **^{1}H NMR** (500 MHz, DMSO-d_6) ^{1}H NMR (500 MHz, DMSO) δ 8.58 – 8.37 (m, 3H), 8.09 (d, *J* = 3.3 Hz, 1H), 7.96 (d, *J* = 9.0 Hz, 2H), 7.88 (d, *J* = 3.3 Hz, 1H), 7.05 (d, *J* = 9.0 Hz, 2H), 5.24 – 5.15 (m, 1H), 3.83 – 3.76 (m, 1H), 2.75 – 2.65 (m, 2H), 2.49 – 2.45 (m, 2H). **^{13}C NMR** (126 MHz, DMSO-d_6) δ 176.4, 161.1, 145.4, 144.0, 125.9, 122.5, 115.9, 69.5, 41.3, 33.9. **LC-MS** (HPLC, acidic): t_r: 3.13 min, purity: 97% (254 nm), λ_{max}: 388 nm, $[M+H]^+$ m/z calc.: 275.10, found 275.05.

(1r,3r)-3-(4-(*(E)*-(1,3,4-thiadiazol-2-yl)diazenyl)phenoxy)cyclobutan-1-amine hydrochloride (15f)

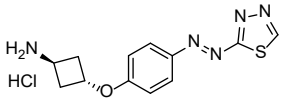

This compound was synthetised according to general procedure **D,** using **14f** (243 mg, 0.647 mmol), MeOH (6.5 mL) and HCl (4 M in dioxane, 1.6 mL, 3.9 mmol). This yielded the title compound as an orange solid (107 mg, 53%). **^{1}H NMR** (500 MHz, CD_3OD) δ 9.44 (s, 1H), 8.06 (d, *J* = 9.1 Hz, 2H), 7.08 (d, *J* = 9.1 Hz, 2H), 5.19 – 5.11 (m, 1H), 4.08 – 4.00 (m, 1H), 2.83 – 2.64 (m, 4H). **^{13}C NMR** (126 MHz, CD_3OD) δ 181.9, 164.0, 155.5, 147.9, 127.9, 117.1, 70.7, 43.7, 35.3. **LC-MS** (HPLC, acidic): t_r: 2.50 min, purity: >99% (254 nm), λ_{max}: 376 nm, $[M+H]^+$ m/z calc.: 276.09, found 276.00.

(1*r*,3*r*)-3-(4-((*E*)-thiazol-4-yldiazenyl)phenoxy)cyclobutan-1-amine (15g)

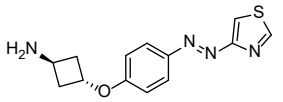

To a solution of **14g** (149 mg, 0.647 mmol) in MeOH (4 mL) was added HCl (4 M in dioxane, 1.0 mL, 4.0 mmol). The reaction mixture was stirred at rt for 2 h and concentrated *in vacuo* whilst keeping the temperature of the water bath below or at 35 °C to counteract observed instability. The crude product was mixed with EtOAc and satd. aq. $NaHCO_3$. The aqueous layer was extracted with EtOAc thrice. The combined organic layers were washed with brine, dried over Na_2SO_4, filtered and concentrated *in vacuo*. The crude product was purified using flash chromatography (2 - 10% MeOH + NH_3 in DCM). This yielded the title compound as an orange solid (72 mg, 66%). **^{1}H NMR** (500 MHz, DMSO) δ 9.25 (d, *J* = 2.1 Hz, 1H), 8.17 (d, *J* = 2.1 Hz, 1H), 7.87 (d, *J* = 9.0 Hz, 2H), 7.00 (d, *J* = 9.0 Hz, 2H), 4.96 (tt, *J* = 6.8, 4.3 Hz, 1H), 3.60 (tt, *J* = 7.8, 5.1 Hz, 1H), 2.35 – 2.15 (m, 4H). **^{13}C NMR** (126 MHz, DMSO) δ 165.4, 160.5, 154.9, 146.2,

124.7, 115.5, 114.1, 70.2, 43.4, 38.5[#]. **LC-MS** (HPLC, acidic): t_r: 2.70 min, purity: >99% (254 nm), λ_{max}: 351 nm, $[M+H]^+$ m/z calc.: 275.10, found 275.10.

(1*r*,3*r*)-3-(4-((*E*)-(1,2,3-thiadiazol-5-yl)diazenyl)phenoxy)cyclobutan-1-amine (15h)

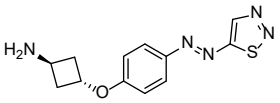

To a solution of **14h** (83 mg, 0.22 mmol) in MeOH (2.3 mL) was added HCl (4 M in dioxane, 0.55 mL, 2.21 mmol). The reaction mixture was stirred at rt for 2 h. The mixture was concentrated *in vacuo*. The crude product was mixed with EtOAc and satd. aq. $NaHCO_3$. The aqueous layer was extracted with EtOAc thrice. The combined organic layers were washed with brine, dried over Na_2SO_4, filtered and concentrated *in vacuo*. The crude product was purified using reverse-phase column chromatography (0-90 % MeCN + 0.1% HCO_2H in H_2O + 0.1% HCO_2H). The desired fractions were diluted with satd. aq. $NaHCO_3$, extracted with EtOAc thrice, dried over Na_2SO_4, filtered and concentrated in vacuo to give the target compound as an orange solid (38 mg, 62%). **^{1}H NMR** (600 MHz, CD_3OD) δ 9.28 (s, 1H), 7.98 – 7.86 (m, 2H), 6.98 (d, *J* = 9.0 Hz, 2H), 4.98 (tt, *J* = 7.0, 3.8 Hz, 1H), 3.72 (tt, *J* = 7.9, 5.6 Hz, 1H), 2.54 – 2.41 (m, 2H), 2.41 – 2.27 (m, 2H). **^{13}C NMR** (151 MHz, CD_3OD) δ 173.3, 164.3, 148.0, 146.9, 127.3, 117.0, 71.7, 44.8, 39.6. **LC-MS** (HPLC, acidic): t_r: 2.99 min, purity: 99% (254 nm), λ_{max}: 387 nm, $[M+H]^+$ m/z calc.: 276.09, found 276.10.

(1*r*,3*r*)-3-(4-((*E*)-isoxazol-3-yldiazenyl)phenoxy)cyclobutan-1-amine hydrochloride (15i)

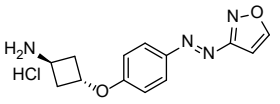

This compound was synthetised according to general procedure **D**, using **14i** (200 mg, 0.56 mmol), MeOH (5.6 mL) and HCl (4 M in dioxane, 1.4 mL, 5.6 mmol). This yielded the title compound as a yellow solid (147 mg, 89%). **^{1}H NMR** (600 MHz, CD_3OD) δ 8.76 (d, *J* = 1.8 Hz, 1H), 8.02 (d, *J* = 8.9 Hz, 2H), 7.05 (d, *J* = 8.8 Hz, 2H), 6.81 (d, *J* = 1.8 Hz, 1H), 5.11 (m, 1H), 4.05 (tt, *J* = 8.4, 5.9 Hz, 1H), 2.79 – 2.65 (m, 4H). **^{13}C NMR** (151 MHz, CD_3OD) δ 174.5, 162.7, 162.5, 148.5, 126.9, 116.7, 96.0, 70.4, 43.8, 35.3. **LC-MS** (HPLC, acidic): t_r: 2.87 min, purity: 99% (254 nm), λ_{max}: 351 nm, $[M+H]^+$ m/z calc.: 259.12, found 259.15.

(1*r*,3*r*)-3-(4-((*E*)-isoxazol-5-yldiazenyl)phenoxy)cyclobutan-1-amine hydrochloride (15j)

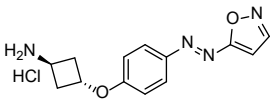

This compound was synthetised according to general procedure **D**, using **14j** (70 mg, 0.195 mmol), MeOH (2.0 mL) and HCl (4 M in dioxane, 0.5 mL, 1.95 mmol). This yielded the title compound as an orange solid (56 mg, 89%). **^{1}H NMR** (600 MHz, CD_3OD) δ 8.52 (d, *J* = 1.9 Hz, 1H), 7.99 (d, *J* = 8.9 Hz, 2H), 7.03 (d, *J* = 8.9 Hz, 2H), 6.78 (d, *J* = 1.9 Hz, 1H), 5.10 (tt, *J* = 7.1, 4.0, Hz, 1H), 4.03 (tt, *J* = 8.4, 5.9 Hz, 1H), 2.77 – 2.61 (m, 4H). **^{13}C NMR** (151 MHz, CD_3OD) δ 175.4, 163.0, 153.5, 148.8, 127.1, 116.8, 97.0, 70.5, 43.7, 35.3. **LC-MS** (HPLC, acidic): t_r: 2.83 min, purity: 98% (254 nm), λ_{max}: 367 nm, $[M+H]^+$ m/z calc.: 259.12, found 259.15.

1-((1*r*,3*r*)-3-(4-((*E*)-(1-methyl-1*H*-imidazol-5-yl)diazenyl)phenoxy)cyclobutyl)piperidine (3a)

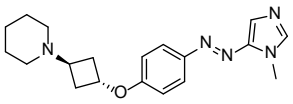

This compound was synthetised according to general procedure **F**, using DIPEA (77 µL, 0.44 mmol), 1,5-dibromopentane (22 µL, 0.18 mmol), **15a** (40 mg, 0.15 mmol), and anhydrous MeCN (0.73 mL). The reaction mixture was stirred at reflux for 19 h. The reaction mixture was concentrated under reduced pressure and extracted with H_2O and EtOAc twice. The aq. layer was made basic with satd. aq. $NaHCO_3$ and extracted thrice with EtOAc. The combined organic layers were dried over Na_2SO_4, filtered, and concentrated under reduced pressure. The crude was purified using reverse-phase column chromatography (5-90 % MeCN + 0.1% HCO_2H in H_2O + 0.1% HCO_2H). The desired fractions were combined, made basic using satd. aq. $NaHCO_3$ and extracted using EtOAc. The combined organic layers were washed with brine, dried over Na_2SO_4, and concentrated under reduced pressure. Lyophilisation yielded the title compound as a yellow solid (6 mg, 12%). **^{1}H NMR** (600 MHz, CD_3OD) δ 7.76 – 7.70 (m, 3H), 7.29 (d, *J* = 1.0 Hz, 1H), 6.84 (d, *J* = 8.8 Hz, 2H), 4.79 – 4.76 (m, 1H), 3.91 – 3.86 (m, 3H), 2.98 (tt, *J* = 7.4, 7.4 Hz, 1H), 2.45 – 2.14 (m, 8H), 1.58 – 1.38 (m, 6H). **^{13}C NMR** (151 MHz, CD_3OD) δ 161.6, 148.7, 146.8, 141.4, 125.4, 120.6, 116.5, 70.8, 58.7, 52.0, 34.4, 32.5, 26.1, 25.0. **LC-MS** (HPLC, acidic): t_r: 2.25 min, purity: 99% (254 nm), λ_{max}: 358 nm, $[M+H]^+$ m/z calc.: 340.21, found 340.15. **HRMS**: $[M+H]^+$ calc. for $C_{19}H_{26}N_5O$: 340.2132, found. 340.2128.

1-((1r,3r)-3-(4-(*(E)*-(1-methyl-1H-imidazol-2-yl)diazenyl)phenoxy)cyclobutyl)piperidine (3b)

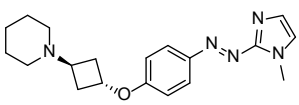

This compound was synthetised according to general procedure **E**, using **5b** (99 mg, 0.49 mmol) in DMF (0.19 mL), NaH (60% dispersion in mineral oil, 24 mg, 0.60 mmol), and **11** (116 mg, 0.375 mmol). The reaction mixture was stirred at 70°C for 17 h, at 75°C for 1.5 h, and at 80°C for 2.5 h. The crude product was purified using normal-phase column chromatography (50-90% EtOAc:MeOH:TEA) (90:5:5) in cHex). Lyophilisation yielded the title compound as a fluffy yellow solid (12 mg, 9%). **^{1}H NMR** (600 MHz, CD_3OD) δ 7.96 (d, *J* = 9.0 Hz, 2H), 7.38 (d, *J* = 1.0 Hz, 1H), 7.18 (d, *J* = 1.1 Hz, 1H), 6.97 (d, *J* = 9.0 Hz, 2H), 4.93 – 4.91 (m, 1H), 4.05 (s, 3H), 3.31 – 3.31 (m, 1H), 2.72 – 2.36 (m, 8H), 1.76 – 1.64 (m, 4H), 1.62 – 1.50 (m, 2H). **^{13}C NMR** (151 MHz, CD_3OD) δ 162.2, 153.7, 148.8, 129.9, 126.2, 125.5, 116.6, 70.4, 58.6, 51.9, 34.1, 33.2, 25.6, 24.4. **LC-MS** (UPLC, acidic): t_r: 1.33 min, purity: 98% (254 nm), λ_{max}: 396 nm, $[M+H]^+$ m/z calc.: 340.21, found 340.10. **HRMS**: $[M+H]^+$ calc. for $C_{19}H_{26}N_5O$: 340.2137, found. 340.2125

1-((1r,3r)-3-(4-(*(E)*-(1-methyl-1*H*-pyrazol-3-yl)diazenyl)phenoxy)cyclobutyl)piperidine (3c)

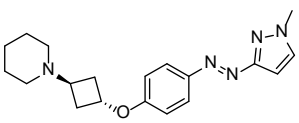

This compound was synthetised according to general procedure **E**, using **5c** (100 mg, 0.495 mmol) in DMF (0.41 mL), NaH (60% dispersion in mineral oil, 25 mg, 0.63 mmol), and **11** (119 mg, 0.385 mmol). The reaction mixture was stirred at 90°C for 16 h. The crude product was purified using normal-phase column chromatography (30-70% EtOAc:MeOH:TEA (90:5:5) in cHex, followed by reverse-phase column chromatography (5-90 % MeCN + 0.1% HCO_2H in H_2O + 0.1% HCO_2H). The desired fractions were combined, made basic using satd. aq. $NaHCO_3$ and extracted using EtOAc. The combined organic layers were washed with brine, dried over $MgSO_4$, and concentrated under reduced pressure. Lyophilisation yielded the title product as a fluffy yellow solid (8 mg, 6%). **^{1}H NMR** (600 MHz, CD_3OD) δ 7.87 (d, J = 8.5 Hz, 2H), 7.64 (d, J = 2.5 Hz, 1H), 6.95 (d, J = 8.5 Hz, 2H), 6.57 (d, J = 2.5 Hz, 1H), 4.88 – 4.83 (m, 1H), 3.99 (s, 3H), 3.16 – 3.01 (m, 1H), 2.61 – 2.18 (m, 8H), 1.70 – 1.59 (m, 4H), 1.58 – 1.44 (m, 2H). **^{13}C NMR** (151 MHz, CD_3OD) δ 165.0, 161.8, 148.3, 134.0, 125.7, 116.5, 95.8, 70.7, 58.6, 52.0, 39.5, 34.3, 26.1, 25.0. **LC-MS** (UPLC, acidic): t_r: 1.37 min, purity: 98% (254 nm), λ_{max}: 347 nm, $[M+H]^+$ m/z calc.: 340.21, found 340.45. **HRMS**: $[M+H]^+$ calc. for $C_{19}H_{26}N_50$: 340.2137, found. 340.2133.

1-((1r,3r)-3-(4-(*(E)*-(1-methyl-1H-1,2,4-triazol-3-yl)diazenyl)phenoxy)cyclobutyl)piperidine (3d)

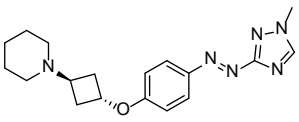

This compound was synthetised according to general procedure **F**, using DIPEA (135 µL, 0.78 mmol), 1,5-dibromopentane (39 µL, 0.29 mmol), **15d** (80 mg, 0.26 mmol) and anhydrous MeCN (2.6 mL). The reaction mixture was stirred at reflux for 19 h. The reaction mixture was concentrated under reduced pressure and extracted with H_2O and EtOAc twice. The aq. layer was made basic with satd. aq. $NaHCO_3$ and extracted thrice with EtOAc and thrice with $CHCl_3$:*i*PrOH (3:1). The combined organic layers were dried over $MgSO_4$, filtered, and concentrated under reduced pressure. The crude product was purified using normal-phase column chromatography (0-3% MeOH + NH_3 in DCM). Lyophilisation yielded the title compound as a fluffy yellow solid (48 mg, 54%). **^{1}H NMR** (500 MHz, CD_3OD) δ 8.50 (s, 1H), 7.99 (d, *J* = 9.0 Hz, 2H), 7.01 (d, *J* = 9.0 Hz, 2H), 5.00 – 4.92 (m, 1H), 4.05 (s, 3H), 3.60 – 3.45 (m, 1H), 2.88 – 2.34 (m, 8H), 1.91 – 1.69 (m, 5H), 1.69 – 1.49 (m, 2H). **^{13}C NMR** (126 MHz, CD_3OD) δ 162.7, 148.4, 146.9, 126.6, 116.7, 70.1, 58.6, 51.8, 37.2, 33.8, 25.1, 23.8. **LC-MS** (HPLC, acidic): t_r: 2.50 min, purity: 97% (254 nm), λ_{max}: 350 nm, $[M+H]^+$ m/z calc.: 341.21, found 341.15. **HRMS**: $[M+H]^+$ calc. for $C_{18}H_{25}N_6O$: 341.2090, found. 341.2093.

2-((*E*)-(4-((1r,3r)-3-(piperidin-1-yl)cyclobutoxy)phenyl)diazenyl)thiazole (3e)

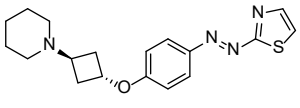

This compound was synthetised according to general procedure **F**, using DIPEA (0.84 mL, 4.83 mmol), 1,5-dibromopentane (0.24 mL, 1.77 mmol), **15e** (500 mg, 1.61 mmol) and anhydrous MeCN (8.0 mL). The reaction mixture was concentrated under reduced pressure and extracted with H_2O and EtOAc twice. The aq. layer was made basic with satd. aq. $NaHCO_3$ and extracted with EtOAc. The combined organic layers were washed with satd. aq. $NaHCO_3$ and brine, dried over $MgSO_4$, filtered, and concentrated under reduced pressure. The crude product was purified using normal-phase column chromatography (0-10% MeOH + NH_3 in DCM). This yielded the title product as a red solid (408 mg, 74%). **^{1}H NMR** (500 MHz, CD_3OD) δ 8.00 (d, *J* = 3.4 Hz, 1H), 7.97 (d, *J* = 9.0 Hz, 2H), 7.66 (d, *J* = 3.4 Hz, 1H), 7.01 (d, *J* = 9.0 Hz, 2H), 4.94 – 4.88 (m, 1H), 3.11 – 3.02 (m, 1H), 2.67 – 2.10 (m, 9H), 1.70 – 1.58 (m, 5H), 1.57 – 1.41 (m, 2H). **^{13}C NMR** (126 MHz, CD_3OD) δ 179.3, 163.7, 144.2, 127.2, 122.6, 117.0, 71.2, 58.6, 52.0, 34.3, 26.1, 25.0. **LC-MS** (acidic): t_r: 3.07 min, purity: 98% (254 nm), λ_{max}: 388 nm, $[M+H]^+$ m/z calc.: 343.16, found 343.15. **HRMS**: $[M+H]^+$ calc. for $C_{18}H_{23}N_4OS$: 343.1593, found. 343.1592.

2-((*E*)-(4-((1r,3r)-3-(piperidin-1-yl)cyclobutoxy)phenyl)diazenyl)-1,3,4-thiadiazole (3f)

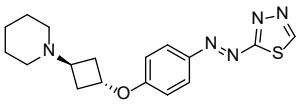

This compound was synthetised according to general procedure **F**, using DIPEA (134 µL, 0.77 mmol), 1,5-dibromopentane (38 µL, 0.28 mmol), **15f** (80 mg, 0.26 mmol) and anhydrous MeCN (1.3 mL). The reaction mixture was stirred at reflux for 22 h. The crude product was purified using reverse-phase column chromatography (5-90 % MeCN + 0.1% HCO_2H in H_2O + 0.1% HCO_2H). The desired fractions were combined, made basic using satd. aq. $NaHCO_3$ and extracted using EtOAc. The combined organic layers were washed with brine, dried over $MgSO_4$, and concentrated under reduced pressure. This yielded the title compound as an orange/yellow solid (36 mg, 41%). **^{1}H NMR** (600 MHz, CD_3OD) δ 9.42 (s, 1H), 8.03 (d, *J* = 9.0 Hz, 2H), 7.05 (d, *J* = 9.1 Hz, 2H), 4.96 – 4.91 (m, 1H), 3.14 – 3.06 (m, 1H), 2.56 – 2.27 (m, 8H), 1.70 – 1.60 (m, 4H), 1.56 – 1.46 (m, 2H). **^{13}C NMR** (151 MHz, CD_3OD) δ 182.0, 164.7, 155.4, 147.6, 127.9, 117.2, 71.4, 58.5, 52.0, 34.3, 26.1, 25.0. **LC-MS** (HPLC, acidic): t_r: 2.76 min, purity: >99% (254 nm), λ_{max}: 376 nm, $[M+H]^+$ m/z calc.: 344.15, found 344.10. **HRMS**: $[M+H]^+$ calc. for $C_{17}H_{22}N_5OS$: 344.1545, found. 344.1547.

4-((*E*)-(4-((1*r*,3*r*)-3-(piperidin-1-yl)cyclobutoxy)phenyl)diazenyl)thiazole (3g)

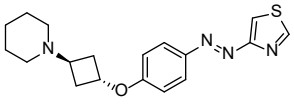

This compound was synthetised according to general procedure **F**, using DIPEA (91 µL, 0.53 mmol), 1,5-dibromopentane (66 mg, 0.29 mmol), **15g** (72 mg, 0.26 mmol) and anhydrous MeCN (1.3 mL). The crude product was purified using using reverse-phase column chromatography (5-90 % MeCN + 0.1% HCO_2H in H_2O + 0.1% HCO_2H). The desired fractions were combined, made basic using satd. aq. $NaHCO_3$ and extracted using EtOAc. The combined organic layers were

washed with brine, dried over $MgSO_4$, and concentrated under reduced pressure. This yielded the title compound as an orange solid (32 mg, 36%). **^{1}H NMR** (600 MHz, CD_3OD) δ 9.13 (d, *J* = 2.2 Hz, 1H), 8.10 (d, *J* = 2.2 Hz, 1H), 7.94 (d, *J* = 8.8 Hz, 2H), 6.98 (d, *J* = 8.9 Hz, 2H), 4.93 – 4.88 (m, 1H), 3.23 – 3.05 (m, 1H), 2.67 – 2.31 (m, 8H), 1.72 – 1.45 (m, 6H). **^{13}C NMR** (151 MHz, CD_3OD) δ 166.9, 162.3, 155.9, 148.2, 126.1, 116.6, 116.2, 70.8, 58.6, 52.0, 34.3, 26.0, 24.9. **LC-MS** (HPLC, acidic): t_r: 2.98 min, purity: >99% (254 nm), λ_{max}: 351 nm, $[M+H]^+$ m/z calc.: 343.16, found 343.15. **HRMS**: $[M+H]^+$ calc. for $C_{17}H_{23}N_4OS$: 343.1587, found. 343.1586.

5-((*E*)-(4-((1*r*,3*r*)-3-(piperidin-1-yl)cyclobutoxy)phenyl)diazenyl)-1,2,3-thiadiazole (3h)

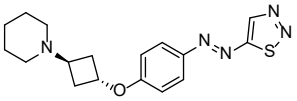

This compound was synthetised according to general procedure **F**, using DIPEA (48 µL, 0.28 mmol), 1,5-dibromopentane (21 µL, 0.15 mmol), **15h** (38 mg, 0.14 mmol) and anhydrous MeCN (0.7 mL). The reaction mixture was stirred at reflux for 17 h. The crude product was purified using reverse-phase column chromatography (5-90 % MeCN + 0.1% HCO_2H in H_2O + 0.1% HCO_2H). The desired fractions were combined, made basic using satd. aq. $NaHCO_3$ and extracted using EtOAc. The combined organic layers were washed with brine, dried over Na_2SO_4, and concentrated under reduced pressure. This yielded the title compound as an orange solid (15 mg, 32%). **^{1}H NMR** (600 MHz, CD_3OD) δ 9.30 (s, 1H), 7.96 (d, *J* = 8.9 Hz, 2H), 7.02 (d, *J* = 8.9 Hz, 2H), 4.92 (tt, *J* = 6.9, 2.7 Hz, 1H), 3.11 (tt, *J* = 7.7, 7.6 Hz, 1H), 2.64 – 2.16 (m, 8H), 1.71 – 1.45 (m, 6H).**^{13}C NMR** (151 MHz, CD_3OD) δ 173.3, 164.1, 148.1, 146.9, 127.3, 117.0, 71.3, 58.5, 52.0, 34.3, 26.0, 24.9. **LC-MS** (HPLC, acidic): t_r: 3.05 min, purity: >99% (254 nm), λ_{max}: 387 nm, $[M+H]^+$ m/z calc.: 344.15, found 344.15. **HRMS**: $[M+H]^+$ calc. for $C_{17}H_{22}N_5OS$: 344.1540, found. 343.1536.

3-((E)-(4-((1r,3r)-3-(piperidin-1-yl)cyclobutoxy)phenyl)diazenyl)isoxazole (3i)

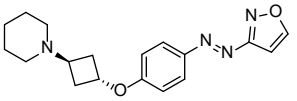

This compound was synthetised according to general procedure **F**, using DIPEA (189 µL, 1.08 mmol), 1,5-dibromopentane (81 µL, 0.60 mmol), **15i** (140 mg, 0.54 mmol) and anhydrous MeCN (3.2 mL). The reaction mixture was stirred at reflux for 17 h. The crude product was purified using reverse-phase column chromatography (5-90 % MeCN + 0.1% HCO_2H in H_2O + 0.1% HCO_2H). The desired fractions were combined, made basic using satd. aq. $NaHCO_3$ and extracted using EtOAc. The combined organic layers were washed with brine, dried over Na_2SO_4, and concentrated under reduced pressure. The crude product was purified using normal-phase column chromatography (0-10% MeOH + NH_3 in DCM). This yielded the title product as a yellow solid (98 mg, 55%). **^{1}H NMR** (600 MHz, CD_3OD) δ 8.73 (d, *J* = 1.8 Hz, 1H), 7.98 (d, *J* = 9.0 Hz, 2H), 7.01 (d, *J* = 8.9 Hz, 2H), 6.79 (d, *J* = 1.8 Hz, 1H), 4.93 – 4.89 (m, 1H), 3.09 (tt, *J* = 7.4, 7.4 Hz, 1H), 2.58 – 2.22 (m, 8H), 1.70 – 1.46 (m, 6H). **^{13}C NMR** (151 MHz, CD_3OD) δ 174.5, 163.5, 162.4, 148.2, 126.9, 116.8, 96.1, 71.1, 58.6, 52.0, 34.3, 26.1, 25.0. **LC-MS** (HPLC, acidic): t_r: 3.19 min, purity: >99% (254 nm), λ_{max}: 345 nm, $[M+H]^+$ m/z calc.: 327.18, found 327.15. **HRMS**: $[M+H]^+$ calc. for $C_{18}H_{23}N_4O_2$: 327.1816, found. 327.1807.

5-((*E*)-(4-((1*r*,3*r*)-3-(piperidin-1-yl)cyclobutoxy)phenyl)diazenyl)isoxazole (3j)

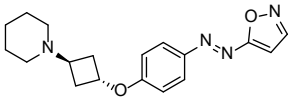

This compound was synthetised according to general procedure **F**, using DIPEA (90 µL, 0.74 mmol), 1,5-dibromopentane (39 µL, 0.28 mmol), **15j** (76 mg, 0.26 mmol) and anhydrous MeCN (1.3 mL). The reaction mixture was stirred at reflux for 17 h. The crude product was purified using using reverse-phase column chromatography (5-90 % MeCN + 0.1% HCO_2H in H_2O + 0.1% HCO_2H). The desired fractions were combined, made basic using satd. aq. $NaHCO_3$ and extracted using EtOAc. The combined organic layers were washed with brine, dried over Na_2SO_4, and concentrated under reduced pressure. The crude product was purified by reverse-phase column chromatography (5-90 % MeCN + 0.1% HCO_2H in H_2O + 0.1% HCO_2H). The title compound was obtained as an orange solid (17 mg, 20%). **^{1}H NMR** (600 MHz, CD_3OD) δ 8.51 (d, *J* = 1.9 Hz, 1H), 7.97 (d, *J* = 8.7 Hz, 2H), 7.01 (d, *J* = 8.8 Hz, 2H), 6.75 (d, *J* = 1.9 Hz, 1H), 4.91 (tt, *J* = 6.8, 2.7 Hz, 1H), 3.08 (tt, *J* = 7.5, 7.5 Hz, 1H), 2.55 – 2.27 (m, 8H), 1.67 – 1.47 (m, 6H). **^{13}C NMR** (151 MHz, CD_3OD) δ 175.5, 163.8, 153.4, 148.5, 127.1, 116.9, 96.6, 71.2, 58.6, 52.0, 34.3, 26.1, 25.0. **LC-MS** (HPLC, acidic): t_r: 3.14 min, purity: 97% (254 nm), λ_{max}: 345 nm, $[M+H]^+$ m/z calc.: 327.18, found 327.15. **HRMS**: $[M+H]^+$ calc. for $C_{18}H_{23}N_4O_2$: 327.1816, found. 327.1818.

3,5-dimethyl-4-((*E*)-(4-((1r,3r)-3-(piperidin-1-yl)cyclobutoxy)phenyl)diazenyl)isoxazole (3k)

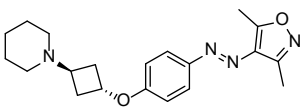

This compound was synthetised according to general procedure **E**, using **5k** (114 mg, 0.525 mmol) in DMF (0.4 mL), NaH (60% dispersion in mineral oil, 32 mg, 0.81 mmol), and **11** (125 mg, 0.405 mmol). The reaction mixture was stirred at 80 °C for 20 h. The crude product was purified using normal-phase column chromatography (10-50% EtOAc:MeOH:TEA (90:5:5) in cHex), followed by reverse-phase column chromatography (0-90 % MeCN + 0.1% HCO_2H in H_2O + 0.1% HCO_2H). The desired fractions were combined, made basic using satd. aq. $NaHCO_3$ and extracted using EtOAc. The combined organic layers were washed with brine, dried over $MgSO_4$, and concentrated under reduced pressure. Lyophilisation yielded the title compound as a fluffy yellow solid (10 mg, 7%). **^{1}H NMR** (600 MHz, CD_3OD) δ 7.79 (d, *J* = 8.9 Hz, 2H), 6.92 (d, *J* = 8.9 Hz, 2H), 4.88 – 4.83 (m, 1H), 3.09 – 3.00 (m, 1H), 2.75 – 2.70 (m, 3H), 2.51 – 2.20 (m, 11H), 1.68 – 1.59 (m, 4H), 1.55 – 1.45 (m, 2H). **^{13}C NMR** (151 MHz, CD_3OD) δ 169.9, 161.5, 155.0, 148.6, 133.2, 125.1, 116.4, 70.7, 58.6, 52.0, 34.4, 26.2, 25.1, 12.1, 11.4. **LC-MS** (UPLC, acidic): t_r: 1.50 min, purity: >99% (254 nm), λ_{max}: 336 nm, $[M+H]^+$ m/z calc.: 355.21, found 355.45. **HRMS**: $[M+H]^+$ calc. for $C_{20}H_{27}N_4O_2$: 355.2134, found. 355.2123.

Chapter 4

Design and synthesis of photoswitchable desloratadine ligands for histamine H_1 receptor photopharmacology

Lars C.P. Binkhorst,[#] Ivana Josimovic,[#] Daan de Vetten, Tyrone J. Nijman, Niels J. Hauwert, Sufyan Ahmad, Oscar P.J. van Linden, Iwan J.P. de Esch, Henry F. Vischer, Maikel Wijtmans and Rob Leurs

RSC Med. Chem., 2025,16, 5041-5051

Amsterdam Institute of Molecular and Life Sciences, Division of Medicinal Chemistry, Faculty of Science, Vrije Universiteit Amsterdam, De Boelelaan 1083, 1081 HV Amsterdam, the Netherlands.

[#] Authors contributed equally to this manuscript.

Abstract

Despite the pharmacological relevance of the histamine H_1 receptor (H_1R), the second most therapeutically targeted G protein-coupled receptor (GPCR), an effective photoswitchable ligand to optically control this receptor remains elusive. In this work, we aimed to identify a suitable photoswitchable H_1R ligand by performing an 'azoscan' on the H_1R antagonist desloratadine. Taking advantage of the synthetic toolbox available for the desloratadine scaffold, aniline groups were regioselectively installed on the aromatic positions of this scaffold to enable the synthesis of azobenzene analogs targeting the orthosteric binding pocket of H_1R. Additionally, we functionalized the piperidine ring of desloratadine with azobenzene moieties. These two strategies resulted in a total of nine photoswitchable compounds, displaying efficient *trans* to *cis* isomerization (PSS_{cis} > 87%) and a broad range of thermal relaxation half-lives. Pharmacological evaluation revealed the 2-position (**10a**) to be most suitable for accommodation of a photoswitchable group, as it exhibits the most balanced profile in absolute affinity (K_i *trans* = 2 nM) and a 3.2-fold light-induced affinity shift. Computational docking studies provide a rationale, with the binding pose of the *trans* and *cis* isomer in the H_1R binding pocket potentially being inverted. While the development of effective photoswitchable ligands for H_1R remains challenging, this study provides promising opportunities for future optimization to achieve optical control of this GPCR.

Introduction

Photopharmacology enables precise spatiotemporal control of protein function using light, offering powerful tools to investigate dynamic signaling processes.[1] Photopharmacology uses photoresponsive ligands[2], employing one of two main strategies: (i) photocaging, which uses ligands with photocleavable protecting groups[3] or (ii) photoswitching, which uses small-molecule ligands that undergo light-induced isomerization.[1,4,5] Successful design of photoswitchable ligands requires incorporation of a photoswitchable moiety in such a way that the two isomers have different pharmacological properties. This can be achieved by (i) azologization, where a bioisoster (azosteres) in the core of the template ligand is replaced by an azobenzene or (ii) azoextension, where the template ligand is expanded with a photoswitchable unit.[5,6]

Photoswitchable ligands have been developed for a broad range of biological targets, including ion channels, enzymes and G protein-coupled receptors (GPCRs).[6,7] GPCRs represent one of the most pharmacologically relevant protein families, with approximately 36% of the approved drugs targeting GPCRs.[8] After the dopamine D_2 receptor, the histamine H_1 receptor (H_1R) is the second most frequent GPCR targeted by approved drugs, with 59 drugs targeting this receptor.[8] H_1R is widely distributed throughout the body, in, for example, smooth muscle cells, endothelial cells and the central nervous system. H_1R antagonists, also known as antihistamines, are a class of drugs used to treat allergic diseases like allergic rhinitis, allergic conjunctivitis, and urticaria.[9] These drugs alleviate symptoms such as itching, swelling, and redness by blocking the action of histamine on the H_1R. Despite significant progress in the

GPCR photopharmacology field,[10–13] and the high number of drugs targeting H_1R,[8] it has proven remarkably difficult to develop a photoswitchable ligand that effectively modulates this receptor. Rustler *et al.* previously published photoswitchable ligands targeting guinea pig H_1R (gpH_1R)[14] based on a clozapine derivative (**1,** Figure 1A).[15] However, the resulting photoswitchable compounds **2** and **3** exhibit low affinity for gpH_1R and no data on human H_1R (hH_1R) were disclosed. Previous in-house efforts with photoswitchable H_1R ligands **5** and **6** based on VUF14454 (**4**)[16] were also unsuccessful with the ligands having low affinity and no appreciable affinity shift between isomers.[12] Likewise, the desmethyl analog[16] of these compounds or substitution of the nitrogen atom with an acidic moiety connected through a linker,[17] were ineffective (unpublished data). Thus, an effective photoswitchable hH_1R ligand remains elusive to date.

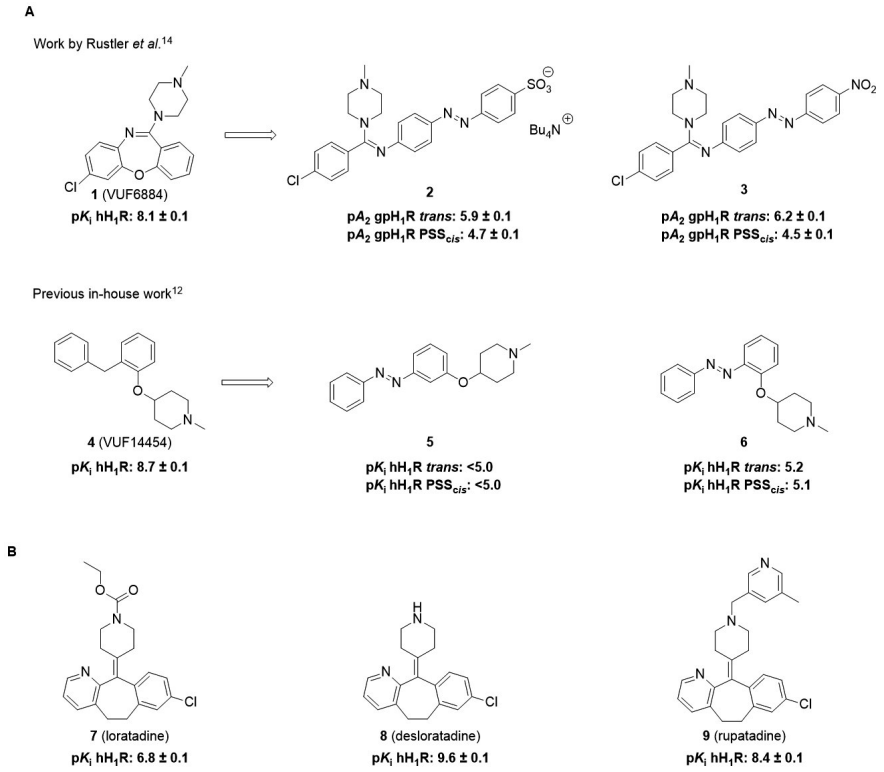

Figure 1. Structures and pharmacological data of key compounds. Except for **2** and **3**, in-house affinity data and associated references are provided. (A) Previously reported photoswitchable ligands targeting gpH_1R[14] based on **1** (VUF6884)[15] or targeting hH_1R[12] based on **4** (VUF14454)[16] (B) Structures of loratadine[23], desloratadine (value from Table 2) and rupatadine.[24]

We reasoned that the 11-(piperidin-4-ylidene)-6,11-dihydro-5H-benzo[5,6]cyclohepta[1,2-b]pyridine core, as in antihistamines loratadine (**7**, Figure 1B) and desloratadine (**8**), provides a promising scaffold. Both are well-characterized compounds that are frequently used in exemplification for late-stage aromatic functionalization.[18–22] In the current work, we

capitalized on this synthetic accessibility by performing an 'azoscan' on desloratidine, a unique approach in which the azobenzene moieties are systematically installed on different positions of the template scaffold to identify a suitable position for placement of a photoswitchable moiety. These include aromatic vectors, but also *N*-substitution on the piperidine ring, generating analogs of rupatadine (**9**).

Results and discussion

Design

The design of new photoswitchable ligands targeting hH_1R (Figure 2) is based on the second-generation antihistamine desloratadine (**8**) as the template. It exhibits an approximately 600-fold higher affinity for hH_1R than loratadine (**7**, Figure 1B).[23,24] The cryo-EM structure of desloratadine bound to hH_1R, published by Wang *et al*.,[25] has revealed that it engages in key hydrogen bonding interactions with $D107^{3.32}$ and $Y431^{6.52}$ within the orthosteric hH_1R pocket. The structure suggests that there is space for growth on desloratadine, particularly on the side of the pyridine ring (Figure S1). Notably, Wang *et al*. also found that the ligand-binding pocket of H_1R shows significant conformational flexibility based on the ligand bound, offering additional opportunities to potentially accommodate a photoswitchable ligand in the orthosteric pocket.[25] The 11-(piperidin-4-ylidene)-6,11-dihydro-5H-benzo[5,6]cyclohepta [1,2-b]pyridine core of desloratadine has proven compatible with several late-stage synthetic functionalization approaches.[18–22] We hypothesized that the use of such literature approaches would enable the installation of aniline moieties on the pyridine and phenyl rings, thereby providing synthetic vectors for the subsequent formation of an azo bond. Leveraging this synthetic accessibility, we conducted a systematic 'azoscan'. By introducing azobenzene moieties at various positions of desloratadine, we sought to identify a photoswitchable ligand where one isomer has a favorable conformation within the binding site, while the other isomer induces steric clashes or unfavorable interactions to induce an affinity shift. In total, three series were explored (Figure 2). The first two series involve introduction of an azobenzene on the pyridine ring on the 2-, 3-, and 4-positions (**10a–c**) and at the phenyl ring on the 7-, 8-, and 9-positions (**11a–c**) to target the orthosteric binding pocket. Substitution of the 8-position required removal of the chlorine of desloratadine. Importantly, Lall *et al.* have shown that replacement of the chlorine atom of loratadine with a hydrogen atom results in an equipotent compound.[26] Furthermore, we did not pursue the 10-position, located on the phenyl ring, due to the significant synthetic challenges expected with this sterically hindered position. The third series we explored is substitution at the piperidine ring (**12a–c**), i.e. based on rupatadine as a template.

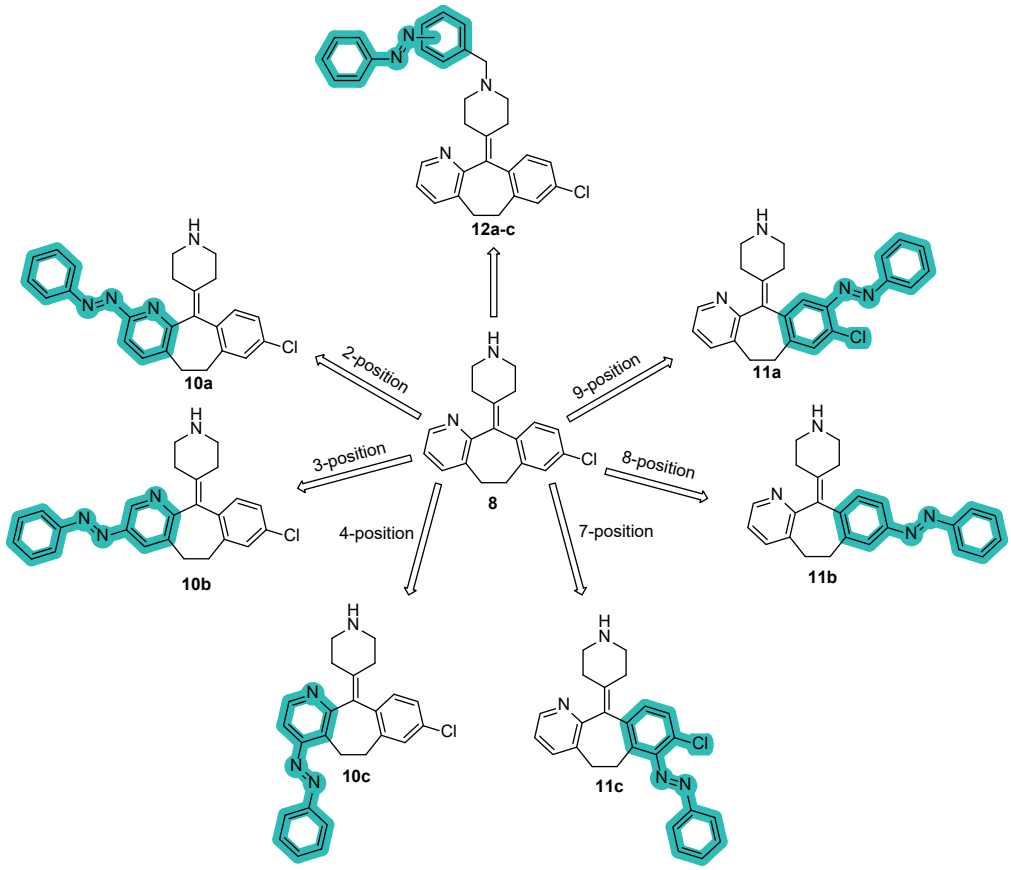

Figure 2. Design strategy towards a photoswitchable hH_1R ligand by performing an 'azoscan' on desloratadine (**8**).

Synthesis

The synthesis routes for the first two series of photoswitchable desloratadine analogs (**10a–c**, **11a–c**) were designed to regio-selectively install aniline groups on the aromatic rings (Scheme 1), enabling subsequent azobenzene formation. For the preparation of the 2-isomer (**10a**), desloratadine (**8**) was first protected to give Boc-protected intermediate **13**, which was oxidized with *m*-CPBA to *N*-oxide **14.** *Ortho*-amination, following the method of Verbeet *et al.*,[27] yielded aminopyridine **15.** Subsequent formation of the azobenzene using PhNO under acidic Mills conditions afforded azobenzene **16**, which was deprotected with HCl to yield **10a**. Intermediate **14** was also used for the preparation of the 4-isomer (**10c**). Substitution of the hydrogen atom through a triflate-intermediate, based on a procedure by Choi *et al.*,[28] gave intermediate **17**. Due to poor reactivity of this intermediate in the Mills reaction under acidic conditions, the aniline was rendered more nucleophilic by deprotonation successfully providing **18**. Deprotection of the Boc group in **18** with HCl afforded **10c**. The 3-isomer was synthesized via regioselective nitration of loratadine (**7**).[29,30] Reduction of the resulting nitro-

compound **19** via a Béchamp reduction provided aniline **20,** which was subjected to acidic Mills conditions (affording **21**) and carbamate deprotection with KOH to yield **10b**.

For installation of the azobenzene at the 8-position (**11b**), a Buchwald-Hartwig amination of loratadine (**7**) with *tert*-butylcarbamate yielded **22**. Boc-deprotection to **23** followed by the Mills reaction under acidic conditions afforded intermediate **24**, which was deprotected using KOH to give **11b**. The 7- and 9-analogs were accessed using a method for the nitration[29] of loratadine that produces the two regioisomers **25** (major) and **28** (minor). For the synthesis of **11c** from **28**, the ethyl-carbamate protecting group was replaced with a Boc protecting group (through intermediacy of **29**) to avoid the formation of side products observed in deprotection attempts of the ethyl-carbamate in the last step (data not shown). Reduction of the nitro group of resulting intermediate **30** gave aniline **31**, which was converted to **32** via *in situ* diazotation and reaction with PhMgBr, based on a procedure of Barbero *et al*.[31] This alternative strategy was chosen because both acidic and basic Mills conditions on **31** were ineffective. Similarly, to obtain **11a**, compound **25** was converted to Boc-protected intermediate **27** via **26**. After reduction of the nitro group to **33** and a Mills reaction to **34**, Boc group deprotection afforded **11a**.

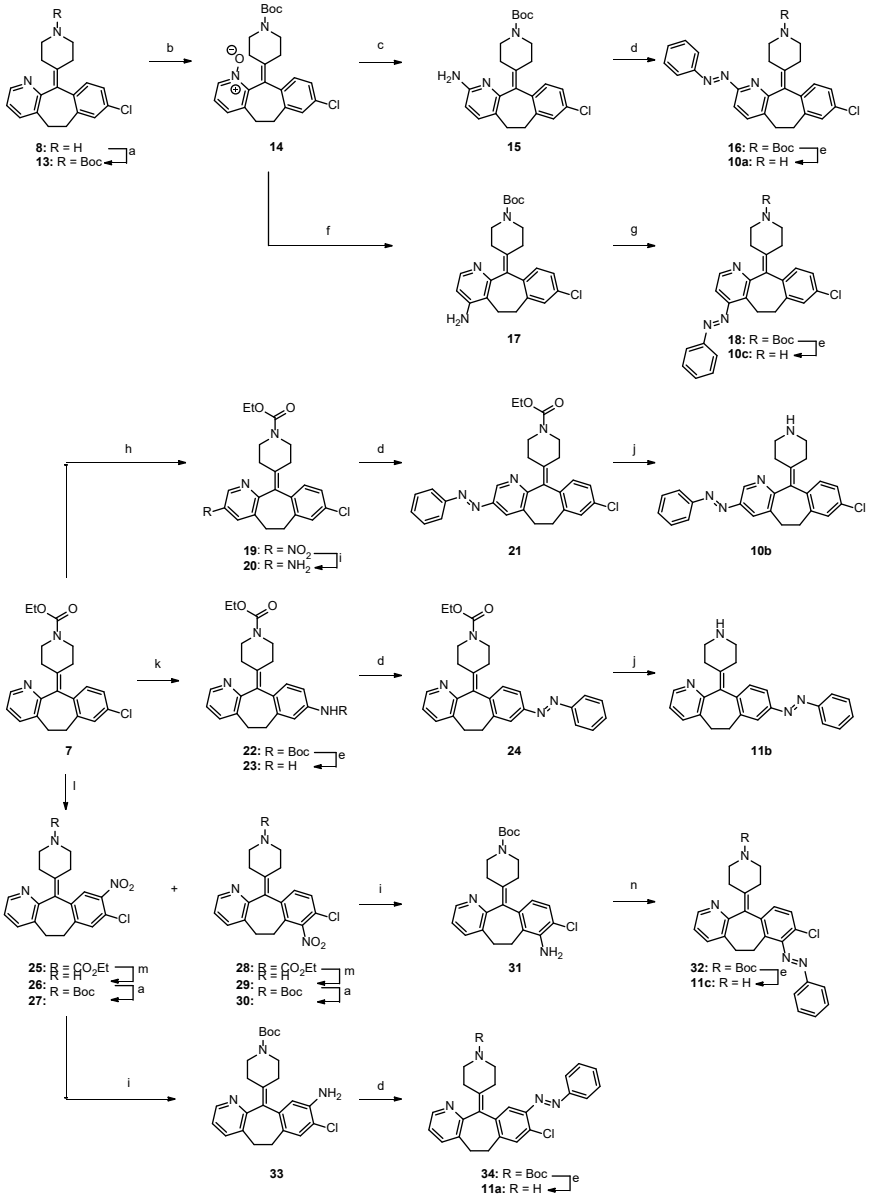

Scheme 1. Synthesis of **10a–c** and **11a–c**. Reagents and conditions: (a) Boc_2O, Et_3N, DCM, rt, 2–16 h, 82–95%; (b) *m*-CPBA, DCM, rt, 50 min, 61%; (c) (i) potassium phthalimide, TsCl, Et_3N, DCM, rt, 20 h; (ii) $H_2NNH_2{\cdot}H_2O$, H_2O, 63%; (d) PhNO, AcOH, PhMe, 18 h–14 d, 75–90 °C, 8–36%; (e) 4M HCl in 1,4-dioxane, MeOH, rt, 16–22 h, 16–98%; (f) (i) 4-cyanopyridine, Tf_2O, DCM, MeCN, 0 °C to rt; (ii) Aq. NH_4OH, rt, 16 h, 25%; (g) PhNO, NaH, THF, rt, 72 h, 23%; (h) Bu_4N^+ NO_3^-, TFAA, DCM, rt, 66 h, 21%; (i) Fe, NH_4Cl, 1,4-dioxane, EtOH, H_2O, 80 °C, 2–3 h, 81–89%; (j) KOH, EtOH, H_2O, 80 °C, 72–100 h, 33–61%; (k) XPhos, $Pd(OAc)_2$, $BocNH_2$, Cs_2CO_3, 1,4-dioxane, 95 °C, 2 h, 82%; (l) Conc. H_2SO_4, KNO_3, -10 °C – rt, 16 h, 81% of **25** and 9% of **28**; (m)

Conc. HCl, 80 °C, 24 h, 82–89%; (n) (i) $BF_3{\cdot}Et_2O$, *t*-$BuNO_2$, THF, rt, 2 h; (ii) PhMgBr, THF, -70 °C, 18 h, 14%.

Rupatadine analogs (**12a–c**) were synthesized using two different routes (Scheme 2). For analogs **12a** (*para*) and **12b** (*meta*), the corresponding anilines **35** and **36** were coupled to PhNO via the Mills reaction under acidic conditions to afford azobenzenes **37** and **38**. These compounds were then oxidized to give aldehydes **39** and **40** using DMP or MnO_2, respectively. Reductive amination with desloratadine (**8**) yielded rupatadine analogs **12a** and **12b**. In contrast, synthesis of **12c** (*ortho*) required an alternative approach, as aldehyde formation from the corresponding azobenzene was unsuccessful. Instead, alkylation of desloratadine (**8**) with alkylbromide **41** gave nitro-compound **42**, which was reduced to aniline **43** and subjected to acidic Mills conditions to afford **12c**.

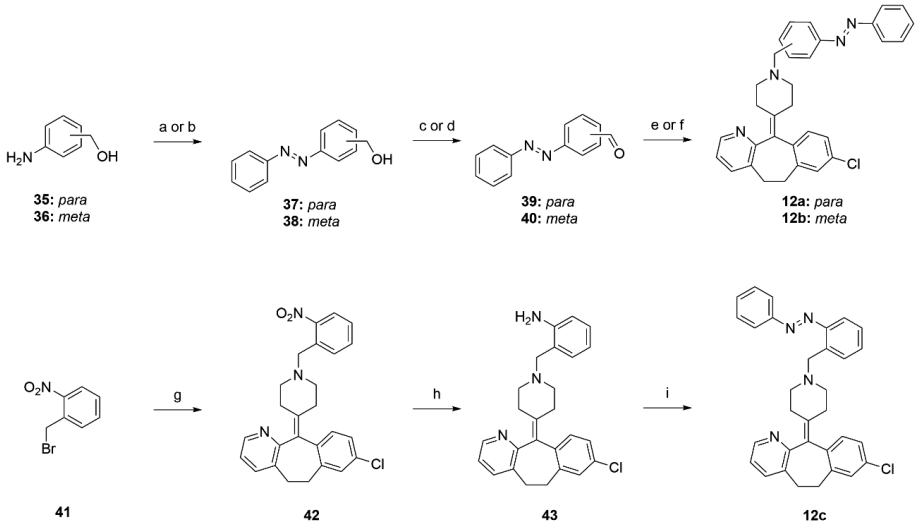

Scheme 2. Synthesis of **12a–c**. Reagents and conditions: (a) For **37**: PhNO, AcOH, rt, 66 h, 12%; (b) For **38**: PhNO, DCM, AcOH, rt, 18 h, 70%; (c) For **39**: DMP, DCM, rt, 1.5 h, 89%; (d) For **40**: MnO_2, DCM, rt, 2 h, 75%; (e) For **12a**: **8**, $NaBH(OAc)_3$, AcOH, DCE, rt, 16 h, 26%; (f) For **12b**: **8**, $NaBH(OAc)_3$, AcOH, DCM, rt, 2h, 62%; (g) **8**, MeCN, K_2CO_3, reflux, 3 h, 91%; (h) Fe, NH_4Cl, 1,4-dioxane, EtOH, H_2O, 80 °C, 3 h, quantitative; (i) PhNO, PhMe, AcOH, 75 °C, 16 h, 12%.

Photochemistry

The photochemical properties of the photoswitchable ligands (Table 1, Figure S2-S10) were first characterized by UV-vis absorption spectroscopy. Spectra were recorded at a concentration of 25 µM in HBSS buffer containing 50% DMSO (Figure S2–10). Most compounds exhibit absorption patterns characteristic for azobenzenes and azopyridines.[32–34] The absorption maxima (λ_{max}) of the *trans* isomers are observed around 310–340 nm (π-π* absorption band).

Table 1. Photochemical parameters of **10a–c**, **11a–c** and **12a–c**.

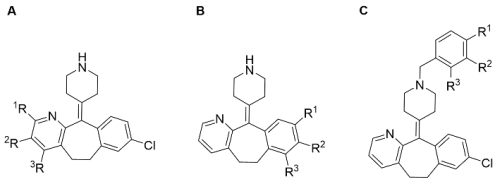

Compound	Structure	R^1	R^2	R^3	λ_{max} *trans*[a] (nm)	λ_{max} *cis*[a] (nm)	PSS_{cis} (area %*cis*)[b]	PSS_{trans} (area %*trans*)[b]	Approximate $t_{1/2}$[c]
10a	A		H	H	332	429	91	85	38 d
10b	A	H		H	335	430	87	79	31 d
10c	A	H	H		319	419	n.d.[d]	n.d.[d]	15 min
11a	B		Cl	H	340	429	97	79	78 d
11b	B	H		H	338	435	91	80	5 d
11c	B	H	Cl		~310[e]	419	67	82	211 d
12a	C		H	H	327	432	93	83	19 d
12b	C	H		H	325	423	91	81	198 d
12c	C	H	H		329	-	n.d.[d]	n.d.[d]	45 s

[a]Determined at 25 µM in HBSS buffer containing 50% DMSO.
[b]Photostationary state area percentages either after illumination of *trans* isomer with 360 ± 20 nm at 10 mM in DMSO as determined by acidic LC-MS analysis at the isosbestic point, or after illumination of PSS_{cis} states with 434 ± 9 nm at 10 mM in DMSO as determined by acidic LC-MS analysis at the isosbestic point.
[c]Thermal relaxation ($t_{1/2}$) of PSS_{cis} states in HBSS buffer containing 50% DMSO, as estimated by the method of Ahmed *et al*.[36] by extrapolating to 20°C. Arrhenius plots are available in SI.
[d]Photostationary state area percentages could not be determined by LC-MS analysis due to the small $t_{1/2}$ value.
[e]Approximate value due to overlapping bands.

Of note is the π–π* transition band of **11c**, which is observed as a shoulder around 310 nm. Next to a potential effect of the *ortho*-Cl atom,[35] the absence of a comparable blue-shift in π–π* band for the related compound **11a** could highlight a steric effect on the absorption profile in **11c**. The λ_{max} values of the *cis* isomers are observed at 419–435 nm (n-π* absorption band). Due to the short thermal half-life of **10c** and **12c** (*vide infra*), determination of the λ_{max} value

of their *cis* isomer and quantification of their photostationary states (PSS) was not feasible. Efficient *trans* to *cis* isomerization for all other compounds was achieved using an illumination wavelength of 360 nm, resulting in PSS_{cis} values ranging from 87–97%. The exception was compound **11c**, which only reaches a moderate PSS_{cis} value of 67% (*vide supra*, Fig. S7C). Indeed, UV analysis (Fig. S7B) clearly shows that 360 nm is near an isosbestic point of **11c**. All compounds show expected PSS_{trans} values between 79–85 % upon illumination with 434 nm. The approximated dark stabilities of these compounds in buffer vary substantially, with thermal half-lives ranging from seconds (**12c**) and minutes (**10c**) to days (**11b**, **12a**) and even months (**10a**, **10b**, **11a**, **11c**, **12b**).

Pharmacology

The affinities (pK_i values) of **10a–c**, **11a–c** and **12a–c** for the hH_1R were evaluated in competition radioligand-binding experiments with the labelled H_1R antagonist [^{3}H]mepyramine (Table 2, Figure S11-S13). For **10c** and **12c**, continuous illumination at 365 nm was used to counteract the short half-lives of their PSS_{cis} states, while for the other compounds PSS_{cis} states were obtained by pre-illumination with 360 nm. In the first series, featuring substitutions on the pyridine ring (**10a–c**), substitution on the 2-position (**10a**) provides a compound with high affinity for the *trans* isomer (pK_i = 8.3, template **8**: pK_i = 9.6) and a lower affinity in the PSS_{cis} state (pK_i = 7.8), resulting in a significant light-induced affinity shift of -0.5 log unit (i.e., a 3.2 fold shift in affinity). Incorporation of an azobenzene at the 3-position (**10b**) is also well tolerated (pK_i *trans* = 8.7). However, a reduced light-induced affinity shift was observed between *trans*-**10b** and **10b**-PSS_{cis} (-0.3 log unit). Placement of the azobenzene on the 4-position (**10c**) reduces affinity for the *trans* isomer compared to **10a** and **10b**, providing high-nM affinities (pK_i **10c** = 6.8). However, **10c** shows no affinity shift upon photoisomerization, indicating that this position is not optimal for azobenzene placement. In the second series (**11a–c**), which involves substitution on the phenyl ring, *trans*-**11a** and *trans*-**11b** have comparable affinity to *trans*-**10c** (pK_i = 6.8). Noteworthy, **11b** shows a significant affinity shift (-0.6 log unit) between *trans* and $PSS_{cis.}$ In contrast, substitution at the 7-position (**11c**) results in a loss of affinity for hH_1R for either state ($pK_i < 6.0$), indicating that this position is not suitable for azologization. The third series (**12a–c**), involving rupatadine analogs, provides high affinities for the *trans* isomers (pK_i = 8.3—8.6, template **9**: pK_i = 8.4, Figure 1). This is in line with other reports showing that the piperidine of **8** can be substituted without eroding H_1R affinities.[24,37,38] However, none of the ligands **12a–c** shows an affinity shift upon photoisomerization, indicating that the *N*-substitution of **8** is not a viable strategy to achieve photochemical modulation of hH_1R. In all, the **10** and **12** series are generally more amenable to appending *trans*-azobenzene moieties while maintaining affinities, with only the **10** series also showing some appreciable affinity shifts upon photoisomerization. The **11** series notably suffers from reduction in H_1R affinity upon appending a *trans* azobenzene, although some members in this series show affinity shifts upon photoisomerization. In all, **10a** and **11b** demonstrate the most pronounced light-induced affinity shifts among the three series (-0.5 and -0.6, respectively). Notably, **10a** displays an approximately 25-fold higher H_1R affinity (pK_i

trans = 8.3) compared to **11b** and therefore emerges as the most suitable photopharmacological H_1R ligand in this study.

Table 2. Human histamine H_1R binding affinity (pK_i) values and affinity shifts of **8, 10a–c**, **11a–c, 12a–c**

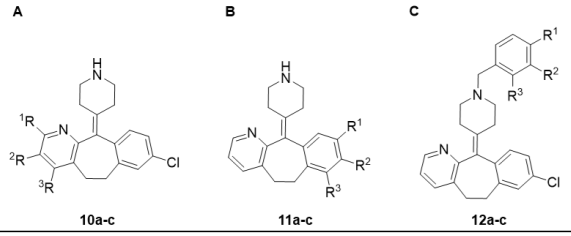

Compound	Structure	R^1	R^2	R^3	pK_i *trans*[a]	pK_i PSS$_{cis}$[a]	pK_i shift[b]
8	A	H	H	H	9.6 ± 0.1	-	-
10a	A		H	H	8.3 ± 0.2	7.8 ± 0.2	-0.5
10b	A	H		H	8.7 ± 0.1	8.4 ± 0.1	-0.3
10c	A	H	H		6.8 ± 0.0	6.8 ± 0.0[c]	0.0
11a	B		Cl	H	6.8 ± 0.2	6.6 ± 0.1	-0.2
11b	B	H		H	6.9 ± 0.0	6.3 ± 0.1	-0.6
11c	B	H	Cl		<6.0	<6.0	-
12a	C		H	H	8.6 ± 0.5	8.5 ± 0.2	-0.1
12b	C	H		H	8.3 ± 0.1	8.2 ± 0.1	-0.1
12c	C	H	H		8.4 ± 0.2	8.3 ± 0.2[c]	-0.1

[a]Affinity (pK_i) values as obtained from radioligand competition experiments with [^{3}H]mepyramine. Values are mean ± SEM of n = 3 experiments, performed in triplicate. Competition binding curves are available in the SI.

[b]Affinity shifts between PSS$_{cis}$ and *trans* states are defined as pK_i PSS$_{cis}$-pK_i *trans*.

[c]Continuous illumination at 365 nm was used during 4 h incubation at 25°C.

Proposed binding mode of 10a

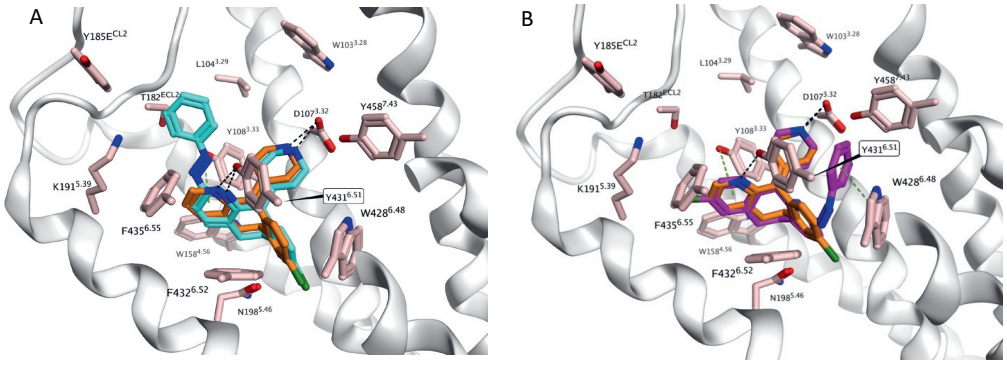

Figure 3. Proposed binding mode of desloratadine (orange) in the H_1R binding pocket as determined by cryo-EM (PDB ID: 8X64)[25] in overlay with the docking pose of (A) *trans*-**10a** (cyan) and (B) *cis*-**10a** (purple)**.**

Molecular modelling using the recently disclosed cryo-EM structure of H_1R with **8** (PDB ID: 8X64)[25] was performed to gain insight in the observed affinities of *trans*- and *cis*-**10a**. We investigated whether both isomers could bind to H_1R in a similar fashion as desloratadine. Indeed, *trans*-**10a** adopts a conformation similar to that of desloratadine (Figure 3A). In this docking pose, the key interactions of the protonated amine with $D107^{3.32}$ and of the pyridine nitrogen atom with $Y431^{6.52}$ are maintained. The azobenzene moiety is directed towards the solvent-exposed region. In contrast, no comparable docking poses could be identified for *cis*-**10a**. Instead, for *cis*-**10a** a binding mode was identified in which the desloratadine core was flipped 180 degrees in the binding pocket. In this binding mode *cis*-**10a** maintains the key interaction with $D107^{3.32}$ via its protonated amine but lacks the hydrogen bond interaction with $Y431^{6.52}$. The azobenzene moiety is buried deep in the pocket where it forms a π-stacking interactions with $W428^{6.48}$, while the chloro-substituted ring of the desloratadine core forms an arene-H interaction with $Y108^{3.33}$. These binding modes explain the reduced affinity of *cis*-**10a** compared to that of *trans*-**10a**, while also providing a rationale for the still appreciable affinity of *cis*-**10a** owing to the maintained key ionic interaction with $D107^{3.32}$ and the two newly formed interactions with $Y108^{3.33}$ and $W428^{6.48}$. Based on these findings, computer-aided approaches could help the design of the next generation of desloratadine-based photoswitchable ligands, for example by focusing on increasing the bulk on the peripheral phenyl ring of **10a**. These modifications may allow the *trans* isomer to maintain a similar binding mode to *trans*-**10a** as its azobenzene moiety is directed towards the solvent-exposed region, while the *cis* isomer in its inverted binding mode would experience steric clashes with the protein. This in turn would lower the affinity of the *cis* isomer and therefore improve the affinity shift.

Conclusion

Finding effective photoswitchable ligands for optical control of the hH_1R remains challenging, which may be attributed to the intrinsic flexibility of the orthosteric binding pocket of hH_1R. Here, a total of nine potential photoswitchable ligands for hH_1R was explored by performing an 'azoscan' on the antihistamine desloratadine (**8**). Late-stage regioselective installation of aniline groups on the aromatic rings of the desloratadine scaffold enabled azobenzene formation and overall an aromatic azoscan. This was supplemented by a concise series of *N*-functionalized derivatives. Most ligands show efficient *trans* to *cis* isomerization (PSS_{cis} > 87%) by using an illumination wavelength of 360 nm, except for **11c** (PSS_{cis} = 67%). Additionally, a wide range of half-lives was observed ranging from seconds to months. Pharmacological evaluation revealed marked differences in effect upon probing azobenzenes in the three regions of **8,** and only a few compounds show an appreciable light-induced H_1R affinity shift upon installation of an azobenzene. Two suitable positions, i.e. the 2-position (**10a**) and the 8-position (**11b**), were identified with similar H_1R affinity shifts between the *trans* and PSS_{cis} states. Of these, **10a** shows the most balanced profile (pK_i *trans* = 8.3, pK_i PSS_{cis} = 7.8). Molecular modeling studies indicate that the docking pose of *trans*-**10a** in H_1R shows good overlap with the binding mode of desloratadine, but that, in contrast, *cis*-**10a** adopts a flipped binding mode. Building on these findings, a light-induced H_1R affinity shift could potentially be improved by decorating the peripheral phenyl ring of the azobenzene of **10a**. Thus, photoswitchable ligand **10a** may provide a promising starting point for future development of improved hH_1R photoswitchable ligands.

Acknowledgments

We acknowledge the Dutch Research Council (NWO) for financial support (OCENW.KLEIN.532, "Towards the next frontiers in GPCR photopharmacology"). We thank Hans Custers for acquiring HRMS analyses, Elwin Janssen for NMR assistance and Andrea van de Stolpe for support with the photochemistry equipment.

References

(1) Velema, W. A.; Szymanski, W.; Feringa, B. L. Photopharmacology: Beyond Proof of Principle. *J Am Chem Soc* **2014**, *136* (6), 2178–2191. https://doi.org/10.1021/ja413063e.

(2) Liu, Y.; Wang, T.; Wang, W. Photopharmacology and Photoresponsive Drug Delivery. *Chem Soc Rev* **2025**, ASAP. https://doi.org/10.1039/d5cs00125k.

(3) Josa-Culleré, L.; Llebaria, A. In the Search for Photocages Cleavable with Visible Light: An Overview of Recent Advances and Chemical Strategies. *ChemPhotoChem* **2021**, *5* (4), 298–316. https://doi.org/10.1002/cptc.202000253.

(4) Fuchter, M. J. On the Promise of Photopharmacology Using Photoswitches: A Medicinal Chemist's Perspective. *J Med Chem* **2020**, *63* (20), 11436–11447. https://doi.org/10.1021/acs.jmedchem.0c00629.

(5) Broichhagen, J.; Frank, J. A.; Trauner, D. A Roadmap to Success in Photopharmacology. *Acc Chem Res* **2015**, *48* (7), 1947–1960. https://doi.org/10.1021/acs.accounts.5b00129.

(6) Kobauri, P.; Dekker, F. J.; Szymanski, W.; Feringa, B. L. Rational Design in Photopharmacology with Molecular Photoswitches. *Angew. Chem. Int. Ed.* **2023**, *62* (30), e202300681. https://doi.org/10.1002/anie.202300681.

(7) Hüll, K.; Morstein, J.; Trauner, D. In Vivo Photopharmacology. *Chem Rev* **2018**, *118* (21), 10710–10747. https://doi.org/10.1021/acs.chemrev.8b00037.

(8) Lorente, J. S.; Sokolov, A. V.; Ferguson, G.; Schiöth, H. B.; Hauser, A. S.; Gloriam, D. E. GPCR Drug Discovery: New Agents, Targets and Indications. *Nature Reviews Drug Discovery 2025* **2025**, 1–22. https://doi.org/10.1038/s41573-025-01139-y.

(9) Simons, F. E. R.; Simons, K. J. Histamine and H1-Antihistamines: Celebrating a Century of Progress. *Journal of Allergy and Clinical Immunology* **2011**, *128* (6), 1139-1150.e4. https://doi.org/10.1016/J.JACI.2011.09.005.

(10) Ricart-Ortega, M.; Font, J.; Llebaria, A. GPCR Photopharmacology. *Mol Cell Endocrinol* **2019**, *488*, 36–51. https://doi.org/10.1016/j.mce.2019.03.003.

(11) Panarello, S.; Rovira, X.; Llebaria, A.; Gómez-Santacana, X. Photopharmacology of G -Protein-Coupled Receptors. In *Molecular Photoswitches*; John Wiley & Sons, Ltd, 2022; Vol. 2–2, pp 921–944. https://doi.org/10.1002/9783527827626.ch37.

(12) Wijtmans, M.; Josimovic, I.; Vischer, H. F.; Leurs, R. Optical Control of Class A G Protein-Coupled Receptors with Photoswitchable Ligands. *Curr Opin Pharmacol* **2022**, *63*. https://doi.org/10.1016/j.coph.2022.102192.

(13) Berizzi, A. E.; Goudet, C. Strategies and Considerations of G-Protein-Coupled Receptor Photopharmacology. *Adv Pharmacol* **2020**, *88*, 143–172. https://doi.org/10.1016/bs.apha.2019.12.001.

(14) Rustler, K.; Pockes, S.; König, B. Light-Switchable Antagonists for the Histamine H 1 Receptor at the Isolated Guinea Pig Ileum. *ChemMedChem* **2019**, *14* (6), 636–644. https://doi.org/10.1002/cmdc.201800815.

(15) Smits, R. A.; Lim, H. D.; Stegink, B.; Bakker, R. A.; De Esch, I. J. P.; Leurs, R. Characterization of the Histamine H4 Receptor Binding Site. Part 1. Synthesis and Pharmacological Evaluation of Dibenzodiazepine Derivatives. *J Med Chem* **2006**, *49* (15), 4512–4516. https://doi.org/10.1021/jm051008s.

(16) Kuhne, S.; Kooistra, A. J.; Bosma, R.; Bortolato, A.; Wijtmans, M.; Vischer, H. F.; Mason, J. S.; De Graaf, C.; De Esch, I. J. P.; Leurs, R. Identification of Ligand Binding Hot Spots of the Histamine H1 Receptor Following Structure-Based Fragment Optimization. *J Med Chem* **2016**, *59* (19), 9047–9061. https://doi.org/10.1021/acs.jmedchem.6b00981.

(17) Kuhne, S.; Bosma, R.; Kooistra, A. J.; Riemens, R.; Stroet, M. C. M.; Vischer, H. F.; de Graaf, C.; Wijtmans, M.; Leurs, R.; de Esch, I. J. P. Probing the Histamine H1 Receptor Binding Site to Explore Ligand Binding Kinetics. *J Med Chem* **2024**, *68*, 448–464. https://doi.org/10.1021/acs.jmedchem.4c02043v.

(18) Nielsen, M. K.; Shields, B. J.; Liu, J.; Williams, M. J.; Zacuto, M. J.; Doyle, A. G. Mild, Redox-Neutral Formylation of Aryl Chlorides through the Photocatalytic Generation of Chlorine Radicals. *Angewandte Chemie* **2017**, *129* (25), 7297–7300. https://doi.org/10.1002/ange.201702079.

(19) Dumoulin, A.; Matsui, J. K.; Gutiérrez-Bonet, Á.; Molander, G. A. Synthesis of Non-Classical Arylated C-Saccharides through Nickel/Photoredox Dual Catalysis. *Angewandte Chemie* **2018**, *130* (22), 6724–6728. https://doi.org/10.1002/ange.201802282.

(20) Nippa, D. F.; Atz, K.; Hohler, R.; Müller, A. T.; Marx, A.; Bartelmus, C.; Wuitschik, G.; Marzuoli, I.; Jost, V.; Wolfard, J.; Binder, M.; Stepan, A. F.; Konrad, D. B.; Grether, U.; Martin, R. E.; Schneider, G. Enabling Late-Stage Drug Diversification by High-Throughput Experimentation with Geometric Deep Learning. *Nat Chem* **2024**, *16* (2), 239–248. https://doi.org/10.1038/s41557-023-01360-5.

(21) Wan, Q.; Hou, Z. W.; Zhao, X. R.; Xie, X.; Wang, L. Organoelectrophotocatalytic C-H Silylation of Heteroarenes. *Org Lett* **2023**, *25* (6), 1008–1013. https://doi.org/10.1021/acs.orglett.3c00144.

(22) Kariofillis, S. K.; Shields, B. J.; Tekle-Smith, M. A.; Zacuto, M. J.; Doyle, A. G. Nickel/Photoredox-Catalyzed Methylation of (Hetero)Aryl Chlorides Using Trimethyl Orthoformate as a Methyl Radical Source. *J Am Chem Soc* **2020**, *142* (16), 7683–7689. https://doi.org/10.1021/jacs.0c02805.

(23) Lim, H. D.; Van Rijn, R. M.; Ling, P.; Bakker, R. A.; Thurmond, R. L.; Leurs, R. Evaluation of Histamine H1-, H2-, and H3-Receptor Ligands at the Human Histamine H4 Receptor: Identification of 4-Methylhistamine as the First Potent and Selective H4 Receptor Agonist. *J Pharmacol Exp Ther* **2005**, *314* (3), 1310–1321. https://doi.org/10.1124/jpet.105.087965.

(24) Bosma, R.; Wang, Z.; Kooistra, A. J.; Bushby, N.; Kuhne, S.; Van Den Bor, J.; Waring, M. J.; De Graaf, C.; De Esch, I. J.; Vischer, H. F.; Sheppard, R. J.; Wijtmans, M.; Leurs, R. Route to

Prolonged Residence Time at the Histamine H1 Receptor: Growing from Desloratadine to Rupatadine. *J Med Chem* **2019**, *62* (14), 6630–6644. https://doi.org/10.1021/acs.jmedchem.9b00447.

(25) Wang, D.; Guo, Q.; Wu, Z.; Li, M.; He, B.; Du, Y.; Zhang, K.; Tao, Y. Molecular Mechanism of Antihistamines Recognition and Regulation of the Histamine H1 Receptor. *Nature Communications 2024 15:1* **2024**, *15* (1), 1–10. https://doi.org/10.1038/s41467-023-44477-4.

(26) Lall, M. S.; Bassyouni, A.; Bradow, J.; Brown, M.; Bundesmann, M.; Chen, J.; Ciszewski, G.; Hagen, A. E.; Hyek, D.; Jenkinson, S.; Liu, B.; Obach, R. S.; Pan, S.; Reilly, U.; Sach, N.; Smaltz, D. J.; Spracklin, D. K.; Starr, J.; Wagenaar, M.; Walker, G. S. Late-Stage Lead Diversification Coupled with Quantitative Nuclear Magnetic Resonance Spectroscopy to Identify New Structure-Activity Relationship Vectors at Nanomole-Scale Synthesis: Application to Loratadine, a Human Histamine H1Receptor Inverse Agonist. *J Med Chem* **2020**, *63* (13), 7268–7292. https://doi.org/10.1021/acs.jmedchem.0c00483.

(27) Verbeet, W.; Husiev, Y.; Bonnet, S. Simple and Efficient Method for Mono- and Di-Amination of Polypyridine N-Oxides. *European J Org Chem* **2024**, *27* (14), e202400054. https://doi.org/10.1002/ejoc.202400054.

(28) Choi, H.; Ham, W. S.; van Bonn, P.; Zhang, J.; Kim, D.; Chang, S. Mechanistic Approach Toward the C4-Selective Amination of Pyridines via Nucleophilic Substitution of Hydrogen. *Angewandte Chemie - International Edition* **2024**, *63* (24), e202401388. https://doi.org/10.1002/anie.202401388.

(29) George Njoroge, F.; Vibulbhan, B.; Pinto, P.; Chan, T. M.; Osterman, R.; Remiszewski, S.; Rosario, J. Del; Doll, R.; Girijavallabhan, V.; Ganguly, A. K. Highly Regioselective Nitration Reactions Provide a Versatile Method of Functionalizing Benzocycloheptapyridine Tricyclic Ring Systems: Application toward Preparation of Nanomolar Inhibitors of Farnesyl Protein Transferase. *Journal of Organic Chemistry* **1998**, *63* (3), 445–451. https://doi.org/10.1021/jo971100z.

(30) George Njoroge, F.; Vibulbhan, B.; Rane, D. F.; Robert Bishop, W.; Petrin, J.; Patton, R.; Bryant, M. S.; Chen, K. J.; Nomeir, A. A.; Lin, C. C.; Liu, M.; King, I.; Chen, J.; Lee, S.; Yaremko, B.; Dell, J.; Lipari, P.; Malkowski, M.; Li, Z.; Catino, J.; Doll, R. J.; Girijavallabhan, V.; Ganguly, A. K. Structure-Activity Relationship of 3-Substituted N-(Pyridinylacetyl)-4- (8-Chloro-5,6-Dihydro-11H-Benzo[5,6]Cyclohepta[1,2-b]Pyridin-11-Ylidene)- Piperidine Inhibitors of Farnesyl-Protein Transferase: Design and Synthesis of in Vivo Active Antitumor Compounds. *J Med Chem* **1997**, *40* (26), 4290–4301. https://doi.org/10.1021/jm970464g.

(31) Barbero, M.; Degani, I.; Dughera, S.; Fochi, R.; Perracino, P. Preparation of Diazenes by Electrophilic C-Coupling Reactions of Dry Arenediazonium o-Benzenedisulfonimides with Grignard Reagents. *Synthesis (Stuttg)* **1998**, *1998* (09), 1235–1237. https://doi.org/10.1055/s-1998-6102.

(32) Nakagawa, M.; Rikukawa, M.; Watanabe, M.; Sanui, K.; Ogata, N. Photochromic, Electrochemical, and Photoelectrochemical Properties of Novel Azopyridinium Derivatives. *Bull Chem Soc Jpn* **1997**, *70* (4), 737–744. https://doi.org/10.1246/BCSJ.70.737.

(33) Xu, Y.; Gao, C.; Andréasson, J.; Grøtli, M. Synthesis and Photophysical Characterization of Azoheteroarenes. *Org Lett* **2018**, *20* (16), 4875–4879. https://doi.org/10.1021/acs.orglett.8b02014.

(34) Otsuki, J.; Narutaki, K. Photochromism of Phenylazopyridines and Its Application to the Fluorescence Modulation of Zinc–Porphyrins. *Bull Chem Soc Jpn* **2004**, *77* (8), 1537–1544. https://doi.org/10.1246/bcsj.77.1537.

(35) Konrad, D. B.; Savasci, G.; Allmendinger, L.; Trauner, D.; Ochsenfeld, C.; Ali, A. M. Computational Design and Synthesis of a Deeply Red-Shifted and Bistable Azobenzene. *J Am Chem Soc* **2020**, *142* (14), 6538–6547. https://doi.org/10.1021/jacs.9b10430.

(36) Ahmed, Z.; Siiskonen, A.; Virkki, M.; Priimagi, A. Controlling Azobenzene Photoswitching through Combined Ortho-Fluorination and -Amination. *Chemical Communications* **2017**, *53* (93), 12520–12523. https://doi.org/10.1039/c7cc07308a.

(37) Wang, Y.; Wang, J.; Lin, Y.; Si-Ma, L. F.; Wang, D. H.; Chen, L. G.; Liu, D. K. Synthesis and Antihistamine Evaluations of Novel Loratadine Analogues. *Bioorg Med Chem Lett* **2011**, *21* (15), 4454–4456. https://doi.org/10.1016/j.bmcl.2011.06.012.

(38) Lin, Y.; Wang, Y.; Sima, L. F.; Wang, D. H.; Cao, X. H.; Chen, L. G.; Chen, B. Design, Synthesis and Biological Activity Evaluation of Desloratadine Analogues as H1 Receptor Antagonists. *Bioorg Med Chem* **2013**, *21* (14), 4178–4185. https://doi.org/10.1016/j.bmc.2013.05.004.

Supplementary information

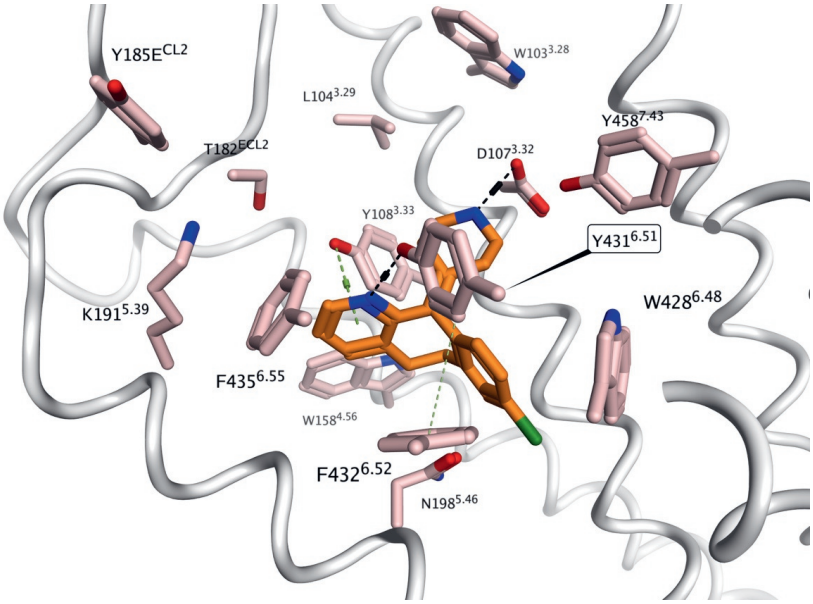

Figure S1. The cryo-EM structure of desloratadine bound to histamine H_1R (PDB:8X63)[1] visualized with MOE. Key interactions with D107$^{3.32}$ and Y431$^{6.52}$ are shown in black dashed lines.

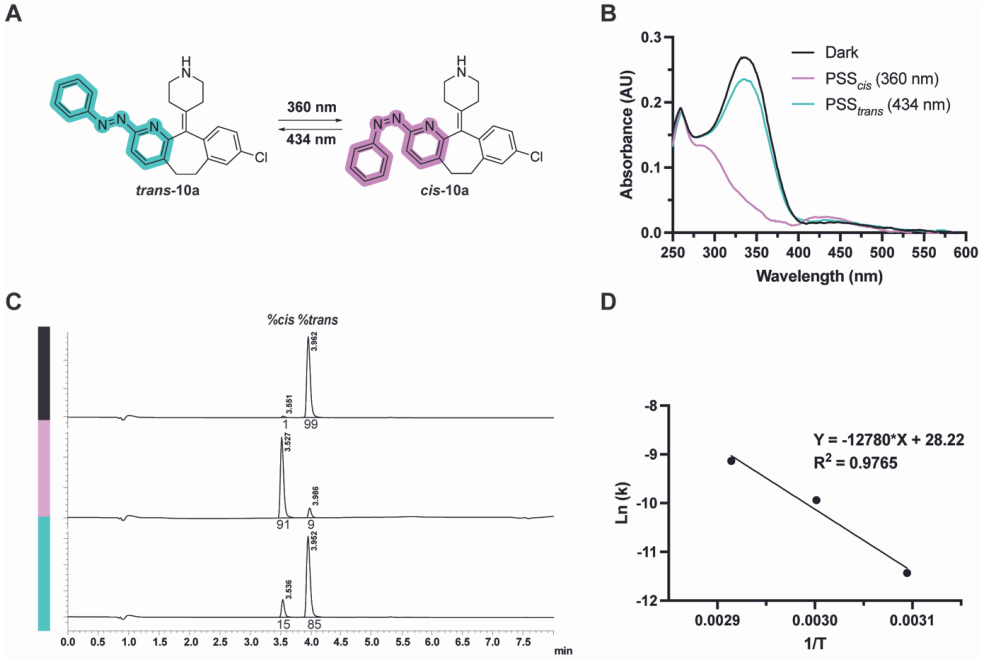

Figure S2. (A) Chemical structures of the *trans* and *cis* isomers of **10a** (B) UV-vis spectra of 25 µM of **10a** in HBSS buffer containing 50% DMSO as the *trans* isomer (black), after illumination with 360 ± 20 nm for 2 min to PSS$_{cis}$ (magenta) and after subsequent illumination with 434 ± 9 nm for 2 min to PSS$_{trans}$ (cyan). (C) *Trans*-**10a** (upper panel) and photostationary state (PSS) area percentages after illumination with 360 ± 20 nm for 10 min to reach PSS$_{cis}$ (middle panel) and after subsequent illumination with 434 ± 9 nm for 10 min to reach PSS$_{trans}$ (lower panel) at 10 mM in DMSO as determined by LC-MS analysis at the isosbestic point (265 nm). (D) Arrhenius fit for the thermal relaxation of **10a** at three different temperatures (50 °C, 60 °C, 70 °C), as measured at 25 µM in HBSS buffer containing 50% DMSO.

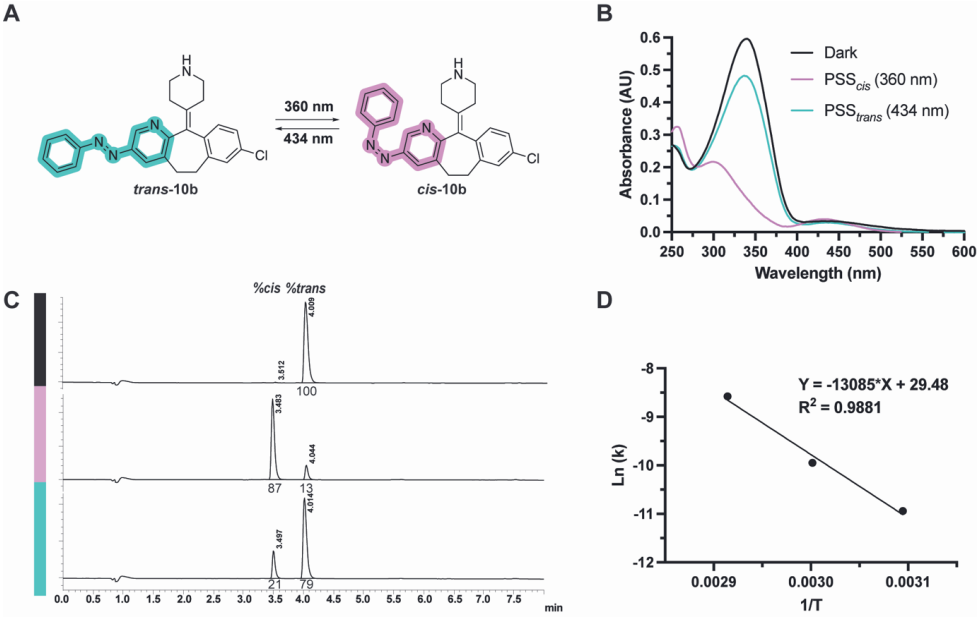

Figure S3. (A) Chemical structures of the *trans* and *cis* isomers of **10b** (B) UV-vis spectra of 25 µM of **10b** in HBSS buffer containing 50% DMSO as the *trans* isomer (black), after illumination with 360 ± 20 nm for 2 min to PSS_{cis} (magenta) and after subsequent illumination with 434 ± 9 nm for 2 min to PSS_{trans} (cyan). (C) *Trans*-**10b** (upper panel) and photostationary state (PSS) area percentages after illumination with 360 ± 20 nm for 20 min to reach PSS_{cis} (middle panel) and after subsequent illumination with 434 ± 9 nm for 10 min to reach PSS_{trans} (lower panel) at 10 mM in DMSO as determined by LC-MS analysis at the isosbestic point (280 nm). (D) Arrhenius fit for the thermal relaxation of **10b** at three different temperatures (50 °C, 60 °C, 70 °C), as measured at 25 µM in HBSS buffer containing 50% DMSO.

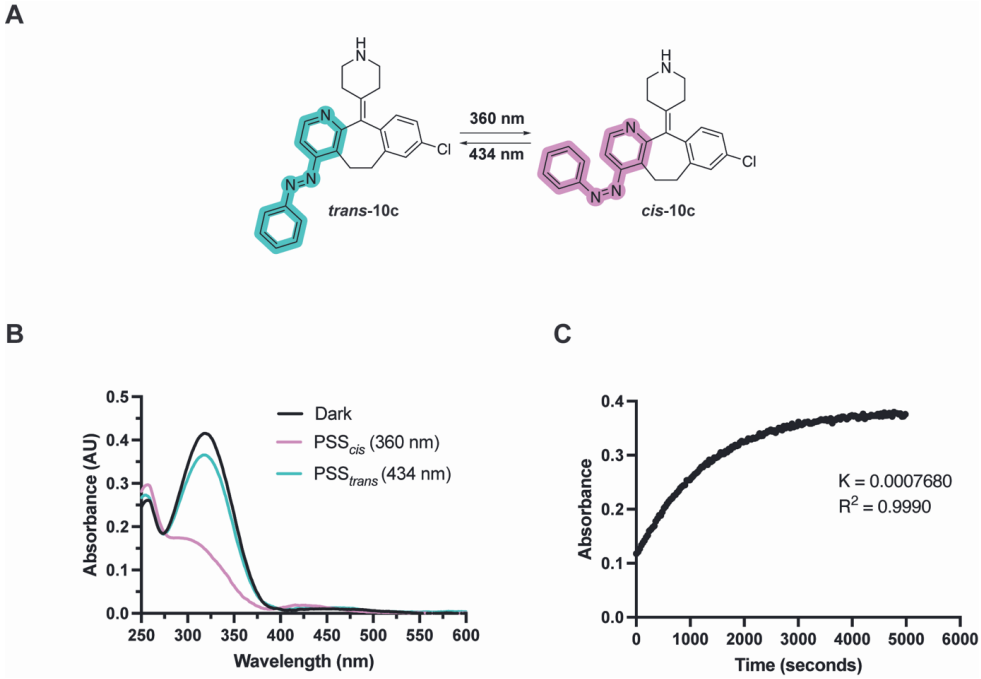

Figure S4. (A) Chemical structures of the *trans* and *cis* isomers of **10c** (B) UV-vis spectra of 25 µM of **10c** in HBSS buffer containing 50% DMSO as the *trans* isomer (black), after illumination with 360 ± 20 nm for 4 min to PSS$_{cis}$ (magenta) and after subsequent illumination with 434 ± 9 nm for 2 min to PSS$_{trans}$ (cyan). (C) Thermal relaxation of *cis*-**10c** at 20°C, as measured at 25 µM in HBSS buffer containing 50% DMSO by UV absorbance at 320 nm.

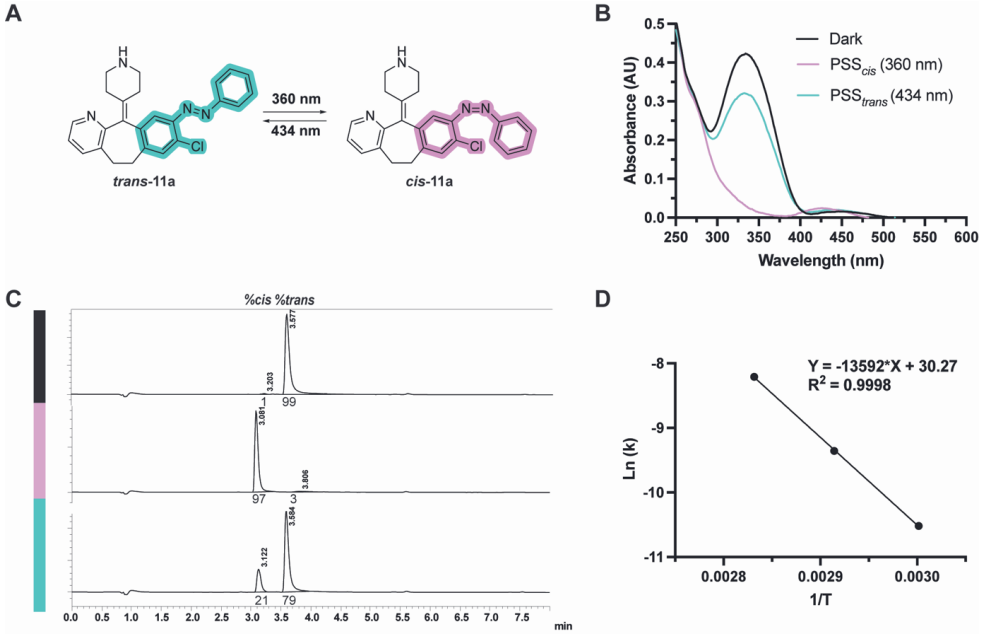

Figure S5. (A) Chemical structures of the *trans* and *cis* isomers of **11a** (B) UV-vis spectra of 25 µM of **11a** in HBSS buffer containing 50% DMSO as the *trans* isomer (black), after illumination with 360 ± 20 nm for 2 min to PSS$_{cis}$ (magenta) and after subsequent illumination with 434 ± 9 nm for 2 min to PSS$_{trans}$ (cyan). (C) *Trans*-**11a** (upper panel) and photostationary state (PSS) area percentages after illumination with 360 ± 20 nm for 5 min to reach PSS$_{cis}$ (middle panel) and after subsequent illumination with 434 ± 9 nm for 10 min to reach PSS$_{trans}$ (lower panel) at 10 mM in DMSO as determined by LC-MS analysis at the isosbestic point (275 nm). (D) Arrhenius fit for the thermal relaxation of **11a** at three different temperatures (60 °C, 70 °C, 80 °C), as measured at 25 µM in HBSS buffer containing 50% DMSO.

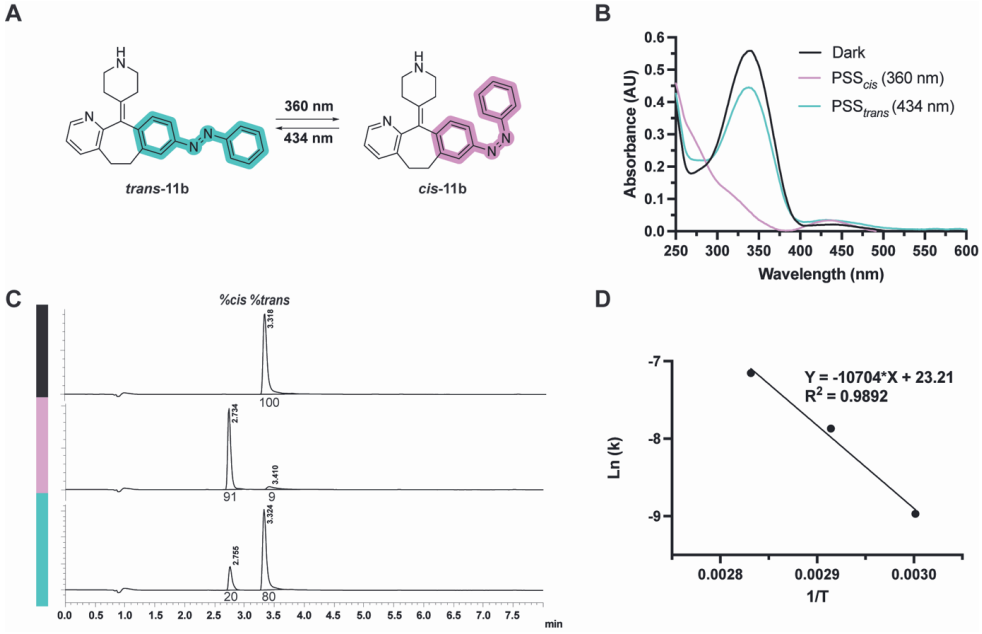

Figure S6. (A) Chemical structures of the *trans* and *cis* isomers of **11b** (B) UV-vis spectra of 25 µM of **11b** in HBSS buffer containing 50% DMSO as the *trans* isomer (black), after illumination with 360 ± 20 nm for 2 min to PSS_{cis} (magenta) and after subsequent illumination with 434 ± 9 nm for 2 min to PSS_{trans} (cyan). (C) *Trans*-**11b** (upper panel) and photostationary state (PSS) area percentages after illumination with 360 ± 20 nm for 5 min to reach PSS_{cis} (middle panel) and after subsequent illumination with 434 ± 9 nm for 10 min to reach PSS_{trans} (lower panel) at 10 mM in DMSO as determined by LC-MS analysis at the isosbestic point (290 nm). (D) Arrhenius fit for the thermal relaxation of **11b** at three different temperatures (60 °C, 70 °C, 80 °C), as measured at 25 µM in HBSS buffer containing 50% DMSO.

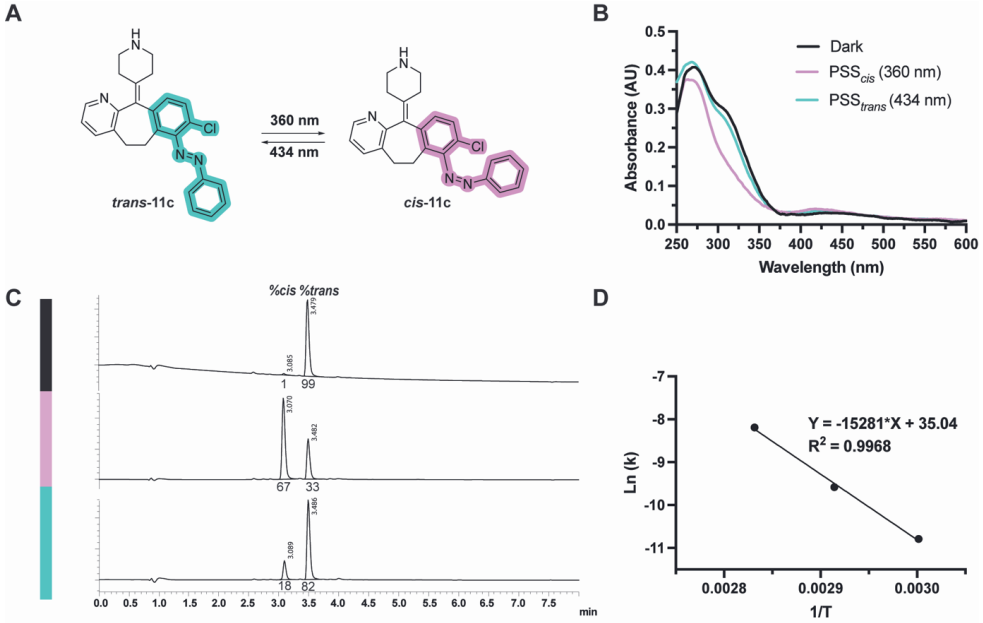

Figure S7. (A) Chemical structures of the *trans* and *cis* isomers of **11c** (B) UV-vis spectra of 25 µM of **11c** in HBSS buffer containing 50% DMSO as the *trans* isomer (black), after illumination with 360 ± 20 nm for 4 min to PSS_{cis} (magenta) and after subsequent illumination with 434 ± 9 nm for 2 min to PSS_{trans} (cyan). (C) *Trans*-**11c** (upper panel) and photostationary state (PSS) area percentages after illumination with 360 ± 20 nm for 10 min to reach PSS_{cis} (middle panel) and after subsequent illumination with 434 ± 9 nm for 10 min to reach PSS_{trans} (lower panel) at 10 mM in DMSO as determined by LC-MS analysis at the isosbestic point (255 nm). (D) Arrhenius fit for the thermal relaxation of **11c** at three different temperatures (60 °C, 70 °C, 80 °C), as measured at 25 µM in HBSS buffer containing 50% DMSO.

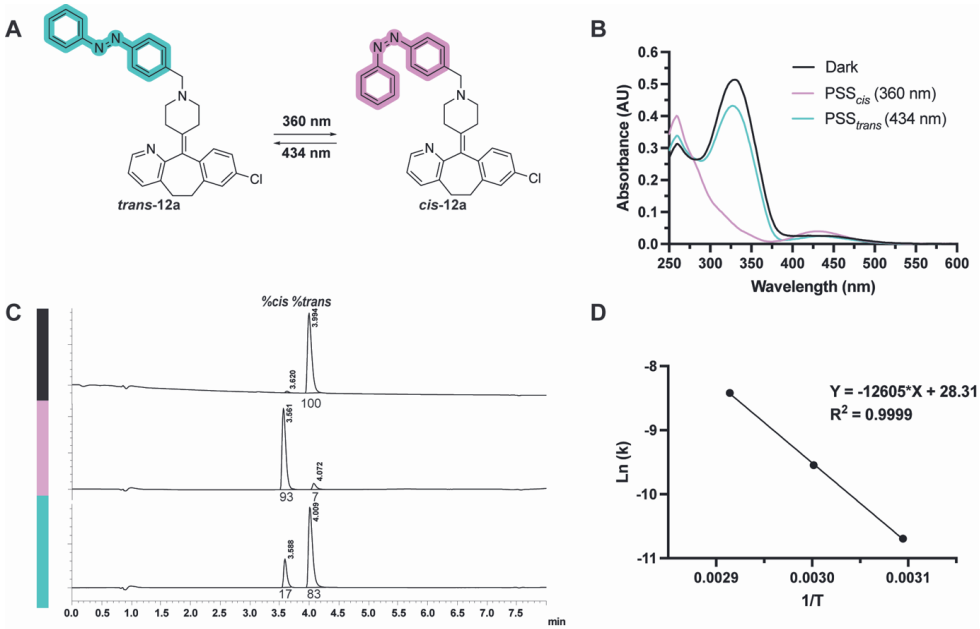

Figure S8. (A) Chemical structures of the *trans* and *cis* isomers of **12a** (B) UV-vis spectra of 25 µM of **12a** in HBSS buffer containing 50% DMSO as the *trans* isomer (black), after illumination with 360 ± 20 nm for 4 min to PSS_{cis} (magenta) and after subsequent illumination with 434 ± 9 nm for 4 min to PSS_{trans} (cyan). (C) *Trans*-**12a** (upper panel) and photostationary state (PSS) area percentages after illumination with 360 ± 20 nm for 5 min to reach PSS_{cis} (middle panel) and after subsequent illumination with 434 ± 9 nm for 10 min to reach PSS_{trans} (lower panel) at 10 mM in DMSO as determined by LC-MS analysis at the isosbestic point (280 nm). (D) Arrhenius fit for the thermal relaxation of **12a** at three different temperatures (50 °C, 60 °C, 70 °C), as measured at 25 µM in HBSS buffer containing 50% DMSO.

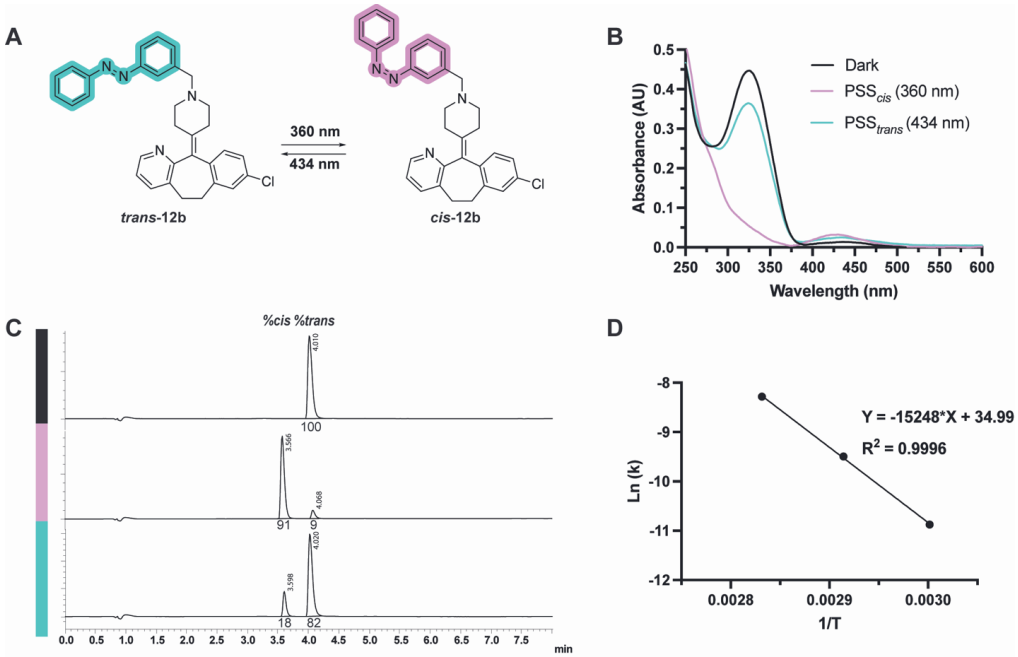

Figure S9. (A) Chemical structures of the *trans* and *cis* isomers of **12b** (B) UV-vis spectra of 25 µM of **12b** in HBSS buffer containing 50% DMSO as the *trans* isomer (black), after illumination with 360 ± 20 nm for 4 min to PSS$_{cis}$ (magenta) and after subsequent illumination with 434 ± 9 nm for 4 min to PSS$_{trans}$ (cyan). (C) *Trans*-**12b** (upper panel) and photostationary state (PSS) area percentages after illumination with 360 ± 20 nm for 5 min to reach PSS$_{cis}$ (middle panel) and after subsequent illumination with 434 ± 9 nm for 10 min to reach PSS$_{trans}$ (lower panel) at 10 mM in DMSO as determined by LC-MS analysis at the isosbestic point (270 nm). (D) Arrhenius fit for the thermal relaxation of **12b** at three different temperatures (60 °C, 70 °C, 80 °C), as measured at 25 µM in HBSS buffer containing 50% DMSO.

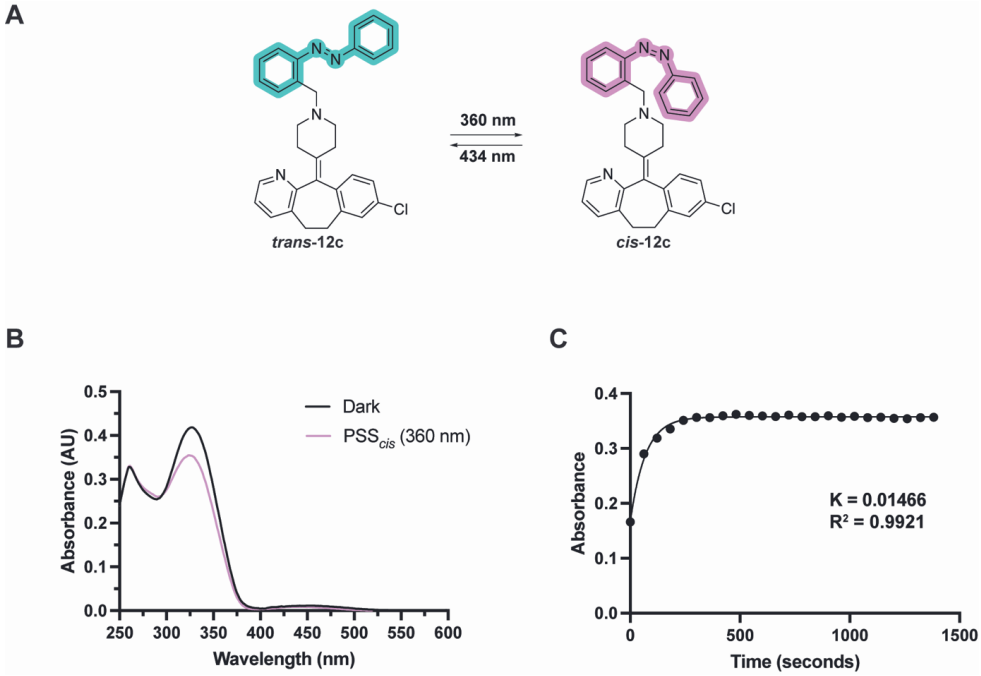

Figure S10. (A) Chemical structures of the *trans* and *cis* isomers of **12c** (B) UV-vis spectra of 25 µM of **12c** in HBSS buffer containing 50% DMSO as the *trans* isomer (black), after illumination with 360 ± 20 nm for 10 min to PSS$_{cis}$ (magenta). (C) Thermal relaxation of *cis*-**12c** at 20°C, as measured at 25 µM in HBSS buffer containing 50% DMSO by UV absorbance at 320 nm.

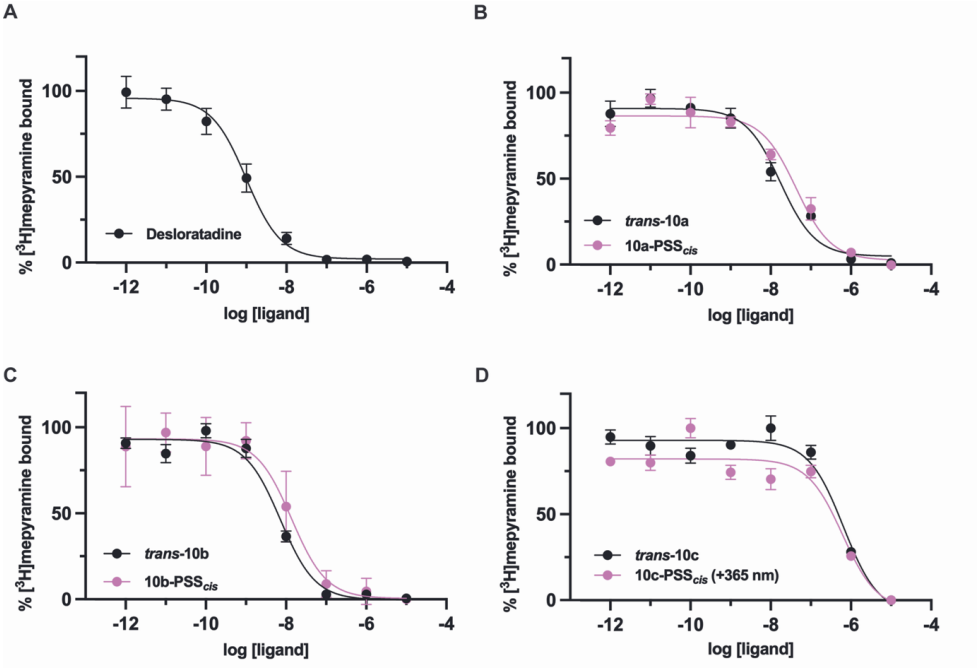

Figure S11. Competition binding curves of (A) desloratadine (**8**) and *trans* and PSS_{cis} states of (B) **10a** (C) **10b** and (D) **10c** in competition with [^{3}H]mepyramine. Pooled data are shown as mean ± SEM of three independent experiments. Due to its short thermal half-life, compound **10c** was continuously illuminated with 365 nm light during incubation.

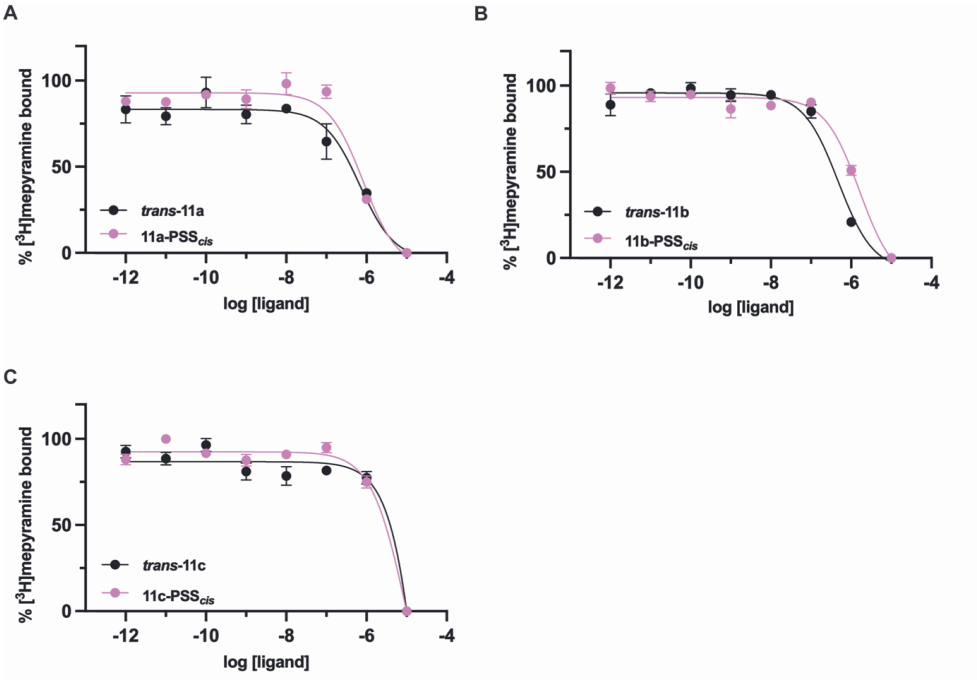

Figure S12. Competition binding curves of *trans* and PSS_{cis} states of (A) **11a** (B) **11b** and (C) **11c** in competition with [^{3}H]mepyramine. Pooled data are shown as mean ± SEM of three independent experiments.

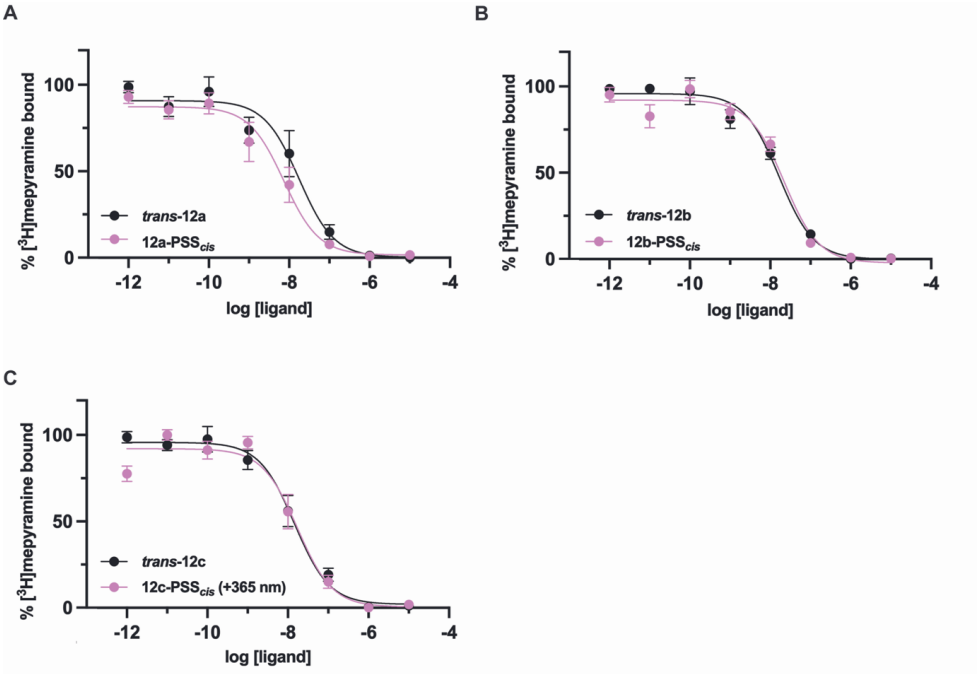

Figure S13. Competition binding curves of *trans* and PSS_{cis} states of (A) **12a** (B) **12b** and (C) **12c** in competition with [^{3}H]mepyramine. Pooled data are shown as mean ± SEM of three independent experiments. Due to its short thermal half-life, compound **12c** was continuously illuminated with 365 nm light during incubation.

Experimental methods – Pharmacology

Radioligand binding experiments were performed in the following manner, as published previously, with minor changes.[2,3] Cell homogenates were made using HEK293T cells, transiently expressing the N-terminally HA-tagged H_1R. The homogenates were stored at −20 °C. For the assay, the HA-H_1R-expressing cell homogenates were resuspended in radioligand binding buffer (Na_2HPO_4 (50 mM) and KH_2PO_4 (50 mM)), pH 7.4, and homogenized with a Branson Sonifier 250 (Branson Ultrasonics, Danbury, CT). Afterwards, the cell homogenates were incubated with the respective (photo)ligands in increasing concentrations (10^{-5}–10^{-12} M) in competition with [^{3}H]mepyramine (2.7–4.9 nM) at 25 °C in black 96 well plates (Greiner). During the incubation time, **10c** and **12c** were continuously illuminated with 365 nm (10 V, 2 mW, constant mode) light (96 LED array plates, LAD-1, LEDA-x, Bio Research Center Co., Ltd. Izumi, Japan) to account for their short-lived *cis* isomers. After a 4-hour incubation time, the binding reaction was stopped using a harvester (PerkinElmer). Upon multiple wash steps through a polyethyleneimine-coated GF/C filter plate (PerkinElmer) receptor-bound radioligand was captured by the GF/C filter plate. After drying the GF/C plate, the filter-bound radioligand was quantified by scintillation counting using MicroScint-O and the Wallac MicroBeta counter (PerkinElmer). IC_{50} values were obtained by analyzing the displacement curves with GraphPad Prism 10 (GraphPad Software, San Diego) and were converted to K_i values using the Cheng–Prusoff equation.[4]

Experimental methods – Computational chemistry

The cryo-EM structure of the H_1R-BRIL/Anti BRIL Fab complex with desloratadine (PDB: 8X64)[1] was prepared using the Structure Preparation module in MOE v2024.06. Hydrogen atoms were added, and partial charges were calculated using the Amber:EHT forcefield. Desloratadine was subsequently extracted from the complex. *Trans*-**10a**, *cis*-**10a** and desloratadine were converted from their SMILES representation into 3D structures using MOE. Each compound was visually inspected and modified to ensure the correct isomeric form. The protonation state of the molecules was checked and corrected as needed during this process.

The docking procedure was validated by redocking of desloratadine into the prepared histamine H_1R structure. MOE's external docking function was applied via the docking user interface, using default settings (Genetic Algorithm placement with PLP and Rigid Receptor refinement). Two hundred docking poses were generated, initially scored using London dG, and then refined. The refined poses were subsequently rescored using the GBVI/WSA dG and twenty poses with the highest score were reported. Docking scores for the desloratadine ranged from -6.5847 kcal/mol to -5.5730 kcal/mol. Interaction fingerprints (IFPs) were used to identify binding modes in which the basic amine of the ligand binds with Asp107$^{3.32}$, a hallmark interaction of aminergic GPCRs. Three out of the twenty reported structures of redocked desloratadine poses exhibited binding modes highly similar to the experimental cryo-EM structure, with RMSD values between 0.8398 and 1.2006 Å.

Trans-**10a** and *cis*-**10a** were docked in the prepared histamine H_1 structure using the same protocol. Docking scores ranged from -7.9736 to -6.5838 kcal/mol for *trans*-**10a** and -8.0865 to -7.0272 kcal/mol for *cis*-**10a**. IFP-based filtering resulted in seven docking poses for *trans*-**10a** with interactions to Asp107$^{3.32}$. The binding mode of *trans*-**10a** that was selected has a docking score of -7.5910 kcal/mol (i.e., the best docking score of the poses that make an interaction with Asp107$^{3.32}$). Applying the same IFP filtering for *cis*-**10a** gave the best docking score of -7.115 kcal/mol.

In most docking poses of *cis*-**10a**, no interaction with Asp107$^{3.32}$ was observed, and a wide range of binding poses was obtained. However, in two poses, an interaction with Asp107$^{3.32}$ was identified. In these cases, the desloratadine core was flipped relative to the experimental structure but could still be adequately overlaid.

Experimental procedures – Photochemistry

UV−Vis spectra were recorded using a Thermo-scientific Evolution 201 PC spectrophotometer equipped with a thermostated cell holder set at 20 °C. Fits of UV−vis spectroscopy data were generated using Prism 10.1.0. Illumination for all photochemical experiments was executed using a Sutter instruments Lambda LS with a 300 W full-spectrum lamp connected to a Sutter instruments Lambda 10-3 optical filter changer equipped with 360 ± 20 nm, 434 ± 9 nm 520 ± 12 nm. The light intensity used for the lambda 10-3 optical filter is 0.93 mW/mm^2 using the 360 ± 20 nm filter, 0.79 mW/mm^2 for the 434 ± 9 nm filter, 0.77 mW/mm^2 for the 494 ± 9 nm filter, and 0.20 mW/mm^2 for the 520 ± 12 nm filter as measured using a Thorlabs PM16−401 power meter. For photochemical analyses, illuminations were performed in Hellma Suprasil quartz 114QS cuvettes. Thermal relaxation experiments and Arrhenius extrapolations were performed according to Priimagi *et al,*[5] using a compound concentration of 25 µM in HBSS +50% DMSO at temperatures of 50, 60, 70, or 80 °C. Illuminations for pharmacological experiments were performed in cylindrical clear glass vials with a volume of 4.5 mL. The typical distance between light source and vial or cuvette was 2 cm.

Experimental procedures - Chemistry

All chemicals and solvents were obtained from commercial suppliers (primarily Sigma-Aldrich, BLD pharma and Combi-Blocks) and used without purification. DCM, DMF, THF and Et_2O were dried by passing through a PureSolv solvent purification system. All reactions were carried out under N_2 atmosphere unless mentioned otherwise. All reactions with photoresponsive compounds were carried out in the dark or under red light. IUPAC names were adapted from Chemdraw Professional 21.0 (PerkinElmer). Reactions were monitored by thin layer chromatography (Merck Silicagel 60 F254) by visualization under 254 nm lamp. Flash column chromatography was performed with Screening Devices 40-63 µm (Biotage) or GraceResolv (Büchi) cartridges on Isolera One with UV-Vis detection (Biotage). Nuclear magnetic resonance (NMR) spectra were determined with a Bruker Avance II 500 MHz or a Bruker Avance III HD 600 MHz spectrometer. Chemical shifts are reported in parts per million (ppm) against the reference compound using the signal of the residual non-deuterated solvent ($CDCl_3$ δ = 7.26 ppm (^{1}H), δ = 77.16 ppm (^{13}C); DMSO-d_6 δ = 2.50 ppm (^{1}H), δ = 39.52 ppm (^{13}C)). NMR spectra were processed using MestReNova 14.1 software. The peak multiplicities are defined as follows: s, singlet; d, doublet; t, triplet; q, quartet; dd, doublet of doublets; ddd, doublet of doublets of doublets; dt, doublet of triplets; dq, doublet of quartets; td, triplet of doublets; tt, triplet of triplets; qd, quartet of doublets; p, pentet; dp, doublet of pentets; br, broad signal; m, multiplet. For NMR listings, in addition to specific instructions that are given by the journal in the guidelines for authors the following additional procedures were used: 1) Multiplicity is not solely reported based on peak shapes, but also distinguishes the coupling to all non-equivalent protons that have similar J values; 2) If additional smaller couplings are observed but are too small for accurate quantitation because the precision is smaller than the digital resolution, a symbol $^{\Delta}$ will be used; 3) The notation 'm' is used in case of obscured accurate interpretation as a result of (i) overlapping signals for different protons, or (ii) a result of overlapping signal lines within the same proton signal; 4) For any rotamers or diastereomers, signals will be listed separately; 5) NMR signals that could only be detected with HSQC analysis are denoted with a $^{\#}$ symbol; 6) NMR signals that could only be detected with HMBC analysis are denoted with a * symbol; 7) If one or more signals remain undetected after extensive 1D and 2D NMR analyses, this will be mentioned. 8) Signals for exchangeable proton atoms (such as NH and OH groups) are only listed if clearly visible (excluding e.g. the use of D_2O or CD_3OD) and if confirmed by a D_2O shake and/or HSQC. Analytical HPLC analyses were performed using a Shimadzu LC-20AD liquid chromatography pump system, equipped with a Waters XBridge C18 column 5 µm 4.6 x 50 mm (used at 40 °C), connected to a Shimadzu SPDM20A photodiode array detector. MS detection was performed using Shimadzu LCMS-2010EV mass spectrometer operating in both positive and negative ionization mode. The mobile phase used for acidic mode was a mixture of A = H_2O + 0.1% HCO_2H and B = MeCN + 0.1% HCO_2H. The mobile phase used for basic mode was a mixture of A = H_2O and B = MeCN + 0.4% w/v NH_4HCO_3. The method used is as follows: flow rate: 1.0 mL/min, start 95% A in a linear gradient to 10% A over 4.5 min, hold 1.5 min at 10% A, in 0.5 min in a linear gradient to 95% A, hold 1.5 min at 95% A, total runtime: 8.0 min. Analytical UPLC analyses were

performed using a Shimadzu LC-40D liquid chromatograph pump system, equipped with an Xbridge (BEH C18) 2.5 µm column (50 mm, 2.1 mm), connected to a Shimadzu SPD-M40 diode array detector. MS detection was performed using a Shimadzu LCMS-2020 EV mass spectrometer. The mobile phase used for acidic mode was a mixture of A = H_2O + 0.1% HCO_2H and B = MeCN + 0.1% HCO_2H, The method used is as follows: flow rate: flow rate: 0.4 mL/min, start 95% A in a linear gradient to 10% A over 1.75 min, hold 0.25 min at 10% A, in 0.25 min in a linear gradient to 95% A, hold 0.75 min at 95% A, total run time: 3 min. Compound purities were calculated as the percentage peak area of the analysed compound by UV detection at 254 nm. Unless mentioned otherwise, all compounds have a LC purity of >95 %. High-resolution mass spectra (HRMS) were recorded on a Bruker micrOTOF mass spectrometer using ESI in positive ion mode (HRMS). λ_{max} values provided in the procedures are those extracted from the LC analysis.

General procedure A - Baeyer-Mills reaction

The aniline was dissolved in the indicated volume of PhMe. The solution was purged with N_2 before addition of PhNO (1.1 eq) and glacial AcOH (4.0 eq). The solution was stirred at the indicated temperature until LC-MS indicated full consumption of the aniline (LC-MS). The mixture was diluted with EtOAc and quenched with satd. aq. $NaHCO_3$ solution. The aqueous layer was extracted with three times with EtOAc. The combined organic layers were washed with brine, dried over Na_2SO_4, filtered, and concentrated under reduced pressure. The crude product was purified using column chromatography to give the desired azobenzene.

General procedure B – Deprotection of *N*-Boc moiety

The Boc-protected amine was dissolved in the indicated volume of MeOH. To this was added 4M HCl in 1,4-dioxane (10.0 eq). The solution was stirred at rt until full consumption of the starting material (LC-MS). The solution was poured on ice, and the organic solvent was evaporated under reduced pressure. The aqueous residue was made basic with satd. aq. $NaHCO_3$ solution and was extracted three times with EtOAc. The combined organic layers were washed with brine, dried over Na_2SO_4, and concentrated under reduced pressure. When indicated, the crude product was purified using column chromatography to give the desired product.

General procedure C – Béchamp reduction

The nitro-compound was dissolved in 1,4-dioxane (0.09 M), EtOH (0.11 M) and water (0.17 M). Solid NH_4Cl (3.6 eq) and Fe powder (4.6 eq) were added. The resulting reaction mixture was stirred at 75 °C until full consumption of the starting material (LC-MS). The reaction mixture was diluted with EtOAc, filtered over Celite and washed with EtOAc. The organic solvents were evaporated under reduced pressure and the aqueous residue was extracted three times with EtOAc. The combined organic layers were washed with brine, dried over Na_2SO_4, filtered, and concentrated under reduced pressure to give the desired aniline.

General procedure D – Deprotection of ethylcarbamate moiety

The carbamate (1.0 eq) was dissolved in EtOH:H_2O (4:1, 0.10 M), after which KOH (10.0 eq) was added. The reaction mixture was heated at reflux until full consumption of the starting material (LC-MS). The solvent was evaporated under reduced pressure and the aqueous residue was extracted three times with EtOAc. The combined organic layers were washed with brine, dried over Na_2SO_4, filtered, and concentrated under reduced pressure. The crude product was purified using column chromatography to give the desired product.

tert-butyl 4-(8-chloro-5,6-dihydro-11H-benzo[5,6]cyclohepta[1,2-b]pyridin-11-ylidene)piperidine-1-carboxylate (13)

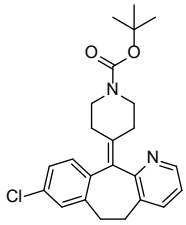

Desloratadine (**8**, 2.00 g, 6.43 mmol, 1.0 eq) was dissolved in DCM (55 mL). To this was added Boc_2O (1.55 g, 7.08 mmol, 1.1 eq) and Et_3N (1.0 mL, 7.19 mmol, 1.1 eq). The solution was stirred at rt for 16 h. The mixture was diluted with DCM (50 mL), and the organic layer was washed with water (3 x 30 mL) and brine. The organic layer was dried over Na_2SO_4, filtered, and concentrated under reduced pressure. This yielded **8** as a white solid (2.50 g, 95%). **^{1}H NMR** (500 MHz, $CDCl_3$) δ 8.39 (dd, *J* = 4.8, 1.6 Hz, 1H), 7.46 – 7.40 (m, 1H), 7.17 – 7.05 (m, 4H), 3.76 (s, 2H), 3.43 – 3.29 (m, 2H), 3.07 (dddd, *J* = 13.2, 9.6, 4.3, 4.3 Hz, 2H), 2.88 – 2.74 (m, 2H), 2.46 (ddd, *J* = 14.2, 9.4, 4.6 Hz, 1H), 2.39 – 2.23 (m, 3H), 1.44 (s, 9H). **^{13}C NMR** (126 MHz, $CDCl_3$) δ 157.3, 154.9, 146.8, 139.7, 137.9, 137.8, 137.6, 134.1, 133.5, 133.0, 130.7, 129.1, 126.3, 122.4, 79.7, 45.4, 44.6, 31.8, 31.6, 30.9, 30.7, 28.6. **LC-MS**: t_r = 4.32 min, purity: > 99%, $[M+H]^+$ m/z calc. 411.15, found 411.18.

11-(1-(tert-butoxycarbonyl)piperidin-4-ylidene)-8-chloro-6,11-dihydro-5H-benzo[5,6]cyclohepta[1,2-b]pyridine 1-oxide (14)

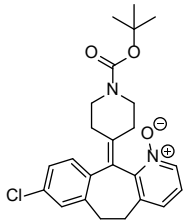

Pyridine **13** (2.50 g, 6.09 mmol, 1.0 eq) was dissolved in DCM (30 mL). To this was added *m*-CPBA (1.58 g, 9.13 mmol, 1.5 eq). The solution was stirred at rt for 50 min. The solution was diluted with DCM and made basic using satd. aq. $NaHCO_3$. The mixture was extracted with DCM (3 x 40 mL). The combined organic layers were washed with brine, dried over Na_2SO_4, filtered, and concentrated under reduced pressure. The crude product was purified using normal-phase column chromatography (0% -> 10% MeOH in EtOAc). This yielded the *N*-oxide **14** as a white solid (1.59 g, 61%). **^{1}H NMR** (500 MHz, CD_3OD) δ 8.17 (dd, *J* = 6.6, 1.2 Hz, 1H), 7.48 (dd, *J* = 7.8, 1.1 Hz, 1H), 7.35 (dd, *J* = 7.8, 6.5 Hz, 1H), 7.32 – 7.27 (m, 1H), 7.20 – 7.14 (m, 2H), 3.71 (dddd, *J* = 17.7, 11.1, 5.1, 5.1 Hz, 2H), 3.48 – 3.22 (m, 4H), 2.99 – 2.86 (m, 2H), 2.48 (ddd, *J* = 13.4, 8.6, 4.5 Hz, 1H), 2.34 (ddd, *J* = 14.2, 6.4, 4.0 Hz, 1H), 2.28 – 2.19 (m, 1H), 1.94 (ddd, *J* = 14.1, 6.3, 3.9 Hz, 1H), 1.46 (s, 9H). **^{13}C NMR** (126 MHz, CD_3OD) δ 156.4, 150.7, 143.0, 140.4, 140.3, 138.5, 134.9, 134.8, 133.6, 131.3, 130.2, 127.0, 126.1, 124.4, 81.3, 45.9, 44.7, 32.8, 31.3, 31.1, 28.7. **LC-MS:** t_r = 4.70 min, purity: > 99%, $[M+H]^+$ m/z calc. 427.20, found 427.17.

tert-butyl 4-(2-amino-8-chloro-5,6-dihydro-11H-benzo[5,6]cyclohepta[1,2-b]pyridin-11-ylidene)piperidine-1-carboxylate (15)

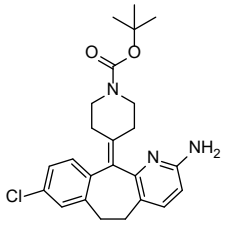

N-oxide **14** (650 mg, 1.52 mmol, 1.0 eq), potassium phthalimide (564 mg, 3.04 mmol, 2.0 eq), and Et_3N (423 µL, 3.04 mmol, 2.0 eq) were dissolved in DCM (1.5 mL). The solution was cooled to 0 ºC. TsCl (580 mg, 3.045 mmol, 2.0 eq) in DCM (6 mL) was added dropwise. The solution was stirred at rt for 20 h. The solution was diluted with water (3 mL) and $H_2NNH_2 \cdot H_2O$ (370 µL, 7.63 mmol, 5.0 eq) was added. The solution was heated at 80 °C for 1.5 h. The mixture was cooled to rt and extracted with DCM (3 x 25 mL). The combined organic layers were washed with 1M NaOH (40 mL). The organic layers were dried over Na_2SO_4, filtered, and concentrated under reduced pressure. The crude product was purified using flash column chromatography (50% -> 80% EtOAc in cHex). This yielded the title compound as a white solid (405 mg, 63%). **^{1}H NMR** (500 MHz, $CDCl_3$) δ 7.18 (d, *J* = 8.2 Hz, 1H), 7.16 – 7.14 (m, 1H), 7.14 – 7.08 (m, 2H), 6.34 (d, *J* = 8.3 Hz, 1H), 4.38 (s, 2H), 3.94 – 3.70 (m, 2H), 3.31 (ddd, *J* = 12.9, 9.0, 4.4 Hz, 1H), 3.23 – 3.13 (m, 1H), 3.04 – 2.92 (m, 2H), 2.78 – 2.64 (m, 2H), 2.50 – 2.39 (m, 2H), 2.32 – 2.26 (m, 2H), 1.45 (s, 9H). **^{13}C NMR** (126 MHz, $CDCl_3$) δ 155.9, 155.0, 154.5, 140.2, 140.0, 138.2, 137.6, 134.1, 132.8, 130.4, 129.0, 126.1, 122.9, 107.7, 79.7, 45.5, 44.4, 32.1, 31.0, 30.8, 28.6. **LC-MS:** t_r = 3.98 min, purity: >99%, $[M+H]^+$ m/z calc. 426.18, found 426.20.

***tert*-butyl (*E*)-4-(8-chloro-2-(phenyldiazenyl)-5,6-dihydro-11*H*-benzo[5,6]cyclohepta[1,2-*b*]pyridin-11-ylidene)piperidine-1-carboxylate (16)**

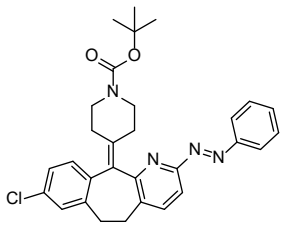

This compound was synthetised according to general procedure **A** using aniline **15** (600 mg, 1.41 mmol, 1.0 eq), PhNO (181 mg, 1.69 mmol, 1.2 eq), AcOH (324 µL, 5.63 mmol, 4.0 eq), PhMe (14.6 mL) and a reaction time of 18h. The crude product was purified using reverse-phase column chromatography (5->95% MeCN + 0.1% H_2COH in H_2O + 0.1% H_2COH). The desired fractions were combined, made basic with satd. aq. $NaHCO_3$ and extracted three times with EtOAc. The combined organic layers were washed with brine, dried over Na_2SO_4, filtered, and concentrated under reduced pressure. This gave **16** as an orange solid (61 mg, 8%). **^{1}H NMR** (600 MHz, $CDCl_3$) δ 8.06 – 8.00 (m, 2H), 7.61 (d, *J* = 8.2 Hz, 1H), 7.58 (d, *J* = 8.1 Hz, 1H), 7.55 – 7.49 (m, 3H), 7.23 – 7.18 (m, 2H), 7.16 (dd, *J* = 8.1, 2.2 Hz, 1H), 3.98 – 3.68 (m, 2H), 3.49 – 3.39 (m, 2H), 3.06 (ddd, *J* = 13.3, 9.9, 3.7 Hz, 2H), 2.96 (ddd, *J* = 16.2, 10.2, 4.5 Hz, 1H), 2.84 (ddd, *J* = 16.1, 8.0, 4.5 Hz, 1H), 2.64 – 2.57 (m, 1H), 2.49 – 2.43 (m, 1H), 2.40 – 2.31 (m, 2H), 1.45 (s, 9H). **^{13}C NMR** (151 MHz, $CDCl_3$) δ 161.4, 156.7, 155.0, 152.4, 140.0, 139.7, 139.0, 137.9, 135.8, 133.3, 133.1, 132.1, 131.0, 129.2, 129.0, 126.4, 123.8, 110.5, 79.7, 31.8, 31.7, 29.8, 28.6. **LC-MS:** t_r = 6.58 min, purity: 97%, λ_{max}: 331 nm, $[M+H]^+$ m/z calc. 515.22, found 515.30.

(*E*)-8-chloro-2-(phenyldiazenyl)-11-(piperidin-4-ylidene)-6,11-dihydro-5*H*-benzo[5,6]cyclohepta[1,2-*b*]pyridine (10a)

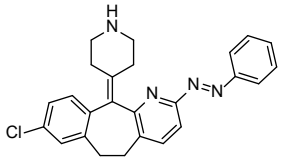

This compound was synthetised according to general procedure **B** using Boc-protected amine **16** (55 mg, 0.11 mmol, 1.0 eq), 4M HCl in 1,4-dioxane (0.27 mL, 1.07 mmol, 10.0 eq), MeOH (1.1 mL) and a reaction time of 17h. The crude product was purified using reverse-phase column chromatography (5->90% MeCN + 0.1% H_2COH in H_2O + 0.1% H_2COH). The desired fractions were combined, made basic with satd. aq. $NaHCO_3$ and extracted three times with EtOAc. The combined organic layers were washed with brine, dried over Na_2SO_4, filtered, and concentrated under reduced pressure. This gave **10a** as an orange solid (7 mg, 16%). **^{1}H NMR** (600 MHz, $(CD_3)_2SO$) δ 7.94 – 7.90 (m, 2H), 7.82 (d, *J* = 8.1 Hz, 1H), 7.64 – 7.59 (m, 3H), 7.55 (d, *J* = 8.0 Hz, 1H), 7.32 (d, *J* = 2.3 Hz, 1H), 7.24 (dd, *J* = 8.2, 2.3 Hz, 1H), 7.15 (d, *J* = 8.2 Hz, 1H), 3.41 – 3.33 (m, 3H), 3.03 – 2.80 (m, 4H), 2.63 – 2.53 (m, 2H), 2.37 – 2.28 (m, 1H), 2.28 – 2.14 (m, 3H). **^{13}C NMR** (151 MHz, $(CD_3)_2SO$) δ 160.6, 156.9, 152.0, 140.3, 140.3, 139.8, 137.9, 136.3, 132.5, 131.8, 131.1, 131.0, 129.8, 129.1, 125.9, 123.1, 111.4, 47.5, 47.4, 32.1, 32.0, 31.0, 30.7. **LC-MS:** t_r = 3.95 min, purity: 97%, λ_{max}: 334 nm, $[M+H]^+$ m/z calc. 415.17, found 415.15. **HRMS**: $[M+H]^+$ calc. for $C_{25}H_{24}ClN_4$: 415.1684, found 415.1694.

tert-butyl 4-(4-amino-8-chloro-5,6-dihydro-11H-benzo[5,6]cyclohepta[1,2-b]pyridin-11-ylidene)piperidine-1-carboxylate (17)

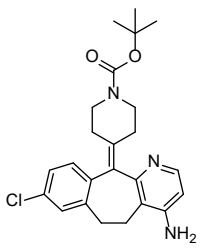

N-oxide **14** (950 mg, 2.31 mmol, 1.0 eq) and 4-cyanopyridine (481 mg, 4.62 mmol, 2.0 eq) were dissolved in MeCN (10 mL). The mixture was cooled to 0 °C. Tf_2O (1M in DCM, 2.3 mL, 2.3 mmol, 1.0 eq) was added. The solution was warmed to rt and stirred for 2 h. Conc. aq. NH_4OH (28-30 wt%) was added (1.0 mL, 15 mmol, 6.4 eq) and the solution was stirred at rt for 16 h. The mixture was diluted with water and the pH was adjusted to 8 using 2M HCl. The reaction mixture was extracted with DCM (3 x 30 mL). The combined organic layers were washed with brine, dried over Na_2SO_4, filtered, and concentrated under reduced pressure. The crude product was purified twice with normal-phase column chromatography (40% -> 75% EtOAc:MeOH:Et_3N (90:5:5) in cHex, followed by 0% -> 10% MeOH in DCM). This yielded **17** (247 mg, 25%) as a brown solid. **^{1}H NMR** (500 MHz, $CDCl_3$) δ 8.03 (d, *J* = 5.5 Hz, 1H), 7.21 (d, *J* = 2.0 Hz, 1H), 7.17 – 7.09 (m, 2H), 6.45 (d, *J* = 5.6 Hz, 1H), 4.28 (s, 2H), 3.92 – 3.65 (m, 2H), 3.44 (ddd, *J* = 14.1, 12.2, 4.2 Hz, 1H), 3.04 (m, 2H), 2.91 (ddd, *J* = 16.1, 4.7, 4.7 Hz, 1H), 2.80 (ddd, *J* = 14.1, 4.8, 4.8 Hz, 1H), 2.58 – 2.45 (m, 2H), 2.40 (ddd, *J* = 14.3, 4.5, 4.5 Hz, 1H), 2.32 – 2.16 (m, 2H), 1.44 (s, 9H). **^{13}C NMR** (126 MHz, $CDCl_3$) δ 155.0, 152.2, 145.7, 140.0, 139.6, 138.4, 132.9, 129.7, 128.1, 126.6, 116.5, 108.7, 80.1, 44.2, 31.0, 30.9, 30.7, 28.6, 26.9. Two missing quaternary carbons **LC-MS**: t_r = 3.69 min, purity: >99%, $[M+H]^+$ m/z calc. 426.19, found 426.15.

tert-butyl (E)-4-(8-chloro-4-(phenyldiazenyl)-5,6-dihydro-11H-benzo[5,6]cyclohepta[1,2-b]pyridin-11-ylidene)piperidine-1-carboxylate (18)

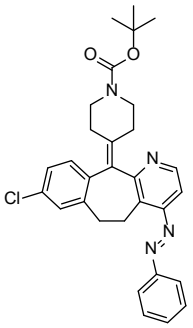

Aniline **17** (247 mg, 0.58 mmol, 1.0 eq) was dissolved in THF (2.5 mL). NaH (60% dispersion in mineral oil, 50 mg, 2.1 mmol, 3.6 eq) and PhNO (124 mg, 1.16 mmol, 2.0 eq) in THF (2.5 mL) were added. The mixture was stirred for 72 h at rt. The crude product was purified using reverse-phase column chromatography (5->90% MeCN + 0.1% H_2COH in H_2O + 0.1% H_2COH). The desired fractions were combined, made basic with satd. aq. $NaHCO_3$ and extracted three times with EtOAc. The combined organic layers were washed with brine, dried over Na_2SO_4, filtered, and concentrated under reduced pressure. This yielded **18** (70 mg, 23%) as an orange oil. **^{1}H NMR** (500 MHz, $CDCl_3$) δ 8.54 (d, *J* = 5.4 Hz, 1H), 7.99 – 7.91 (m, 2H), 7.61 – 7.50 (m, 3H), 7.30 (d, *J* = 5.4 Hz, 1H), 7.20 (d, *J* = 13.0 Hz, 3H), 3.96 – 3.71 (m, 2H), 3.63 (ddd, *J* = 16.8, 9.4, 4.7 Hz, 1H), 3.56 – 3.45 (m, 2H), 3.13 (ddd, *J* = 13.1, 9.4, 3.8 Hz, 2H), 2.93 (ddd, *J* = 15.2, 8.5, 4.7 Hz, 1H), 2.64 – 2.53 (m, 1H), 2.49 – 2.27 (m, 3H), 1.46 (s, 9H). **^{13}C NMR** (126 MHz, $CDCl_3$) δ 157.5*, 154.9, 152.8, 139.5, 136.8, 133.5, 132.9, 132.1*, 131.1, 129.5, 129.3, 126.6, 123.8, 109.0, 79.8, 45.1*, 31.9, 31.0, 28.6, 26.0. Four carbon signals could not be identified despite extensive 2D-NMR analysis (three quaternary carbon atoms, one tertiary aromatic carbon atom). **LC-MS**: t_r = 6.28 min, purity: >99%, λ_{max}: 316 nm, $[M+H]^+$ m/z calc. 515.20, found 515.30.

(E)-8-chloro-4-(phenyldiazenyl)-11-(piperidin-4-ylidene)-6,11-dihydro-5H-benzo[5,6]cyclohepta[1,2-b]pyridine (10c)

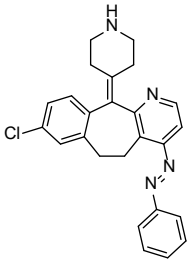

This compound was synthetised according to General procedure **B** using Boc-protected amine **18** (70 mg, 0.14 mmol, 1.0 eq), HCl in 1,4-dioxane (0.34 mL, 1.36 mmol, 10 eq), MeOH (1.4 mL) and a reaction time of 22h. The crude product was purified using flash column chromatography (3%-> 6% MeOH + NH_3 in DCM). Compound **10c** was obtained as an orange solid (35 mg, 62%) **^{1}H NMR** (500 MHz, $CDCl_3$) δ 8.51 (d, *J* = 5.2 Hz, 1H), 7.98 – 7.88 (m, 2H), 7.59 – 7.49 (m, 3H), 7.21 (d, *J* = 5.3 Hz, 1H), 7.19 – 7.16 (m, 2H), 7.14 (dd, *J* = 7.8, 2.1 Hz, 1H), 3.70 – 3.60 (m, 1H), 3.55 – 3.44 (m, 2H), 3.13 – 3.05 (m, 2H), 2.93 (ddd, *J* = 15.4, 9.6, 4.6 Hz, 1H), 2.75 (dddd, *J* = 15.6, 12.2, 9.5, 3.7 Hz, 2H), 2.51 – 2.32 (m, 4H). **^{13}C NMR** (126 MHz, $CDCl_3$) δ 160.8, 155.9, 152.8, 147.8, 139.7, 139.5, 137.3, 133.0, 132.7, 132.4, 131.1, 131.0, 129.4, 129.4, 126.2, 123.6, 108.4, 48.2, 48.1, 32.6, 31.9, 25.7. **LC-MS:** t_r = 3.94 min, purity 99%, λ_{max}: 317 nm, $[M+H]^+$ m/z calc. 415.16, found 415.15. **HRMS**: $[M+H]^+$ calc. for $C_{25}H_{24}ClN_4O_2$: 415.1684, found 415.1688.

Ethyl 4-(8-chloro-3-nitro-5,6-dihydro-11H-benzo[5,6]cyclohepta[1,2-b]pyridin-11-ylidene)piperidine-1-carboxylate (19)

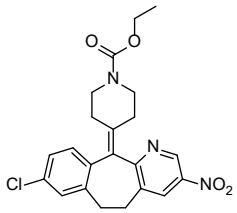

Loratadine (**7**, 2.00 g, 5.22 mmol, 1.0 eq) was dissolved in DCM (15 mL). The solution was cooled to -5 °C. A solution of $Bu_4N^+NO_3^-$ (1.84 g, 6.04 mmol, 1.16 eq) and TFAA (0.85 mL, 6.0 mmol, 1.2 eq) in DCM (8 mL) was added dropwise, keeping the temperature below 0 °C. The solution was stirred for 2 h at 0 °C, after which the solution was warmed to rt and stirred for 66 h. The mixture was quenched with satd. aq. $NaHCO_3$ and the aqueous layer was extracted three times with DCM. The combined organic layers were washed with brine, dried over Na_2SO_4, filtered, and concentrated under reduced pressure. The crude product was purified using normal-phase column chromatography (10% -> 30% EtOAc in cHex). This yielded **19** (473 mg, 21%) as a yellow solid. **^{1}H NMR** (600 MHz, $CDCl_3$) δ 9.21 (d, *J* = 2.5 Hz, 1H), 8.24 (d, *J* = 2.4 Hz, 1H), 7.20 (d$^\Delta$, *J* = 2.1 Hz, 1H), 7.17 (dd, *J* = 8.1, 2.2 Hz, 1H), 7.10 (d$^\Delta$, *J* = 8.1 Hz, 1H), 4.14 (q, *J* = 7.1 Hz, 2H), 3.85 – 3.66 (m, 2H), 3.49 – 3.40 (m, 2H), 3.22 (dddd, *J* = 12.8, 8.8, 8.8, 3.9 Hz, 2H), 3.01 (ddd, *J* = 16.9, 9.9, 4.7 Hz, 1H), 2.85 (ddd, *J* = 15.2, 8.2, 4.6 Hz, 1H), 2.53 – 2.45 (m, 1H), 2.43 – 2.35 (m, 1H), 2.35 – 2.28 (m, 1H), 2.28 – 2.21 (m, 1H), 1.25 (t, *J* = 7.1 Hz, 3H). **^{13}C NMR** (151 MHz, $CDCl_3$) δ 162.9, 155.6, 143.0, 142.1, 140.4, 139.1, 136.5, 134.7, 133.8, 132.9, 132.6, 130.9, 129.2, 126.8, 61.6, 44.9, 44.8, 31.8, 31.2, 14.8. **LC-MS:** t_r = 5.38 min, purity >99%, $[M+H]^+$ m/z calc. 428.13, found 428.15.

Ethyl 4-(3-amino-8-chloro-5,6-dihydro-11H-benzo[5,6]cyclohepta[1,2-b]pyridin-11-ylidene)piperidine-1-carboxylate (20)

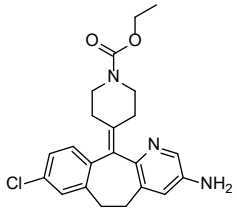

This compound was synthetised according to general procedure **C** using nitro-compound **19** (473 mg, 1.11 mmol, 1.0 eq), Fe (278 mg, 4.97 mmol, 4.5 eq), NH_4Cl (213 mg, 3.98 mmol, 3.6 eq), 1,4-dioxane (13 mL), EtOH (8 mL), water (6.5 mL), and a reaction time of 3h. This yielded the title compound as a brown oil (387 mg, 88%). **^{1}H NMR** (500 MHz, $(CD_3)_2SO$) δ 7.71 (d, *J* = 2.6 Hz, 1H), 7.29 (d, *J* = 2.3 Hz, 1H), 7.19 (dd, *J* = 8.1, 2.3 Hz, 1H), 7.02 (d$^\Delta$, *J* = 8.1 Hz, 1H), 6.66 (d, *J* = 2.6 Hz, 1H), 4.03 (qd, *J* = 7.1, 1.7 Hz, 2H), 3.60 (ddd, *J* = 12.7, 5.2, 5.2 Hz, 2H), 3.31 – 3.08 (m, 4H), 2.78 – 2.61 (m, 2H), 2.36 – 2.08 (m, 4H), 1.22 – 1.12 (m, 3H). **LC-MS:** t_r = 3.59 min, purity >99%, $[M+H]^+$ m/z calc. 398.16, found 398.10.

Ethyl (E)-4-(8-chloro-3-(phenyldiazenyl)-5,6-dihydro-11H-benzo[5,6]cyclohepta[1,2-b]pyridin-11-ylidene)piperidine-1-carboxylate (21)

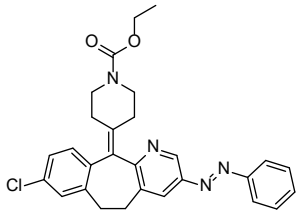

This compound was synthetised according to general procedure **A** using aminopyridine **20** (0.387 g, 0.973 mmol, 1.0 eq), AcOH (0.22 mL, 3.9 mmol, 4.0 eq), PhNO (104 mg, 0.97 mmol, 1.0 eq), PhMe (10 mL) and a reaction time of 25h. The crude product was purified using flash column chromatography (10% -> 30% EtOAc in cHex). This yielded **21** as an orange solid (152 mg, 32%). **^{1}H NMR** (600 MHz, $CDCl_3$) δ 9.01 (d, *J* = 2.2 Hz, 1H), 7.98 – 7.94 (m, 1H), 7.93 – 7.89 (m, 2H), 7.57 – 7.48 (m, 3H), 7.21 – 7.19 (m, 1H), 7.19 – 7.16 (m, 2H), 4.14 (q, *J* = 7.1 Hz, 2H), 3.94 – 3.74 (m, 2H), 3.53 – 3.37 (m, 2H), 3.17 (m, 2H), 3.00 (ddd, *J* = 15.7, 9.6, 4.6 Hz, 1H), 2.87 (ddd, *J* = 15.2, 8.4, 4.6 Hz, 1H), 2.63 – 2.51 (m, 1H), 2.46 – 2.31 (m, 3H), 1.26 (t, *J* = 7.1 Hz, 3H). **^{13}C NMR** (151 MHz, $CDCl_3$) δ 159.3, 155.6, 152.6, 147.0, 144.2, 139.4, 139.1, 137.1, 134.7, 133.4, 131.9, 130.9, 129.4, 129.2, 128.5, 126.6, 123.2, 61.5, 44.9, 31.8, 31.6, 31.0, 14.8. One carbon signal is not visible (quaternary carbon atom). **LC-MS:** t_r = 6.29 min, purity 96%, λ_{max}: 339 nm, $[M+H]^+$ m/z calc. 487.18, found 487.20.

(E)-8-chloro-3-(phenyldiazenyl)-11-(piperidin-4-ylidene)-6,11-dihydro-5H-benzo[5,6]cyclohepta[1,2-b]pyridine (10b)

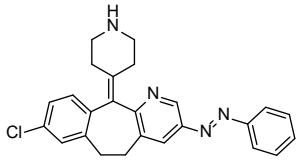

This compound was synthetised according to General procedure **D** using protected amine **21** (60 mg, 0.12 mmol, 1 eq), KOH (270 mg, 4.81 mmol, 39.0 eq), EtOH (4 mL), water (1 mL) and a reaction time of 4d. The crude product was purified using reverse-phase column chromatography (5->90% MeCN + 0.1% H_2COH in H_2O + 0.1% H_2COH). The desired fractions were combined, made basic with satd. aq. $NaHCO_3$ and extracted three times with EtOAc. The combined organic layers were washed with brine, dried over Na_2SO_4, filtered, and concentrated under reduced pressure. This gave **10b** as an orange solid (17 mg, 33%). **^{1}H NMR** (600 MHz, $(CD_3)_2SO$) δ 8.91 (d, *J* = 2.3 Hz, 1H), 8.00 (d, *J* = 2.3 Hz, 1H), 7.91 – 7.88 (m, 2H), 7.63 – 7.57 (m, 3H), 7.32 (d^{Δ}, *J* = 2.3 Hz, 1H), 7.23 (dd, *J* = 8.2, 2.3 Hz, 1H), 7.11 (d^{Δ}, *J* = 8.2 Hz, 1H), 3.44 – 3.35 (m, 2H), 2.99 (ddd, *J* = 16.7, 9.1, 4.7 Hz, 1H), 2.93 – 2.85 (m, 3H), 2.60 (dddd, *J* = 15.0, 12.2, 8.9, 3.5 Hz, 2H), 2.33 – 2.21 (m, 2H), 2.20 – 2.12 (m, 2H). **^{13}C NMR** (151 MHz, $(CD_3)_2SO$) δ 160.2, 152.0, 146.2, 143.8, 140.4, 140.1, 137.3, 134.6, 132.0, 131.6, 131.1, 131.0, 129.6, 129.1, 127.4, 125.8, 122.7, 47.7, 47.6, 32.3, 32.2, 30.9, 30.6. **LC-MS:** t_r = 4.02 min, purity 98%, λ_{max}: 337 nm, $[M+H]^+$ m/z calc. 415.16, found 415.15. **HRMS**: $[M+H]^+$ calc. for $C_{25}H_{24}ClN_4$: 415.1684, found 415.1689.

ethyl 4-(8-((tert-butoxycarbonyl)amino)-5,6-dihydro-11H-benzo[5,6]cyclohepta[1,2-b]pyridin-11-ylidene)piperidine-1-carboxylate (22)

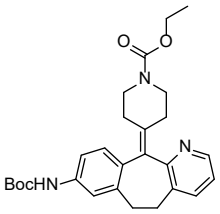

Loratadine (**7**, 500 mg, 1.31 mmol, 1.0 eq) was dissolved in 1,4-dioxane (12 mL). XPhos (224 mg, 0.47 mmol, 0.36 eq), $Pd(OAc)_2$ (35 mg, 0.16 mmol, 0.12 eq), $BocNH_2$ (184 mg, 1.57 mmol, 1.2 eq) and Cs_2CO_3 (596 mg, 1.83 mmol, 1.4 eq) were added. The reaction mixture was stirred at 95 °C for 2 h, after which it was cooled to rt. The reaction mixture was diluted with EtOAc and filtered over Celite. The filtrate was diluted with water and extracted three times with EtOAc. The combined organic layers were washed with brine, dried over Na_2SO_4, filtered, and concentrated under reduced pressure. The crude product was purified using normal-phase column chromatography (30 -> 60 % EtOAc:MeOH:Et_3N (90:5:5) in cHex). This yielded **22** as an off-white solid (499 mg, 82%). **^{1}H NMR** (500 MHz, $CDCl_3$) δ 8.38 (dd, *J* = 4.8, 1.7 Hz, 1H), 7.43 (dd, *J* = 7.6, 1.7 Hz, 1H), 7.39 – 7.33 (m, 1H), 7.12 – 7.05 (m, 2H), 6.98 (dd, *J* = 8.2, 2.3 Hz, 1H), 6.48 (s, 1H), 4.13 (q, *J* = 7.1 Hz, 2H), 3.88 – 3.72 (m, 2H), 3.44 – 3.28 (m, 2H), 3.16 – 3.05 (m, 2H), 2.90 – 2.76 (m, 2H), 2.47 (ddd, *J* = 14.2, 9.5, 4.6 Hz, 1H), 2.40 – 2.24 (m, 3H), 1.50 (s, 9H), 1.24 (t, *J* = 7.1 Hz, 3H). **^{13}C NMR** (126 MHz, $CDCl_3$) δ 157.8, 155.7, 152.9, 146.5, 138.6, 137.7, 137.6, 136.9, 134.1, 133.9, 130.0, 122.2, 119.2, 116.4, 80.7, 61.4, 45.0, 45.0, 32.2, 31.7, 30.9, 30.7, 28.5, 14.8. **LC-MS**: t_r = 3.74 min, purity: >99%, [M+H]+ m/z calc. 464.30, found 464.25.

ethyl 4-(8-amino-5,6-dihydro-11H-benzo[5,6]cyclohepta[1,2-b]pyridin-11-ylidene)piperidine-1-carboxylate (23)

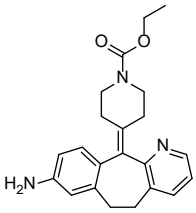

This compound was synthetised according to general procedure **B** using protected amine **22** (486 mg, 1.05 mmol, 1.0 eq), HCl in dioxane (2.6 mL, 10.50 mmol, 10.0 eq), MeOH (15 mL) and a reaction time of 17h. This gave **23** (375 mg, 98%) as a yellow powder. **^{1}H NMR** (500 MHz, $CDCl_3$) δ 8.38 (dd, *J* = 4.8, 1.7 Hz, 1H), 7.44 (dd, *J* = 7.7, 1.7 Hz, 1H), 7.07 (dd, *J* = 7.6, 4.8 Hz, 1H), 7.00 – 6.95 (m, 1H), 6.52 – 6.47 (m, 2H), 4.13 (q, *J* = 7.1 Hz, 2H), 3.91 – 3.68 (m, 2H), 3.38 – 3.28 (m, 2H), 3.17 – 3.04 (m, 2H), 2.86 – 2.67 (m, 2H), 2.50 – 2.33 (m, 3H), 2.27 (ddd, *J* = 14.6, 4.5 Hz, 1H), 1.24 (t, *J* = 7.1 Hz, 3H). **^{13}C NMR** (126 MHz, $CDCl_3$) δ 158.5, 155.7, 146.3, 145.8, 138.6, 137.4, 134.0, 130.7, 129.3, 122.1, 115.6, 113.0, 61.4, 45.1, 45.0, 32.3, 31.7, 30.8, 30.7, 14.8. Two carbon signal nots are not visible (quaternary carbon atoms). **LC-MS**: t_r = 2.58 min, purity: >99%, $[M+H]^+$ m/z calc. 364.19, found 364.15.

ethyl (E)-4-(8-(phenyldiazenyl)-5,6-dihydro-11H-benzo[5,6]cyclohepta[1,2-b]pyridin-11-ylidene)piperidine-1-carboxylate (24)

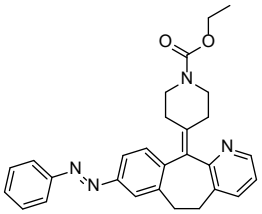

This compound was synthetised according to general procedure **A** using aniline **23** (375 mg, 1.03 mmol, 1.0 eq), PhNO (173 mg, 1.62 mmol, 1.6 eq), AcOH (0.24 mL, 4.1 mmol, 4.0 eq), PhMe (10 mL) and a reaction time of 72h. The crude product was purified using normal-phase column chromatography (5% -> 40% EtOAc:MeOH:Et_3N (90:5:5) in cHex). This gave **24** as an orange solid (170 mg, 36%). **^{1}H NMR** (600 MHz, $CDCl_3$) δ 8.43 (dd, *J* = 4.8, 1.6 Hz, 1H), 7.91 – 7.85 (m, 2H), 7.77 – 7.71 (m, 2H), 7.54 – 7.42 (m, 4H), 7.36 (d^{Δ}, *J* = 8.6 Hz, 1H), 7.13 (dd, *J* = 7.7, 4.8 Hz, 1H), 4.14 (q, *J* = 7.1 Hz, 2H), 3.92 – 3.76 (m, 2H), 3.56 – 3.48 (m, 1H), 3.41 (ddd, *J* = 15.9, 8.6, 4.6 Hz, 1H), 3.17 (ddd, *J* = 13.1, 9.0, 3.7 Hz, 2H), 3.01 – 2.89 (m, 2H), 2.54 (ddd, *J* = 14.0, 9.4, 4.6 Hz, 1H), 2.47 – 2.31 (m, 3H), 1.25 (t, *J* = 7.1 Hz, 3H). **^{13}C NMR** (151 MHz, $CDCl_3$) δ 156.9, 155.7, 152.8, 152.1, 146.7, 142.4, 138.9, 138.2, 138.0, 134.6, 133.8, 131.1, 130.3, 129.2, 123.2, 122.9, 122.5, 121.2, 61.5, 45.0, 44.9, 32.0, 31.9, 31.0, 30.8, 14.8. **LC-MS**: t_r = 4.48 min, purity: 98%, $[M+H]^+$ m/z calc. 453.22 found 453.25, λ_{max}: 329 nm. **HRMS**: $[M+H]^+$ calc. for $C_{25}H_{25}N_4$: 381.2074, found 381.2076.

(E)-8-(phenyldiazenyl)-11-(piperidin-4-ylidene)-6,11-dihydro-5H-benzo[5,6]cyclohepta[1,2-b]pyridine (11b)

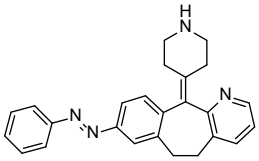

This compound was synthetised according to general procedure **D** using protected amine **24** (113 mg, 0.25 mmol, 1.0 eq), KOH (140 mg, 2.50 mmol, 10.0 eq), EtOH (8 mL), water (2 mL) and a reaction time of 100h. The crude product was purified using normal-phase column chromatography (3.5% -> 6.5% MeOH + NH_3 in DCM). This yielded **11b** as an orange solid (58 mg, 61%). **^{1}H NMR** (500 MHz, $CDCl_3$) δ 8.41 (dd, *J* = 4.8, 1.7 Hz, 1H), 7.91 – 7.85 (m, 2H), 7.76 – 7.69 (m, 2H), 7.50 (ddd, *J* = 8.3, 6.4, 1.8 Hz, 2H), 7.49 – 7.42 (m, 3H), 7.38 – 7.32 (m, 1H), 7.09 (dd, *J* = 7.7, 4.8 Hz, 1H), 3.54 (ddd, *J* = 13.2, 8.7, 4.5 Hz, 1H), 3.43 (ddd, *J* = 15.6, 7.0, 4.3 Hz, 1H), 3.10 (dddd, *J* = 16.4, 12.0, 4.8, 4.7 Hz, 2H), 3.01 – 2.86 (m, 2H), 2.75 (dddd, *J* = 13.0, 9.4, 4.2, 4.2 Hz, 2H), 2.53 – 2.34 (m, 4H). **^{13}C NMR** (126 MHz, $CDCl_3$) δ 157.4, 152.9, 152.0, 146.8, 142.6, 139.1, 138.9, 137.6, 133.8, 133.6, 131.0, 130.4, 129.2, 123.3, 122.9, 122.3, 121.0, 48.1, 48.1, 32.6, 32.3, 32.1, 31.8. **LC-MS**: t_r = 3.29 min, purity > 99%, $[M+H]^+$ calculated 381.21, found 381.20, λ_{max}: 329 nm. **HRMS**: $[M+H]^+$ calc. for $C_{28}H_{29}N_4$: 381.2079, found 381.2076.

ethyl 4-(8-chloro-9-nitro-5,6-dihydro-11*H*-benzo[5,6]cyclohepta[1,2-*b*]pyridin-11-ylidene)piperidine-1-carboxylate (25) and ethyl 4-(8-chloro-7-nitro-5,6-dihydro-11*H*-benzo[5,6]cyclohepta[1,2-*b*]pyridin-11-ylidene)piperidine-1-carboxylate (28)

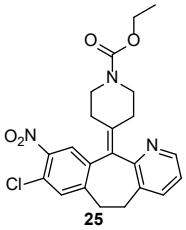

25
major

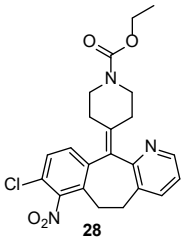

28
minor

Loratadine (**7**, 6.28 g, 16.4 mmol, 1.0 eq) was dissolved in conc. H_2SO_4 (30 mL). The solution was cooled between -10 °C and -5 °C. To this solution was slowly added solid KNO_3 (1.66 g, 16.4 mmol, 1.0 eq), while keeping the temperature between -10 °C and -5 °C. The mixture was stirred for 3 h in this temperature range, after which it was warmed to rt and stirred for 17 h at rt. The mixture was poured onto crushed ice and made basic using aq. NH_4OH (28-30 wt%). The resulting mixture was extracted three times with DCM. The combined organic layers were washed with brine, dried over Na_2SO_4, filtered, and concentrated under reduced pressure. The two products were separated using flash column chromatography (20% -> 100% EtOAc in cHex). Compound **25** (5.665 g, 81%) was obtained as a white solid and compound **28** (640 mg, 9%) as a yellow solid. Compound **25** (major): **^{1}H NMR** (500 MHz, $CDCl_3$) δ 8.43 (dd, *J* = 4.8, 1.7 Hz, 1H), 7.79 – 7.73 (m, 1H), 7.48 (dd, *J* = 7.7, 1.7 Hz, 1H), 7.40 – 7.34 (m, 1H), 7.15 (dd, *J* = 7.7, 4.8 Hz, 1H), 4.14 (q, *J* = 7.1 Hz, 2H), 3.89 – 3.75 (m, 2H), 3.55 – 3.32 (m, 2H), 3.17 (dddd, *J* = 18.5, 13.3, 9.3, 3.9 Hz, 2H), 2.88 (dddd, *J* = 14.0, 10.5, 8.4, 5.4 Hz, 2H), 2.52 (ddd, *J* = 14.1, 9.4, 4.7 Hz, 1H), 2.42 (ddd, *J* = 14.0, 9.3, 4.7 Hz, 1H), 2.35 – 2.24 (m, 2H), 1.25 (t, *J* = 7.1 Hz, 3H).**^{13}C NMR** (126 MHz, $CDCl_3$) δ 156.1, 155.6, 147.2, 145.6, 144.5, 140.0, 138.9, 137.8, 133.1, 132.5, 132.2, 126.6, 125.8, 122.9, 61.6, 44.7, 31.8, 31.0, 30.9, 30.7, 14.8. **LC-MS:** t_r = 4.00 min, purity 95%, $[M+H]^+$ m/z calc. 428.13, found 428.10.

Compound **28** (minor): **^{1}H NMR** (500 MHz, $CDCl_3$) δ 8.43 (dd, *J* = 4.7, 1.7 Hz, 1H), 7.47 (d^{Δ}, *J* = 7.5 Hz, 1H), 7.33 (d, *J* = 8.3 Hz, 1H), 7.27 (d, *J* = 8.3 Hz, 1H), 7.16 (dd, *J* = 7.7, 4.8 Hz, 1H), 4.14 (q, *J* = 7.1 Hz, 2H), 3.89 – 3.76 (m, 2H), 3.40 – 3.28 (m, 2H), 3.18 (dddd, *J* = 13.1, 9.3, 6.8, 3.9 Hz, 2H), 2.96 (ddd, *J* = 13.8, 13.1, 5.5 Hz, 1H), 2.76 (ddd, *J* = 15.1, 7.6, 4.4 Hz, 1H), 2.53 (ddd, *J* = 14.1, 9.4, 4.6 Hz, 1H), 2.42 – 2.23 (m, 3H), 1.25 (t, *J* = 7.1 Hz, 3H). **^{13}C NMR** (126 MHz, $CDCl_3$) δ 155.6, 155.4, 149.8, 147.0, 140.6, 138.4, 132.9, 131.6, 131.1, 128.3, 123.7, 122.9, 61.6, 44.8, 31.1, 30.8, 27.0, 14.8. A signal for one quaternary carbon is missing. **LC-MS:** t_r = 4.14 min, purity 99%, $[M+H]^+$ m/z calc. 428.13, found 428.10.

8-chloro-9-nitro-11-(piperidin-4-ylidene)-6,11-dihydro-5H-benzo[5,6]cyclohepta[1,2-b]pyridine (26)

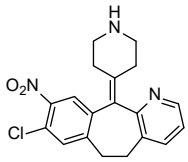

Protected amine **25** (3.00 g, 7.01 mmol, 1.0 eq) was dissolved in conc. HCl (12.0 mL, 139 mmol, 19.9 eq). The solution was heated at 80 °C for 24 h. The mixture was made basic with aq. NH_4OH (28-30 wt%). The resulting mixture was extracted three times with DCM. The combined organic layers were washed with brine, dried over Na_2SO_4, filtered, and concentrated under reduced pressure. This yielded **26** as a yellow solid (2.23 g, 89%). **^{1}H NMR** (500 MHz, CD_3OD) δ 8.36 (dd, J = 4.9, 1.6 Hz, 1H), 7.75 – 7.71 (m, 1H), 7.69 (dd, J = 7.8, 1.6 Hz, 1H), 7.53 – 7.49 (m, 1H), 7.29 (dd, J = 7.7, 4.9 Hz, 1H), 3.54 – 3.40 (m, 2H), 3.06 – 2.88 (m, 4H), 2.69 (dddd, J = 33.3, 12.7, 9.4, 3.7 Hz, 2H), 2.47 – 2.28 (m, 3H), 2.24 – 2.15 (m, 1H). **^{13}C NMR** (126 MHz, CD_3OD) δ 157.9, 147.5, 146.9, 146.1, 139.8, 139.6, 135.7, 133.9, 131.5, 127.3, 126.0, 124.5, 48.2, 48.0, 32.9, 32.8, 32.7, 31.3. **LC-MS:** t_r = 2.86 min, purity 98%, $[M+H]^+$ m/z calc. 356.11, found 356.10.

tert-butyl 4-(8-chloro-9-nitro-5,6-dihydro-11H-benzo[5,6]cyclohepta[1,2-b]pyridin-11-ylidene)piperidine-1-carboxylate (27)

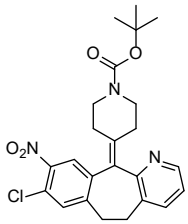

Amine **26** (1.87 g, 5.26 mmol, 1.0 eq) was dissolved in DCM (48 mL). Et_3N (0.80 mL, 5.75 mmol, 1.1 eq) and Boc_2O (1.36 g, 6.24 mmol, 1.2 eq) were added. The solution was stirred at rt for 2 h. The solution was diluted with DCM and washed with water (3 x 50 mL). The organic layer was washed with brine, dried over Na_2SO_4, filtered, and concentrated under reduced pressure. This gave **27** as a yellow solid (2.25 g, 94%). **^{1}H NMR** (500 MHz, $CDCl_3$) δ 8.43 (dd, *J* = 4.8, 1.7 Hz, 1H), 7.78 – 7.74 (m, 1H), 7.47 (dd, *J* = 7.7, 1.7 Hz, 1H), 7.37 – 7.33 (m, 1H), 7.14 (dd, *J* = 7.7, 4.8 Hz, 1H), 3.83 – 3.74 (m, 2H), 3.50 – 3.34 (m, 2H), 3.10 (dddd, *J* = 13.2, 13.2, 10.4, 3.6 Hz, 2H), 2.94 – 2.82 (m, 2H), 2.45 (m, 2H), 2.30 (dddd, *J* = 14.5, 5.2 Hz, 2H), 1.45 (s, 9H). **^{13}C NMR** (126 MHz, $CDCl_3$) δ 156.3, 154.8, 147.3, 145.6, 144.5, 140.3, 139.0, 137.7, 133.0, 132.5, 132.0, 126.7, 125.8, 122.9, 79.9, 45.9, 31.9, 31.0, 31.0, 30.8, 28.5. **LC-MS:** t_r = 4.54 min, purity 97 %, $[M+H]^+$ m/z calc. 456.16 found 456.20.

tert-butyl 4-(9-amino-8-chloro-5,6-dihydro-11H-benzo[5,6]cyclohepta[1,2-b]pyridin-11-ylidene)piperidine-1-carboxylate (33)

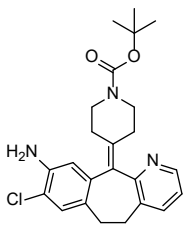

This compound was synthetised according to general procedure **C** using nitro-compound **27** (2.00 g, 4.39 mmol, 1.0 eq), Fe (980 mg, 17.55 mmol, 4.0 eq), NH_4Cl (821 mg, 15.4 mmol, 3.5 eq), 1,4-dioxane (24 mL), EtOH (20 mL), water (20 mL) and a reaction time of 3h. This gave **33** as a white solid (1.67 g, 89%). **^{1}H NMR** (500 MHz, $CDCl_3$) δ 8.38 (dd, *J* = 4.8, 1.7 Hz, 1H), 7.42 (dd, *J* = 7.7, 1.7 Hz, 1H), 7.08 (dd, *J* = 7.7, 4.8 Hz, 1H), 7.05 (s, 1H), 6.61 (s, 1H), 3.91 (s, 2H), 3.77 (s, 2H), 3.34 – 3.23 (m, 2H), 3.05 (dddd, *J* = 13.4, 9.8, 9.7, 4.0 Hz, 2H), 2.81 (ddd, *J* = 16.8, 9.5, 4.7 Hz, 1H), 2.73 – 2.64 (m, 1H), 2.48 – 2.30 (m, 3H), 2.26 (ddd, *J* = 14.2, 4.6 Hz, 1H), 1.45 (s, 9H). **^{13}C NMR** (126 MHz, $CDCl_3$) δ 157.2, 154.9,

146.5, 140.9, 139.0, 137.9, 137.5, 134.3, 133.8, 129.6, 128.6, 122.3, 118.3, 116.4, 79.7, 45.3, 32.1, 30.9, 30.8, 30.7, 28.6. **LC-MS:** t_r = 3.86 min, purity: 95%, $[M+H]^+$ m/z calc. 426.19, found 426.20.

tert-butyl (E)-4-(8-chloro-9-(phenyldiazenyl)-5,6-dihydro-11H-benzo[5,6]cyclohepta[1,2-b]pyridin-11-ylidene)piperidine-1-carboxylate (34)

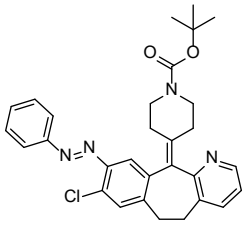

This compound was synthetised according to general procedure **A** using aniline **33** (300 mg, 0.70 mmol, 1.0 eq), PhNO (83 mg, 0.78 mmol, 1.1 eq) and AcOH (0.16 mL, 2.8 mmol, 4.0 eq) and PhMe (7 mL). The mixture was stirred for 14 d at 80 °C, after which approximately 40% consumption of the starting material was achieved. The reaction mixture was made basic using satd. aq. $NaHCO_3$ (40 mL). The resulting solution was extracted with EtOAc (3 x 40 mL). The combined organic layers were washed with brine, dried over Na_2SO_4, filtered, and concentrated under reduced pressure. The crude product was purified using normal-phase column chromatography (10% -> 35% EtOAc in cHex). This gave **34** as an orange solid (90 mg, 25%).**^{1}H NMR** (500 MHz, $CDCl_3$) δ 8.43 (dd, *J* = 4.9, 1.7 Hz, 1H), 7.95 – 7.89 (m, 2H), 7.63 (m, 1H), 7.56 – 7.43 (m, 4H), 7.38 (m, 1H), 7.12 (dd, *J* = 7.7, 4.8 Hz, 1H), 3.78 (m, 2H), 3.51 – 3.35 (m, 2H), 3.12 (ddd, *J* = 13.0, 9.2, 4.0 Hz, 2H), 2.94 – 2.84 (m, 2H), 2.53 (ddd, *J* = 14.0, 9.3, 4.6 Hz, 1H), 2.44 – 2.28 (m, 3H), 1.45 (s, 9H). **^{13}C NMR** (126 MHz, $CDCl_3$) δ 154.8, 152.7, 146.7, 146.7, 142.2, 138.5, 137.5, 134.1, 133.3, 131.4, 130.9, 129.1, 123.3, 122.4, 118.2, 79.6, 45.2, 31.6, 31.5, 30.9, 30.7, 28.4. The signals for three quaternary carbon atoms are missing. **LC-MS:** t_r = 5.41 min, purity 98%, λ_{max}: 325 nm, $[M+H]^+$ m/z calc. 515.22, found 515.30.

(E)-8-chloro-9-(phenyldiazenyl)-11-(piperidin-4-ylidene)-6,11-dihydro-5H-benzo[5,6]cyclohepta[1,2-b]pyridine (11a)

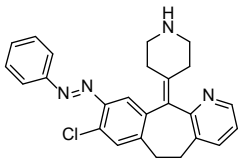

This compound was synthetised according to general procedure **B** using protected amine **34** (65 mg, 0.13 mmol, 1.0 eq), HCl in 1,4-dioxane (0.32 mL, 1.3 mmol, 10.0 eq), MeOH (1.3 mL). The mixture was stirred at rt for 20 h. This gave **11a** as an orange solid (37 mg, 71%). **^{1}H NMR** (600 MHz, $CDCl_3$) δ 8.41 (dd, *J* = 4.8, 1.7 Hz, 1H), 7.94 – 7.89 (m, 2H), 7.64 – 7.61 (m, 1H), 7.54 – 7.46 (m, 3H), 7.44 (dd, *J* = 7.7, 1.7 Hz, 1H), 7.39 – 7.35 (m, 1H), 7.09 (dd, *J* = 7.7, 4.7 Hz, 1H), 3.52 – 3.45 (m, 1H), 3.45 – 3.37 (m, 1H), 3.10 (dddd, *J* = 17.3, 11.8, 4.3, 4.3 Hz, 2H), 2.92 – 2.84 (m, 2H), 2.81 – 2.71 (m, 2H), 2.49 (ddd, *J* = 13.9, 9.6, 4.4 Hz, 1H), 2.43 – 2.34 (m, 3H). **^{13}C NMR** (151 MHz, $CDCl_3$) δ 157.2, 152.8, 147.0, 146.7, 142.5, 139.4, 138.8, 137.6, 134.1, 133.4, 132.6, 131.5, 131.0, 129.2, 123.4, 122.3, 118.4, 48.0, 47.9, 32.4, 32.2, 31.8, 31.6. **LC-MS:** t_r = 3.54 min, purity 98%, λ_{max}: 330 nm, $[M+H]^+$ m/z calc. 415.16, found 415.15. **HRMS**: $[M+H]^+$ calc. for $C_{25}H_{24}ClN_4$: 415.1684, found 415.1685.

8-chloro-7-nitro-11-(piperidin-4-ylidene)-6,11-dihydro-5H-benzo[5,6]cyclohepta[1,2-b]pyridine (29)

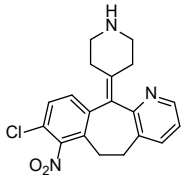

Protected amine **28** (640 mg, 1.50 mmol, 1.0 eq) was dissolved in conc. HCl (2.5 mL, 29.0 mmol, 19 eq). The solution was heated at 80 °C for 22 h. The pH was adjusted to 8 using aq. NH_4OH (28-30 wt%), after which the reaction mixture was diluted with water. The mixture was extracted with DCM (3 x 30 mL). The combined organic layers were washed with brine, dried over Na_2SO_4, filtered, and concentrated under reduced pressure. This yielded **29** as a yellow solid (475 mg, 89%). **^{1}H NMR** (500 MHz, $CDCl_3$) δ 8.42 (dd, *J* = 4.7, 1.7 Hz, 1H), 7.44 (dd, *J* = 7.8, 1.7 Hz, 1H), 7.31 (d, *J* = 8.3 Hz, 1H), 7.27 (d, *J* = 8.5 Hz, 1H), 7.12 (dd, *J* = 7.7, 4.7 Hz, 1H), 3.41 – 3.30 (m, 2H), 3.09 (ddd, *J* = 16.8, 8.5, 4.8 Hz, 2H), 3.00 – 2.87 (m, 1H), 2.75 (dddd, *J* = 12.3, 10.8, 9.2, 4.9 Hz, 3H), 2.49 (ddd, *J* = 14.1, 9.6, 4.5 Hz, 1H), 2.42 – 2.27 (m, 3H). **^{13}C NMR** (126 MHz, $CDCl_3$) δ 155.9, 149.8, 147.2, 141.1, 140.8, 138.0, 132.8, 131.7, 131.6, 131.2, 128.1, 123.4, 122.7, 47.9, 47.9, 32.5, 32.2, 30.7, 27.0. **LC-MS**: t_r = 2.99 min, purity 98%, $[M+H]^+$ m/z calc. 356.10, found 356.11.

tert-butyl 4-(8-chloro-7-nitro-5,6-dihydro-11H-benzo[5,6]cyclohepta[1,2-b]pyridin-11-ylidene)piperidine-1-carboxylate (30)

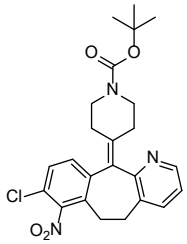

Amine **29** (459 mg, 1.29 mmol, 1.0 eq) was dissolved in DCM (11.5 mL). To this solution were added Et_3N (0.20 mL, 1.4 mmol, 1.1 eq) and Boc_2O (310 mg, 1.42 mmol, 1.1 eq). The solution was stirred at rt for 2 h. The mixture was diluted with DCM and washed with water (3 x 25 mL). The organic layer was washed with brine, dried over Na_2SO_4, filtered, and concentrated under reduced pressure. This yielded **30** as a light brown solid (484 mg, 82%). **^{1}H NMR** (500 MHz, $CDCl_3$) δ 8.42 (dd, *J* = 4.8, 1.7 Hz, 1H), 7.46 (dd, *J* = 7.8, 1.7 Hz, 1H), 7.32 (d, *J* = 8.2 Hz, 1H), 7.27 (d, *J* = 8.0 Hz, 1H), 7.14 (dd, *J* = 7.7, 4.8 Hz, 1H), 3.86 – 3.73 (m, 2H), 3.40 – 3.28 (m, 2H), 3.16 – 3.06 (m, 2H), 2.99 – 2.90 (m, 1H), 2.76 (ddd, *J* = 15.1, 7.6, 4.3 Hz, 1H), 2.51 (ddd, *J* = 14.2, 9.4, 4.7 Hz, 1H), 2.40 – 2.22 (m, 3H), 1.45 (s, 9H). **^{13}C NMR** (126 MHz, $CDCl_3$) δ 155.4, 154.7, 149.7, 146.9, 140.5, 140.2, 138.1, 132.7, 132.4, 131.5, 131.0, 128.1, 123.5, 122.7, 79.8, 45.8, 31.0, 30.6, 28.4, 26.9. **LC-MS**: t_r = 4.69 min, purity: 98%, $[M+H]^+$ m/z calc. 456.16, found 456.15.

tert-butyl 4-(7-amino-8-chloro-5,6-dihydro-11H-benzo[5,6]cyclohepta[1,2-b]pyridin-11-ylidene)piperidine-1-carboxylate (31)

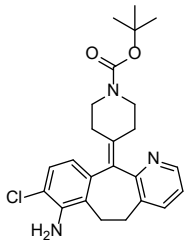

This compound was synthetised according to general procedure **C** using nitro-compound **30** (463 mg, 1.02 mmol, 1.0 eq), Fe (199 mg, 3.57 mmol, 3.5 eq), NH_4Cl (217 mg, 4.08 mol, 4.0 eq), 1,4-dioxane (11 mL), EtOH (9 mL), water (6 mL) and a reaction time of 2h. This yielded **31** as a yellow solid (350 mg, 81%). **^{1}H NMR** (500 MHz, $CDCl_3$) δ 8.42 (dd, *J* = 4.9, 1.7 Hz, 1H), 7.53 (dd, *J* = 7.6, 1.6 Hz, 1H), 7.18 – 7.10 (m, 2H), 6.64 (d, *J* = 8.3 Hz, 1H), 4.06 (s, 2H), 3.76 (s, 2H), 3.46 (ddd, *J* = 15.1, 11.3, 4.3 Hz, 1H), 3.15 (ddd, *J* = 13.1, 8.5, 4.7 Hz, 1H), 3.09 (ddd, *J* = 8.7, 3.2, 3.2 Hz, 2H), 2.89 (ddd, *J* = 14.6, 6.2, 4.5 Hz, 1H), 2.63 (ddd, *J* = 16.0, 11.3, 4.5 Hz, 1H), 2.52 – 2.35 (m, 3H), 2.22 – 2.13 (m, 1H), 1.47 (s, 9H). **^{13}C NMR** (126 MHz, $CDCl_3$) δ 159.4, 154.9, 146.9, 141.1, 137.0, 136.4, 134.6, 133.7, 126.7, 122.5, 122.4, 120.8, 118.8, 79.7, 45.2, 30.8, 30.2, 28.6, 28.4. One signal for a quaternary carbon atom is missing. **LC-MS**: t_r = 3.73 min, purity: 97%, [M+H]+ m/z calc. 426.19, found 426.30.

tert-butyl (E)-4-(8-chloro-7-(phenyldiazenyl)-5,6-dihydro-11H-benzo[5,6]cyclohepta[1,2-b]pyridin-11-ylidene)piperidine-1-carboxylate (32)

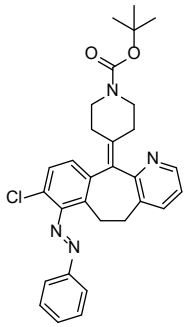

Aniline **31** (200 mg, 0.47 mmol, 1.0 eq) was dissolved in THF (2.4 mL). To this solution was added BF_3•Et_2O (87 µL, 0.70 mmol, 1.5 eq). The mixture was stirred at 0 °C for 15 min. Subsequently, *t*BuONO (67 µL, 0.56 mmol, 1.2 eq) was added and the solution was stirred at rt for 2 h. The solution was cooled to -70 °C and PhMgBr (172 µL, 0.52 mmol, 1.1 eq) was added. The reaction mixture was warmed to rt and stirred for 18 h. The reaction mixture was diluted with water and extracted with EtOAc (3 x 40 mL). The combined organic layers were washed with brine, dried over Na_2SO_4, filtered, and concentrated under reduced pressure. The crude product was purified using reverse-phase column chromatography (5->90% MeCN + 0.1% H_2COH in H_2O + 0.1% H_2COH). The desired fractions were combined, made basic with satd. aq. $NaHCO_3$ and extracted three times with EtOAc. The combined organic layers were washed with brine, dried over Na_2SO_4, filtered, and concentrated under reduced pressure. This yielded **32** as an orange oil (35 mg, 14%). **^{1}H NMR** (600 MHz, $CDCl_3$) δ 8.41 (dd, J = 4.8, 1.6 Hz, 1H), 7.97 – 7.92 (m, 2H), 7.62 – 7.52 (m, 3H), 7.47 – 7.40 (m, 1H), 7.31 (d, J = 8.2 Hz, 1H), 7.16 – 7.07 (m, 2H), 3.92 – 3.66 (m, 2H), 3.30 (ddd, J = 16.2, 6.8, 4.3 Hz, 1H), 3.21 – 3.06 (m, 3H), 2.96 – 2.79 (m, 2H), 2.52 (ddd, J = 14.1, 9.2, 4.6 Hz, 1H), 2.44 – 2.32 (m, 3H), 1.46 (s, 9H). **^{13}C NMR** (151 MHz, $CDCl_3$) δ 156.3, 154.9, 152.5, 150.2, 146.6, 140.6, 138.7, 138.2, 133.9, 133.6, 132.2, 130.9, 129.4, 129.1, 128.2, 123.1, 122.5, 79.8, 45.3, 44.5, 31.5, 31.1, 30.8, 28.6, 26.7. **LC-MS**: t_r = 5.15 min, purity: 95%, $[M+H]^+$ m/z calc. 515.30, found 515.30, λ_{max}: 277 nm.

(E)-8-chloro-7-(phenyldiazenyl)-11-(piperidin-4-ylidene)-6,11-dihydro-5H-benzo[5,6]cyclohepta[1,2-b]pyridine (11c)

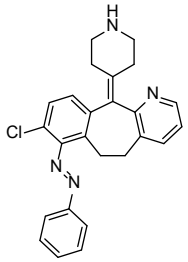

This compound was synthetised according to general procedure **B** using protected amine **32** (35 mg, 0.067 mmol, 1.0 eq), HCl in dioxane (0.17 mL, 0.68 mmol, 10.0 eq), MeOH (0.7 mL) and a reaction time of 22h. The crude product was purified using flash column chromatography (4% -> 6% MeOH + NH_3 in DCM). This yielded **11c** as an orange solid (16 mg, 57%). **^{1}H NMR** (600 MHz, $(CD_3)_2SO$) δ 8.53 – 8.50 (m, 1H), 8.38 – 8.32 (m, 1H), 7.91 (dd, *J* = 6.6, 3.0 Hz, 2H), 7.65 (dd, *J* = 5.2, 1.9 Hz, 3H), 7.54 (dd, *J* = 7.7, 1.7 Hz, 1H), 7.42 (d, *J* = 8.2 Hz, 1H), 7.18 (dd, *J* = 7.7, 4.7 Hz, 1H), 7.11 (d, *J* = 8.2 Hz, 1H), 3.32 – 3.24 (m, 1H), 3.11 (ddd, *J* = 14.9, 10.0, 4.5 Hz, 1H), 2.91 – 2.78 (m, 3H), 2.66 (ddd, *J* = 15.1, 7.5, 4.5 Hz, 1H), 2.58 (m, 2H), 2.31 – 2.09 (m, 4H). **^{13}C NMR** (151 MHz, $(CD_3)_2SO$) δ 156.7, 151.9, 149.5, 146.4, 140.8, 140.1, 137.6, 132.9, 132.6, 131.2, 130.7, 129.7, 129.4, 127.5, 122.8, 122.6, 122.2, 47.9, 47.8, 32.7, 32.4, 30.5, 26.6. **LC-MS**: t_r = 3.49 min, purity: 95%, $[M+H]^+$ m/z calc. 415.17, found 415.15, λ_{max}: 278 nm (not the π-π* band). **HRMS**: $[M+H]^+$ calc. for $C_{25}H_{24}ClN_4$: 415.1684, found 415.1691.

(E)-(4-(phenyldiazenyl)phenyl)methanol (37)

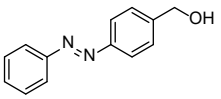

4-Aminobenzylalcohol (**35**, 2.58 g, 20.9 mmol, 1.0 eq) was dissolved in glacial AcOH (100 mL). To this solution was added PhNO (2.55 g, 23.8 mmol, 1.1 eq). The solution was stirred for 66 h at rt. The solution was concentrated under reduced pressure. The crude product was dissolved in EtOAc. The mixture was made basic using satd. aq. $NaHCO_3$ and extracted three times with EtOAc. The combined organic layers were washed with brine, dried over Na_2SO_4, filtered, and concentrated under reduced pressure. The crude product was purified using flash column chromatography (100% DCM) to afford alcohol **37** as an orange solid (530 mg, 12%). **^{1}H NMR** (600 MHz, $CDCl_3$) δ 7.95 – 7.90 (m, 4H), 7.55 – 7.50 (m, 4H), 7.50 – 7.46 (m, 1H), 4.81 – 4.78 (m, 2H), 1.80 (t, *J* = 5.5 Hz, 1H). **^{13}C NMR** (151 MHz, $CDCl_3$) δ 152.75, 152.23, 143.94, 131.16, 129.24, 127.58, 123.23, 122.98, 65.04. **LC-MS:** t_r = 4.42 min, purity >99%, λ_{max}: 325 nm, $[M+H]^+$ m/z calc. 213.10, found 213.00.

(E)-4-(phenyldiazenyl)benzaldehyde (39)

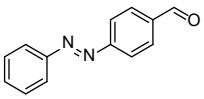

Alcohol **37** (530 mg, 2.50 mmol, 1.0 eq) was dissolved in DCM (45 mL). To this mixture was added DMP (2.457 g, 5.79 mmol, 2.3 eq). The solution was stirred at rt for 1.5 h. The reaction mixture was diluted with DCM, made basic using satd. aq. $NaHCO_3$ and extracted three times with DCM. The combined organic layers were washed with brine, dried over Na_2SO_4, filtered, and concentrated under reduced pressure. The crude product was purified using normal-phase column chromatography (0 -> 10% EtOAc in cHex). This yielded the aldehyde **30** as an orange solid (469 mg, 89%). **^{1}H NMR** (600 MHz, $CDCl_3$) δ 10.11 (s, 1H), 8.06 – 8.03 (m, 4H), 7.99 – 7.95 (m, 2H), 7.58 – 7.51 (m, 3H). **^{13}C NMR** (151 MHz, $CDCl_3$) δ 191.8, 156.0, 152.7, 137.6, 132.1, 130.9, 129.4, 123.5, 123.4. **LC-MS:** t_r = 5.13 min, purity > 99%, λ_{max}: 327 nm, $[M+H]^+$ m/z calc. 211.08, found 210.80.

(*E*)-8-chloro-11-(1-(4-(phenyldiazenyl)benzyl)piperidin-4-ylidene)-6,11-dihydro-5*H*-benzo[5,6]cyclohepta[1,2-*b*]pyridine (12a)

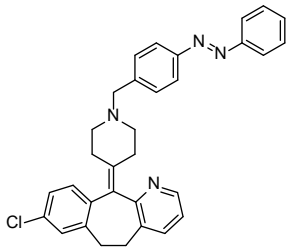

Aldehyde **39** (245 mg, 1.17 mmol, 1.7 eq) and desloratadine (**8**, 210 mg, 0.68 mmol, 1.0 eq) were dissolved in DCE (4.5 mL). The solution was purged with N_2 before the addition of $NaBH(OAc)_3$ (286 mg, 1.35 mmol, 2.0 eq) and a catalytic amount of AcOH (3 drops). The solution was stirred at rt for 16 h. The solution was made basic using satd. aq. $NaHCO_3$ and extracted with DCM thrice. The combined organic layers were washed with brine, dried over Na_2SO_4, filtered, and concentrated under reduced pressure. The crude product was purified using normal-phase column chromatography (0% to 10% MeOH in EtOAc). The title compound **4a** was obtained as an orange solid (87 mg, 26%). **^{1}H NMR** (600 MHz, $CDCl_3$) δ 8.4 (dd, *J* = 4.9, 1.7 Hz, 1H), 7.9 – 7.9 (m, 2H), 7.9 – 7.8 (m, 2H), 7.5 – 7.5 (m, 2H), 7.5 – 7.5 (m, 2H), 7.5 – 7.4 (m, 1H), 7.4 (dd, *J* = 7.7, 1.7 Hz, 1H), 7.2 – 7.1 (m, 2H), 7.1 (dd, *J* = 8.2, 2.0 Hz, 1H), 7.1 (dd, *J* = 7.6, 4.8 Hz, 1H), 3.6 (s, 2H), 3.5 – 3.3 (m, 2H), 2.9 – 2.8 (m, 2H), 2.8 – 2.7 (m, 2H), 2.6 (ddd, *J* = 14.1, 9.9, 4.2 Hz, 1H), 2.5 (ddd, *J* = 13.9, 9.7, 4.2 Hz, 1H), 2.4 – 2.3 (m, 2H), 2.2 – 2.1 (m, 2H). **^{13}C NMR** (151 MHz, $CDCl_3$) δ 157.7, 152.8, 152.0, 146.8, 141.9, 139.6, 139.0, 138.0, 137.4, 133.5, 132.8, 131.0, 131.0, 129.9, 129.2, 129.1, 126.1, 122.9, 122.9, 122.2, 62.6, 55.0, 54.9, 32.0, 31.6, 31.1, 30.9. One missing carbon. **LC-MS:** t_r = 4.00 min, purity 98%, λ_{max}: 318 nm, $[M+H]^+$ m/z calc. 505.21, found 505.20. **HRMS**: $[M+H]^+$ calc. for $C_{32}H_{30}ClN_4$: 505.2154, found 505.2165.

(*E*)-(3-(phenyldiazenyl)phenyl)methanol (38)

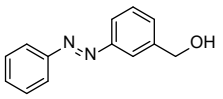

A solution of (3-aminophenyl)methanol (**36**, 3.00 g, 24.4 mmol) and PhNO (2.49 g, 23.2 mmol) in DCM (58 mL) and AcOH (58 mL) was stirred for 18 h at rt. The resulting mixture was concentrated and purified using normal-phase column chromatography (0 -> 10% EtOAc in cHex) to give the title compound **38** (3.420 g, 67%). **^{1}H NMR** (500 MHz, $CDCl_3$) δ 7.95 – 7.89 (m, 3H), 7.86 (ddd, *J* = 7.5, 1.8, 1.8 Hz, 1H), 7.57 – 7.45 (m, 5H), 4.89 – 4.76 (m, 2H), 1.98 (d, *J* = 5.1 Hz, 1H). **^{13}C NMR** (126 MHz, $CDCl_3$) δ 153.0, 152.7, 142.2, 131.2, 129.5, 129.4, 129.2, 123.0, 122.8, 120.7, 65.1. **LC-MS**: t_r = 4.40 min, purity: 97%, $[M+H]^+$ m/z calc. 213.10, found 213.00.

(*E*)-3-(phenyldiazenyl)benzaldehyde (40)

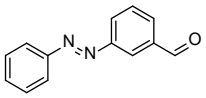

A mixture of alcohol **38** (3.40 g, 16.0 mmol) and MnO_2 (8.36 g, 96 mmol) in DCM (100 mL) was stirred at rt for 2 h. The reaction mixture was filtered over Celite and the filtrate was concentrated *in vacuo* to give the title compound **40** (2.508 g, 75%). **^{1}H NMR** (500 MHz, $CDCl_3$) δ 10.14 (s, 1H), 8.41 (dd, *J* = 1.8, 1.8 Hz, 1H), 8.19 (ddd, *J* = 7.9, 2.1, 1.3 Hz, 1H), 8.01 (ddd, *J* = 7.6, 1.4, 1.4 Hz, 1H), 7.99 – 7.93 (m, 2H), 7.70 (dd, *J* = 7.7, 7.7 Hz, 1H), 7.59 – 7.49 (m, 3H). **^{13}C NMR** (126 MHz, $CDCl_3$) δ 191.9, 153.1, 152.5, 137.5, 131.8, 131.2, 130.0, 129.4, 128.9, 124.0, 123.2. **LC-MS**: t_r = 5.08 min, purity: >99%, $[M+H]^+$ m/z calc. 211.09, found 211.00.

(*E*)-8-chloro-11-(1-(3-(phenyldiazenyl)benzyl)piperidin-4-ylidene)-6,11-dihydro-5*H*-benzo[5,6]cyclohepta[1,2-*b*]pyridine (12b)

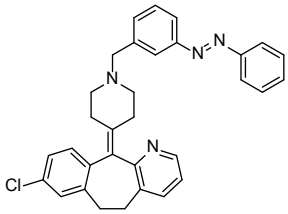

To a solution of aldehyde **40** (304 mg, 1.45 mmol), desloratadine (**8**, 150 mg, 0.48 mmol) and AcOH (221 µL) in DCM (4.8 mL) was added $NaBH(OAc)_3$. The reaction mixture was stirred for 2 h at rt. Satd. aq. $NaHCO_3$ (20 mL) was added. The organic layer was separated, dried over Na_2SO_4 and concentrated. The resulting crude compound was purified using normal-phase column chromatography (0 -> 40% EtOAc in cHex) to give the title compound **12b** as an orange solid (150 mg, 62%). **^{1}H NMR** (600 MHz, $CDCl_3$) δ 8.38 (dd, *J* = 4.8, 1.6 Hz, 1H), 7.93 – 7.89 (m, 2H), 7.87 – 7.84 (m, 1H), 7.82 – 7.77 (m, 1H), 7.54 – 7.49 (m, 2H), 7.49 – 7.44 (m, 3H), 7.42 (dd, *J* = 7.6, 1.7 Hz, 1H), 7.15 – 7.09 (m, 3H), 7.07 (dd, *J* = 7.6, 4.8 Hz, 1H), 3.61 (s, 2H), 3.45 – 3.33 (m, 2H), 2.87 – 2.73 (m, 4H), 2.55 (ddd, *J* = 14.2, 10.0, 4.3 Hz, 1H), 2.45 (ddd, *J* = 14.0, 9.9, 4.3 Hz, 1H), 2.40 – 2.30 (m, 2H), 2.25 – 2.13 (m, 2H). **^{13}C NMR** (151 MHz, $CDCl_3$) δ 157.8, 152.8, 152.8, 146.8, 139.8, 139.6, 139.2, 138.0, 137.3, 133.5, 132.8, 131.8, 131.1, 131.0, 129.2, 129.1, 126.1, 123.6, 123.0, 122.2, 121.8, 62.7, 55.0, 54.9, 32.0, 31.6, 31.2, 30.9. **LC-MS:** t_r = 3.92 min, purity >99%, λ_{max}: 316 nm, $[M+H]^+$ m/z calc. 505.21, found 505.25. **HRMS**: $[M+H]^+$ calc. for $C_{32}H_{30}ClN_4$: 505.2154, found 505.2159.

8-chloro-11-(1-(2-nitrobenzyl)piperidin-4-ylidene)-6,11-dihydro-5*H*-benzo[5,6]cyclohepta[1,2-*b*]pyridine (42)

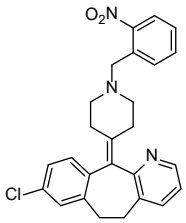

Desloratadine (**8**, 515 mg, 1.66 mmol, 1.0 eq) was dissolved in MeCN (5.5 mL). To this were added 2-nitrobenzyl bromide (391 mg, 1.81 mmol, 1.1 eq) and K_2CO_3 (313 mg, 2.27 mmol, 1.4 eq). The mixture was heated at reflux for 3 h. The mixture was concentrated under reduced pressure and the residue was dissolved in EtOAc. The mixture was washed with satd. aq. $NaHCO_3$ (30 mL) and brine (25 mL). The organic layer was dried over Na_2SO_4, filtered, and concentrated under reduced pressure. The crude product was purified with normal-phase column chromatography (60% -> 100% EtOAc in cHex). Product **42** was obtained as a dark brown solid (669 mg, 91%). ^{1}H NMR (600 MHz, $CDCl_3$)

δ 8.38 (dd, *J* = 4.8, 1.7 Hz, 1H), 7.81 (dd, *J* = 8.1, 1.3 Hz, 1H), 7.68 (d, *J* = 7.7 Hz, 1H), 7.53 (ddd, *J* = 7.6, 7.6, 1.3 Hz, 1H), 7.42 (dd, *J* = 7.6, 1.7 Hz, 1H), 7.40 – 7.34 (m, 1H), 7.18 – 7.09 (m, 3H), 7.07 (dd, *J* = 7.6, 4.8 Hz, 1H), 3.78 (s, 2H), 3.44 – 3.30 (m, 2H), 2.88 – 2.74 (m, 3H), 2.73 – 2.66 (m, 2H), 2.49 (ddd, *J* = 14.1, 9.9, 4.3 Hz, 1H), 2.40 (ddd, *J* = 14.0, 9.8, 4.3 Hz, 1H), 2.36 – 2.25 (m, 2H), 2.25 – 2.12 (m, 2H).**^{13}C NMR** (151 MHz, $CDCl_3$) δ 157.7 , 149.9, 146.7, 139.7, 138.7$^{\#}$, 137.9, 137.4, 134.3$^{\#}$, 133.6, 132.9, 132.8, 132.6, 131.0, 130.9, 129.1, 127.9, 126.1, 124.5, 122.2, 58.8, 55.0, 54.9, 31.9, 31.6, 31.1, 30.9.**LC-MS**: t_r = 3.31 min, purity: >99%, $[M+H]^+$ m/z calc. 446.16, found 446.15.

2-((4-(8-chloro-5,6-dihydro-11*H*-benzo[5,6]cyclohepta[1,2-*b*]pyridin-11-ylidene)piperidin-1-yl)methyl)aniline (43)

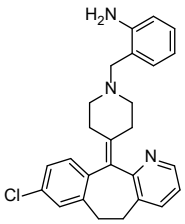

This compound was synthetised according to general procedure **C**, using nitro-compound **42** (649 mg, 1.46 mmol, 1.0 eq), Fe (460 mg, 8.24 mmol, 5.6 eq), NH_4Cl (308 mg, 5.76 mmol, 4.0 eq), 1,4-dioxane (24 mL), EtOH (14 mL), water (8.6 mL), and a reaction time of 3h. This yielded aniline **43** as a brown oil (620 mg, quant.). **^{1}H NMR** (500 MHz, $CDCl_3$) δ 8.37 (dd, *J* = 4.8, 1.7 Hz, 1H), 7.41 (dd, *J* = 7.6, 1.7 Hz, 1H), 7.15 (d, *J* = 1.3 Hz, 1H), 7.11 (d, *J* = 1.3 Hz, 2H), 7.09 – 7.05 (m, 2H), 6.96 – 6.91 (m, 1H), 6.67 – 6.60 (m, 2H), 4.98 (br s, 2H), 3.56 (s, 2H), 3.46 – 3.28 (m, 2H), 2.92 – 2.71 (m, 4H), 2.61 – 2.09 (m, 6H). **^{13}C NMR** (126 MHz, $CDCl_3$) δ 157.4, 147.2, 146.7, 139.6, 137.8, 137.5, 133.5, 132.9, 130.9, 130.7, 129.1, 128.8, 126.1, 122.3, 117.7, 115.9, 61.5, 54.5, 54.4, 31.8, 31.5, 30.7, 30.6. The signals for three quaternary carbon atoms are missing. **UPLC-MS:** t_r = 1.45 min, purity > 99%, $[M+H]^+$ m/z calc. 416.18, found 416.25.

(*E*)-8-chloro-11-(1-(2-(phenyldiazenyl)benzyl)piperidin-4-ylidene)-6,11-dihydro-5*H*-benzo[5,6]cyclohepta[1,2-*b*]pyridine (12c)

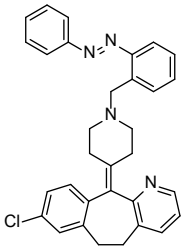

This compound was synthetised according to general procedure **A** with aniline **43** (200 mg, 0.481 mmol, 1.0 eq), PhNO (58 mg, 0.54 mmol, 1.1 eq), AcOH (0.11 mL, 1.9 mmol, 4.0 eq), PhMe (5 mL), and a reaction time of 16h. The crude product was purified using flash column chromatography (19:1 EtOAc:Et_3N). This yielded product **12c** as an orange solid (30 mg, 12%). **^{1}H NMR** (600 MHz, $CDCl_3$) δ 8.37 (dd, *J* = 4.8, 1.6 Hz, 1H), 7.92 – 7.86 (m, 2H), 7.66 – 7.60 (m, 2H), 7.52 (dd, *J* = 8.3, 6.5 Hz, 2H), 7.50 – 7.47 (m, 1H), 7.45 (ddd, *J* = 8.8, 7.6, 2.0 Hz, 1H), 7.41 (dd, *J* = 7.7, 1.7 Hz, 1H), 7.34 (dd$^{\Delta}$, *J* = 7.6, 7.5 Hz, 1H), 7.13 – 7.10 (m, 2H), 7.09 (dd, *J* = 8.1, 2.0 Hz, 1H), 7.06 (dd, *J* = 7.7, 4.7 Hz, 1H), 4.14 (s, 2H), 3.43 – 3.28 (m, 2H), 2.89 – 2.81 (m, 2H), 2.81 – 2.73 (m, 2H), 2.53 (ddd, *J* = 14.2, 10.0, 4.3 Hz, 1H), 2.43 (ddd, *J* = 14.0, 9.8, 4.2 Hz, 1H), 2.37 – 2.29 (m, 2H), 2.29 – 2.18 (m, 2H). **^{13}C NMR** (151 MHz, $CDCl_3$) δ 157.8, 153.0, 151.0, 146.7, 139.6, 139.0, 138.0, 137.4, 137.3, 133.5, 132.7, 132.5, 131.1, 131.0, 131.0, 130.9, 129.2, 129.1, 127.8, 126.1, 123.1, 122.2, 115.4, 56.6, 54.8, 54.7, 32.0, 31.6, 31.2, 31.0. **LC-MS**: t_r = 3.87 min, purity 98%, λ_{max}: 324 nm, $[M+H]^+$ m/z

calculated 505.21, found 505.20. **HRMS**: $[M+H]^+$ calc. for $C_{32}H_{30}ClN_4$: 505.2154, found 505.2168.

Chapter 5

Investigating the effect of positional arylazopyrazole isomers of a photoswitchable H_3R agonist

Lars C.P. Binkhorst, Ivana Josimovic, Henry F. Vischer, Maikel Wijtmans and Rob Leurs

Amsterdam Institute of Molecular and Life Sciences, Division of Medicinal Chemistry, Faculty of Science, Vrije Universiteit Amsterdam, De Boelelaan 1083, 1081 HV Amsterdam, the Netherlands.

Abstract

The use of photoswitchable ligands enables reversible, light-controlled modulation of biological targets, offering precise spatiotemporal control over protein activity. Azobenzenes are the most widely used photoswitches in this field, but these rely on UV and blue light for photoswitching, and suboptimal photostationary states (PSS) limit their usage. Arylazopyrazoles have emerged as better alternatives owing to their improved photochemical properties and compatibility with biologically preferred wavelengths. Here, we report the design, synthesis, and evaluation of photoswitchable histamine H_3 receptor (H_3R) ligands incorporating arylazopyrazole photoswitches. Building on the azobenzene-based agonists VUF15000 and VUF16003, we designed analogs with an arylazopyrazole moiety installed at either the central or peripheral position. While an arylazopyrazole is typically introduced at peripheral sites of a ligand, this study explores how positional variation affects the photochemical and pharmacological properties of a photoswitchable H_3R agonist. The arylazopyrazole-based ligands exhibit high PSS_{cis} values (97–98%) and enhanced PSS_{trans} values (up to 92%) and could be efficiently switched from the *cis* to *trans* configuration with green light. However, despite favorable photochemical profiles, radioligand competition binding assays revealed that the arylazopyrazole-based ligands lack affinity for H_3R. These findings highlight both the potential and challenges of integrating alternative photoswitches into azobenzene-based GPCR ligands.

Introduction

Photopharmacology has emerged as a powerful tool for spatiotemporal control of biological activity using light. By incorporating light-responsive moieties into biologically active compounds, protein function can be modulated with high precision, offering a method to regulate biological systems.[1] In photoswitching, the light-responsive molecules undergo reversible *trans* to *cis* isomerization upon illumination, producing isomers with different biological properties. Among photoswitchable moieties, azobenzenes are the most widely used in photopharmacology.[2,3] Their prevalence is primarily attributed to their well-established photochemical properties, and synthetic accessibility.[2,3] However, integrating azobenzenes into biologically active ligands can present challenges. The switching from the thermodynamically more stable *trans* to the metastable *cis* isomer typically requires ultraviolet (UV) light. Converting the *cis* isomer back to the *trans* isomer typically requires blue light (400–450 nm), and spectral overlap between the isomers in this region can lead to suboptimal photostationary state (PSS) values.[4]

Nonetheless, azobenzenes have been used for photoswitchable ligands targeting a broad spectrum of proteins, amongst which are G protein-coupled receptors (GPCRs).[5–8] GPCRs are the target of approximately 36% of all marketed drugs.[9] They have been effectively targeted in the photopharmacology field, with numerous photoswitchable ligands reported.[5–8] In this work, we focused on the histamine H_3 receptor (H_3R). It is an intensively studied GPCR and is implicated in sleep-wake regulation and cognitive disorders such as Alzheimer's and Parkinson's disease. Currently, the H_3R antagonist pitolisant is marketed for the treatment of narcolepsy (Wakix®) and for the treatment of excessive daytime sleepiness in adults with obstructive sleep apnea (Ozawade®).[10,11] Interestingly, our 2022 review revealed that only a

small percentage of known photoswitchable class A GPCR ligands incorporate a heteroarylazo moiety (5%), compared with those that contain an azobenzene moiety (84%).[6] In recent years, though, arylazopyrazoles have become a more popular photoswitch in photopharmacology owing to their favorable photochemical properties.[12–20] Specifically, with this photoswitch moiety, lower-energy wavelengths for biological applications can be used for *cis* to *trans* switching, and improved PSS_{trans} values are typically obtained. Furthermore, the heteroatoms in these photoswitches offer new interaction opportunities with targets, such as metal coordination or hydrogen bonding. These properties allow for tuning of both the photochemical and pharmacological properties of a light-responsive ligand.[3,21] As an example, we have successfully replaced the azobenzene photoswitch with an arylazopyrazole moiety in the core of a known H_3R photoswitchable antagonist.[22] Installation of this moiety allowed growing from the pyrazole, resulting in antagonists with improved photochemical properties, affinity, and affinity shift.

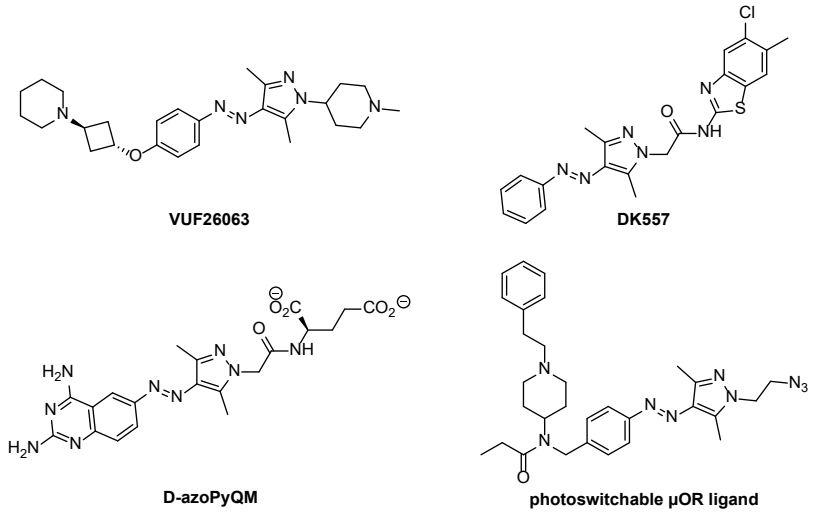

Figure 1. Examples of photoswitchable ligands containing an arylazopyrazole photoswitch in the core of the ligand.[18–20,22]

Although a few additional examples of arylazopyrazole incorporation into the core of a photoswitchable ligand (Figure 1) have been reported, all focus only on a single positional isomer. [18–20,22] In the current study, we aimed to investigate how the position of the arylazopyrazole within a ligand affects both its photochemical and pharmacological properties. Toward that end, the azobenzene moieties of two photoswitchable H_3R agonists were replaced with arylazopyrazole, either in the core or in the periphery, affording positional isomers that have the potential to improve both the photochemical and pharmacological properties.

Results and discussion

Design

Hauwert *et al.*[23] reported azobenzene-based H_3R agonists VUF15000 (**2**; Figure 2) and VUF16003 (**3**), both based on the non-photoswitchable agonist VUF5980 (**1**).[24] Building on these agonists [23] two compounds were selected as starting points for further optimization. Agonist **2** (Figure 2) has been reported as the key compound with a high affinity in the *trans* configuration (pK_i = 8.4) and an almost 10-fold affinity shift upon isomerization. Additionally, compound **3** with an *o*-fluoro substituent shows a similar affinity in the *trans* configuration (pK_i = 8.3) and a significant affinity shift (~16-fold). However, in functional assays, **2** exhibits higher potency (pEC_{50} *trans* = 7.6) than **3** (pEC_{50} *trans* = 6.3) with a similar decrease in potency (~20-fold) upon illumination. In the current work, we introduced the arylazopyrazole at different positions of **2** and **3**, by replacing either the central phenyl ring of these ligands to give arylazopyrazole **4** and **6,** or the peripheral phenyl ring, which is only possible for **2** and affords arylazopyrazole **5**.

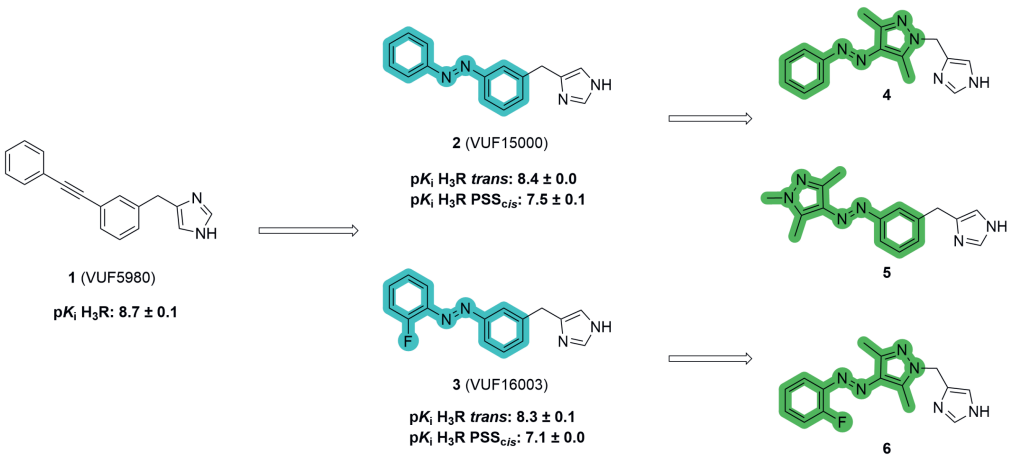

Figure 2. Design towards arylazopyrazole-based photoswitchable agonists **4**, **5** and **6** based on agonists VUF15000 (**2**) and VUF16003 (**3**), [23] themselves developed based on template VUF5980 (**1**). [24]

Synthesis

To prepare the ligands, (1H-imidazol-4-yl)methanol (**7**) was first protected with a trityl group to afford **8** (Scheme 1). Treatment of alcohol **8** with $SOCl_2$ yielded chloride **9**.[25] Anilines **10** and **11** were converted by diazonium coupling with acetylacetone to diones **12** and **13**, respectively. Subsequent ring closure with $NH_2NH_2{\cdot}H_2O$ yielded pyrazoles **14** and **15**, which were then reacted with chloride **9** to give **16** and **17**. Deprotection of the trityl group under acidic conditions yielded ligands **4** and **6**. For the synthesis of ligand **5**, 3-bromoaniline (**18**) was converted to dione **19** by diazonium salt coupling with acetylacetone. Ring closure with $MeNHNH_2$ afforded pyrazole **20**, which was subjected to Miyaura borylation with B_2pin_2 to

pinacol ester **21**. Suzuki coupling of chloride **9** and pinacol ester **21** yielded intermediate **22**, which was deprotected under acidic conditions to yield ligand **5**.

Scheme 1. Synthesis of arylazopyrazole-based photoswitchable ligands **4**–**6**.[a]

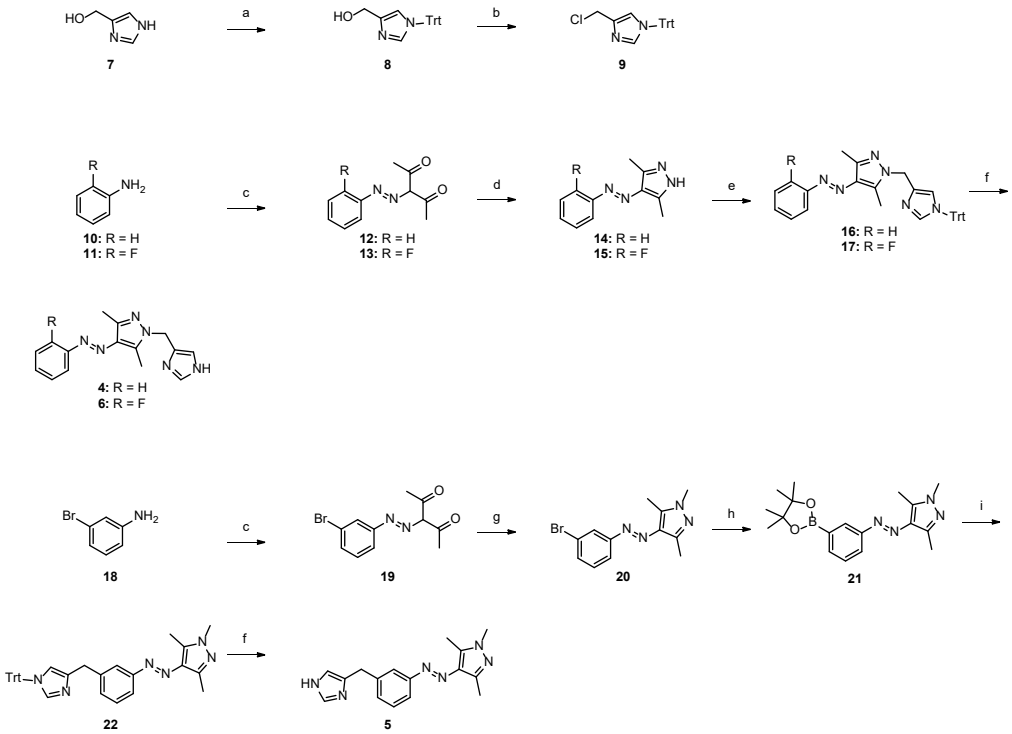

[a]**Reagents and conditions:** (a) TrtCl, Et_3N, DMF, rt, 5 h, 59%; (b) $SOCl_2$, DCM, 0 °C, 30 min, 97%; (c) (i) $NaNO_2$, aq. HCl, H_2O/AcOH, 0 °C, 45 min; (ii) Acetylacetone, NaOAc, H_2O/EtOH, 0 °C, 1 h, 66–97%; (d) $NH_2NH_2{\cdot}H_2O$, TEA, EtOH, reflux, 17 h, 86–97%; (e) **9**, Cs_2CO_3, DMF, 80 °C, 1 h, 82–85%; (f) Aq. 2M HCl, EtOH, reflux, 1 h, 37-81%; (g) $MeNHNH_2$, EtOH, reflux, 17 h, 86%; (h) B_2pin_2, Pd(dppf)Cl_2, KOAc, 1,4-dioxane, reflux, 2 h, 66%; (i) **9**, Pd(dppf)Cl_2, Cs_2CO_3, 1,4-dioxane/H_2O, 80 °C, 1 h, 62%.

Photochemistry and pharmacology

Table 1. Photochemical parameters and H_3R affinity of photoswitchable ligands **2–6**.

#	Structure	λ_{max} *trans* [a] (nm)	λ_{max} *cis*[a] (nm)	Illumination wavelength for PSS_{cis} (nm)	PSS_{cis} (area %*cis*)[b]	Illumination wavelength for PSS_{trans} (nm)	PSS_{trans} (area %*trans*)[c]	Half-life[d] (days)	pK_i *trans* ± SEM[e]	pK_i PSS_{cis} ± SEM[e]
2[f]	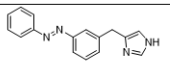	320	427	360	91	434	82	106	8.4 ± 0.0	7.5 ± 0.1
3[f]	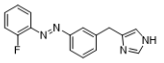	323	425	360	92	434	77	128	8.3 ± 0.1	7.1 ± 0.0
4	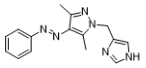	334	429	360	97	494	90	6	<5.0	<5.0
5	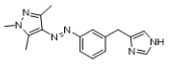	338	436	360	98[g]	520	92[g]	6	<5.0	<5.0
6	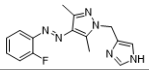	337	426	360	97	520	91	7	<5.0	<5.0

[a]Determined at 25 µM in HBSS buffer containing 1% DMSO.
[b]Photostationary state area percentages after illumination of *trans* isomer with the indicated illumination wavelength to PSS_{cis} at 10 mM in DMSO as determined by acidic LC-MS analysis at the isosbestic point.
[c]Photostationary state area percentages after illumination of PSS_{cis} states with the indicated illumination wavelength for PSS_{trans} at 10 mM in DMSO as determined by acidic LC-MS analysis at the isosbestic point.
[d]Approximate thermal relaxation ($t_{1/2}$) of PSS_{cis} states in HBSS buffer containing 1% DMSO at 20 °C as determined by acidic LC-MS analysis at the isosbestic point.
[e]Affinity (pK_i) values obtained from radioligand competition experiments with 1.6 nM [^{3}H]NAMH. Values are means of n = 3 experiments ± SEM, performed in triplicate.
[f]Previously published data by Hauwert *et al*.[23]
[g]Photostationary state area percentages determined by ^{1}H NMR analysis due to significant tailing of peaks with acidic LC-MS.

Photochemical and pharmacological properties were systematically examined (Table 1, Figure 3). Arylazopyrazoles **4–6** show slightly red-shifted λ_{max} *trans* values (334–338 nm) compared to azobenzene-based ligands **2,3** (320–323 nm). All compounds were switched from the *trans* configuration to the metastable *cis* configuration using UV light (360 nm). High PSS_{cis} values were observed for both series, with the azobenzenes reaching PSS_{cis} values of 91–92% and the arylazopyrazoles achieving PSS_{cis} values of 97–98%. As by design, green light (494 and 520 nm) was used to switch the arylazopyrazoles **4–6** back to the *trans* configuration, in contrast to blue light (434 nm) required for azobenzenes. The wavelengths used for illumination were based on a qualitative analysis of UV spectra. As anticipated, improved PSS_{trans} values were obtained for the arylazopyrazoles (>90%) compared with those for the azobenzenes (77–82%). Interestingly, despite the PSS_{cis} states of arylazopyrazoles being generally regarded as more thermally stable compared to their azobenzene counterpart,[26] the estimated thermal half-lives of the *cis* isomers of compounds **4–6** are shorter (~6–7 days) compared to the

azobenzene derivatives (106 and 128 days). This observation may be attributed to the combination of the pyrazole and imidazole linker. The polarity of the molecule is significantly increased, lowering the activation barrier for thermal *cis* to *trans* relaxation.[4]

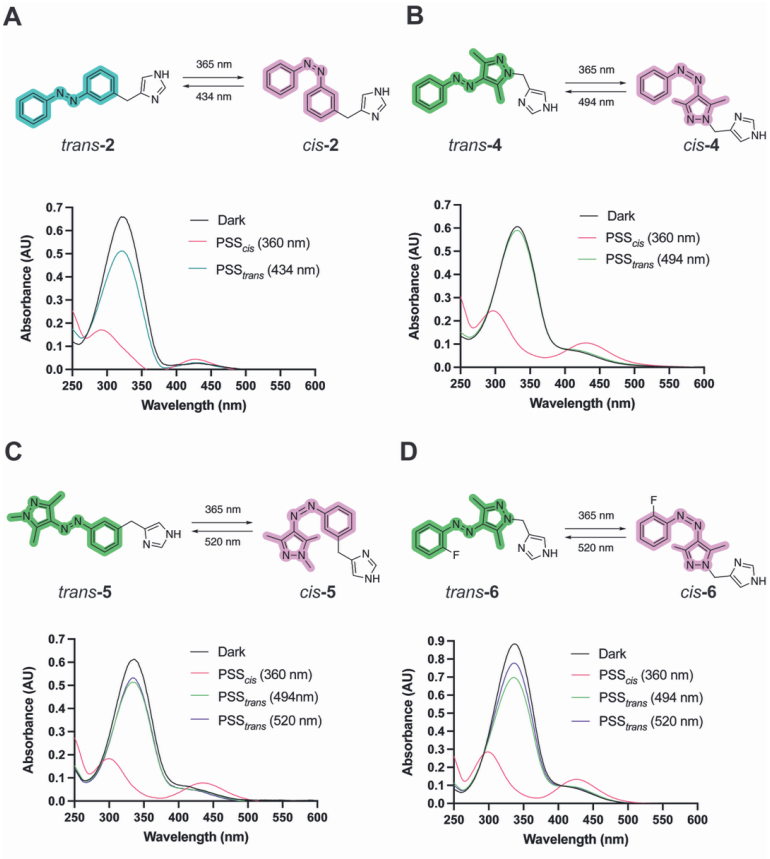

Figure 3. Chemical structures of the *trans* and *cis* isomers and UV-vis spectra of 25 µM of (A) **2**, (B) **4**, (C) **5**, (D) **6** in HBSS buffer containing 1% DMSO as the *trans* isomer (black), after illumination with 360 ± 20 nm to PSS$_{cis}$ (magenta) and after subsequent illumination with 494 ± 9 nm or 520 ± 12 nm to PSS$_{trans}$ (green).

Only minimal differences were observed between the positional isomers, with absorption maxima differing by approximately 5 nm for compounds **4** and **5** and nearly identical PSS values and thermal half-lives. This suggests that, for the substituents introduced here, the position has little influence on the photochemical properties. However, the introduction of different substituents could result in more pronounced differences in photochemical properties.

Compared to their azobenzene counterparts, arylazopyrazoles **4–6** demonstrate improved photoswitching properties, i.e., higher PSS$_{trans}$ values and red-shifted wavelength for *cis* to *trans* isomerization. However, they showed no measurable affinity for the H_3R in either the

trans or *cis* configuration (Table 1). Thus, their affinities are considerably lower than those of the azobenzene-based agonists **2** and **3**. More conceptually, this outcome contrasts with the previously published H_3R antagonist VUF26063,[22] which shows improved affinity upon introduction of the arylazopyrazole for the same receptor. However, the SAR of template compound **1** and parent compounds **2** and **3** has already demonstrated that minor modifications can result in significant changes in affinity.[23,24] For example, Hauwert *et al.* introduced methyl groups at various positions of the inner and outer rings of the azobenzene (Table 2). A moderate decrease in affinity of the *trans* isomers can be observed for **23** and **25**, with a more significant drop in affinity for the *cis* isomers compared to **2.** Notably, placement of a methyl group between the azobond and the imidazole linker (**24**) is detrimental for the affinity of both the *trans* and *cis* isomers. Thus, for **4–6**, the incorporation of arylazopyrazoles bearing two methyl groups in the *ortho* position appears to be unfavorable, possibly due to increased steric hindrance that results in a drop in affinity. However, in the absence of the '*ortho*-methyl' substituents, the *trans* and *cis* isomers will likely show substantial overlap of their n-π* absorption bands,[26] preventing high PSS_{trans} values from being achieved using green light. These observations reinforce the notion that steric considerations and spatial orientation play a critical role in H_3R ligand affinity, especially in the context of photoswitchable scaffolds.

Overall, the results of the current work suggest that while arylazopyrazoles can offer improved photochemical properties, particularly higher PSS_{trans} values and compatibility with green light, they do not always translate into improved affinity, even for the same receptor and at multiple isomeric positions within a template azobenzene. These findings underscore the importance of carefully selecting the desired photoswitch moiety. Even within the same receptor, i.e., the H_3R, outcomes can differ significantly depending on the parent scaffold, orientation, and pharmacophore compatibility. Using positional isomers of a photoswitch moiety could theoretically expand the design space for photoswitchable ligands, but as this study shows, it is also subject to the constraints generally at play in the photopharmacology field.

Table 2. The H_3R affinity of photoswitchable H_3R agonists as reported by Hauwert *et al.*[23]

#	Structure	pK_i *trans* ± SEM	pK_i PSS_{cis} ± SEM
2	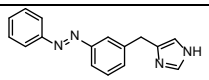	8.4 ± 0.0	7.5 ± 0.1
23	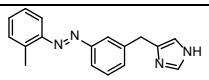	7.7 ± 0.0	6.4 ± 0.0
24	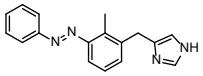	5.6 ± 0.1	5.5 ± 0.0
25	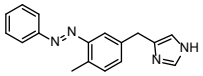	7.2 ± 0.0	5.9 ± 0.1

Conclusions

In this study, we report the design, synthesis, and evaluation of positional isomers of arylazopyrazole-based H_3R agonists. While these compounds exhibit favorable photochemical properties, including red-shifted absorption, improved PSS_{trans} values, and *cis* to *trans* isomerization with green light, these compounds do not show any affinity for the H_3R in either the *trans* or PSS_{cis} state. Our findings suggest that, despite the photochemical advantages of arylazopyrazoles, which are maintained between positional isomers, their incorporation into ligands does not necessarily yield the desired pharmacological outcome, highlighting the need for careful consideration. The results show the importance of a case-by-case approach when replacing azobenzenes with alternative photoswitch moieties and provide valuable insights for the future design of light-responsive ligands.

Acknowledgments

We acknowledge The Dutch Research Council (NWO) for financial support (OCENW.KLEIN.532, "Towards the next frontiers in GPCR photopharmacology"). We thank, Hans Custers for acquiring HRMS analyses, Elwin Janssen for NMR assistance, and Andrea van de Stolpe for setting up the photochemistry equipment.

References

(1) Velema, W. A.; Szymanski, W.; Feringa, B. L. Photopharmacology: Beyond Proof of Principle. *J Am Chem Soc* **2014**, *136* (6), 2178–2191. https://doi.org/10.1021/ja413063e.

(2) Volarić, J.; Szymanski, W.; Simeth, N. A.; Feringa, B. L. Molecular Photoswitches in Aqueous Environments. *Chem Soc Rev* **2021**, *50* (22), 12377–12449. https://doi.org/10.1039/d0cs00547a.

(3) Fuchter, M. J. On the Promise of Photopharmacology Using Photoswitches: A Medicinal Chemist's Perspective. *J Med Chem* **2020**, *63* (20), 11436–11447. https://doi.org/10.1021/acs.jmedchem.0c00629.

(4) Tavassoli, A.; Hamilton, A. D.; Spring, D. R.; Beharry, A. A.; Woolley, G. A. Azobenzene Photoswitches for Biomolecules. *Chem Soc Rev* **2011**, *40* (8), 4422–4437. https://doi.org/10.1039/c1cs15023e.

(5) Panarello, S.; Rovira, X.; Llebaria, A.; Gómez-Santacana, X. Photopharmacology of G -Protein-Coupled Receptors. In *Molecular Photoswitches*; John Wiley & Sons, Ltd, 2022; Vol. 2–2, pp 921–944. https://doi.org/10.1002/9783527827626.ch37.

(6) Wijtmans, M.; Josimovic, I.; Vischer, H. F.; Leurs, R. Optical Control of Class A G Protein-Coupled Receptors with Photoswitchable Ligands. *Curr Opin Pharmacol* **2022**, *63*, 102192. https://doi.org/10.1016/j.coph.2022.102192.

(7) Ricart-Ortega, M.; Font, J.; Llebaria, A. GPCR Photopharmacology. *Mol Cell Endocrinol* **2019**, *488*, 36–51. https://doi.org/10.1016/j.mce.2019.03.003.

(8) Berizzi, A. E.; Goudet, C. Strategies and Considerations of G-Protein-Coupled Receptor Photopharmacology. *Adv Pharmacol* **2020**, *88*, 143–172. https://doi.org/10.1016/bs.apha.2019.12.001.

(9) Lorente, J. S.; Sokolov, A. V.; Ferguson, G.; Schiöth, H. B.; Hauser, A. S.; Gloriam, D. E. GPCR Drug Discovery: New Agents, Targets and Indications. *Nature Reviews Drug Discovery 2025* **2025**, 1–22. https://doi.org/10.1038/s41573-025-01139-y.

(10) *Wakix | European Medicines Agency (EMA)*. https://www.ema.europa.eu/en/medicines/human/EPAR/wakix (accessed 2025-10-31).

(11) *Ozawade | European Medicines Agency (EMA)*. https://www.ema.europa.eu/en/medicines/human/EPAR/ozawade (accessed 2025-10-31).

(12) Matsuo, K.; Ogawa, H.; Yamaoka, S.; Waku, T.; Kobori, A. A Chemical Platform for the Efficient Screening of Arylazopyrazole-Based Photoswitchable CENP-E Inhibitors Using Mild Cyclization Reactions. *Bioorg Med Chem Lett* **2024**, *111*, 129892. https://doi.org/10.1016/j.mbcl.2024.129892.

(13) Wirth, U.; Raabe, K.; Kalaba, P.; Keimpema, E.; Muttenthaler, M.; König, B. Photoswitchable Probes of Oxytocin and Vasopressin. *J Med Chem* **2023**, *66* (21), 14853–14865. https://doi.org/10.1021/acs.jmedchem.3c01415.

(14) Kolarski, D.; Miró-Vinyals, C.; Sugiyama, A.; Srivastava, A.; Ono, D.; Nagai, Y.; Iida, M.; Itami, K.; Tama, F.; Szymanski, W.; Hirota, T.; Feringa, B. L. Reversible Modulation of Circadian Time

with Chronophotopharmacology. *Nature Communications 2021 12:1* **2021**, *12* (1), 1–12. https://doi.org/10.1038/s41467-021-23301-x.

(15) Sink, A.; Gerwe, H.; Hübner, H.; Boivin-Jahns, V.; Fender, J.; Lorenz, K.; Gmeiner, P.; Decker, M. "Photo-Adrenalines": Photoswitchable B2-Adrenergic Receptor Agonists as Molecular Probes for the Study of Spatiotemporal Adrenergic Signaling. *Chemistry – A European Journal* **2024**, *30* (11), e202303506. https://doi.org/10.1002/chem.202303506.

(16) Wirth, U.; Erl, J.; Azzam, S.; Höring, C.; Skiba, M.; Singh, R.; Hochmuth, K.; Keller, M.; Wegener, J.; König, B. Monitoring the Reversibility of GPCR Signaling by Combining Photochromic Ligands with Label-Free Impedance Analysis. *Angewandte Chemie* **2023**, *135* (21), e202215547. https://doi.org/10.1002/ange.202215547.

(17) Aguirre, T.; Teichmann, E.; Römpp, F. Q.; Vivier, R.; Bryant, C.; Hulverson, M. A.; Van Voorhis, W. C.; Ojo, K. K.; Doggett, J. S.; Fiedler, D.; Hecht, S. Photoswitchable Inhibitors to Optically Control Specific Kinase Activity. *ACS Chem Biol* **2023**, *18* (6), 1378–1387. https://doi.org/10.1021/acschembio.3c00119.

(18) Sarkar, H. S.; Mashita, T.; Kowada, T.; Hamaguchi, S.; Sato, T.; Kasahara, K.; Matubayasi, N.; Matsui, T.; Mizukami, S. Arylazopyrazole-Based Photoswitchable Inhibitors Selective for Escherichia Coli Dihydrofolate Reductase. *ACS Chem Biol* **2023**, *18* (2), 340–346. https://doi.org/10.1021/acschembio.2c00749.

(19) Schulte, A. M.; Kolarski, D.; Sundaram, V.; Srivastava, A.; Tama, F.; Feringa, B. L.; Szymanski, W. Light-Control over Casein Kinase 1δ Activity with Photopharmacology: A Clear Case for Arylazopyrazole-Based Inhibitors. *Int J Mol Sci* **2022**, *23* (10), 5326. https://doi.org/10.3390/ijms23105326.

(20) Lahmy, R.; Hübner, H.; Lachmann, D.; Gmeiner, P.; König, B. Development of Photoswitchable Tethered Ligands That Target the μ-Opioid Receptor. *ChemMedChem* **2023**, *18* (23), e202300228. https://doi.org/10.1002/cmdc.202300228.

(21) Crespi, S.; Simeth, N. A.; König, B. Heteroaryl Azo Dyes as Molecular Photoswitches. *Nature Reviews Chemistry*. Nature Publishing Group March 1, 2019, pp 133–146. https://doi.org/10.1038/s41570-019-0074-6.

(22) Binkhorst, L. C. P.; Josimovic, I.; Boer, B. De; Simon, I. A.; Aa, F. Van Der; Zarzycka, B. A.; Esch, I. J. P. De; Vischer, H. F.; Windhorst, A. D.; Wijtmans, M.; Leurs, R. A Radiolabeled Photoswitchable G Protein-Coupled Receptor Antagonist Enlightens Ligand Binding Kinetics Associated with Photoswitching. *J Am Chem Soc* **2025**. https://doi.org/10.1021/JACS.5C07349.

(23) Hauwert, N. J.; Mocking, T. A. M.; Da Costa Pereira, D.; Lion, K.; Huppelschoten, Y.; Vischer, H. F.; De Esch, I. J. P.; Wijtmans, M.; Leurs, R. A Photoswitchable Agonist for the Histamine H3 Receptor, a Prototypic Family A G Protein-Coupled Receptor. *Angewandte Chemie International Edition* **2019**, *58* (14), 4531–4535. https://doi.org/10.1002/anie.201813110.

(24) Wijtmans, M.; Celanire, S.; Snip, E.; Gillard, M. R.; Gelens, E.; Collart, P. P.; Venhuis, B. J.; Christophe, B.; Hulscher, S.; Van Der Goot, H.; Lebon, F.; Timmerman, H.; Bakker, R. A.; Lallemand, B. I. L. F.; Leurs, R.; Talaga, P. E.; De Esch, I. J. P. 4-Benzyl-1H-Imidazoles with Oxazoline Termini as Histamine H3 Receptor Agonists. *J Med Chem* **2008**, *51* (10), 2944–2953. https://doi.org/10.1021/JM7014149.

(25) Houssin, R.; Pommery, J.; Salaün, M. C.; Deweer, S.; Goossens, J. F.; Chavatte, P.; Hénichart, J. P. Design, Synthesis, and Pharmacological Evaluation of New Farnesyl Protein Transferase Inhibitors. *J Med Chem* **2001**, *45* (2), 533–536. https://doi.org/10.1021/JM010297R.

(26) Weston, C. E.; Richardson, R. D.; Haycock, P. R.; White, A. J. P.; Fuchter, M. J. Arylazopyrazoles: Azoheteroarene Photoswitches Offering Quantitative Isomerization and Long Thermal Half-Lives. *J Am Chem Soc* **2014**, *136* (34), 11878–11881. https://doi.org/10.1021/ja505444d.

Experimental procedures – Photochemistry

UV–Vis spectra were recorded using a Thermo-scientific Evolution 201 PC spectrophotometer equipped with a thermostated cell holder set at 20 °C. Fits of UV–vis spectroscopy data were generated using Prism 10.1.0. Illumination for all photochemical experiments was executed using a Sutter instruments Lambda LS with a 300 W full-spectrum lamp connected to a Sutter instruments Lambda 10-3 optical filter changer equipped with 360 ± 20 nm, 434 ± 9 nm, 494 ± 9 nm filter, and 520 ± 12 nm. The light intensity used for the lambda 10-3 optical filter is 0.93 mW/mm^2 using the 360 ± 20 nm filter, 0.79 mW/mm^2 for the 434 ± 9 nm filter, 0.77 mW/mm^2 for the 494 ± 9 nm filter, and 0.20 mW/mm^2 for the 520 ± 12 nm filter as measured using a Thorlabs PM16−401 power meter. For photochemical analyses, illuminations were performed in Hellma Suprasil quartz 114QS cuvettes. Illuminations for pharmacological experiments were performed in cylindrical clear glass vials with a volume of 4.5 mL. The typical distance between light source and vial or cuvette was 2 cm.

Experimental procedures - Chemistry

All chemicals and solvents were obtained from commercial suppliers (primarily Sigma-Aldrich, BLD pharma and Combi-Blocks) and used without purification. DCM, DMF, THF and Et_2O were dried by passing through a PureSolv solvent purification system. All reactions were carried out under N_2 atmosphere unless mentioned otherwise. All reactions with photoresponsive compounds were carried out in the dark or under red light. IUPAC names were adapted from Chemdraw Professional 21.0 (PerkinElmer). Reactions were monitored by thin layer chromatography (Merck Silicagel 60 F254) by visualization under 254 nm lamp. Flash column chromatography was performed with Screening Devices 40-63 µm (Biotage) or GraceResolv (Büchi) cartridges on Isolera One with UV-Vis detection (Biotage). Nuclear magnetic resonance (NMR) spectra were determined with a Bruker Avance II 500 MHz or a Bruker Avance III HD 600 MHz spectrometer. Chemical shifts are reported in parts per million (ppm) against the reference compound using the signal of the residual non-deuterated solvent ($CDCl_3$ δ = 7.26 ppm (^{1}H), δ = 77.16 ppm (^{13}C); DMSO-d_6 δ = 2.50 ppm (^{1}H), δ = 39.52 ppm (^{13}C)). NMR spectra were processed using MestReNova 14.1 software. The peak multiplicities are defined as follows: s, singlet; d, doublet; t, triplet; q, quartet; dd, doublet of doublets; ddd, doublet of doublets of doublets; dt, doublet of triplets; dq, doublet of quartets; td, triplet of doublets; tt, triplet of triplets; qd, quartet of doublets; p, pentet; dp, doublet of pentets; br, broad signal; m, multiplet. For NMR listings, in addition to specific instructions that are given by the journal in the guidelines for authors the following additional procedures were used: 1) Multiplicity is not solely reported based on peak shapes, but also distinguishes the coupling to all non-equivalent protons that have similar J values; 2) If additional smaller couplings are observed but are too small for accurate quantitation because the precision is smaller than the digital resolution, a symbol $^{\Delta}$ will be used; 3) The notation 'm' is used in case of obscured accurate interpretation as a result of (i) overlapping signals for different protons, or (ii) a result of overlapping signal lines within the same proton signal; 4) For any rotamers or diastereomers, signals will be listed separately; 5) NMR signals that could only be detected with HSQC analysis are denoted with a $^{\#}$ symbol; 6) NMR signals that could only be detected with HMBC analysis are denoted with a * symbol; 7) If one or more signals remain undetected after extensive 1D and 2D NMR analyses, this will be mentioned. 8) Signals for exchangeable proton atoms (such as NH and OH groups) are only listed if clearly visible (excluding e.g. the use of D_2O or CD_3OD) and if confirmed by a D_2O shake and/or HSQC. Analytical HPLC analyses were performed using a Shimadzu LC-20AD liquid chromatography pump system, equipped with a Waters XBridge C18 column 5 µm 4.6 x 50 mm (used at 40 °C), connected to a Shimadzu SPDM20A photodiode array detector. MS detection was performed using Shimadzu LCMS-2010EV mass spectrometer operating in both positive and negative ionization mode. The mobile phase used for acidic mode was a mixture of A = H_2O + 0.1% HCO_2H and B = MeCN + 0.1%

HCO_2H. The mobile phase used for basic mode was a mixture of A = H_2O and B = MeCN + 0.4% w/v NH_4HCO_3. The method used is as follows: flow rate: 1.0 mL/min, start 95% A in a linear gradient to 10% A over 4.5 min, hold 1.5 min at 10% A, in 0.5 min in a linear gradient to 95% A, hold 1.5 min at 95% A, total runtime: 8.0 min. Analytical UPLC analyses were performed using a Shimadzu LC-40D liquid chromatograph pump system, equipped with an Xbridge (BEH C18) 2.5 µm column (50 mm, 2.1 mm), connected to a Shimadzu SPD-M40 diode array detector. MS detection was performed using a Shimadzu LCMS-2020 EV mass spectrometer. The mobile phase used for acidic mode was a mixture of A = H_2O + 0.1% HCO_2H and B = MeCN + 0.1% HCO_2H, The method used is as follows: flow rate: flow rate: 0.4 mL/min, start 95% A in a linear gradient to 10% A over 1.75 min, hold 0.25 min at 10% A, in 0.25 min in a linear gradient to 95% A, hold 0.75 min at 95% A, total run time: 3 min. Compound purities were calculated as the percentage peak area of the analysed compound by UV detection at 254 nm. Unless mentioned otherwise, all compounds have a LC purity of >95 %. High-resolution mass spectra (HRMS) were recorded on a Bruker micrOTOF mass spectrometer using ESI in positive ion mode (HRMS). λ_{max} values provided in the procedures are those extracted from the LC analysis.

(1-trityl-1*H*-imidazol-4-yl)methanol (8)

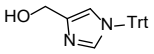

To a solution of (1H-imidazol-4-yl)methanol (**7**, 2.50 g, 25.5 mmol, 1.0 eq) and Et_3N (10.6 mL, 76.5 mmol, 3.0 eq) in DMF (50 mL) was added dropwise TrtCl (7.8 g, 28.0 mmol, 1.1 eq). The resulting mixture was stirred at rt for 5 h. The reaction mixture was poured into water (150 mL). The resulting solid was collected by vacuum filtration, washed with water and cold Et_2O. The crude product was recrystallized from dioxane to yield the title compound as a white solid (5.1 g, 59%). **^{1}H NMR** (500 MHz, DMSO-d_6) δ 7.44 – 7.35 (m, 9H), 7.29 (d, *J* = 1.5 Hz, 1H), 7.12 – 7.06 (m, 6H), 6.72 (s, 1H), 4.87 (t, *J* = 5.6, 5.6 Hz, 1H), 4.33 (d, *J* = 5.6 Hz, 2H). **^{13}C NMR** (126 MHz, DMSO-d_6) δ 142.3, 142.2, 137.7, 129.2, 128.2, 128.0, 118.0, 74.4, 57.7. **LC-MS** (HPLC, acidic): t_r: 3.54 min, purity: 96% (254 nm), $[M+H]^+$ m/z calc.: 341.16, found 243.10 (Trt^+ cation).

4-(chloromethyl)-1-trityl-1*H*-imidazole (9)

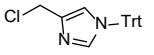

A suspension of **8** (3.00g, 8.81 mmol, 1.0 eq) in DCM was cooled to 0 °C. $SOCl_2$ (0.77 mL, 10.5 mmol, 1.2 eq) was added dropwise. The reaction mixture was stirred for 30 min in the ice bath. The reaction mixture was washed using satd. aq. $NaHCO_3$. The organic layer was dried over $MgSO_4$ and concentrated under reduced pressure. The resulting oil was co-evaporated with Et_2O to give the title compound as a while solid (3.1g, 97%). **^{1}H NMR** (600 MHz, DMSO-d_6) δ 7.56 (s, 1H), 7.47 – 7.36 (m, 9H), 7.26 – 7.21 (m, 1H), 7.12 – 7.06 (m, 6H), 4.65 (s, 2H).

(*E*)-3-(phenyldiazenyl)pentane-2,4-dione (12)

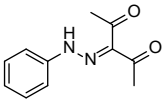

A solution of $NaNO_2$ (889 mg, 12.9 mmol, 1.2 eq) in H_2O (4 mL) was added dropwise to a solution of aniline (**10**, 1.00 g, 10.7 mmol) in AcOH (16 mL) and conc. aq. HCl (2.5 mL) that was cooled at 0-4°C. The resulting suspension was stirred at 0 °C for 45 min. The diazonium salt solution was added to a suspension of pentane-2,4-dione (1.4 mL, 14.0 mmol, 1.3 eq) and NaOAc (2.64 g, 32.2 mmol, 3.0 eq) in EtOH (28 mL) and H_2O (17 mL). The mixture was stirred at 0 °C for 1 h and filtered. The residue was washed with water, water:EtOH (1:1), and cHex. This yielded the title compound as a pale brown solid (1.49 g, 68%). **^{1}H NMR** (500 MHz, $CDCl_3$) δ 14.73 (s, 1H), 7.45 – 7.38 (m, 4H), 7.24 – 7.17 (m, 1H), 2.60 (s, 3H), 2.49 (s, 3H). **^{13}C NMR** (126 MHz, $CDCl_3$) δ 198.1, 197.3, 141.7, 133.4, 129.8, 126.0, 116.4, 31.8, 26.8. **LC-MS** (HPLC, acidic): t_r: 4.53 min, purity: >99% (254 nm), $[M+H]^+$ m/z calc.: 205.09, found 205.05.

(*E*)-3,5-dimethyl-4-(phenyldiazenyl)-1*H*-pyrazole (14)

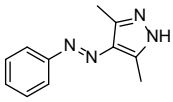

To a solution of dione **12** (500 mg, 2.45 mmol, 1.0 eq) in EtOH (12.2 mL) was added $NH_2NH_2 \cdot H_2O$ (0.12 mL, 2.45 mmol, 1.0 eq). The reaction mixture was heated at reflux for 17 h. The reaction mixture was cooled to rt and concentrated under reduced pressure to give the title compound as an orange solid (477 mg, 97%). **^{1}H NMR** (500 MHz, $CDCl_3$) δ 7.80 (d, *J* = 7.3 Hz, 2H), 7.47 (dd, *J* = 7.7, 7.2 Hz, 2H), 7.39 (dd, *J* = 7.4, 7.2 Hz, 1H), 2.62 (s, 6H). **^{13}C NMR** (126 MHz, $CDCl_3$) δ 153.7, 141.6, 134.9, 129.6, 129.1, 122.0, 12.3. **LC-MS** (UPLC, acidic): t_r: 1.90 min, purity: 94% (254 nm), $[M+H]^+$ m/z calc.: 201.11, found 201.05

(*E*)-3,5-dimethyl-4-(phenyldiazenyl)-1-((1-trityl-1*H*-imidazol-4-yl)methyl)-1*H*-pyrazole (16)

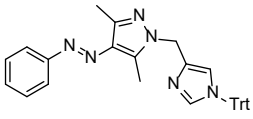

To a solution of pyrazole **14** (200 mg, 1.00 mmol, 1.0 eq) in DMF (5 mL) were added Cs_2CO_3 and chloride **9** (430 mg, 1.20 mmol, 1.2 eq). The resulting solution was stirred at 80 °C for 1 h. The reaction mixture was poured on ice containing brine, and extracted with EtOAc thrice. The combined organic layers were washed with cold brine, dried over Na_2SO_4, and concentrated. The crude product was purified using flash chromatography (20 -> 60% EtOAc in cHex) to give the title compound as a yellow solid (429 mg, 82%). **^{1}H NMR (**500 MHz, $CDCl_3$) δ 7.79 – 7.73 (m, 2H), 7.45 (dd, *J* = 8.5, 7.0 Hz, 2H), 7.39 – 7.28 (m, 11H), 7.14 – 7.06 (m, 6H), 6.81 – 6.76 (m, 1H), 5.17 (s, 2H), 2.64 (s, 3H), 2.47 (s, 3H). **^{13}C NMR** (126 MHz, $CDCl_3$) δ 154.3, 142.4, 142.3, 139.4, 139.1, 137.0, 135.0, 129.8, 129.2, 128.9, 128.1, 128.1, 121.8, 119.8, 75.5, 44.1, 15.1, 10.3. **LC-MS** (UPLC, acidic): t_r: 2.40 min, purity: 97% (254 nm), $[M+H]^+$ m/z calc.: 523.26, found 523.35.

(E)-1-((1H-imidazol-4-yl)methyl)-3,5-dimethyl-4-(phenyldiazenyl)-1H-pyrazole (4)

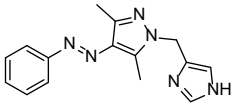

To a solution of **16** (400 mg, 0.77 mmol, 1.0 eq) in EtOH (7.7 mL) was added aq. 2M HCl (0.77 mL, 1.53 mmol, 2.0 eq). The mixture was heated to reflux for 1 h. The reaction mixture was concentrated. The residue was mixed with water and EtOAc. The aq. layer was made basic using aq. sat. $NaHCO_3$, and extracted with EtOAc thrice. The combined organic layers were dried over Na_2SO_4, filtered and concentrated *in vacuo*. The crude product was purified using reverse phase column chromatography (5 -> 95% ACN + 0.1% HCO_2H in water + 0.1% HCO_2H). The desired fractions were combined, made basic using satd. aq. $NaHCO_3$ and extracted using EtOAc. The combined organic layers were washed with brine, dried over $MgSO_4$, and concentrated under reduced pressure. This yielded the title compound as a yellow solid (174 mg, 81%). **^{1}H NMR** (600 MHz, $CDCl_3$) δ 7.82 – 7.76 (m, 2H), 7.58 (d, *J* = 1.2 Hz, 1H), 7.50 – 7.45 (m, 2H), 7.39 (dddd, *J* = 7.2, 7.2, 1.2, 1.2 Hz, 1H), 6.91 (s, 1H), 5.29 – 5.21 (m, 2H), 2.68 (s, 3H), 2.51 (s, 3H). **^{13}C NMR** (151 MHz, $CDCl_3$) δ 153.7, 142.8, 139.5, 135.6, 135.3, 129.5, 129.0, 121.9, 46.7[#], 14.2, 10.1. **LC-MS** (HPLC, acidic): t_r: 3.30 min, λ_{max}: 329 nm, purity: >99% (254 nm), $[M+H]^+$ m/z calc.: 281.15, found 281.15. **HRMS**: $[M+H]^+$ calc. for $C_{15}H_{16}N_6$: 281.1515, found 281.1510.

(*E*)-3-((2-fluorophenyl)diazenyl)pentane-2,4-dione (13)

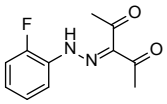

A solution of $NaNO_2$ (745 mg, 10.8 mmol, 1.2 eq) in H_2O (4 mL) was added dropwise to a solution of 2-fluoroaniline (**11**, 0.87 mL, 10.7 mmol, 1.0 eq) in AcOH (13.5 mL) and conc. aq. HCl (2.1 mL) that was cooled at 0-4°C. The resulting suspension was stirred at 0 °C for 45 min. The diazonium salt solution was added to a suspension of pentane-2,4-dione (1.2 mL, 11.7 mmol, 1.3 eq) and NaOAc (2.22 g, 27.0 mmol, 3.0 eq) in EtOH (9

mL) and H_2O (5.4 mL). The mixture was stirred at 0 °C for 1 h and filtered. The residue was washed with water, water:EtOH (1:1), and cHex. This yielded the title compound as a pale brown solid (1.32 g, 66%). **^{1}H NMR** (600 MHz, $CDCl_3$) δ 14.69 (s, 1H), 7.75 (ddd, *J* = 8.0, 7.7, 1.5 Hz, 1H), 7.23 – 7.18 (m, 1H), 7.17 – 7.09 (m, 2H), 2.60 (s, 3H), 2.49 (s, 3H). **^{13}C NMR** (151 MHz, $CDCl_3$) δ 198.0, 197.2, 152.2 (d, *J* = 247.1 Hz), 134.5, 130.2 (d, *J* = 8.8 Hz), 126.0 (d, *J* = 7.2 Hz), 125.3 (d, *J* = 3.7 Hz), 116.5, 116.1 (d, *J* = 17.8 Hz). 31.8, 26.7.**^{19}F NMR** (471 MHz, $CDCl_3$) δ -131.9. **LC-MS** (HPLC, acidic): t_r: 4.79 min, purity: >99% (254 nm), $[M+H]^+$ m/z calc.: 223.09, found 223.05.

(*E*)-4-((2-fluorophenyl)diazenyl)-3,5-dimethyl-1*H*-pyrazole (15)

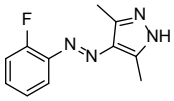

To a solution of dione **13** (400 mg,1.8 mmol, 1.0 eq) in EtOH (9.0 mL) was added $NH_2NH_2{\cdot}H_2O$ (87 µL, 1.8 mmol, 1.0 eq). The reaction mixture was heated at reflux for 17 h. The reaction mixture was cooled to rt and concentrated under reduced pressure. The crude product was purified using column chromatography (30 -> 80% EtOAc in cHex) to give the title compound as a yellow solid (338 mg, 86%). **^{1}H NMR** (500 MHz, $CDCl_3$) ^{1}H NMR (600 MHz, $CDCl_3$) δ 7.69 (ddd, *J* = 7.9, 7.8, 1.8 Hz, 1H), 7.35 (dddd, *J* = 8.9, 7.0, 4.9, 1.7 Hz, 1H), 7.24 – 7.14 (m, 2H), 2.63 (s, 6H). **^{13}C NMR** (151 MHz, $CDCl_3$) δ 159.4 (d, *J* = 255.7 Hz), 141.4 (d, *J* = 6.8 Hz), 135.5, 130.7 (d, *J* = 8.2 Hz), 124.1 (d, *J* = 3.8 Hz), 117.1, 116.8 (d, *J* = 19.8 Hz), 12.2. **^{19}F NMR** (471 MHz, $CDCl_3$) δ -125.9. **LC-MS** (HPLC, acidic): t_r: 4.26 min, purity: >99% (254 nm), $[M+H]^+$ m/z calc.: 219.10, found 219.05.

(*E*)-4-((2-fluorophenyl)diazenyl)-3,5-dimethyl-1-((1-trityl-1*H*-imidazol-4-yl)methyl)-1*H*-pyrazole (17)

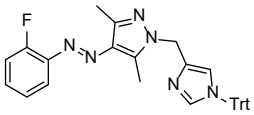

To a solution of pyrazole **15** (200 mg, 0.92 mmol, 1.0 eq) in DMF (4.5 mL) were added Cs_2CO_3 (597 mg, 1.83 mmol, 2.0 eq) and chloride **9** (395 mg, 1.1 mmol, 1.2 eq). The resulting solution was stirred at 80 °C for 1h. The reaction mixture was poured on ice containing brine, and extracted with EtOAc thrice. The combined organic layers were washed with cold brine, dried over Na_2SO_4, and concentrated. The crude product was purified using flash chromatography (5 -> 50% EtOAc in DCM) to give the title compound as a yellow solid (422 mg, 85%). **^{1}H NMR** (600 MHz, $CDCl_3$) δ 7.65 (ddd, *J* = 7.9, 7.9, 1.8 Hz, 1H), 7.38 (d, *J* = 1.4 Hz, 1H), 7.36 – 7.28 (m, 10H), 7.22 – 7.14 (m, 2H), 7.13 – 7.07 (m, 6H), 6.79 (d, *J* = 1.4 Hz, 1H), 5.18 (s, 2H), 2.66 (s, 3H), 2.48 (s, 3H). **^{13}C NMR** (151 MHz, $CDCl_3$) δ 159.4 (d, *J* = 255.0 Hz), 143.0, 142.3, 141.7 (d, *J* = 7.1 Hz) 139.7, 139.3, 136.6, 136.2, 130.4 (d, *J* = 7.8 Hz), 129.8, 128.2, 128.2, 124.2 (d, *J* = 3.7 Hz), 119.9, 117.2, 116.8 (d, *J* = 19.7 Hz), 75.6, 47.8, 14.1, 10.3. **^{19}F NMR** (471 MHz, $CDCl_3$) δ -126.1. **LC-MS** (HPLC, acidic): t_r: 5.546 min, purity: >99% (254 nm), $[M+H]^+$ m/z calc 541.25, found 243.10 (Trt^+ cation).

(*E*)-1-((1*H*-imidazol-4-yl)methyl)-4-((2-fluorophenyl)diazenyl)-3,5-dimethyl-1*H*-pyrazole (6)

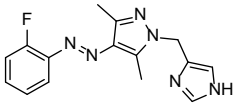

To a solution of **17** (310 mg, 0.57 mmol, 1.0 eq) in EtOH (5.7 mL) was added aq. 2M HCl (0.57 mL, 1.15 mmol, 2.0 eq). The mixture was heated to reflux for 1h. The reaction mixture was concentrated. The residue was mixed with water and EtOAc. The aq. layer was made basic using aq. sat. $NaHCO_3$, and extracted with EtOAc thrice. The combined organic layers were dried over Na_2SO_4, filtered and concentrated *in vacuo*. The crude product was purified using reverse phase column chromatography (5 -> 95% ACN + 0.1% HCO_2H in water + 0.1% HCO_2H). The desired fractions were combined, made basic using satd. aq. $NaHCO_3$ and extracted using EtOAc. The combined organic layers were washed with brine, dried over Na_2SO_4, and concentrated under reduced pressure. This yielded the title compound as a yellow solid (64 mg, 37%). **^{1}H NMR (600 MHz, $CDCl_3$)** δ 7.66 (ddd, *J* = 7.9, 7.9, 1.8 Hz, 1H), 7.61 (d, *J* = 1.2 Hz, 1H), 7.35 – 7.30 (m, 1H), 7.22 – 7.14 (m, 2H), 6.96 – 6.92 (m, 1H), 5.24 (s, 2H), 2.68 (s, 3H), 2.50 (s, 3H). **^{13}C NMR (151 MHz, $CDCl_3$)** δ 159.5 (d, *J* = 255.4 Hz), 143.4, 141.6 (d, *J* = 7.1 Hz), 139.7, 136.2, 135.5, 130.7 (d, *J* = 8.2 Hz), 124.2 (d, *J* = 3.8 Hz), 117.2, 116.9 (d, *J* = 19.9 Hz), 46.6, 14.1, 10.2. **^{19}F NMR** (471 MHz, $CDCl_3$) δ -126.0. **LC-MS** (HPLC, acidic): t_r: 3.25 min, purity: >99% (254 nm), $[M+H]^+$ m/z calc.: 299.14, found 299.10. **HRMS**: $[M+H]^+$ calc. for $C_{15}H_{15}FN_6$: 299.1420, found 299.1421.

(*E*)-3-((3-bromophenyl)diazenyl)pentane-2,4-dione (19)

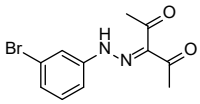

A solution of $NaNO_2$ (481 mg, 6.98 mmol, 1.2 eq) in H_2O (2.5 mL) was added dropwise to a solution of 3-bromoaniline (**18**, 1.00 g, 5.8 mmol) in AcOH (8.7 mL) and conc. aq. HCl (1.3 mL) that was cooled at 0-4°C. The resulting suspension was stirred at 0°C for 45 min. The diazonium salt solution was added to a suspension of pentane-2,4-dione (0.77 mL, 7.55 mmol, 1.3 eq) and NaOAc (1.43 g, 17.4 mmol, 3.0 eq) in EtOH (5.8 mL) and H_2O (3.5 mL). The mixture was stirred at 0 °C for 1 h and filtered. The residue was washed with water, water:EtOH (1:1), and cHex. This yielded the title compound as a pale brown solid (1.61 g, 97%). **^{1}H NMR** (500 MHz, $CDCl_3$) δ 14.59 (s, 1H), 7.59 (dd, *J* = 1.9, 1.9 Hz, 1H), 7.33 – 7.26 (m, 3H), 2.61 (s, 3H), 2.50 (s, 3H).**^{13}C NMR** (126 MHz, $CDCl_3$) δ 198.4, 197.2, 143.0, 133.9, 131.1, 128.7, 123.7, 119.2, 115.1, 31.9, 26.8. **LC-MS** (HPLC, acidic): t_r: 5.07 min, purity: >99% (254 nm), $[M+H]^+$ m/z calc.: 283.00, found 282.95.

(*E*)-4-((3-bromophenyl)diazenyl)-1,3,5-trimethyl-1*H*-pyrazole (20)

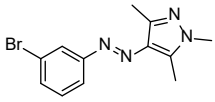

To a solution of dione **19** (500 mg, 1.77 mmol, 1.0 eq) in EtOH (8.8 mL) was added $MeNHNH_2$ (93 µL, 1.77 mmol, 1.0 eq). The reaction mixture was heated at reflux for 17 h. The reaction mixture was cooled to rt and concentrated under reduced pressure to give the title compound as a yellow solid (446 mg, 86%). **^{1}H NMR** (500 MHz, $CDCl_3$) δ 7.94 (dd, *J* = 1.9, 1.9 Hz, 1H), 7.75 (ddd, *J* = 7.9, 1.9, 1.0 Hz, 1H), 7.51 (ddd, *J* = 7.9, 2.1, 1.0 Hz, 1H), 7.36 (dd, *J* = 7.9, 7.9 Hz, 1H), 3.82 (s, 3H), 2.61 (s, 3H), 2.52 (s, 3H). **^{13}C NMR** (126 MHz, $CDCl_3$) δ 154.8, 142.7, 139.6, 135.3, 132.0, 130.4, 123.8, 123.1, 121.9, 36.2, 14.0, 10.1. **LC-MS** (UPLC, acidic): t_r: 2.27 min, purity: >99% (254 nm), $[M+H]^+$ m/z calc.: 293.04, found 293.60.

(*E*)-1,3,5-trimethyl-4-((3-(4,4,5,5-tetramethyl-1,3,2-dioxaborolan-2-yl)phenyl)diazenyl)-1*H*-pyrazole (21)

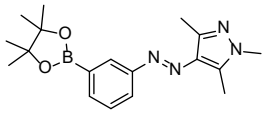

To a solution of bromide **20** (400 mg, 1.36 mmol, 1.0 eq) in 1,4-dioxane (6.5 mL) were added KOAc (268 mg, 2.72 mmol, 2.0 eq) and B_2pin_2 (520 mg, 2.05 mmol, 1.5 eq). The resulting mixture was purged with N_2. Subsequently, Pd(dppf)Cl_2 (30 mg, 0.041 mmol, 0.03 eq) was added. The reaction mixture was stirred at reflux for 2 h. The mixture was cooled to room temperature and filtered over celite. The filtrate was concentrated *in vacuo*. The resulting crude product was purified using flash chromatography (0 -> 50% EtOAc in cHex) to give the title compound as a yellow solid (306 mg, 66%). **^{1}H NMR** (500 MHz, $CDCl_3$) δ 8.23 – 8.19 (m, 1H), 7.85 (ddd, *J* = 8.0, 2.1, 1.3 Hz, 1H), 7.81 (ddd, *J* = 7.2, 1.2, 1.2 Hz, 1H), 7.45 (dd, *J* = 7.6, 7.6 Hz, 1H), 3.78 (s, 3H), 2.59 (s, 3H), 2.50 (s, 3H), 1.37 (s, 12H). **^{13}C NMR** (126 MHz, $CDCl_3$) δ 153.0, 142.5, 138.7, 135.8, 135.2, 129.7, 128.4, 122.9, 84.0, 36.0, 24.9, 13.9, 10.1. **^{11}B NMR** (160 MHz, $CDCl_3$) δ 30.7. **LC-MS** (UPLC, acidic): t_r:2.36 min, purity: 90% (254 nm), $[M+H]^+$ m/z calc.: 341.21, found 341.60.

(*E*)-1,3,5-trimethyl-4-((3-((1-trityl-1*H*-imidazol-4-yl)methyl)phenyl)diazenyl)-1*H*-pyrazole (22)

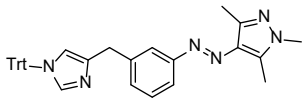

To a solution of **21** (380 mg, 1.12 mmol, 1.0 eq) in 1,4-dioxane (5.1 mL) were added Cs_2CO_3 (1.09 g, 3.35 mmol, 3.0 eq) and chloride **9** (400 mg, 1.12 mmol, 1.0 eq). Water (1.0 mL) was added and the reaction mixture was purged with N_2. Pd(dppf)Cl_2 (82 mg, 0.11 mmol, 0.10 eq) was added and the solution was stirred at 80 °C for 1 h. The reaction mixture was filtered over celite and the filter cake was washed with EtOAc. The filtrate was diluted with EtOAc. The organic layer was washed with brine, dried over Na_2SO_4 and concentrated *in vacuo*. The crude product was purified using flash chromatography (0 -> 30% EtOAc) in cHex to give the title compound as a yellow solid (370 mg, 62%). **^{1}H NMR** (600 MHz, $CDCl_3$) δ 7.65 (dd, *J* = 2.0, 2.0 Hz, 1H), 7.59 (ddd, *J* = 7.9, 1.5, 1.5 Hz, 1H), 7.39 – 7.28 (m, 11H), 7.26 – 7.23 (m, 1H), 7.16 – 7.10 (m, 6H), 6.58 (d, *J* = 1.3 Hz, 1H), 3.98 (s, 2H), 3.78 (s, 3H), 2.56 (s, 3H), 2.48 (s, 3H). **^{13}C NMR** (151 MHz, $CDCl_3$) δ 153.8, 142.6, 142.5, 141.5, 140.8, 139.7*, 138.9, 138.8, 135.2, 129.9, 128.9, 128.1, 128.1, 122.5, 119.4, 119.0, 75.3, 36.1, 35.0, 14.0, 10.5. **LC-MS** (UPLC, acidic): t_r: 1.82 min, purity: 95% (254 nm), $[M+H]^+$ m/z calc.: 537.28, found 537.60.

(*E*)-4-((3-((1*H*-imidazol-4-yl)methyl)phenyl)diazenyl)-1,3,5-trimethyl-1*H*-pyrazole (5)

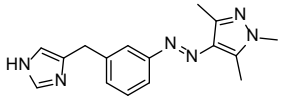

To a solution of **22** (350 mg, 0.65 mmol, 1.0 eq) in EtOH (6.5 mL) was added aq. 2M HCl (0.65 mL, 1.31 mmol, 2.0 eq). The mixture was heated to reflux for 1 h. The reaction mixture was concentrated, and diluted with water and EtOAc. The aqueous layer was made basic using aq. satd. $NaHCO_3$, and extracted with EtOAc thrice. The combined organic layers were dried over Na_2SO_4, filtered and concentrated *in vacuo*. The crude product was purified using reverse phase column chromatography (5 -> 95% ACN + 0.1% HCO_2H in water + 0.1% HCO_2H). The desired fractions were combined, made basic using satd. aq. $NaHCO_3$ and extracted using EtOAc. The combined organic layers were washed with brine, dried over $MgSO_4$, and concentrated under reduced pressure. This yielded the title compound as a yellow solid (134 mg, 70%). **^{1}H NMR** (600 MHz, $CDCl_3$) δ 7.67 – 7.60 (m, 2H), 7.55 (d, *J* = 1.1 Hz, 1H), 7.37 (dd, *J* = 7.7, 7.7 Hz, 1H), 7.26 – 7.23 (m, 1H), 6.78 (s, 1H), 4.04 (s, 2H), 3.74 (s, 3H), 2.54 (s, 3H), 2.47 (s, 3H). **^{13}C NMR** (151 MHz, $CDCl_3$) δ 153.9, 142.5, 140.5, 139.0, 135.2, 135.0, 129.9, 129.2, 122.3, 119.9, 36.1, 33.6, 14.0, 10.1. **LC-MS** (HPLC, acidic): t_r: 2.94 min, λ_{max}: 335 nm, purity: >99% (254 nm), $[M+H]^+$ m/z calc.: 295.17, found 295.15. **HRMS**: $[M+H]^+$ calc. for $C_{16}H_{18}N_6$: 295.1671, found 295.1665.

Chapter 6

Discussion and future perspectives

Discussion

This thesis describes the development of photoswitchable ligands (Figure 1) to explore emerging photoswitch moieties and concepts in the field of GPCR photopharmacology. In **Chapter 2**, the first radiolabeled photoswitchable ligand ([^{3}H]VUF26063) was disclosed. This ligand is an arylazopyrazole-based antagonist for the histamine H_3 receptor (H_3R) with subnanomolar affinity (K_i *trans* = 501 pM) and a 50-fold affinity shift upon illumination. This ligand was used to investigate whether ligands can isomerize in the binding pocket of the receptor. Kinetic data revealed that this ligand, upon illumination, undergoes isomerization within the binding pocket. In **Chapter 3**, a systematic "photoswitch hop" was performed by replacing the azobenzene moiety of a known H_3R antagonist with a diverse set of heteroarylazo switches. The synthesis, physicochemical, photochemical, and pharmacological properties of twelve different photoswitchable ligands were explored. These heteroaryl compounds exhibit diverse photochemical properties, often with red-shifted absorption but reduced PSS_{cis} values, while consistently achieving higher PSS_{trans} values and in multiple instances *cis* to *trans* isomerization using green light. An arylazoisoxazole ligand (VUF26257) emerged as the most promising compound having picomolar affinity (K_i *trans* = 158 pM), which is, to our knowledge, the highest affinity for a small-molecule ligand within the GPCR photopharmacology field. Upon illumination, this ligand showed a 13-fold decrease in affinity. In **Chapter 4**, efforts were directed toward developing a photoswitchable ligand for the human histamine H_1 receptor (H_1R), a GPCR for which such a ligand had remained elusive. An "azoscan" on the antihistamine desloratadine was carried out by functionalizing aromatic positions of the scaffold and introducing azobenzene moieties on the piperidine ring. This strategy resulted in nine photoswitchable ligands, which were characterized for their photochemical and pharmacological properties. It was found that an azobenzene located at the 2-position of desloratadine (as in VUF27037) is the most favorable position for placement of a photoswitchable group. This compound showed the best absolute affinity (K_i *trans* = 5 nM) and a 3.2-fold affinity shift upon isomerization. In **Chapter 5**, arylazopyrazoles were used to probe the isomeric effect of photoswitch placement, while simultaneously improving the photochemical and pharmacological properties. Building on the azobenzene-based H_3R agonists VUF15000 and VUF16003, analogues were designed with arylazopyrazole moieties introduced at central and peripheral positions to probe structure-activity relationships. These ligands exhibit good photochemical properties, including high PSS_{cis} and PSS_{trans} values and the ability to switch from *cis* to *trans* with green light. However, radioligand binding assays revealed a lack of affinity for H_3R, emphasizing both the potential as well as the design challenges of incorporating arylazopyrazoles into GPCR ligands.

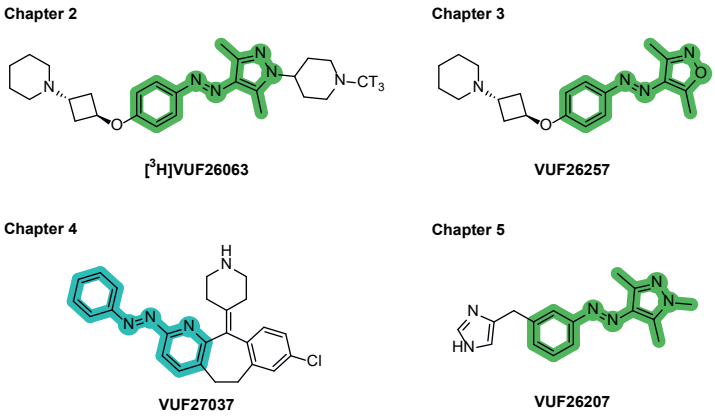

Figure 1. Structures of key compounds [^{3}H]VUF26063 (**Chapter 2**), VUF26257 (**Chapter 3**) and VUF27037 (**Chapter 4**), and of the ligand VUF26207 (**Chapter 5**).

Building on the findings reported in this thesis, this chapter will discuss the challenges and opportunities for photoresponsive ligands in GPCR photopharmacology. A key consideration remains the selection of a photoswitch moiety. It is important to consider both the physicochemical and photochemical properties of the photoswitchable ligand into which the moiety will be incorporated.

Physicochemical, photochemical, and kinetic properties of a photoswitch

Solubility

One of the limitations of azobenzenes is their poor aqueous solubility. This is predominantly the case for the hydrophobic *trans* isomer, which is 5-40 times less soluble than the *cis* isomer.[1–3] In early-stage drug discovery, solubility cut-offs of >100 µM are regularly applied for the aqueous solubility of organic compounds, and often *trans* azobenzenes do not reach these thresholds.[1,4] Substituents can significantly affect solubility, and several strategies have been proposed to improve it, including the formation of salts, decreasing planarity, and introducing polar (e.g., incorporating heteroatoms) or ionizable groups. In **Chapters 2** and **3**, the latter approach was used by replacing azobenzene moieties with heteroarylazo scaffolds. In **Chapter 2**, the approximate solubility was assessed by nephelometry, which revealed that VUF26063 displays improved aqueous solubility compared to the first-generation azobenzene VUF14682.[5] However, in **Chapter 3**, where a systematic "photoswitch hop" was performed, it was found that contrary to the hypothesis, incorporation of a heteroaromatic group not always results in improved aqueous solubility. While nephelometry can be used to obtain quantitative solubility data, in practice it is most often applied as a rapid, qualitative screening method, in contrast to the shake-flask approach.[6,7] However, nephelometry could be used to detect ligand aggregation, which may cause artifacts in assays.[8] A disadvantage of methods like the shake-flask method is that they require a significant amount of compound to establish aqueous solubility.[9]

In addition to heteroaryl incorporation, other strategies to reduce planarity were attempted and included the increase of the 3D character of photoswitch itself. Most photoswitches, including azobenzenes, are nearly planar, with a very high fraction of sp^2-hybridized atoms. Higher sp^3 content has been associated with improved solubility and also a higher success in drug discovery campaigns.[10] More recently, it has been suggested that this relationship has become less pronounced over the past 15 years, and that more complex factors contribute to the success of a drug.[11] Nevertheless, solubility remains an important consideration for photoswitchable ligands, as poor aqueous solubility can limit their biological application. One strategy to increase the sp^3-character is to use partially saturated azobenzene photoswitches such as cyclohexylphenyldiazene derivatives (Figure 2A), which introduce sp^3 character while keeping the ability to photoswitch. This scaffold has been described previously, but not in the context of photopharmacology.[12] However, within this PhD work, limitations were encountered regarding its chemical stability and air-sensitivity,[13] which limit their suitability for biological applications.

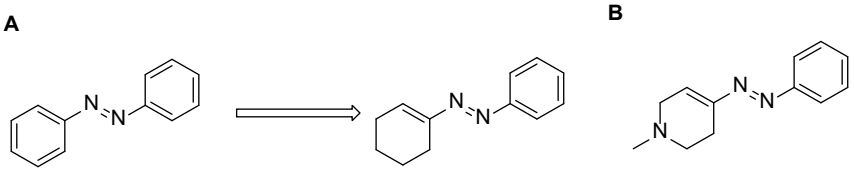

Figure 2. Structures of (A) an azobenzene and cyclohexylphenyldiazene[12] and (B) tetrahydropyridinyl phenyldiazine.

Basicity of photoswitches

To date, no reported photoswitches contain sp^3-hybridised basic alkylamines into the switch scaffold, despite such amines being ubiquitous in ligands, especially those for aminergic GPCRs. The cyclohexylphenyldiazene moiety provides an opportunity to introduce an alkylamine. In this PhD work, attempts were made to incorporate a sp^3-hybridised basic alkylamine in a cyclohexylphenyldiazene moiety (Figure 2B). The synthetic approach towards such ligands involves the reaction of phenylhydrazine with α-haloketones to form an arylhydrazone intermediate (Scheme 1).[14,15] The formation of this arylhydrazone is followed by 1,4-elimination after treatment with a mild base. First, attempts were made to prepare α-haloketones or α-hydroxyketones with one alpha position blocked to avoid complex mixtures of compounds. The synthesis and purification of these α-haloketones or α-hydroxyketones proved difficult, particularly for compounds containing a basic nitrogen atom. Additionally, the reaction conditions for the formations of hydrazones and subsequent elimination did not yield the desired product or afforded a significant amount of side products. Various conditions were probed, but none yielded clean formation and allowed isolation of the target compounds. Boc protection of the amine (R = Boc) did provide limited success, but upon deprotection compound decomposition was observed.

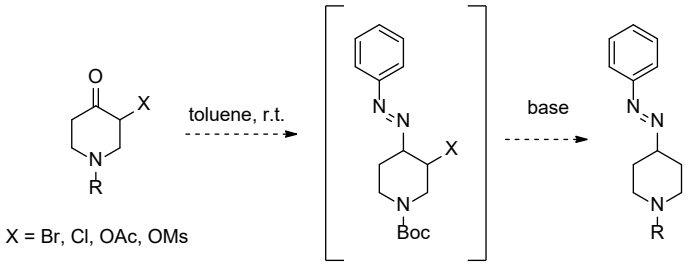

Scheme 1. Approach towards photoswitches with an embedded basic alkylamine.

Even if the compounds can be obtained, challenges will include a pronounced blue-shift in absorption features compared to the azobenzene, and multiple conformations of the photoswitching unit (*s*-trans and *s*-cis).[16] Preliminary evidence also suggests chemical stability must be addressed before these switches are explored further.

Photochemical properties

Another important consideration for photoswitchable ligands is their photochemical properties. Parameters for photoswitches such as absorption maxima, PSS, and thermal half-lives ($t_{½}$) are usually determined in organic solvents such as DMSO or acetonitrile. However, these conditions are often not representative of biological conditions, where the aqueous environment can influence photochemical properties.[17–20] Thus, a comparison between (reported) compounds may be complicated due to the lack of photochemical data in aqueous solvents and can affect the interpretation of structure–property relationships. Moreover, the effects of substituents on photochemical performance remain insufficiently understood. For example, while electron-donating and electron-withdrawing groups are known to shift absorption spectra, their influence on PSS values and thermal relaxation is often context-dependent. If the photopharmacology field aims to progress toward more rational design, standardized methodologies for photochemical characterization will be essential to further support the design. Ideally, all photoswitching properties are measured under biologically relevant conditions (e.g., aqueous buffer) and standardized light sources would substantially improve reproducibility and comparison across laboratories. An analogy can be drawn from the electrochemistry field, where standardized devices such as the ElectraSyn have been introduced to unify experimental setups and enhance reproducibility.[21] Establishing similar standards in photopharmacology would accelerate discovery and improve the robustness of structure–property relationships and improve design. However, in practice this will be difficult to achieve logistically.

Binding kinetics: can compounds switch in the pocket?

Most studies on photoswitchable ligands focus on properties such as the PSS values and binding affinity. However, less attention has been given to the kinetics, i.e., both the photoswitching kinetics but also the binding kinetics. However, in recent years more attention has been given to these phenomena, particularly concerning how photoswitchable ligands

behave inside the receptor pocket. This represents an important area to study, because switching events during binding can fundamentally change ligand residence times and thereby alter outcomes in functional biological effects. The azobenzene-based ligands for $mGluR_5$ and A_{2A} receptors discussed in **Chapter 2** illustrates that the local protein environment can strongly influence photoswitching behavior,[22,23] which can affect the overall observed binding kinetics of the ligand, because the two isomers may interact with distinct conformations of the receptor.[24] In this thesis, **Chapter 2** provides direct evidence that photoswitchable ligands can undergo isomerization inside the GPCR binding pocket. Using the first radiolabeled photoswitchable ligand ([^{3}H]VUF26063), kinetic binding experiments revealed a light-dependent kinetic pattern that is consistent with isomerization occurring inside the receptor. Molecular modeling suggests that this ligand occupies the extended binding pocket of the H_3R, providing enough space for photoswitching. For the H_3R ligands studied in **Chapter 2**, this meant that in-pocket photoswitching could directly alter the dynamic behavior of the ligand-receptor complex. Such effects need to be considered in future ligand design, as they provide both an opportunity for controlling receptor function at the kinetic level, but also a challenge in predicting behavior from their properties alone.

Rational design, computational aided design and synthesis

Design workflow for photoswitchable ligands

The development of photoswitchable ligands and the use of approaches such as the "photoswitch hop" described in this thesis tend to be time-consuming and inefficient. They require significant synthetic effort, photochemical characterization, and pharmacological efforts. Perhaps due to substantial synthetic and characterization effort required, many photopharmacology studies select a photoswitchable ligand once acceptable properties have been identified, rather than pursuing more extensive optimization. Thus, unlike traditional medicinal chemistry campaigns, where projects typically evolve from hit identification to lead optimization and eventually clinical candidates,[25] photopharmacology has so far remained limited to relatively small structure-activity relationships explorations.[26] This likely hampers the transition from proof-of-concept tools to ligands that could eventually be developed as drug candidates.

Other factors also affect further optimization of a photoswitchable hit ligands. While the chemistry for azobenzene incorporation is relatively well established,[27–29] it can still alter compound reactivity and stability. Moreover, synthetic throughput is often lower than in conventional medicinal chemistry campaigns, because in addition to chemical analyses, also photochemical analyses are required for each compound. The challenge of designing compounds is further complicated by the need to balance the usual physicochemical and pharmacological properties with additional photochemical requirements such as PSS values, thermal half-lives, and switching wavelengths. Notably, each compound represents effectively two ligands. Both the *trans* and *cis* isomers (often as PSS_{cis}) must be evaluated, and the

properties of each compound should be established.[30] Additionally, the general limitations of most photoswitches discussed earlier, such as the solubility and reliance on UV light for many scaffolds, remain.

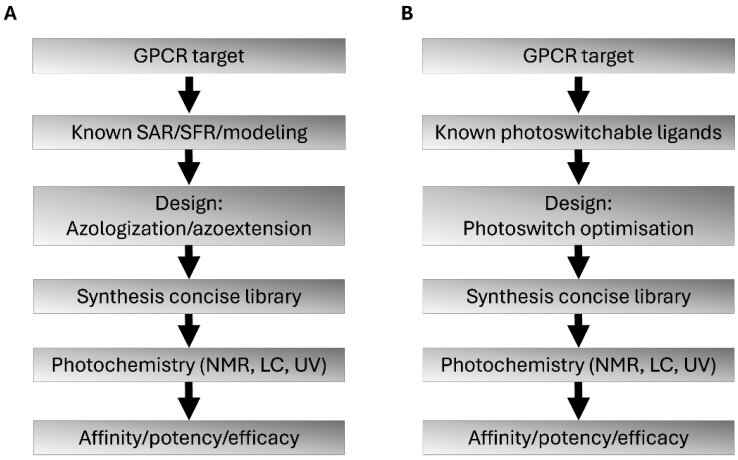

Figure 3. (A) First-generation workflow for the design of photoswitchable GPCR ligands. (B) New workflow for the design of for the design of photoswitchable GPCR ligands.

In this thesis, an alternative design strategy was explored compared to the "first-generation" approach that was used by our group (Figure 3A). As described in **Chapter 1,** the common workflow typically begins by selecting a GPCR target, analyzing available structure-activity relationships or structure-functional relationships data, and selecting an azologization or azoextension strategy. A small library is then synthesized and characterized for photochemical and pharmacological properties, after which a single key compound is selected for more detailed study. In contrast to this approach, in **Chapters 2**, **3**, and **5** previously validated azobenzene-based ligands were used as a starting point and attempts were made to improve their properties by introducing emerging photoswitches (Figure 3B). This approach was successful in some cases, i.e., VUF26063 and VUF26257, but not in **Chapter 5**, where incorporation of arylazopyrazoles resulted in complete loss of affinity. In **Chapter 4**, we followed the more traditional strategy, which resulted in a ligand that showed moderate success but did not yet meet the desired profile. These outcomes demonstrate the challenges, and suboptimal efficiencies remain in the design process, even when starting from well-characterized photoswitchable ligands.

Computer-aided design

Given the surge of GPCR structures released in recent years, computational modeling appears to be a potential solution to the design challenges faced by the field. However, prospective applications in photopharmacology remain very limited. Often, modeling is used retrospectively to rationalize observed results (e.g., **Chapters 2** and **4**) rather than to guide

design. Predicting the binding of both *trans* and *cis* isomers is inherently difficult, as some computational tools do not preserve the correct geometry of the azobond. Furthermore, modeling the inactive isomer can be challenging because docking algorithms may attempt to force the ligand in the binding pocket regardless of whether binding is possible. Flexible parts of a ligand present an additional layer of complexity, as docking algorithms often force them into conformations that appear to fit even when binding is unlikely. Any flexibility of photoswitchable ligands is not only a challenge for modelling. Schehr *et al*. postulated that the flexibility of a ligand and conformational changes of a receptor could lead to an induced fit. Therefore, no differences may be observed between the two isomers.[31] Moreover, subtle differences in pocket shape can determine whether a ligand functions as a compound that is more active in the *cis* configuration ("*cis*-on") or in the *trans* configuration ("*trans*-on"), making predictions difficult.

Despite these challenges, advances in computational methodologies could transform the design of photoswitchable ligands. In addition to computational methods such as docking and molecular dynamics of photoswitchable ligands, Kobauri *et al*. highlighted the exploration of methods including 3D pharmacophores, 3D-QSAR and AI-based approaches for the design of photoswitchable ligands.[32] Recently, Simon *et al.* reported an open-source computational platform for the design and virtual screening of new photoswitchable ligands.[33] This platform uses activity data of known ligands and incorporates photoswitchable moieties in the parent ligands through azologization or azoextension.[33] Altogether, these computational methods will offer new opportunities to aid the rational design of photoswitchable ligands.

Synthesis of photoswitchable ligands

In addition to the design challenges, the synthetic feasibility of photoswitchable ligands is an important subject. The synthesis of photoswitchable ligands is generally well established, particularly for azobenzenes, which can be prepared through the Mills reaction or diazonium coupling. In our experience, arylazopyrazoles can also be introduced relatively easily. Ideally, the photoswitchable moiety is installed as late as possible in the synthesis route. However, bioactive scaffolds may contain reactive functional groups that complicate late-stage functionalization and require careful selection of protecting groups and conditions. Purification can also be challenging, as photoswitchable compounds often show atypical behavior during column chromatography as a result of poor solubility and their sensitivity to light. The development of red-shifted photoswitches, such as tetra-*ortho*-substituted azobenzenes and heteroarylazo switches, requires improved synthetic strategies to overcome issues like steric demands, low reactivity, or instability. In recent years, several methods have been developed to address these challenges. However, as shown in **Chapter 3**, up to five different methods were applied to obtain a range of heteroarylazo scaffolds. Despite these efforts, several target compounds could not be synthesized, and some reactions were inefficient. These results emphasize that while the synthesis is feasible, further improvements are required to make these systems more synthetically accessible and applicable to a wider range of ligands. Overall, development of methods that allow late-stage functionalization with

photoswitchable moieties would be desirable. Such approaches would simplify synthesis and expand the accessible chemical space for photopharmacological applications and improve the efficiency of photopharmacology projects.

Emerging photoswitch moieties in GPCR photopharmacology

Although significant progress has been made in the photopharmacology field over the past decade, a 2021 study showed that over 80% of photoswitchable ligands in class A GPCR photopharmacology comprised an azobenzene moiety.[26] Azobenzenes suffer from poor aqueous solubility and rely on UV light to switch from the *trans* to the *cis* isomer, which can cause problems in biological systems due to limited tissue penetration.[18,30] Isomerization to the *trans* isomer requires blue light (>400 nm) and overlap in the absorption spectrum of both isomers in that region reduces the photostationary state (PSS_{trans}) values. To address these limitations, recent strategies have attempted to explore ligands that can be switched using visible light to overcome the limitations associated with the use of UV light. The use of emerging photoswitch classes, such as heteroaryl and tetra-*ortho*-substituted azobenzene photoswitches, has gained significantly more attention over the past decade.[34–36] Various combinations of *ortho* substituents are possible. However, only photoswitchable ligands with tetra-*ortho*-fluoro-azobenzenes and tetra-*ortho*-chloro-azobenzenes have been reported.[34] Additionally, heteroaryl photoswitches are emerging in the field of photopharmacology.[35,37] Especially the arylazopyrazoles have become an important photoswitch moiety.[38–46]

The work described in **Chapters 2** and **5** demonstrates how these different photoswitch moieties, in these cases specifically the arylazopyrazoles, can affect the photochemical properties and affinity. In **Chapter 2**, the incorporation of an arylazopyrazole scaffold resulted in a compound with improved photochemical properties, including enhanced PSS_{trans} value, improved physicochemical properties such as solubility, and an increased affinity for H_3R compared to the first-generation azobenzene-based antagonist VUF14862. In contrast, in **Chapter 5**, replacing the azobenzene with an arylazopyrazole in a first-generation agonist for the same receptor, i.e., H_3R, resulted in a completely different outcome in terms of affinity. While the compounds showed excellent photochemical properties, they exhibited a complete loss of affinity upon incorporation of this scaffold. This suggests that steric factors and subtle structural modifications, such as placement of a methyl group in the *ortho* position, strongly influence receptor binding. On the other hand, these methyl substituents are required for optimal PSS_{trans} values in the arylazopyrazole scaffold. This highlights both the potential but also the challenges of incorporating novel photoswitch moieties into already known photoswitchable ligands, and provides insights for future optimization. Specifically, the result of replacing an azobenzene by an alternative siwtch is also dependent on the selected scaffold, its orientation in the binding pocket, and the compatibility with the pharmacophore.

Although more heteroaryl photoswitches have emerged in recent years, there are still many five-membered heteroarylazo switches that are unknown in the photopharmacology field. Additionally, the photochemical and pharmacological properties of these switches have not yet been systematically compared, which may be due to the limited availability of synthetic procedures for incorporating these photoswitches into drug-like structures.[47,48] In **Chapter 3**, a "photoswitch hop" on a H_3R ligand was performed and the physicochemical and photochemical properties of twelve known and underexplored five-membered heteroarylazo photoswitches were compared to those of the azobenzene.[49,50] While several photoswitchable ligands still require UV light (360 nm) for *trans* to *cis* isomerization, other heteroarylazo photoswitches exhibit red-shifted λ_{max} *trans* values, enabling the use of blue light for *trans* to *cis* isomerization. However, this results in reduced PSS_{cis} values. This demonstrates the trade-off between using red-shifted wavelengths and achieving optimal PSS values. Notably, however, all heteroarylazo photoswitches show improved wavelengths for switching (494-560 nm) and improved PSS_{trans} values compared to the azobenzene. Moreover, the thermal stability of the *cis* isomers varies significantly across the series, indicating that the thermal relaxation can be tuned with these switches. While several of these heteroarylazo photoswitches show promising properties, their successful implementation in photopharmacology switches will depend on their application and specific target. Although only a selected subset of five-membered heterocycles was probed in this chapter, it does not fully cover the vast diversity of heterocycles available. Other substitution patterns should be investigated, as well as different substituents and even fused-ring systems. Moreover, based on their potential, further tuning of the photochemical properties of these heteroaromatic photoswitches could be pursued. The primary focus should be on moving away from the UV spectrum for *trans* to *cis* switching. Additionally, other modifications could be attempted to improve *cis* to *trans* switching, like *ortho*-methyl substituents since they been shown to lead to better separation of the n-π* absorption in arylazopyrazoles.[51] However, such optimization would require more fundamental studies and extensive computational investigations to predict their properties accurately. Initial efforts toward this have been made by the group of Lopez for heteroarylazo switches.[52,53]

Systematic comparison of emerging photoswitches

In addition to the incorporation of heteroarylazo photoswitches examined in **Chapters 2, 3, and 5**, throughout the thesis work several occasions emerged to also investigate photoswitchable ligands comprising other emerging photoswitches. One case involved H_3R as a protein target (Table 1) and the ligands included tetra-*ortho*-substituted azobenzenes, albeit connected to a more flexible linker compared to the rigid linker used in **Chapters 2** and **3**. These ligands could be switched using visible light in both directions, i.e., red-shifted wavelengths (520/560 nm) could be used instead of UV to switch from the *trans* to the *cis* isomers and the same wavelength as the azobenzene (434 nm) could be used to switch from the *cis* to the *trans* isomer. However, despite the advantage of visible light switching, the incorporation of these photoswitch moieties resulted in a more than 10-fold decrease in

affinity for both the *trans* and at PSS_{cis} states (Table 1). In contrast, upon incorporation of arylazopyrazole moieties, the affinity of the ligands increases. However, no affinity shift was observed for these ligands.

Table 1. Photchemical parameters and human H_3R binding affinity values for red-shifted photoswitchable H_3R ligands.

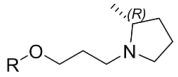

R		PSS_{cis} (wavelength used)[a]	PSS_{trans} (wavelength used)[b]	pK_i hH$_3$R *trans* ± SEM[c]	pK_i hH$_3$R PSS_{cis} ± SEM[c]	pK_i shift
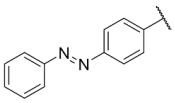	**1a**	96% (360 nm)	70% (434 nm)	8.6 ± 0.2	8.2 ± 0.1	-0.4
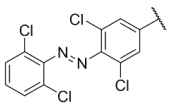	**1b**	76% (520 nm)	n.d.	6.0 ± 0.1	6.7 ± 0.1	0.7
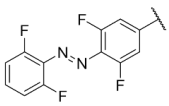	**1c**	84% (560 nm)	81% (434 nm)	6.9 ± 0.2	7.0 ± 0.2	0.1
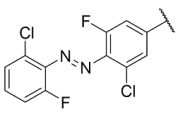	**1d**	90% (560 nm)	86% (434 nm)	6.3 ± 0.1	6.9 ± 0.2	0.6
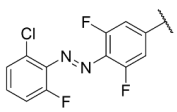	**1e**	88% (560 nm)	83% (434 nm)	6.9 ± 0.2	7.0 ± 0.2	0.1
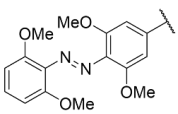	**1f**	70% (520 nm)	97% (434 nm)	5.2 ± 0.0	5.7 ± 0.1	0.5
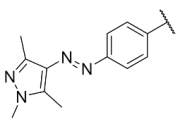	**1g**	94% (360 nm)	94% (494 nm)	9.3 ± 0.2	9.1 ± 0.2	-0.2
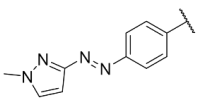	**1h**	95% (360 nm)	81% (460 nm)	9.0 ± 0.1	9.1 ± 0.2	0.1

[a]Photostationary state area percentages after illumination of *trans* isomer with the indicated illumination wavelength to PSS_{cis} at 10 mM in DMSO as determined by acidic LC-MS analysis at the isosbestic point.

[b]Photostationary state area percentages after illumination of PSS_{cis} states with the indicated illumination wavelength for PSS_{trans} at 10 mM in DMSO as determined by acidic LC-MS analysis at the isosbestic point.

[c]Affinity (pK_i) values obtained from radioligand competition experiments with 1.6 nM [^{3}H]NAMH. Values are means of n = 3 experiments ± SEM, performed in triplicate.

A similar approach was applied to another class A GPCR, the beta adrenergic 1 receptor (β_1AR). That study was based on Opto-prop-3 (Figure 4), which shows an absolute affinity of 12 nM in the *trans* state and an 18-fold decrease in affinity upon illumination.[54] Similar results were obtained for these compounds as in the H_3R case. They can be switched in both directions using visible light, yet the incorporation reduces the affinity for β_1AR. In this case, however, and in contrast to H_3R, the use of arylazopyrazoles also results in a significant decrease in affinity.

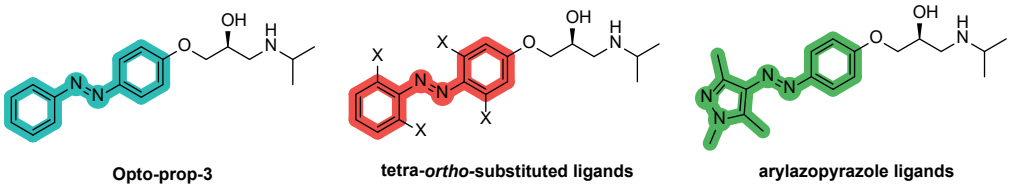

Figure 4. Structures of opto-prop-3 and examples of tetra-*ortho*-substituted and arylazopyrazole-based β_1AR photoswitchable ligands.

When looking at the photochemical properties of the involved tetra-*ortho*-substituted photoswitches, irradiation is performed in the tail of the n–π* absorption band. As a result, the photoswitching at higher wavelengths often requires substantially longer irradiation times to reach the PSS. Although UV light is not optimal for biological applications due to its poor tissue penetration and potential toxicity, for multiple ligands similar PSS_{cis} values could be obtained faster by irradiating at 365 nm. Additional challenges were encountered regarding physicochemical properties. For compounds containing *ortho*-fluorine atoms, chemical stability was limited due to the increased reactivity imposed on the aromatic rings by the fluorine atoms. This may compromise their usefulness over the long term and for biological applications. Moreover, solubility also became a limiting factor for both tetra-*ortho*-chloro- and tetra-*ortho*-methoxy-substituted derivatives. These showed precipitation in buffer compared to the other ligands.

These findings demonstrate that while new photoswitch scaffolds such as tetra-*ortho*-azobenzenes and arylazopyrazoles hold promise for expanding the photopharmacological toolbox, their successful integration into bioactive GPCR ligands remains highly context-dependent and outcomes can significantly differ between receptors. The balance between photochemical performance and pharmacological activity is therefore a recurring challenge and highlights the need for systematic evaluations and methods to identify which scaffolds are most suitable for a specific receptor and application.

Approaches towards photoswitchable ligands with signalling bias

GPCRs can activate both G protein and β-arrestin mediated pathways. Ligands that preferentially activate one pathway over the other can result in different physiological responses.[55,56] Designing biased ligands therefore provides an interesting opportunity in GPCR drug discovery. The use of photopharmacological approaches offers a unique opportunity to study these signaling processes and gain spatial and temporal control over bias. To date, only a few biased photoswitchable ligands have been reported. While some can preferentially activate either G protein or β-arrestin pathways, [57–60] none are able to activate either one of the two reversibly upon illumination. In this thesis, attempts were made to find ligands that could achieve photoswitching of biased signalling. Ligands based on the histamine H_3/H_4 receptor ligand clobenpropit were studied, and earlier studies suggested that variations in chlorine substitution on the phenyl ring could give differences in signaling preference at the H_4R (Figure 5A).[61]

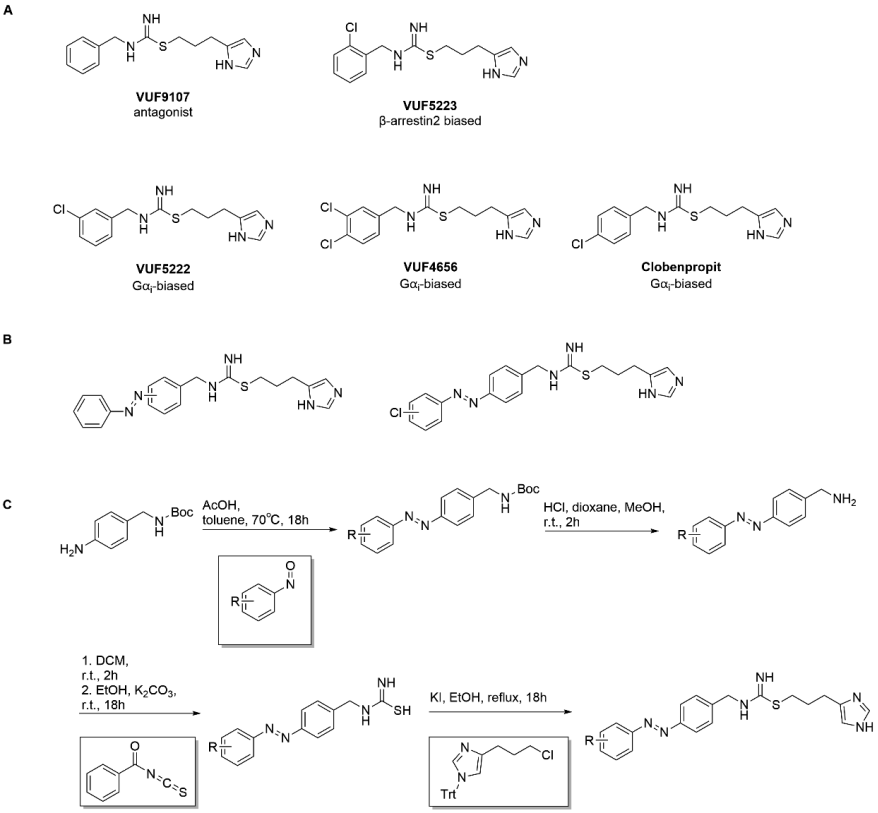

Figure 5. (A) Structure of clobenpropit as well as its derivatives with various chlorine substituents and their signalling bias for H_4R. (B) Photoswitchable ligands based on clobenpropit. (C) Synthetic approach towards photoswitchable clobenpropit analogs.

To explore this concept, analogues were designed (Figure 5B) and synthesized (Figure 5C) in which the phenyl ring was extended with azobenzenes. However, challenges were encountered like chemical stability issues, particularly for the *ortho*- and *meta*-substituted ligands, indicating that the choice of scaffold is important. Initial photopharmagological studies show that some compounds provide a potency switch on H_4R, but not a pronounced bias switch.

In general, the current understanding of how proteins translate ligand binding into signaling bias remains incomplete and therefore the design of such ligands is even more complicated. Signalling bias may depend on subtle changes in the structure of a ligand, as demonstrated by the varying position of the chlorine in clobenpropit. This adds another layer of complexity to the already intricate design process. Another important challenge lies in the quantification of signaling bias itself.[62] Direct comparisons can be obscured upon use of different methods, which can result in different verdicts on whether a ligand is biased or not.[62] These considerations suggest that while photoswitchable biased ligands remain interesting, a deeper mechanistic understanding of biased signaling is required at the structural level and improved strategies for design are needed.

Towards photoswitchable ligands for *in vivo* use

All the pharmacological work described in this thesis has been carried out *in vitro*. Translating these approaches into *in vivo* will face challenges. The major limitation remains the use of UV light, which is typically used for photoswitching from the *trans* to *cis* isomer, and has limited tissue penetration and possible toxicity. While implantable optical fibers represent possible solutions,[63–65] ideally, photopharmacology should be applied in a minimally invasive manner. For this reason, future progress will depend heavily on improving photoswitch scaffolds themselves and/or devising innovative methods to enhance the performance of existing ones.

To address the challenges of the azobenzene-based photoswitchable ligands for the H_1 receptor as described in **Chapter 4**, we explored the development of another photoresponsive ligand with photochemical properties desirable for *in vivo* use. Specifically, we pursued the design of a Cy7 photocaged ligand (Figure 6).[66,67] Within our group, several desloratadine-based photocages had already been developed. Building on that work, we selected a red-shifted cage that could, in principle, be uncaged using NIR light (>780 nm). Although the ligand was prepared successfully, no uncaging of the ligand was observed under the tested conditions even in the presence of salts, which has been reported to promote the uncaging.[66]

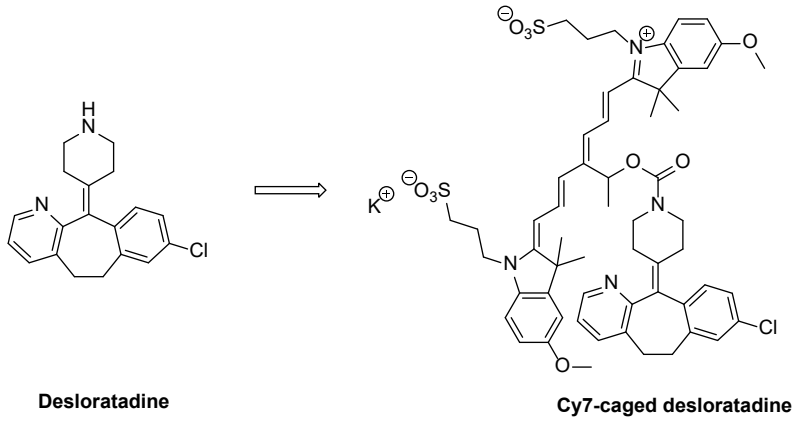

Figure 6. Structure of Desloratadine and Cy7-caged desloratadine

Moreover, to gain a better understanding of the behavior of photoswitchable ligands *in vivo*, new tools are needed. In addition to the tritium ligand described in **Chapter 2**, a PET ligand, i.e., [^{11}C]VUF26063, was developed (Scheme 2). The ability to radiolabel this compound offers opportunities. During the reaction, both the *trans* and *cis* isomers were formed and could be separated and isolated. This would allow the *in vivo* evaluation of them separately, enabling detailed studies, for example, of their distribution. In later stages this tracer could be used to photoswitch the ligand *in vivo*. PET tracers could be used to study these strategies in live animals. PET tracers like [^{11}C]VUF26063 serve as powerful translational tools that bring together chemistry, pharmacology, and imaging. A photoswitchable PET tracer could further improve the understanding of the behavior of the photoswitchable ligands *in vivo*.

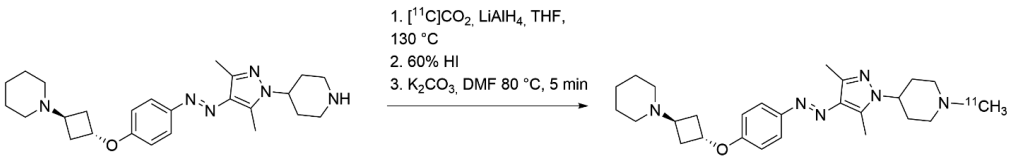

Scheme 2. Synthesis of [^{11}C]VUF26063.

Concluding remarks

This thesis demonstrates how emerging photoswitch moieties, particularly heteroarylazo switches such as arylazopyrazoles, can expand the photopharmacological toolbox and provide opportunities for studying concepts like binding kinetics. Incorporating these scaffolds in well-characterized photoswitchable ligands revealed both advantages and challenges. Ligands such as VUF26063 and VUF26257, described in **Chapters 2** and **3**, demonstrate how incorporation of new photoswitches can give improved photochemical, physicochemical and pharmacological properties. In contrast, the loss of affinity observed for arylazopyrazole-containing H_3R agonists (**Chapter 5**) underscores the fine balance required for photoswitch incorporation. It demonstrates the need for careful balancing of the various properties in

addition to the standard challenges faced in medicinal chemistry. These findings also show that the design of photoswitchable ligands remains a complex task and that a better understanding of the structure-property relationships is important to advance the design process, especially as new scaffolds continue to emerge. However, developments in computer aided design could provide opportunities to aid the design and better predict ligands' properties. Although significant progress has been made in red-shifting the switching wavelengths, optimal photoswitches that can operate in the near-infrared light and are compatible in biological settings have yet to be developed. Achieving this will require development or improvement of synthetic methods. Although a variety of synthetic procedures are known, [29,68–72] this thesis illustrates for heteroarylazo switches that it remains a point of attention. Further improvement of synthetic methodologies is required to develop next-generation photoswitch scaffolds.

Future progress will also depend on gaining a more detailed understanding of how photoswitchable ligands bind to receptors. To date, structural data of GPCRs in complex with photoswitchable ligands is mostly lacking. It often remains unclear how the *trans* and *cis* configurations of these ligands bind in the binding pocket, and in what conformation. These structural insights would significantly improve the ability to design photoswitchable ligands and to rationalize observed pharmacological properties. Systematic studies on emerging photoswitches, prospective computational approaches, and standardized photochemical characterization under biologically relevant conditions will all be essential to advance the photopharmacology field further. Studies on photoswitching kinetics and signaling bias, together with tools such as PET tracers could provide an opportunity to advance from *in vitro* to *in vivo* applications.

Although challenges remain, the field of photopharmacology is progressively advancing to improved and more biologically compatible photoswitches, as well as a better mechanistic understanding of ligand behavior. The work presented in this thesis aids in laying the groundwork for next generation photoswitchable GPCR ligands. The ligands described here offer an opportunity to investigate receptor function with spatial and temporal control and may guide future efforts in the field.

References

(1) Brown, C.; Rastogi, S. K.; Barrett, S. L.; Anderson, H. E.; Twichell, E.; Gralinski, S.; McDonald, A.; Brittain, W. J. Differential Azobenzene Solubility Increases Equilibrium Cis/Trans Ratio in Water. *J Photochem Photobiol A Chem* **2017**, *336*, 140–145. https://doi.org/10.1016/j.jphotochem.2016.12.013.

(2) Hartley, G. S. 113. The Cis-Form of Azobenzene and the Velocity of the Thermal Cis→trans-Conversion of Azobenzene and Some Derivatives. *Journal of the Chemical Society (Resumed)* **1938**, No. 0, 633–642. https://doi.org/10.1039/jr9380000633.

(3) Volarić, J.; Szymanski, W.; Simeth, N. A.; Feringa, B. L. Molecular Photoswitches in Aqueous Environments. *Chem Soc Rev* **2021**, *50* (22), 12377–12449. https://doi.org/10.1039/d0cs00547a.

(4) Hughes, J. P.; Rees, S. S.; Kalindjian, S. B.; Philpott, K. L. Principles of Early Drug Discovery. *Br J Pharmacol* **2011**, *162* (6), 1239. https://doi.org/10.1111/j.1476-5381.2010.01127.x.

(5) Binkhorst, L. C. P.; Josimovic, I.; Boer, B. De; Simon, I. A.; Aa, F. Van Der; Zarzycka, B. A.; Esch, I. J. P. De; Vischer, H. F.; Windhorst, A. D.; Wijtmans, M.; Leurs, R. A Radiolabeled Photoswitchable G Protein-Coupled Receptor Antagonist Enlightens Ligand Binding Kinetics Associated with Photoswitching. *J Am Chem Soc* **2025**. https://doi.org/10.1021/jacs.5c07349.

(6) Brea, J.; Varela, M. J.; Daudey, G. A.; Loza, M. I. High-Throughput Nephelometry Methodology for Qualitative Determination of Aqueous Solubility of Chemical Libraries. *SLAS Discovery* **2024**, *29* (3), 100149. https://doi.org/10.1016/j.slasd.2024.100149.

(7) Hoelke, B.; Gieringer, S.; Arlt, M.; Saal, C. Comparison of Nephelometric, UV-Spectroscopic, and HPLC Methods for High-Throughput Determination of Aqueous Drug Solubility in Microtiter Plates. *Anal Chem* **2009**, *81* (8), 3165–3172. https://doi.org/10.1021/ac9000089.

(8) Sassano, M. F.; Doak, A. K.; Roth, B. L.; Shoichet, B. K. Colloidal Aggregation Causes Inhibition of G Protein-Coupled Receptors. *J Med Chem* **2013**, *56* (6), 2406–2414. https://doi.org/10.1021/jm301749y.

(9) Könczöl, Á.; Dargó, G. Brief Overview of Solubility Methods: Recent Trends in Equilibrium Solubility Measurement and Predictive Models. *Drug Discov Today Technol* **2018**, *27*, 3–10. https://doi.org/10.1016/j.ddtec.2018.06.001.

(10) Lovering, F.; Bikker, J.; Humblet, C. Escape from Flatland: Increasing Saturation as an Approach to Improving Clinical Success. *J Med Chem* **2009**, *52* (21), 6752–6756. https://doi.org/10.1021/jm901241e.

(11) Churcher, I.; Newbold, S.; Murray, C. W. Return to Flatland. *Nature Reviews Chemistry* **2025**, *9* (3), 140–141. https://doi.org/10.1038/s41570-025-00688-5.

(12) Conti, I.; Marchioni, F.; Credi, A.; Orlandi, G.; Rosini, G.; Garavelli, M. Cyclohexenylphenyldiazene: A Simple Surrogate of the Azobenzene Photochromic Unit. *J Am Chem Soc* **2007**, *129* (11), 3198–3210. https://doi.org/10.1021/ja0668466.

(13) Caglioti, L.; Grasselli, P.; Rosini, G. Phenylazoalkenes from the Alkaline Decomposition of Phenyltosylhydrazones. *Tetrahedron Lett* **1965**, *6* (50), 4545–4548. https://doi.org/10.1016/s0040-4039(01)89060-2.

(14) Brodka, S.; Simon, H. Darstellung Verschieden Substituierter 1-Benzolazo-Alkene Und Additionsprodukte. *Chem. Ber* **1969**, *102*, 3647–3655. https://doi.org/10.1002/cber.19691021106.

(15) Caglioti, L.; Rosini, G.; Rossi, F. Azoalkenes as Intermediate Compounds in the Formation of Osazones from α-Acetoxy Ketones. *J Am Chem Soc* **1966**, *88* (16), 3865–3866. https://doi.org/10.1021/ja00968a038.

(16) Schantl, J. G.; Hebeisen, P. 1-Phenylazo-1-Alkenes. *Tetrahedron* **1990**, *46* (2), 395–406. https://doi.org/10.1016/s0040-4020(01)85424-7.

(17) Wijtmans, M.; Josimovic, I.; Vischer, H. F.; Leurs, R. Optical Control of Class A G Protein-Coupled Receptors with Photoswitchable Ligands. *Curr Opin Pharmacol* **2022**, *63*, 102192. https://doi.org/10.1016/j.coph.2022.102192.

(18) Volarić, J.; Szymanski, W.; Simeth, N. A.; Feringa, B. L. Molecular Photoswitches in Aqueous Environments. *Chem Soc Rev* **2021**, *50* (22), 12377–12449. https://doi.org/10.1039/d0cs00547a.

(19) Bandara, H. M. D.; Burdette, S. C. Photoisomerization in Different Classes of Azobenzene. *Chem Soc Rev* **2012**, *41* (5), 1809–1825. https://doi.org/10.1039/c1cs15179g.

(20) Broichhagen, J.; Frank, J. A.; Trauner, D. A Roadmap to Success in Photopharmacology. *Acc Chem Res* **2015**, *48* (7), 1947–1960. https://doi.org/10.1021/acs.accounts.5b00129.

(21) Yan, M.; Kawamata, Y.; Baran, P. S. Synthetic Organic Electrochemistry: Calling All Engineers. *Angewandte Chemie International Edition* **2018**, *57* (16), 4149–4155. https://doi.org/10.1002/anie.201707584.

(22) Saßmannshausen, T.; Glover, H.; Trabuco, M.; Neidhart, W.; Cheng, R.; Hennig, M.; Slavov, C.; Standfuss, J.; Wachtveitl, J. Kinetic Basis for the Design of Azobenzene-Based Photoswitchable A2a Adenosine Receptor Ligands. *J Am Chem Soc* **2024**, *146* (47), 32670–32677. https://doi.org/10.1021/jacs.4c11995.

(23) Ricart-Ortega, M.; Berizzi, A. E.; Pereira, V.; Malhaire, F.; Catena, J.; Font, J.; Gómez-Santacana, X.; Munõz, L.; Zussy, C.; Serra, C.; Rovira, X.; Goudet, C.; Llebaria, A. Mechanistic Insights into Light-Driven Allosteric Control of GPCR Biological Activity. *ACS Pharmacol Transl Sci* **2020**, *3* (5), 883–895. https://doi.org/10.1021/acsptsci.0c00054.

(24) Glover, H.; Saßmannshausen, T.; Bertrand, Q.; Trabuco, M.; Slavov, C.; Bacchin, A.; Andres, F.; Kondo, Y.; Stipp, R.; Wranik, M.; Khusainov, G.; Carrillo, M.; Kekilli, D.; Nan, J.; Gonzalez, A.; Cheng, R.; Neidhart, W.; Weinert, T.; Leonarski, F.; Dworkowski, F.; Kepa, M.; Wachtveitl, J.; Hennig, M.; Standfuss, J. Photoswitch Dissociation from a G Protein-Coupled Receptor Resolved by Time-Resolved Serial Crystallography. *Nat Commun* **2024**, *15* (1), 10837. https://doi.org/10.1038/s41467-024-55109-w.

(25) Brown, D. G. An Analysis of Successful Hit-to-Clinical Candidate Pairs. *J Med Chem* **2023**, *66* (11), 7101–7139. https://doi.org/10.1021/acs.jmedchem.3c00521.

(26) Wijtmans, M.; Josimovic, I.; Vischer, H. F.; Leurs, R. Optical Control of Class A G Protein-Coupled Receptors with Photoswitchable Ligands. *Current Opinion in Pharmacology*. **2022**. https://doi.org/10.1016/j.coph.2022.102192.

(27) Tavassoli, A.; Hamilton, A. D.; Spring, D. R.; Beharry, A. A.; Woolley, G. A. Azobenzene Photoswitches for Biomolecules. *Chem Soc Rev* **2011**, *40* (8), 4422–4437. https://doi.org/10.1039/c1cs15023e.

(28) Küllmer, F.; Gregor, L.; Arndt, H. D. Systematic Modifications of Substitution Patterns for Property Tuning of Photoswitchable Asymmetric Azobenzenes. *Org Biomol Chem* **2022**, *20* (20), 4204–4214. https://doi.org/10.1039/d2ob00214k.

(29) Merino, E. Synthesis of Azobenzenes : The Coloured Pieces of Molecular Materials. *Chem Soc Rev* **2011**, *40* (7), 3835–3853. https://doi.org/10.1039/c0cs00183j.

(30) Fuchter, M. J. On the Promise of Photopharmacology Using Photoswitches: A Medicinal Chemist's Perspective. *J Med Chem* **2020**, *63* (20), 11436–11447. https://doi.org/10.1021/acs.jmedchem.0c00629.

(31) Schehr, M.; Ianes, C.; Weisner, J.; Heintze, L.; Müller, M. P.; Pichlo, C.; Charl, J.; Brunstein, E.; Ewert, J.; Lehr, M.; Baumann, U.; Rauh, D.; Knippschild, U.; Peifer, C.; Herges, R. 2-Azo-, 2-Diazocine-Thiazols and 2-Azo-Imidazoles as Photoswitchable Kinase Inhibitors: Limitations and Pitfalls of the Photoswitchable Inhibitor Approach. *Photochemical and Photobiological Sciences* **2019**, *18* (6), 1398–1407. https://doi.org/10.1039/c9pp00010k.

(32) Kobauri, P.; Dekker, F. J.; Szymanski, W.; Feringa, B. L. Rational Design in Photopharmacology with Molecular Photoswitches. *Angew. Chem. Int. Ed.* **2023**, *62* (30), e202300681. https://doi.org/10.1002/anie.202300681.

(33) Simon, I. A.; Homan, E. J.; Wijtmans, M.; Sundström, M.; Leurs, R.; De Esch, I. J. P.; Zarzycka, B. A. PSW-Designer: An Open-Source Computational Platform for the Design and Virtual Screening of Photopharmacological Ligands. *J Chem Inf Model* **2023**, *63* (21), 6696–6705. https://doi.org/10.1021/acs.jcim.3c01050.

(34) Cardano, F.; Márquez García, R.; Szymanski, W. Manipulation of Chemistry and Biology with Visible Light Using Tetra-ortho-Substituted Azobenzenes and Azonium Ions. *Angewandte Chemie International Edition* **2025**. https://doi.org/10.1002/anie.202423506.

(35) Dang, T.; Zhang, Z. Y.; Li, T. Visible-Light-Activated Heteroaryl Azoswitches: Toward a More Colorful Future. *J Am Chem Soc* **2024**, *146* (29), 19609–19620. https://doi.org/10.1021/jacs.4c03135.

(36) Dong, M.; Babalhavaeji, A.; Samanta, S.; Beharry, A. A.; Woolley, G. A. Red-Shifting Azobenzene Photoswitches for in Vivo Use. *Acc Chem Res* **2015**, *48* (10), 2662–2670. https://doi.org/10.1021/acs.accounts.5b00270.

(37) Crespi, S.; Simeth, N. A.; König, B. Heteroaryl Azo Dyes as Molecular Photoswitches. *Nature Reviews Chemistry*. Nature Publishing Group March 1, **2019**, pp 133–146. https://doi.org/10.1038/s41570-019-0074-6.

(38) Matsuo, K.; Ogawa, H.; Yamaoka, S.; Waku, T.; Kobori, A. A Chemical Platform for the Efficient Screening of Arylazopyrazole-Based Photoswitchable CENP-E Inhibitors Using Mild Cyclization Reactions. *Bioorg Med Chem Lett* **2024**, *111*, 129892. https://doi.org/10.1016/j.mbcl.2024.129892.

(39) Wirth, U.; Raabe, K.; Kalaba, P.; Keimpema, E.; Muttenthaler, M.; König, B. Photoswitchable Probes of Oxytocin and Vasopressin. *J Med Chem* **2023**, *66* (21), 14853–14865. https://doi.org/10.1021/acs.jmedchem.3c01415.

(40) Kolarski, D.; Miró-Vinyals, C.; Sugiyama, A.; Srivastava, A.; Ono, D.; Nagai, Y.; Iida, M.; Itami, K.; Tama, F.; Szymanski, W.; Hirota, T.; Feringa, B. L. Reversible Modulation of Circadian Time with Chronophotopharmacology. *Nature Communications* **2021**, *12* (1), 1–12. https://doi.org/10.1038/s41467-021-23301-x.

(41) Sink, A.; Gerwe, H.; Hübner, H.; Boivin-Jahns, V.; Fender, J.; Lorenz, K.; Gmeiner, P.; Decker, M. “Photo-Adrenalines”: Photoswitchable B2-Adrenergic Receptor Agonists as Molecular Probes for the Study of Spatiotemporal Adrenergic Signaling. *Chemistry – A European Journal* **2024**, *30* (11), e202303506. https://doi.org/10.1002/chem.202303506.

(42) Wirth, U.; Erl, J.; Azzam, S.; Höring, C.; Skiba, M.; Singh, R.; Hochmuth, K.; Keller, M.; Wegener, J.; König, B. Monitoring the Reversibility of GPCR Signaling by Combining Photochromic Ligands with Label-Free Impedance Analysis. *Angewandte Chemie* **2023**, *135* (21), e202215547. https://doi.org/10.1002/ange.202215547.

(43) Aguirre, T.; Teichmann, E.; Römpp, F. Q.; Vivier, R.; Bryant, C.; Hulverson, M. A.; Van Voorhis, W. C.; Ojo, K. K.; Doggett, J. S.; Fiedler, D.; Hecht, S. Photoswitchable Inhibitors to Optically Control Specific Kinase Activity. *ACS Chem Biol* **2023**, *18* (6), 1378–1387. https://doi.org/10.1021/acschembio.3c00119.

(44) Sarkar, H. S.; Mashita, T.; Kowada, T.; Hamaguchi, S.; Sato, T.; Kasahara, K.; Matubayasi, N.; Matsui, T.; Mizukami, S. Arylazopyrazole-Based Photoswitchable Inhibitors Selective for Escherichia Coli Dihydrofolate Reductase. *ACS Chem Biol* **2023**, *18* (2), 340–346. https://doi.org/10.1021/acschembio.2c00749.

(45) Schulte, A. M.; Kolarski, D.; Sundaram, V.; Srivastava, A.; Tama, F.; Feringa, B. L.; Szymanski, W. Light-Control over Casein Kinase 1δ Activity with Photopharmacology: A Clear Case for Arylazopyrazole-Based Inhibitors. *Int J Mol Sci* **2022**, *23* (10), 5326. https://doi.org/10.3390/ijms23105326.

(46) Lahmy, R.; Hübner, H.; Lachmann, D.; Gmeiner, P.; König, B. Development of Photoswitchable Tethered Ligands That Target the μ-Opioid Receptor. *ChemMedChem* **2023**, *18* (23), e202300228. https://doi.org/10.1002/cmdc.202300228.

(47) Crespi, S.; Simeth, N. A.; König, B. Heteroaryl Azo Dyes as Molecular Photoswitches. *Nature Reviews Chemistry* **2019**, pp 133–146. https://doi.org/10.1038/s41570-019-0074-6.

(48) Dang, T.; Zhang, Z. Y.; Li, T. Visible-Light-Activated Heteroaryl Azoswitches: Toward a More Colorful Future. *J Am Chem Soc* **2024**, *146* (29), 19609–19620. https://doi.org/10.1021/jacs.4c03135.

(49) Acharya, A.; Yadav, M.; Nagpure, M.; Kumaresan, S.; Guchhait, S. K. Molecular Medicinal Insights into Scaffold Hopping-Based Drug Discovery Success. *Drug Discov Today* **2024**, *29* (1), 103845. https://doi.org/10.1016/j.drudis.2023.103845.

(50) Sun, H.; Tawa, G.; Wallqvist, A. Classification of Scaffold-Hopping Approaches. *Drug Discov Today* **2012**, *17* (7–8), 310–324. https://doi.org/10.1016/j.drudis.2011.10.024.

(51) Calbo, J.; Weston, C. E.; White, A. J. P.; Rzepa, H. S.; Contreras-García, J.; Fuchter, M. J. Tuning Azoheteroarene Photoswitch Performance through Heteroaryl Design. *J Am Chem Soc* **2017**, *139* (3), 1261–1274. https://doi.org/10.1021/jacs.6b11626.

(52) Adrion, D. M.; Kaliakin, D. S.; Neal, P.; Lopez, S. A. Benchmarking of Density Functionals for Z-Azoarene Half-Lives via Automated Transition State Search. *Journal of Physical Chemistry A* **2021**, *125* (29), 6474–6485. https://doi.org/10.1021/acs.jpca.1c01695.

(53) Mukadum, F.; Nguyen, Q.; Adrion, D. M.; Appleby, G.; Chen, R.; Dang, H.; Chang, R.; Garnett, R.; Lopez, S. A. Efficient Discovery of Visible Light-Activated Azoarene

Photoswitches with Long Half-Lives Using Active Search. *J Chem Inf Model* **2021**, *61* (11), 5524–5534. https://doi.org/10.1021/acs.jcim.1c00954.

(54) Bosma, R.; Dijon, N. C.; Zheng, Y.; Schihada, H.; Hauwert, N. J.; Shi, S.; Arimont, M.; Riemens, R.; Custers, H.; van de Stolpe, A.; Vischer, H. F.; Wijtmans, M.; Holliday, N. D.; Kuster, D. W. D.; Leurs, R. Optical Control of the B2-Adrenergic Receptor with Opto-Prop-2: A Cis-Active Azobenzene Analog of Propranolol. *iScience* **2022**, *25* (9), 104882. https://doi.org/10.1016/j.isci.2022.104882.

(55) Smith, J. S.; Lefkowitz, R. J.; Rajagopal, S. Biased Signalling: From Simple Switches to Allosteric Microprocessors. *Nat Rev Drug Discov* **2018**, *17* (4), 243–260. https://doi.org/10.1038/nrd.2017.229.

(56) Wootten, D.; Christopoulos, A.; Marti-Solano, M.; Babu, M. M.; Sexton, P. M. Mechanisms of Signalling and Biased Agonism in G Protein-Coupled Receptors. *Nat Rev Mol Cell Biol* **2018**, *19* (10), 638–653. https://doi.org/10.1038/s41580-018-0049-3.

(57) Sink, A.; Pottie, E.; Carter, S. J.; Tombari, R. J.; Weber, V.; Carloni, P.; Rossetti, G.; Olson, D. E.; Stove, C. P.; Decker, M. Design, Synthesis, and In Vitro Characterization of a Tryptamine-Based Visible-Light Photoswitchable 5-HT2AR Ligand Showing Efficacy Preference for β-Arrestin over Mini-Gq. *J Med Chem* **2025**, *68* (13), 13628–13639. https://doi.org/10.1021/acs.jmedchem.5c00442.

(58) Esmaeili, A. J.; Montazeri, P.; Gomez, J. C.; Dumervil, D. J.; Nezhad, F. S.; Steinhardt, R. C. Photoswitchable TCB-2 for Control of the 5-HT2A Receptor and Analysis of Biased Agonism. *Chemical Communications* **2024**, *60* (83), 11956–11959. https://doi.org/10.1039/d4cc03892d.

(59) Broichhagen, J.; Podewin, T.; Meyer-Berg, H.; Von Ohlen, Y.; Johnston, N. R.; Jones, B. J.; Bloom, S. R.; Rutter, G. A.; Hoffmann-Röder, A.; Hodson, D. J.; Trauner, D. Optical Control of Insulin Secretion Using an Incretin Switch. *Angewandte Chemie - International Edition* **2015**, *54* (51), 15565–15569. https://doi.org/10.1002/anie.201506384.

(60) Steinmüller, S. A. M.; Fender, J.; Deventer, M. H.; Tutov, A.; Lorenz, K.; Stove, C. P.; Hislop, J. N.; Decker, M. Visible-Light Photoswitchable Benzimidazole Azo-Arenes as β-Arrestin2-Biased Selective Cannabinoid 2 Receptor Agonists. *Angewandte Chemie - International Edition* **2023**, *62* (49). https://doi.org/10.1002/anie.202306176.

(61) Nijmeijer, S.; Vischer, H. F.; Rosethorne, E. M.; Charlton, S. J.; Leurs, R. Analysis of Multiple Histamine H4 Receptor Compound Classes Uncovers Gαi Protein- and β-Arrestin2-Biased Ligands. *Mol Pharmacol* **2012**, *82* (6), 1174–1182. https://doi.org/10.1124/mol.112.080911.

(62) Kolb, P.; Kenakin, T.; Alexander, S. P. H.; Bermudez, M.; Bohn, L. M.; Breinholt, C. S.; Bouvier, M.; Hill, S. J.; Kostenis, E.; Martemyanov, K. A.; Neubig, R. R.; Onaran, H. O.; Rajagopal, S.; Roth, B. L.; Selent, J.; Shukla, A. K.; Sommer, M. E.; Gloriam, D. E. Community Guidelines for GPCR Ligand Bias: IUPHAR Review 32. *Br J Pharmacol* **2022**, *179* (14), 3651–3674. https://doi.org/10.1111/bph.15811.

(63) Rezapour Sarabi, M.; Jiang, N.; Ozturk, E.; Yetisen, A. K.; Tasoglu, S. Biomedical Optical Fibers. *Lab Chip* **2021**, *21* (4), 627–640. https://doi.org/10.1039/d0lc01155j.

(64) Frank, J. A.; Antonini, M. J.; Chiang, P. H.; Canales, A.; Konrad, D. B.; Garwood, I. C.; Rajic, G.; Koehler, F.; Fink, Y.; Anikeeva, P. In Vivo Photopharmacology Enabled by Multifunctional Fibers. *ACS Chem Neurosci* **2020**, *11* (22), 3802–3813. https://doi.org/10.1021/acschemneuro.0c00577.

(65) McClain, S. P.; Ma, X.; Johnson, D. A.; Johnson, C. A.; Layden, A. E.; Yung, J. C.; Lubejko, S. T.; Livrizzi, G.; He, X. J.; Zhou, J.; Chang-Weinberg, J.; Ventriglia, E.; Rizzo, A.; Levinstein, M.; Gomez, J. L.; Bonaventura, J.; Michaelides, M.; Banghart, M. R. In Vivo Photopharmacology with Light-Activated Opioid Drugs. *Neuron* **2023**, *111* (24), 3926-3940.e10. https://doi.org/10.1016/j.neuron.2023.09.017.

(66) Russo, M.; Janeková, H.; Meier, D.; Generali, M.; Štacko, P. Light in a Heartbeat: Bond Scission by a Single Photon above 800 Nm. *J Am Chem Soc* **2024**, *146* (12), 8417–8424. https://doi.org/10.1021/jacs.3c14197.

(67) Alachouzos, G.; Schulte, A. M.; Mondal, A.; Szymanski, W.; Feringa, B. L. Computational Design, Synthesis, and Photochemistry of Cy7-PPG, an Efficient NIR-Activated Photolabile Protecting Group for Therapeutic Applications. *Angewandte Chemie - International Edition* **2022**, *61* (27), e202201308. https://doi.org/10.1002/anie.202201308.

(68) Barbero, M.; Degani, I.; Dughera, S.; Fochi, R.; Perracino, P. Preparation of Diazenes by Electrophilic C-Coupling Reactions of Dry Arenediazonium o-Benzenedisulfonimides with Grignard Reagents. *Synthesis (Stuttg)* **1998**, *1998* (09), 1235–1237. https://doi.org/10.1055/s-1998-6102.

(69) Curtin, D. Y.; Tveten, J. L. Reaction of Diarylzinc Reagents with Aryldiazonium Salts. Direct Formation of Cis-Azo Compounds. *Journal of Organic Chemistry* **1961**, *26* (6), 1764–1768. https://doi.org/10.1021/jo01065Aa017.

(70) Curtin, D. Y.; Arnheim Ursprung, J. Reaction of Organometallic Compounds with Diazonium Salts. Synthesis of Arylazoalkanes. *Journal of Organic Chemistry* **1956**, *21* (11), 1221–1225. https://doi.org/10.1021/jo01117a005.

(71) Hansen, M. J.; Lerch, M. M.; Szymanski, W.; Feringa, B. L.; Hansen,] M J; Lerch, M. M.; Szymanski, W.; Eringa, B. L. F. Direct and Versatile Synthesis of Red-Shifted

Azobenzenes. *Angewandte Chemie International Edition* **2016**, *55* (43), 13514–13518. https://doi.org/10.1002/anie.201607529.

(72) Sahu, S.; Tamaoki, N. A Versatile One-Pot Strategy for Thiazolylazo Extensions: Visible Light-Driven Photoswitches. *J Am Chem Soc* **2025**. https://doi.org/10.1021/jacs.5c08259.

Appendix

English Summary

English Summary

The ability to control biological processes with high spatial and temporal precision remains a major challenge in modern drug discovery. Light-based approaches have emerged to address this challenge, enabling dynamic control of biological targets while reducing off-target effects. Among these approaches, photopharmacology uses light-responsive ligands the biological activity of which can be reversibly controlled through irradiation with light. Photoswitchable ligands offer the possibility to modulate protein function with high precision, making them attractive compounds for research. Despite substantial advances in the field, many photoswitchable ligands still rely on the azobenzene scaffold, and switching this group from its *trans* to its *cis* configuration generally calls for ultraviolet (UV) irradiation. As a result, their applicability in living systems is limited, since UV wavelengths are absorbed before they can reach deeper tissue layers.

G protein-coupled receptors (GPCRs) constitute one of the most important classes of drug targets and have become a major focus of photopharmacological research. Several photoswitchable ligands for histamine receptors have already been developed in the past. Building on this foundation, this thesis explores the design, synthesis, and characterization of next-generation photoswitchable GPCR ligands. Particular emphasis is placed on expanding the photopharmacological toolbox beyond conventional azobenzenes by exploring alternative heteroaryl photoswitches and evaluating how these structural modifications influence both photochemical and pharmacological properties. Together, these studies aim to contribute to the development of more effective and biologically compatible photoswitchable ligands for GPCR photopharmacology.

Chapter 2 describes the development of a second-generation series of arylazopyrazole-based histamine H_3 receptor (H_3R) antagonists, designed to improve properties compared to the earlier azobenzene photoswitchable ligands. Introducing the arylazopyrazole photoswitch led to more efficient photoswitching, better solubility, and improved binding to H_3R than the azobenzene-based template ligand. The optimization process led to the identification of key compound **VUF26063**, which combines picomolar H_3R binding in its *trans* isomer with a pronounced erosion of affinity upon conversion to the *cis* state. A key structural feature of this ligand also made it possible to introduce a tritium label, generating the first radiolabelled photoswitchable ligand. This tool was used to study the kinetics of this ligand, indicating that it photochemically isomerizes while residing inside the receptor pocket. Beyond the specific case of H_3R, these results offer a more general mechanistic picture of how photoswitchable ligands behave once bound to their target, information that will be valuable for designing future generation tools.

Chapter 3 introduces a 'photoswitch hop' as a design strategy. The phenyl ring of an azobenzene-based H_3R antagonist is substituted with a range of heteroaryl azo (HAA) groups to examine how the incorporation of heteroaromatic rings affects the photochemical, physicochemical and pharmacological properties of the resulting ligands. The study revealed that exchanging the photoswitch scaffold can profoundly influence properties, yielding compounds with red-shifted switching wavelengths, improved photostationary states, and a

wide range of thermal relaxation times. While no single HAA photoswitch outperforms azobenzene across all parameters, several analogues display superior receptor affinity and improved photoswitching wavelengths. In particular, arylazoisoxazole ligand **VUF26257** exhibits picomolar H_3R affinity together with a 13-fold light-induced affinity shift, showing the potential of using HAA photoswitches for optimizing photopharmacological ligands beyond the azobenzene scaffold.

Chapter 4 targets the histamine H_1 receptor (H_1R), a clinically important GPCR for which no sufficiently effective photoswitchable ligand has yet been developed, despite several prior attempts. Desloratadine was used as the template scaffold for an "azoscan" approach, in which azobenzene units were installed at available positions, yielding nine ligands with a wide range of photoswitching properties and half-lives. Among these, the 2-substituted analogue emerged as the most promising candidate, combining nanomolar H_1R affinity in the *trans* state with a 3.2-fold drop in affinity when switched to the *cis* state. While a fully optimized H_1R photoswitchable ligand was not obtained, these ligands form a basis for further exploration of photoswitchable ligands to optically control the H_1R.

Chapter 5 examines how the position and orientation of an arylazopyrazole photoswitch affects the photochemical and pharmacological properties of a ligand. Starting from two previously reported azobenzene-based H_3R agonists, three ligands were prepared by substituting either the central or the peripheral phenyl ring with an arylazopyrazole moiety. The resulting compounds switch efficiently from the *cis* to the *trans* state under green light and show red-shifted absorption together with higher photostationary states than their azobenzene counterparts. Despite this, none of the three compounds show H_3R affinity in either the *trans* or *cis* state. Relative to the agonists that the ligands are based on, this loss of affinity indicates the steric demands of the dimethyl-substituted pyrazole ring as the likely cause, outweighing any gain from its improved photoswitching behavior. This outcome underlines that favourable photoswitching properties do not guarantee retained pharmacological activity, and that compatibility between a photoswitch and a given scaffold needs to be assessed individually rather than generalized across positions or receptors.

Chapter 6 discusses the overall findings of this thesis in light of the broader opportunities and challenges in photoswitchable GPCR ligand design. Newer photoswitch classes, such as arylazopyrazoles and other heteroarylazo scaffolds, show the potential to improve photochemical parameters, but their compatibility with a given bioactive ligand cannot be assumed and instead depends strongly on the specific receptor and ligand. The work presented here demonstrates that simultaneous optimization of all the parameters is challenging, and that improvement of one property can come at the expense of another. Further advancement of the field will depend on more efficient synthetic methods for accessing red-shifted and heteroaromatic photoswitches, photochemical characterization carried out under standardized biologically relevant conditions, structural data clarifying how *trans* and *cis* isomers occupy the receptor binding pocket, and earlier incorporation of

computational approaches into the design process itself. Such developments will be necessary to move photoswitchable ligands from proof-of-concept studies toward more complex biological and, eventually, *in vivo* applications.

In all, this thesis explored the design, synthesis, and characterization of next-generation photoswitchable ligands for the histamine receptors, with particular emphasis on photoswitch scaffolds beyond the azobenzene. Across the photoswitch replacement strategies and positional studies described in the individual chapters, even subtle structural changes were found to substantially affect photochemical properties and receptor affinity. Beyond the individual ligands, this work provides new mechanistic insight into ligand behavior within the receptor binding pocket and establishes structure-property relationships that can inform future photopharmacological design. Collectively, the findings advance the understanding of how light-responsive ligands can be designed to achieve precise spatiotemporal control of GPCRs and establish a framework for the development of future photopharmacological tools.

Appendix

Acknowledgements

Dankwoord

Al het werk in dit proefschrift zou nooit mogelijk zijn geweest zonder de hulp van anderen. Ik wil daarom graag iedereen bedanken die de afgelopen jaren, op welke manier dan ook, heeft bijgedragen aan mijn onderzoek, maar ook zeker aan de vele leuke momenten daarbuiten.

Allereerst wil ik mijn promotor **Rob** bedanken voor de samenwerking in de afgelopen vier jaar. Ik denk dat we samen een aantal mooie projecten hebben neergezet waarop we met trots kunnen terugkijken. Ik waardeer al het wetenschappelijke advies dat je mij hebt gegeven en de manier waarop je mij scherp hield en bleef uitdagen om kritisch naar onze projecten te kijken. Daarnaast wil ik mijn copromotor **Maikel** bedanken. Het is inmiddels meer dan tien jaar geleden dat we elkaar leerden kennen. Hoewel we elkaar voor de start van mijn promotietraject dus al behoorlijk goed kenden, denk ik dat we de afgelopen vier jaar toch weer nieuwe kanten van elkaar hebben gezien. Ik heb het altijd enorm gewaardeerd dat jouw deur openstaat en dat ik op ieder moment bij je naar binnen kan lopen, voor wat dan ook. Ondanks onze compleet verschillende persoonlijkheden en de kleine misverstanden die daar soms bij hoorden, kijk ik met veel plezier terug op onze samenwerking.

Naast mijn promotieteam wil ik graag de collega's bedanken met wie ik de afgelopen jaren heb samengewerkt. **Laura**, jij hebt mij vanaf het begin van mijn promotietraject meegemaakt. In het begin konden we nog zonder al te veel problemen alle borrels afgaan, maar inmiddels zijn we een paar jaar ouder en moeten we toch concluderen dat we daar iets minder goed tegen kunnen (ik in ieder geval). We hebben de afgelopen jaren ontelbaar veel koffietjes gedronken en zijn bijna failliet gegaan aan onze bezoeken aan het Science Café en de AH to go. Daarnaast is het heerlijk om iemand naast je op het lab te hebben bij wie je altijd je frustraties kwijt kunt als de chemie tegenzit, maar met wie je ook zonder problemen de nodige scherpe opmerkingen tegen kunt maken. **Peter**, aan het begin van mijn promotietraject begon je nog als mijn literatuurstudent. Sindsdien is onze band uitgegroeid tot een mooie vriendschap. Naast alle gezelligheid in en rondom het lab hebben we samen ook de nodige voetbalwedstrijden bezocht: van Nederland-Duitsland, Telstar-FC Emmen en Ajax-PSV tot wedstrijden in Londen. Ik hoop dat er in de toekomst nog veel meer wedstrijden aan deze lijst zullen worden toegevoegd. **Jaap**, met jou heb ik veel mooie en bijzondere avonturen meegemaakt. Van samen Formule 1 kijken tot het delen van een twijfelaar in Kopenhagen, met wat mij betreft als ultiem hoogtepunt de ULLA Summer School in Uppsala. Op naar nog veel meer gezelligheid de komende jaren. **Yang**, I first joined the group as your bachelor's student and later became your colleague and fellow member of the photo team. Looking back on the past years, I realise that much of what I have learned in the lab came from you. Thank you for your patience, for sharing your knowledge, and for always being willing to think along whenever I encountered a problem. Of course, I will also never forget our trip to Nice and all the memorable moments we shared there.

Hans en Andrea, jullie blijven toch altijd een beetje de vader en moeder van de groep. Ik heb het altijd enorm gewaardeerd dat ik bij jullie kon binnenlopen om even te kletsen, advies te

vragen of mijn hart te luchten. Ook jullie betrokkenheid en de gezellige sfeer die jullie binnen de groep creëren, heb ik enorm gewaardeerd. Daarnaast weet ik dat ik, wanneer Ajax scoort, vrijwel direct een bericht van Hans op WhatsApp kan verwachten. I would also like to thank **Ivana** for the great collaboration throughout our PhDs. Without your work, much of what is presented in this thesis would not have been possible. I think we experienced both the highs and lows of research together, and I always appreciated that we could have a coffee and vent whenever our projects were not progressing as we had hoped. One of the highlights of our PhDs was undoubtedly our trip to Hong Kong, where we not only had the opportunity to present our work, but also to explore the city together. I would also like to thank **Yangzhi** and **Sophie** for the pleasant collaboration and for your contributions to the photo team. I greatly appreciated your enthusiasm, your input during our discussions, and your willingness to always think along. It was a pleasure to work with you on our shared projects. **Tom,** bedankt voor de etentjes bij het VUmc (toen dat nog te betalen was) op de avonden dat we tot laat hebben doorgewerkt en natuurlijk voor onze gezamenlijke passie voor het kugelrohren. **Bas**, bedankt voor de prettige samenwerking op het gebied van computational modelling. Ook **Icaro**, **Barbara** en **Oscar** wil ik bedanken voor jullie bijdragen en de fijne samenwerking op computational gebied. **Job**, bedankt voor de gezelligheid, je altijd droge opmerkingen en onze FPL met Peter (die jullie aanzienlijk serieuzer nemen dan ik). **Elwin**, bedankt voor je hulp en input op het gebied van NMR en de gezellige praatjes ‘s ochtends. Ook **Iwan** wil ik graag bedanken voor al je waardevolle input tijdens meetings.

Frank and **Lukas**, thank you for the pleasant collaboration at the RNC and for all the time and energy you invested in our joint work. I greatly appreciated your help, involvement, and enthusiasm throughout our collaboration. It was always a pleasure working with you, and your contributions have been very valuable to the projects presented in this thesis.

Tijdens mijn promotietraject heb ik daarnaast verschillende lab- en literatuurstudenten mogen begeleiden. Zonder hun werk was dit proefschrift nooit geworden wat het nu is. **Hidde**, **Steffi** en **Valeria**, bedankt voor jullie inzet en jullie bijdragen aan de verschillende projecten. In het bijzonder wil ik **Daan** en **Tess** bedanken voor al het werk dat jullie hebben verricht. Ik ben ontzettend trots op de manier waarop jullie je als onderzoekers hebben ontwikkeld. Het is mooi om te zien dat jullie inmiddels allebei zelf aan een promotietraject zijn begonnen. Ik heb er alle vertrouwen in dat jullie daarin nog veel mooie dingen zullen bereiken.

Naast alle collega’s die bij mijn onderzoek betrokken waren, wil ik ook de mensen bedanken die ervoor zorgden dat er tijdens mijn promotietraject voldoende ruimte bleef voor ontspanning en gezelligheid.

Bas en **Haye**, hoewel we elkaar niet altijd even vaak spreken, voelt het wanneer we elkaar zien direct weer vertrouwd. We hebben samen veel mooie momenten meegemaakt, van padellen tot stappen in Haarlem. Bedankt voor jullie vriendschap. Ik hoop dat er nog veel van zulke momenten zullen volgen. **Suzanne**, bedankt voor alle gezelligheid van de afgelopen jaren. We hebben samen heel wat koffietjes gedronken, zijn regelmatig naar de bioscoop geweest en

natuurlijk zorgde onze vakantie naar Malta voor de nodige ontspanning buiten het werk. **Nick**, **Jelle** en **Twan**, bedankt voor de fantastische week die we samen hebben gehad tijdens de Summer School in Uppsala. Het blijft toch een van de mooiste weken van de afgelopen vier jaar.

Natuurlijk wil ik ook mijn lieve ouders, **Ron** en **Willemke**, bedanken. Ik weet dat jullie altijd voor mij klaarstaan en dat ik altijd op jullie volledige steun kan rekenen. Zonder jullie was ik nooit zo ver gekomen.

En als laatste, lieve **Es**, dat ik jou tijdens de ULLA Summer School in Zweden heb leren kennen, zal toch altijd het mooiste moment van mijn PhD blijven. Bedankt dat je er altijd voor mij bent, mij altijd steunt en dat je mij af en toe achter mijn kont aan zit wanneer dat nodig is. Ik weet niet of dit boekje zonder jou nu al af was geweest. Ik kan soms behoorlijk eigenwijs zijn, maar juist daarom heb ik iemand zoals jij nodig, die mij af en toe een zetje in de juiste richting geeft. We hebben samen al veel mooie dingen meegemaakt en ik kan niet wachten om te ontdekken wat de toekomst ons nog allemaal zal brengen!